SCATTERING OF ELECTROMAGNETIC WAVES BY HUMAN BODY AND ITS APPLICATIONS

By

Devendra K. Misra

A DISSERTATION

Submitted to
Michigan State University
in partial fulfillment of the requirements
for the degree of

DOCTOR OF PHILOSOPHY

Department of Electrical Engineering and Systems Science

1984

ABSTRACT

SCATTERING OF ELECTROMAGNETIC WAVES

BY HUMAN BODY AND ITS

APPLICATIONS

By

Devendra K. Misra

This dissertation presents a study on the scattering of electromagentic waves by the human body alongwith some related applications. After introducing the aim and scope of this study in Chapter 1, the responses of three orthogonally aligned E-field probes, near a cylindrical model of human body illuminated by TE and TM waves, are determined theoretically in Chapter 2. In Chapter 3, theoretical results of the probe responses are verified experimentally using a cylindrical dielectric shell filled with saline solution and at the frequencies of 2GHz, 2.45GHz and 3GHz. The theoretically computed results are also compared with the experimentally recorded probe responses when the shell is empty. An excellent agreement is found between the theory and the experiments. Some additional theoretical results of the response of the probe near the biological body are also presented in this chapter. A large shadow region behind the body and the difference in the probe response with and without the presence of the body are noted.

In Chapter 4, the expressions for the backscattered electric fields from a cylindrical and a spherical body illuminated by plane EM

waves are obtained and their behaviours are studied when the body-radius changes with time. It is observed that the phase of the return signal changes approximately linearly with change in the radius, while the magnitude of this signal is not linearly affected.

Two different techniques for detecting the breathing and heart beats of humans from large distances are presented in Chapter 5 using a magic tee in one and a circulator in the other. Detection of the breathing and heart beats from about 100 feet and also through a concrete wall is reported in this chapter.

Finally, Chapter 6 summarizes the whole work and Appendices A to D present the computer programs and the printouts.

To My Father

Sri Koshadhish Misra

ACKNOWLEDGEMENTS

The author expresses his gratitude to his major professor Dr. K.M. Chen, for his sincere guidance and encouragement throughout the course of this work. He also wishes to thank the members of his guidance committee, Dr. D.P. Nyquist, Dr. D.K. Reinhard and Dr. B. Drachman, for their assistance and constructive criticisms.

Thanks are also due to Li Sheng Sun, H. Chuang and H. Wang for the assistance during the experimental phases of the work.

The research reported in this thesis was supported in part by the Naval Medical Research and Development Command under contract N00014-82-K-0355.

Finally, an expression of appreciation is reserved for my wife, Ila and son, Shashank for their patience and understanding.

TABLE OF CONTENTS

TABLE OF CONTENTS (Continued)

LIST OF FIGURES

LIST OF FIGURES (Continued)

LIST OF FIGURES (Continued)

LIST OF FIGURES (Continued)

LIST OF FIGURES (Continued)

LIST OF FIGURES (Continued)

CHAPTER 1

INTRODUCTION

Many reports and papers are available in the scientific literature dealing with the interaction of EM field with the biological systems. These studies were motivated by the controversy over the potential health hazards due to non-ionizing EM radiation and increasing medical applications in therapeutic and diagnostic treatment involving EM energy. For that purpose, theoretical methods of calculating the internal EM field accurately in an irradiated body have been developed [1]. However, the EM field scattered by the biological body,which is the subject of this thesis, has not been studied thoroughly so far [2,3]. In the present work, the scattered EM field near as well as away from the simplified models of human body, has been studied and some of its possible applications have been demonstrated.

In Chapter 2, the human body is modeled as two concentric cylinders of infinite length, illuminated by a linearly polarized plane EM wave. The responses of single and orthogonal E-field probes near the body are determined by solving the boundary value problem. These results are experimentally verified in Chapter 3 using a cylindrical dielectric shell filled with saline water. A few computed results for the probe response under various conditions are also presented in this chapter.

An expression for the backscattered electric field from a cylindrical body illuminated by a plane wave with electric field parallel to its axis, is first obtained in Chapter 4. The behaviour of this field is then studied when the radius of the cylinder changes with time. In the latter part of this chapter, an expression for the backscattered electric field from a spherical body exposed to the plane EM waves is obtained and the effect of the change in the radius of the sphere on the magnitude and phase of the field is studied.

Chapter 5 presents two different techniques, one using a magic tee and the other using a circulator, to detect the breathing and heart signals of the human beings from the long distances (~ 100 feet or so) as well as through a concrete wall. These techniques may be useful for remotely detecting the physiological status of humans at distance or trapped living beings behind barriers.

Finally, Chapter 6 summarizes the whole work and the computer programs are given in Appendices A to D alongwith the computed results.

CHAPTER 2

RESPONSE OF E-FIELD PROBES IN THE PROXIMITY OF HUMAN BODY - THEORETICAL CONSIDERATIONS

An E-field probe is often carried by a man on his body surface for sensing the intensity of the EM field he is exposed to. It is, therefore, worthwhile to study the response of these probes in the proximity of human body. In this chapter, the two cases - TE and TM polarized incident fields are considered. For simplicity, the human body is assumed as circular cylinder of infinite length with complex permittivity. The equivalent voltages induced in the receiving probes have been determined after obtaining the expressions for the scattered fields from a two-layer concentric cylindrical model. The experimental verification is presented in the following chapter using a cylindrical dielectric shell filled with saline water.

2.1 Human body exposed to a TE-polarized EM wave

In order to determine the equivalent voltage induced in the receiving probe near the human body, the total fields at the location are required. Since, by superposition, total field is sum of the incident and scattered fields, the expression for the latter is first obtained in the following section and then the expression for induced voltage is obtained.

2.1.1 Determination of scattered EM fields

The geometry and the coordinate systems related to the problem are shown in Figure 2.1.1 Specialized form of Maxwell's equations suitable for the present system are,

$$\frac{1}{r}\frac{\partial E_z}{\partial \phi} = -j\omega\mu_0 H_r \tag{2.1.1}$$

$$\frac{-\partial E_z}{\partial r} = -j\omega\mu_0 H_\phi \tag{2.1.2}$$

$$\frac{1}{r}\frac{\partial}{\partial r}(rH_\phi) - \frac{1}{r}\frac{\partial Hr}{\partial \phi} = -\frac{k^2}{j\omega\mu_0} E_z \tag{2.1.3}$$

with the assumption of $\frac{\partial}{\partial z} \to 0$ and $E_r = E_\phi = 0$, and

$$k^2 = \omega^2 \mu_0 \epsilon \left(1 - j\frac{\sigma}{\omega\epsilon}\right) \tag{2.1.4}$$

The time dependence $\exp(j\omega t)$ is assumed and suppressed throughout.

The expression for $\hat{z}$-polarized incident plane wave is assumed to be

$$\vec{E}^i = \hat{z}\, E_{0z} \exp(-jk_0 x) = \hat{z}\, E_{0z} \exp(-jk_0 r \cos\phi) \tag{2.1.5}$$

From equations (2.1.1) - (2.1.3), the partial differential equation for $E_z(r,\phi)$ is obtained as,

$$\frac{\partial^2 E_z}{\partial r^2} + \frac{1}{r}\frac{\partial E_z}{\partial r} + \frac{1}{r^2}\frac{\partial^2 E_z}{\partial \phi^2} + k^2 E_z = 0 \tag{2.1.6}$$

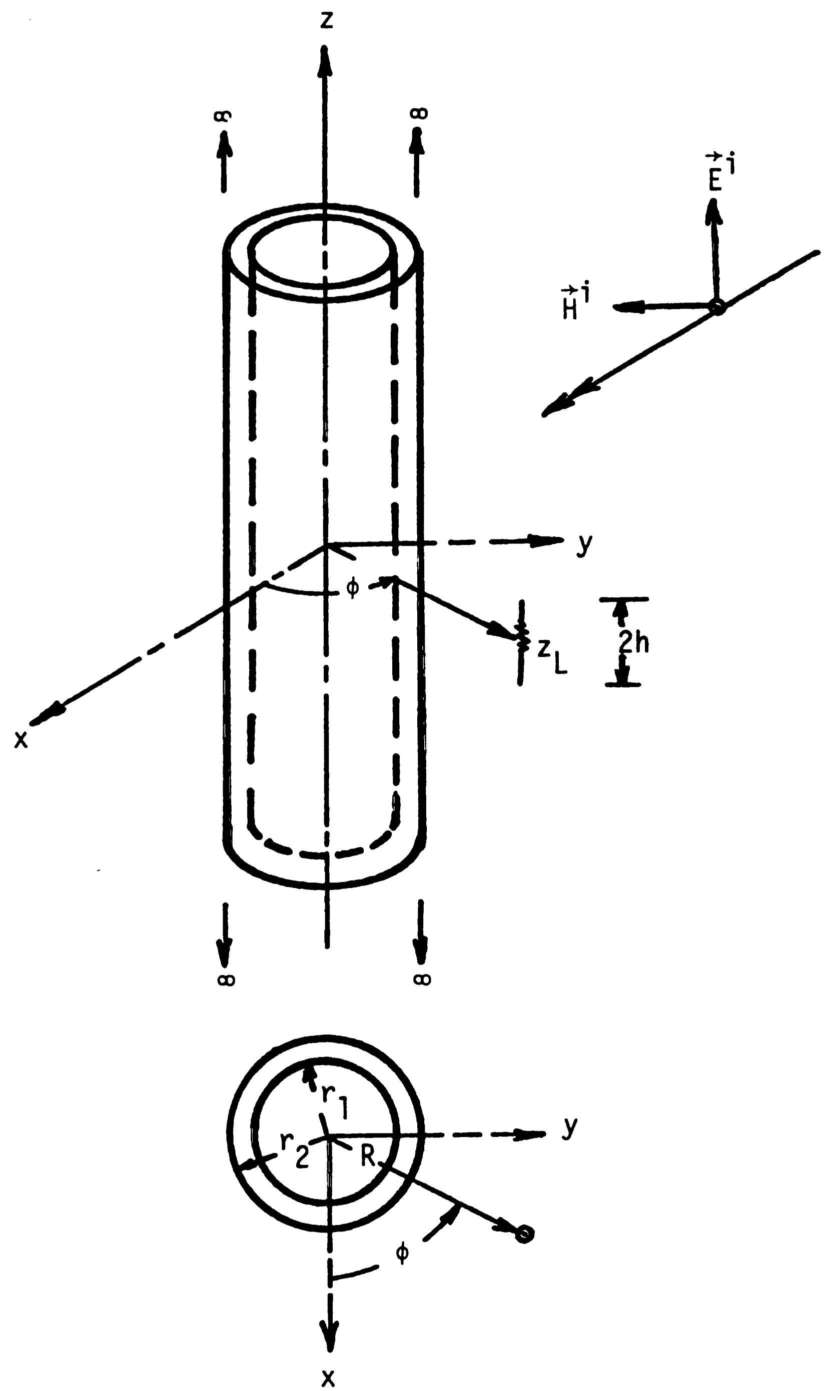

Fig. 2.1.1. A TE-polarized plane wave illuminates a vertical receiving probe located near a long sheathed conducting cylinder.

Now assuming $E_z(r,\phi) = R(r)\Phi(\phi)$ to obtain a separation of variables solution, equation (2.1.6) gives,

$$\frac{r^2}{R}\frac{d^2R}{dr^2} + \frac{r}{R}\frac{dR}{dr} + k^2r^2 = -\frac{1}{\Phi}\frac{d^2\Phi}{d\phi^2} \qquad (2.1.7)$$

Since the left hand side of equation (2.1.7) is only r-dependent, both should be equal to the same constant. Furthermore, the field is single valued, i.e.,

$$E_z(r,\phi) = E_z(r,\phi + 2\pi)$$

Therefore, the above mentioned constant should be an integer. Now since the incident field, expressed by equation (2.1.5) is even in ϕ, the scattered field $\vec{E}^s$ is expected to be even in ϕ. Hence, keeping in mind the properties of Bessel functions, the scattered field in three regions may be written as,

$$E^s_{zn}(r,\phi) = \begin{cases} a_n\, J_n(k_1r)\cos(n\phi) & r < r_1 \\ [b_nH_n^{(1)}(k_2r) + c_nH_n^{(2)}(k_2r)]\cos(n\phi) & r_1 < r < r_2 \\ d_n\, H_n^{(2)}(k_0r)\cos(n\phi) & r > r_2 \end{cases} \qquad (2.1.8)$$

Where a_n, b_n, c_n and d_n are constants and usual notations for Bessel and Hankel functions are employed. Hence the total electric field $E_z(r,\phi)$ in three regions are,

$$E_z(r,\phi) = \begin{cases} \sum\limits_{n=0}^{\infty} a_n\, J_n(k_1 r) \cos(n\phi) & r < r_1 \\ \sum\limits_{n=0}^{\infty} [b_n H_n^{(1)}(k_2 r) + c_n H_n^{(2)}(k_2 r)] \cos(n\phi) & r_1 < r < r_2 \\ E_{0z} \exp(-jk_0 r \cos\phi) + \sum\limits_{n=0}^{\infty} d_n H_n^{(2)}(k_0 r) \cos(n\phi) & r > r_2 \end{cases} \tag{2.1.9}$$

For evaluation of constants, boundary conditions, the continuity of tangential fields, E_z and H_ϕ, at r_1 and r_2 are used. For that H_ϕ is evaluated from equation (2.1.2) as

$$H_\phi(r,\phi) = \frac{1}{j\omega\mu_0} \begin{cases} k_1 \sum\limits_{n=0}^{\infty} a_n\, J_n'(k_1 r) \cos(n\phi) & r < r_1 \\ k_2 \sum\limits_{n=0}^{\infty} [b_n H_n^{(1)'}(k_2 r) + c_n H_n^{(2)'}(k_2 r)] \cos(n\phi) & r_1 < r < r_2 \\ -jk_0 \cos\phi\, E_{0z} \exp(-jk_0 r \cos\phi) + & \\ \qquad k_0 \sum\limits_{n=0}^{\infty} d_n H_n^{(2)'}(k_0 r) \cos(n\phi) & r > r_2 \end{cases} \tag{2.1.10}$$

Now, in order to satisfy boundary conditions, the following four equations must be satisfied.

$$\sum_{n=0}^{\infty} [a_n J_n(k_1 r_1) - b_n H_n^{(1)}(k_2 r_1) - c_n H_n^{(2)}(k_2 r_1)] \cos(n\phi) = 0 \tag{2.1.11}$$

$$\sum_{n=0}^{\infty} [b_n H_n^{(1)}(k_2 r_2) + c_n H_n^{(2)}(k_2 r_2) - d_n H_n^{(2)}(k_0 r_2)] \cos(n\phi)$$

$$= E_{0z} \exp(-jk_0 r_2 \cos\phi) \tag{2.1.12}$$

$$\sum_{n=0}^{\infty} [a_n J_n'(k_1 r_1) - \frac{k_2}{k_1} \{b_n H_n^{(1)'}(k_2 r_1) + c_n H_n^{(2)'}(k_2 r_1)\}]\cos(n\phi) = 0 \tag{2.1.13}$$

and

$$\sum_{n=0}^{\infty} [d_n H_n^{(2)'}(k_0 r_2) - \frac{k_2}{k_1} \{b_n H_n^{(1)'}(k_2 r_2) + c_n H_n^{(2)'}(k_2 r_2)\}]\cos(n\phi)$$

$$= j \cos \phi \; E_{0z} \exp(-jk_0 r_2 \cos \phi) \tag{2.1.14}$$

Equations (2.1.11) - (2.1.14) can be solved for a_n, b_n, c_n and d_n. From equation (2.1.11),

$$a_n J_n(k_1 r_1) = b_n H_n^{(1)}(k_2 r_1) + c_n H_n^{(2)}(k_2 r_1) \tag{2.1.15}$$

while from equation (2.1.13),

$$a_n J_n'(k_1 r_1) = \frac{k_2}{k_1} [b_n H_n^{(1)'}(k_2 r_1) + c_n H_n^{(2)'}(k_2 r_1)] \tag{2.1.16}$$

From equations (2.1.15) and (2.1.16),

$$b_n = -X_n c_n \tag{2.1.17}$$

where

$$X_n = \frac{H_n^{(2)}(k_2 r_1)}{H_n^{(1)}(k_2 r_1)} \left\{ \frac{\dfrac{J_n'(k_1 r_1)}{J_n(k_1 r_1)} - \dfrac{k_2}{k_1} \dfrac{H_n^{(2)'}(k_2 r_1)}{H_n^{(2)}(k_2 r_1)}}{\dfrac{J_n'(k_1 r_1)}{J_n(k_1 r_1)} - \dfrac{k_2}{k_1} \dfrac{H_n^{(1)'}(k_2 r_1)}{H_n^{(1)}(k_2 r_1)}} \right\} \tag{2.1.18}$$

Now, using equation (2.1.17), equation (2.1.12) may be written as,

$$\sum_{n=0}^{\infty} \{[-X_n H_n^{(1)}(k_2 r_2) + H_n^{(2)}(k_2 r_2)]\, c_n - d_n H_n^{(2)}(k_0 r_2)\} \cos(n\phi)$$

$$= E_{0z} \exp(-jk_0 r_2 \cos \phi) \qquad (2.1.19)$$

Multiplying both the sides of equation (2.1.19) by $\cos(m\phi)$ and then integrating over 0 to 2π, one gets,

$$[-X_m H_m^{(1)}(k_2 r_2) + H_m^{(2)}(k_2 r_2)]\, c_m - d_m H_m^{(2)}(k_0 r_2)$$

$$= \frac{\epsilon_m}{2\pi} E_{0z} I_m(k_0 r_2) \qquad (2.1.20)$$

where

$$I_m(k_0 r_2) = 2\pi j^{-m} J_m(k_0 r_2) \qquad (2.1.21)$$

and

$$\epsilon_m = \text{Neumann number}$$

The orthogonality property of cosine functions is utilized in equation (2.1.20).

From equations (2.1.14) and (2.1.17),

$$\sum_{n=0}^{\infty} \{ \frac{k_2}{k_1}[-X_n H_n^{(1)'}(k_2 r_2) + H_n^{(2)'}(k_2 r_2)]c_n - d_n H_n^{(2)'}(k_0 r_2)\}\cos(n\phi)$$

$$= -j \cos \phi \; E_{0z} \exp(-jk_0 r_2 \cos \phi)$$

As before, multiplying by cos m , integrating them over 0 to 2π, and provoking the orthogonality property of cosine functions, the above equation reduces to,

$$\frac{k_2}{k_0}\,[-X_m H_m^{(1)'}(k_2r_2) + H_m^{(2)'}(k_2r_2)]c_m - d_m H_m^{(2)'}(k_0r_2)$$

$$= \frac{\epsilon_m}{2\pi}\, E_{0z} I_m'(k_0r_2) \tag{2.1.22}$$

where,

$$I_m'(k_0r_2) = 2\pi j^{-m} J_m'(k_0r_2) \tag{2.1.23}$$

and

$$\epsilon_m = \text{Neumann number}$$

c_m can be expressed in terms of d_m using equations (2.1.20) and (2.1.21) as follows:

$$c_m = \frac{H_m^{(2)}(k_0r_2)}{H_m^{(2)}(k_2r_2)-X_m H_m^{(1)}(k_2r_2)}\, d_m + $$

$$+ \frac{J_m(k_0r_2)}{H_m^{(2)}(k_2r_2)-X_m H_m^{(1)}(k_2r_2)}\, j^{-m}\epsilon_m E_{0z} \tag{2.1.24}$$

Now, substituting for c_m from equation (2.1.24) into equation (2.1.22) and then solving for d_m, one gets,

$$d_m = E_{0z}\epsilon_m j^{-m}\, \frac{J_m(k_0r_2)}{H_m^{(2)}(k_0r_2)} \left[\frac{\dfrac{J_m'(k_0r_2)}{J_m(k_0r_2)} - y_m}{y_m - \dfrac{H_m^{(2)'}(k_0r_2)}{H_m^{(2)}(k_0r_2)}} \right] \tag{2.1.25}$$

where

$$y_m = \frac{k_2}{k_0} \left[\frac{H_m^{(2)'}(k_2 r_2) - X_m H_m^{(1)'}(k_2 r_2)}{H_m^{(2)}(k_2 r_2) - X_m H_m^{(1)}(k_2 r_2)} \right] \qquad (2.1.26)$$

Thus, the electric field outside cylinder is given by,

$$E_z(r,\phi) = E_{0z} \exp(-jk_0 r \cos \phi) + \sum_{n=0}^{\infty} d_n H_n^{(2)}(k_0 r) \cos n\phi \qquad (2.1.27)$$

Where d_n is given by equation (2.1.25) with m replaced by n.

2.1.2 Equivalent voltage induced in a receiving probe

The EM fields in three different regions have been determined in the previous subsection. Now, consider that there is a small cylindrical receiving antenna at a distance of R ($R > r_2$) from the axis of the cylinder and aligned along z-axis, as shown in Figure 2.1.1. Then the boundary condition to be satisfied at the antenna surface is

$$\hat{z} \cdot \vec{E}_p = V_0 \, \delta(z) = Z_L I_0 \, \delta(z) \qquad (2.2.1)$$

Where V_0 is the voltage across the load Z_L due to current I_0 at $z = 0$ of the receiving antenna, and

$$\vec{E}_p = \vec{E}_t^i + \vec{E}_{self}^a + \vec{E}_{image}^a \qquad (2.2.2)$$

$\vec{E}_t^i$ is the total $\vec{E}$ field given by equation (2.1.27), $\vec{E}_{self}^a$ is the electric field maintained by the induced current on the receiving probe and $\vec{E}^a_{image}$ is the electric field maintained by its image created by the presence of the cylindrical body.

The induced current in the antenna is a function of z and can be expressed as

$$I(z) = I_0 f(z)$$

Where f(z) is the current distribution function. Since,

$$I(z=0) = I_0, \; f(0) = 1.$$

Therefore, from equation (2.2.1),

$$\int_{-h}^{h} f(z)\hat{z}\cdot\vec{E}_p dz = Z_L I_0 \tag{2.2.3}$$

or

$$Z_L I_0 = \int_{-h}^{h} f(z)\hat{z}\cdot\vec{E}^i_t dz + \int_{-h}^{h} f(z)\hat{z}\cdot\vec{E}^a_{self}\, dz + \\ + \int_{-h}^{h} f(z)\hat{z}\cdot\vec{E}^a_{image}\, dz \tag{2.2.4}$$

Therefore, if

$$\int_{-h}^{h} f(z)\hat{z}\cdot\vec{E}^i_t dz \triangleq V_{eq} \tag{2.2.5}$$

$$\int_{-h}^{h} f(z)\hat{z}\cdot\vec{E}^a_{self}\, dz \triangleq - Z_{in} I_0 \tag{2.2.6}$$

and,

$$\int_{-h}^{h} f(z)\hat{z}\cdot\vec{E}^a_{image}\, dz \triangleq - Z_m \Gamma_z I_0 \tag{2.2.7}$$

Here the induced EMF method [4] is used to get equation (2.2.6). The effect of probe-body coupling is included via image theory, except that the strenth of the image is approximated by weighting it with appropriate reflection coefficient [5,6,7]. Z_m is the mutual impedance of the antenna and its image for the perfect conducting body case.

Hence from equations (2.2.4) - (2.2.7),

$$I_0 = \frac{V_{eq}}{Z_L + Z_{in} + \Gamma_z Z_m}$$

For a small probe, Z_{in} is very large. For example, for a probe of $2h = 1.3$ cm, Z_{in} at 2.45 GHz is found to be about 2-j1137 Ohm [8]. The load impedance, Z_L, for a 10 k Ohm in parallel with 6pF capacitor which is a typical value for the probe, is approximately -j10.8 Ohm, If two of these probes are placed in parallel 2.54 cm apart, which represent the probe and its image, the mutual impedance, Z_m, can be computed [9] as 2.06 - j2.07 Ohm. Since $|\Gamma_z| \leq 1$, $|Z_L + Z_{in}| >> |\Gamma_z Z_m|$. Therefore, for practical purposes,

$$I_0 \simeq \frac{V_{eq}}{Z_L + Z_{in}} \tag{2.2.8}$$

V_{eq} is determined as follows:

$$V_{eq} = \int_{-h}^{h} f(z)\hat{z}\cdot\vec{E}_t^i dz$$

$$= \int_{-h}^{h} f(z)[E_{0z} \exp(-jk_0R \cos \phi) + \sum_{n=0}^{\infty} d_n H_n^{(2)}(k_0R)\cos(n\phi)]dz$$

or

$$V_{eq} = [E_{0z} \exp(-jk_0 R \cos\phi) + \sum_{n=0}^{\infty} d_n H_n^{(2)}(k_0 R)\cos(n\phi)] \int_{-h}^{h} f(z)dz \tag{2.2.9}$$

Assuming a triangular distribution of current over the probe which is a short dipole as,

$$f(z) = 1 - \frac{|z|}{h} \qquad 0 \leq |z| \leq h$$

The equation (2.2.9) reduces to

$$V_{eq} = h[E_{0z} \exp(-jk_0 R \cos\phi) + \sum_{n=0}^{\infty} d_n H_n^{(2)}(k_0 R)\cos(n\phi)] \tag{2.2.10}$$

Hence, the load current I_0 can be determined for a given probe with known input-impedance Z_{in} and load impedance Z_L.

2.2 Human body exposed to a TM-polarized EM wave

When the human body is exposed to a TM-polarized EM wave, the electric field will be coupled to both azimuthally as well as radially aligned probes. Again, the human-body is modeled as two layered infinite cylinder of complex permittivities. The expressions for the scattered field distributions are obtained in the following sub-section. The induced voltages in the two probes are then obtained from the total E-field.

2.2.1 Determination of the scattered EM-field

The geometry and the coordinate system for the analysis are depicted in Figure 2.2.1. The magnetic field components H_r and H_ϕ are zero. The electric field component E_z is also zero. The relations

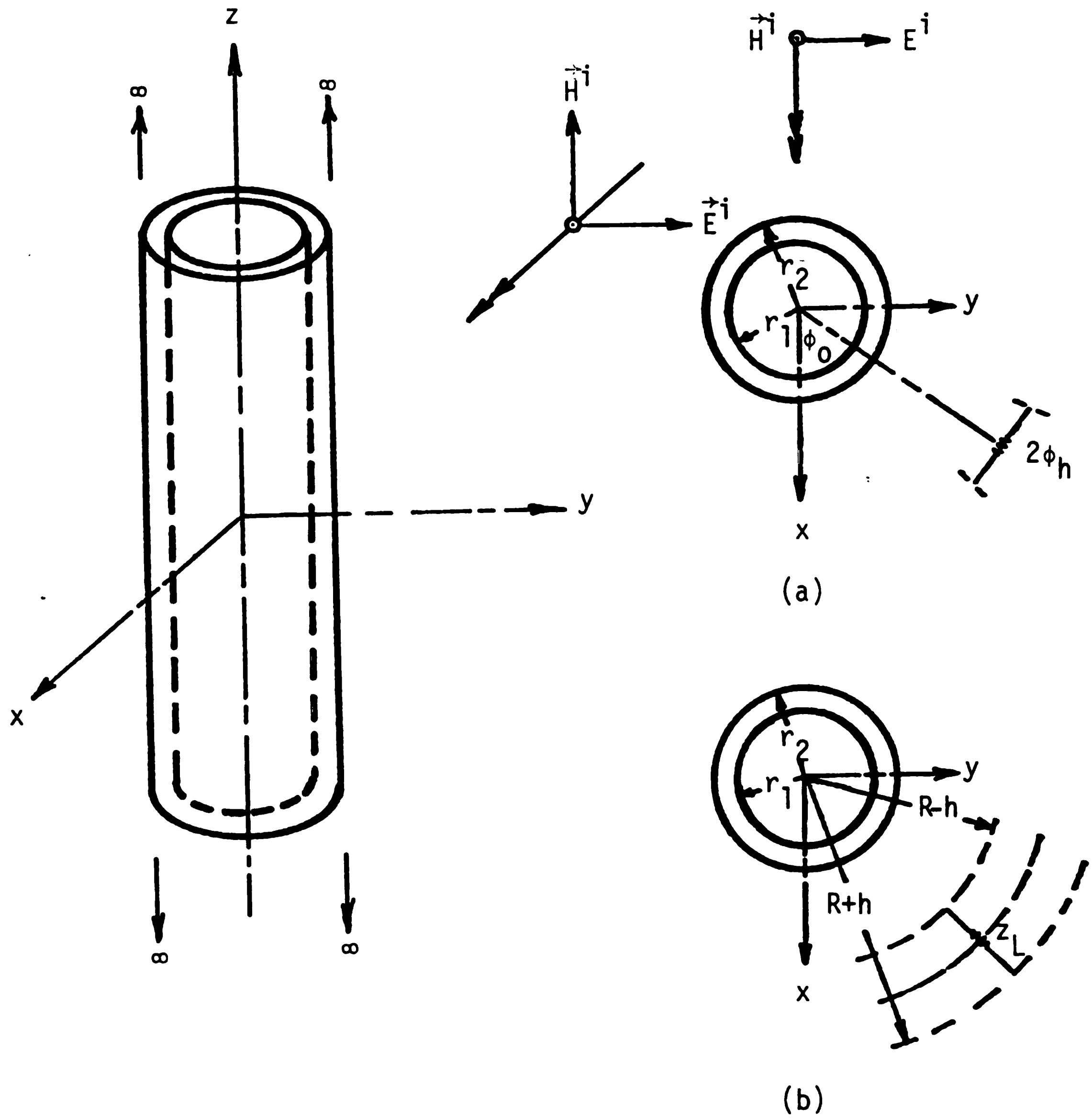

Fig. 2.2.1. A TM-polarized plane wave illuminates a horizontal receiving probe located near a long sheathed conducting cylinder for (a) the probe oriented azimuthally and (b) the probe oriented radially.

among other three field components are obtained via Maxwell's equation, assuming that the partial derivative with respect to z is zero, as follows:

$$E_r = -\frac{j\omega\mu_0}{k^2}\frac{1}{r}\frac{\partial H_z}{\partial\phi} \tag{2.2.1}$$

$$E_\phi = \frac{j\omega\mu_0}{k^2}\frac{\partial H_z}{\partial r} \tag{2.2.2}$$

while H_z satisfies the following partial differential equaiton:

$$\frac{\partial^2 H_z}{\partial r^2} + \frac{1}{r}\frac{\partial H_z}{\partial r} + \frac{1}{r^2}\frac{\partial^2 H_z}{\partial\phi^2} + k^2 H_z = 0 \tag{2.2.3}$$

Now using the method of separation of variables and following the procedure similar to the TE-wave case, the scattered magnetic field $H_z^s(r,\phi)$ in the three regions is found as,

$$H_z^s(r,\phi) = \sum_{n=0}^{\infty}\begin{cases} a_n J_n(k_1 r)\cos(n\phi) & r < r_1 \\ [b_n H_n^{(1)}(k_2 r) + c_n H_n^{(2)}(k_2 r)]\cos(n\phi) & r_1 < r < r_2 \\ d_n H_n^{(2)}(k_0 r)\cos(n\phi) & r > r_2 \end{cases} \tag{2.2.4}$$

Where a_n, b_n, c_n and d_n are constants. Hence the total magnetic field $H_z(r,\phi)$ in the three regions can be expressed as

$$H_z(r,\phi) = \begin{cases} \sum_{n=0}^{\infty} a_n J_n(k_1 r)\cos(n\phi) & r < r_1 \\ \sum_{n=0}^{\infty} [b_n H_n^{(1)}(k_2 r) + c_n H_n^{(2)}(k_2 r)]\cos(n\phi) & r_1 < r < r_2 \\ H_{0z}\exp(-jk_0 r\cos\phi) + \sum_{n=0}^{\infty} d_n H_n^{(2)}(k_0 r)\cos(n\phi) & r > r_2 \end{cases} \tag{2.2.5}$$

For evaluating the constants, the continuity of the tangential fields, H_z and E_ϕ, at r_1 and r_2 is imposed. E_ϕ is evaluated using equation (2.2.2) as follows:

$$E_\phi(r,\phi) = \begin{cases} \dfrac{j\omega\mu_0}{k_1} \displaystyle\sum_{n=0}^{\infty} a_n J_n'(k_1 r) \cos(n\phi) & r < r_1 \\ \dfrac{j\omega\mu_0}{k_2} \displaystyle\sum_{n=0}^{\infty} [b_n H_n^{(1)'}(k_2 r) + c_n H_n^{(2)'}(k_2 r)]\cos(n\phi) & r_1 < r < r_2 \\ \dfrac{j\omega\mu_0}{k_0} [-j \cos\phi \, H_{0z} \exp(-jk_0 r \cos\phi) + & \\ \quad + \displaystyle\sum_{n=0}^{\infty} d_n H_n^{(2)'}(k_0 r)\cos(n\phi) & r > r_2 \end{cases} \tag{2.2.6}$$

Now enforcing the boundary conditions at r_1 and r_2, the following equations are obtained:

$$\sum_{n=0}^{\infty} [a_n J_n(k_1 r_1) - b_n H_n^{(1)}(k_2 r_1) - c_n H_n^{(2)}(k_2 r_1)]\cos(n\phi) = 0 \tag{2.2.7}$$

$$\sum_{n=0}^{\infty} [b_n H_n^{(1)}(k_2 r_2) + c_n H_n^{(2)}(k_2 r_2) - d_n H_n^{(2)}(k_0 r_2)]\cos(n\phi)$$
$$= H_{0z} \exp(-jk_0 r_2 \cos\phi) \tag{2.2.8}$$

$$\sum_{n=0}^{\infty} [b_n H_n^{(1)'}(k_2 r_1) + c_n H_n^{(2)'}(k_2 r_1) - \frac{k_2}{k_1} a_n J_n'(k_1 r_1)]$$
$$\cdot \cos(n\phi) = 0 \tag{2.2.9}$$

and,

$$\sum_{n=0}^{\infty}\left[\frac{k_0}{k_2}\{b_n H_n^{(1)'}(k_2r_2) + c_n H_n^{(2)'}(k_2r_2)\} - d_n H_n^{(2)'}(k_0r_2)\right]\cdot$$

$$\cdot\cos(n\phi) = -j\cos\phi\, H_{0z}\exp(-jk_0r_2\cos\phi) \tag{2.2.10}$$

Thus a_n, b_n, c_n and d_n can be evaluated from equations (2.2.7) - (2.2.10). Equations (2.2.7) and (2.2.9) can be solved to get

$$b_n = -X_n c_n \tag{2.2.11}$$

where

$$X_n = \frac{H_n^{(2)}(k_2r_1)}{H_n^{(1)}(k_2r_1)}\left\{\frac{\dfrac{J_n'(k_1r_1)}{J_n(k_1r_1)} - \dfrac{k_1}{k_2}\dfrac{H_n^{(2)'}(k_2r_1)}{H_n^{(2)}(k_2r_1)}}{\dfrac{J'_n(k_1r_1)}{J_n(k_1r_1)} - \dfrac{k_1}{k_2}\dfrac{H_n^{(1)'}(k_2r_1)}{H_n^{(1)}(k_2r_1)}}\right\} \tag{2.2.12}$$

Now substituting for b_n from equation (2.2.11) into equation (2.2.8) and then multiplying the resulting equation by $\cos m\phi$, and integrating over 0 to 2π, one gets,

$$[-X_m H_m^{(1)}(k_2r_2) + H_m^{(2)}(k_2r_2)]c_m - d_m H_m^{(2)}(k_0r_1)$$

$$= \frac{\epsilon_m}{2\pi} H_{0z} I_m(k_0r_2) \tag{2.2.13}$$

where

$$I_m(k_0r_2) = 2\pi j^{-m} J_m(k_0r_2) \tag{2.2.14}$$

And by a similar process, equations (2.2.10) and (2.2.11) lead to,

$$\frac{k_0}{k_2}[-X_m H_m^{(1)'}(k_2r_2) + H_m^{(2)'}(k_2r_2)]c_m - d_m H_m^{(2)'}(k_0r_2)$$
$$= \frac{\epsilon_m}{2\pi} H_{0z} I_m'(k_0r_2) \qquad (2.2.15)$$

where

$$I_m'(k_0r_2) = 2\pi j^{-m} J_m'(k_0r_2) \qquad (2.2.16)$$

and, ϵ_m in equations (2.2.13) and (2.2.15) is Neumann number.

Now equations (2.2.13) and (2.2.15) can be solved for d_m to get

$$d_m = \epsilon_m H_{0z} j^{-m} \frac{J_m(k_0r_2)}{H_m^{(2)}(k_0r_2)} \left\{ \frac{\dfrac{J_m'(k_0r_2)}{J_m(k_0r_2)} - y_m}{y_m - \dfrac{H_n^{(2)'}(k_0r_2)}{H_m^{(2)}(k_0r_2)}} \right\} \qquad (2.2.17)$$

where

$$y_m = \frac{k_0}{k_2}\left[\frac{H_m^{(2)'}(k_2r_2) - X_m H_m^{(1)'}(k_2r_2)}{H_m^{(2)}(k_2r_2) - X_m H_m^{(1)}(k_2r_2)}\right] \qquad (2.2.18)$$

Thus, the magnetic field outside cylinder is given by,

$$H_z(r,\phi) = H_{0z}\exp(-jk_0 r\cos\phi) + \sum_{n=0}^{\infty} d_n H_n^{(2)}(k_0 r)\cos(n\phi) \qquad (2.2.19)$$

where d_n is given by equation (2.2.17) with dummy integer m changing to n.

2.2.2 Equivalent voltage induced in an azimuthally aligned receiving probe

The expression for $H_z(r,\phi)$ is now known. Therefore, the expressions for $E_r(r,\phi)$ and $E_\phi(r,\phi)$ outside the cylinder can be obtained from equations (2.2.1), (2.2.2) and (2.2.19) as follows:

$$E_r(r,\phi) = \zeta_0 H_{0z} \sin\phi \exp(-jk_0 r\cos\phi) + \frac{j\zeta_0}{k_0 r} \sum_{n=0}^{\infty} n d_n H_n^{(2)}(k_0 r) \sin(n\phi) \tag{2.2.20}$$

and,

$$E_\phi(r,\phi) = \zeta_0 H_{0z} \cos\phi \exp(-jk_0 r\cos\phi) + \sum_{n=0}^{\infty} d_n H_n^{(2)'}(k_0 r) \cos(n\phi) \tag{2.2.21}$$

where d_n is given by equation (2.2.17) and $\zeta_0 = \frac{\omega\mu_0}{k_0} = \sqrt{\frac{\mu_0}{\epsilon_0}} =$ intrinsic impedance of the free space.

Thus, the total electric field at any point is region $r > r_2$ is given by

$$\vec{E}_t(r,\phi) = \hat{r}E_r(r,\phi) + \hat{\phi}E_\phi(r,\phi) \tag{2.2.22}$$

where $E_r(r,\phi)$ and $E_\phi(r,\phi)$ are given by equations (2.2.20) and (2.2.21), respectively.

When the probe is parallel to ϕ-axis and located at $\phi = \phi_0$, the boundary condition to be satisfied at its surface is

$$\hat{\phi}\cdot\vec{E}(r,\phi) = V_0 \frac{\delta(\phi-\phi_0)}{r} = Z_L I_0 \frac{\delta(\phi-\phi_0)}{r} \tag{2.2.23}$$

where

$$\vec{E}(r,\phi) = \vec{E}_t(r,\phi) + \vec{E}^a_{self}(r,\phi) + \vec{E}^{a\phi}_{image}(r,\phi)$$

If $f(\phi)$ is the current distribution function over the antenna and I_0 is the current at its center, then

$$I(\phi) = I_0 f(\phi)$$

and, since

$$I(\phi = \phi_0) = I_0 \; ; \; f(\phi_0) = 1$$

Hence

$$\int_{\phi_0-\phi_h}^{\phi_0+\phi_h} f(\phi)\hat{\phi}\cdot\vec{E}(r,\phi) r d\phi = V_0 f(\phi_0) = Z_L I_0 \tag{2.2.24}$$

As before, the effect of probe-body coupling may be included through the image theory. Therefore,

$$\int_{\phi_0-\phi_h}^{\phi_0+\phi_h} f(\phi)\hat{\phi}\cdot\vec{E}^{a\phi}_{image}(r,\phi) r d\phi \stackrel{\Delta}{=} - Z_{m\phi}\Gamma_\phi I_0 \tag{2.2.25}$$

Where $Z_{m\phi}$ is mutual impedance of the probe and its image, while Γ_ϕ is weighting coefficient.

$$\int_{\phi_0-\phi_h}^{\phi_0+\phi_h} f(\phi)\hat{\phi}\cdot\vec{E}^a_{self} r d\phi \stackrel{\Delta}{=} - Z_{in} I_0 \tag{2.2.26}$$

and

$$\int_{\phi_0-\phi_h}^{\phi_0+\phi_h} f(\phi)\hat{\phi}\cdot\vec{E}_t(r,\phi)rd\phi = \int_{\phi_0-\phi_h}^{\phi_0+\phi_h} f(\phi)E_\phi(r,\phi)rd\phi \triangleq V_{eq}^{TM,\phi} \quad (2.2.27)$$

Hence, from equations (2.2.24) - (2.2.27),

$$I_0 = \frac{V_{eq}^{TM,\phi}}{Z_L + Z_{in} + \Gamma_\phi Z_{m\phi}}$$

Noting that $|Z_L + Z_{in}| >> |\Gamma_\phi Z_{m\phi}|$ for a short dipole, as illustrated in TE-wave case, the expression for I_0 may be approximated as

$$I_0 \approx \frac{V_{eq}^{TM,\phi}}{Z_L + Z_{in}} \quad (2.2.28)$$

Evaluation of $V_{eq}^{TM,\phi}$:

As the probe is very small, a triangular distribution of current over it can be assumed. Hence

$$f(\phi) = \begin{cases} (1-\dfrac{\phi-\phi_0}{\phi_h}) = (\dfrac{\phi_0+\phi_h}{\phi_h} - \dfrac{\phi}{\phi_h}) & \phi_0<\phi< (\phi_h+\phi_0) \\ \\ (1-\dfrac{\phi_0-\phi}{\phi_h}) = (\dfrac{\phi_h-\phi_0}{\phi_h} + \dfrac{\phi}{\phi_h}) & \phi_0 >\phi> (\phi_0-\phi_h) \end{cases} \quad (2.2.29)$$

Therefore, from equations (2.2.21), (2.2.27) and (2.2.29) $V_{eq}^{TM,\phi}$ for $r = R$ may be found as

$$V_{eq}^{TM,\phi} = \zeta_0 R \left[\frac{\phi_h - \phi_0}{\phi_h}\right] \int_{\phi_0-\phi_h}^{\phi_0} [H_{0z} \cos\phi \exp(-jk_0 R \cos\phi) +$$

$$+ j \sum_{n=0}^{\infty} d_n H_n^{(2)'}(k_0 R) \cos(n\phi)] d\phi +$$

$$+ \zeta_0 R \left[\frac{\phi_h + \phi_0}{\phi_h}\right] \int_{\phi_0}^{\phi_0+\phi_h} [H_{0z} \cos\phi \exp(-jk_0 R \cos\phi) +$$

$$+ j \sum_{n=0}^{\infty} d_n H_n^{(2)'}(k_0 R) \cos(n\phi)] d\phi +$$

$$+ \frac{\zeta_0 R}{\phi_h} \int_{\phi_0-\phi_h}^{\phi_0} [H_{0z} \cos\phi \exp(-jk_0 R \cos\phi) +$$

$$+ j \sum_{n=0}^{\infty} d_n H_n^{(2)'}(k_0 R) \cos(n\phi)]\phi \, d\phi +$$

$$- \frac{\zeta_0 R}{\phi_h} \int_{\phi_0}^{\phi_0+\phi_h} [H_{0z} \cos\phi \exp(-jk_0 R \cos\phi) +$$

$$+ j \sum_{n=0}^{\infty} d_n H_n^{(2)'}(k_0 r) \cos(n\phi)]\phi \, d\phi \qquad (2.2.30)$$

Thus, the integrals involved in equation (2.2.30) are of the form

$$I_1 = A \int_{\phi_1}^{\phi_2} \cos\phi \exp(-ja \cos\phi) d\phi$$

$$I_2 = B \int_{\phi_1}^{\phi_2} \cos n\phi \, d\phi$$

$$I_3 = C \int_{\phi_1}^{\phi_2} \phi \cos\phi \exp(-ja \cos\phi) d\phi$$

and

$$I_4 = D\int_{\phi_1}^{\phi_2} \phi \cos n\phi \, d\phi$$

Clearly, the evaluation of I_2 and I_4 is straight forward,

$$I_2 = \begin{cases} B\,(\phi_2 - \phi_1) & n = 0 \\ \frac{B}{n}\,[\sin(n\phi_2) - \sin(n\phi_1)] & n \geq 1 \end{cases}$$

and

$$I_4 = \begin{cases} \frac{D}{2}\,[\phi_2^2 - \phi_1^2\,] & n = 0 \\ D\,[\frac{\phi_2 \sin(n\phi_2) - \phi_1\, \sin(n\phi_1)}{n} + \\ \qquad + \frac{\cos(n\phi_2) - \cos(n\phi_1)}{n^2}\,] & n \geq 1 \end{cases}$$

However, evaluation of I_1 and I_3 is a bit tricky. The integrals can be evaluated in form of series, using Jacobi-Anger expansion [10]. Alternatively, the numerical techniques can be employed for this purpose. For the present case, however, integration interval is small because of the very short probe. Therefore, the exponential term $\exp(-ja \cos \phi)$ can be pulled out of the integrals I_1 and I_3. Hence

$$I_1 \approx A[\sin \phi_2 - \sin \phi_1] \exp(-ja \cos \phi_a)$$

and

$$I_3 \approx C[\phi_2 \sin \phi_2 - \phi_1 \sin \phi_1 + \cos \phi_2 - \cos \phi_1]\exp(-ja \cos \phi_a)$$

where $\phi_a = (\phi_1 + \phi_2)/2$

Further, using the trignometric relations

$$\phi_0 \sin(n\phi_0) - (\phi_0 - \phi_h)\sin n(\phi_0 - \phi_h) - (\phi_0 + \phi_h)\sin n(\phi_0 + \phi_h) + \phi_0 \sin(n\phi_0)$$

$$= 2\phi_0 \sin(n\phi_0)[1 - \cos n\phi_h] - 2\phi_h \cos(n\phi_0)\sin(n\phi_h)$$

$$(\phi_h - \phi_0)\sin n(\phi_0 - \phi_h) - (\phi_h + \phi_0)\sin n(\phi_h + \phi_0)$$

$$= -2\phi_h \cos(n\phi_0)\sin(n\phi_h) - 2\phi_0 \sin(n\phi_0)\cos(n\phi_h)$$

and, noting that ϕ_h is very small, therefore

$$\sin\left(\frac{\phi_h}{2}\right) \approx \phi_{h/2}$$

the expression for $V_{eq}^{TM,\phi}$ is found from equation (2.2.30) as,

$$V_{eq}^{TM,\phi} \approx \frac{\zeta_0 H_{0z}\phi_h R}{2} \quad [\cos(\phi_0 - \frac{\phi_h}{4}) \exp\{-jk_0R \cos(\phi_0 - \frac{\phi_h}{2}\} +$$

$$+ \cos(\phi_0 + \frac{\phi_h}{4}) \exp\{-jk_0R \cos(\phi_0 + \frac{\phi_h}{2})\}] +$$

$$+ j\zeta_0 d_0 \phi_h R \, H_0^{(2)'}(k_0R) +$$

$$+ \frac{j2\zeta_0 R}{\phi_h} \sum_{n=1}^{\infty} \frac{d_n}{n^2} \{1 - \cos(n\phi_h)\}\cos(n\phi_0) H_n^{(2)'}(k_0R) \tag{2.2.31}$$

2.2.3 Equivalent voltage induced in a radially aligned receiving probe

When the probe is radially aligned and its center is at $r = R$, the boundary condition that must be satisfied at its surface is

$$\hat{r}\cdot\vec{E}(r,\phi) = V_0\delta(r-R) = Z_L I_0\delta(r-R) \tag{2.2.32}$$

where

$$\vec{E}(r,\phi) = \vec{E}_t(r,\phi) + \vec{E}^a_{self}(r,\phi) + \vec{E}^{ar}_{image}(r,\phi)$$

Assuming $f(r)$ as the current distribution function over the probe and I_0, the current at its center,

$$I(r) = I_0 f(r)$$

and, since

$$I(r = R) = I_0,$$

$$f(r = R) = 1$$

Therefore,

$$\int_{R-h}^{R+h} f(r)\hat{r}\cdot\vec{E}(r,\phi)dr = V_0 f(R) = Z_L I_0 \tag{2.2.33}$$

Also,

$$\int_{R-h}^{R+h} f(r)\hat{r}\cdot\vec{E}^{ar}_{image}(r,\phi)d\phi \overset{\Delta}{=} -Z_{mr}\Gamma_r I_0 \tag{2.2.34}$$

Where Z_{mr} is mutual impedance of the probe and its image, which is collinear. Γ_r is a suitable reflection coefficient weighting factor.

$$\int_{R-h}^{R+h} f(r)\hat{r}\cdot\vec{E}^{a}_{self}dr \triangleq - Z_{in}I_0 \tag{2.2.35}$$

and

$$\int_{R-h}^{R+h} f(r)\hat{r}\cdot\vec{E}_t(r,\phi)dr = \int_{R-h}^{R+h} f(r)E_r(r,\phi)dr \triangleq V_{eq}^{TM,r} \tag{2.2.36}$$

Thus, from equations (2.2.33) - (2.2.36),

$$I_0 = \frac{V_{eq}^{TM,r}}{Z_L + Z_{in} + \Gamma_r Z_{mr}}$$

As illustrated for TE-wave case in section 2.1.2, for the typical probe and the load, $Z_{in} + Z_L$ is approximately 2-j1148 Ohm at 2.45GH_Z. When two similar probes are collinear, then the mutual impedance, Z_{mr}, can be computed [9] as 2.51 + j6.50 Ohm. Since $|\Gamma_r| \leq 1$, $|Z_L + Z_{in}| >> |\Gamma_r Z_{mr}|$ still holds for a small probe. Therefore, I_0 can be approximated as

$$I_0 \approx \frac{V_{eq}^{TM,r}}{Z_L + Z_{in}} \tag{2.2.37}$$

Evaluation of $V_{eq}^{TM,r}$:

For a short probe, current distribution function, f(r), can be assumed as triangular. Hence,

$$f(r) = \begin{cases} \left[\frac{R+h}{h} - \frac{r}{h} \right] & R < r < (R + h) \\ \\ \left[\frac{h-R}{h} + \frac{r}{h} \right] & R > r > (R - h) \end{cases} \tag{2.2.38}$$

Therefore, from equations (2.2.20), (2.2.36) and (2.2.38), an expression for $V_{eq}^{TM,r}$ can be found as follows:

$$V_{eq}^{TM,r} = [\frac{h-R}{h}] \ \zeta_0 \int_{R-h}^{R} [H_{0z} \sin\phi \exp(-jk_0 r \cos\phi) +$$

$$+ \frac{j}{k_0 r} \sum_{n=1}^{\infty} nd_n \sin(n\phi) H_n^{(2)}(k_0 r)]dr +$$

$$+ [\frac{h+R}{h}] \ \zeta_0 \int_{R}^{R+h} [H_{0z} \sin\phi \exp(-jk_0 r \cos\phi) +$$

$$+ \frac{j}{k_0 r} \sum_{n=1}^{\infty} nd_n \sin(n\phi) H_n^{(2)}(k_0 r)]dr +$$

$$+ \frac{\zeta_0}{h} \int_{R-h}^{R} [r\, H_{0z} \sin\phi \exp(-jk_0 r \cos\phi) +$$

$$+ \frac{j}{k_0} \sum_{n=1}^{\infty} nd_n \sin(n\phi) H_n^{(2)}(k_0 r)]dr +$$

$$- \frac{\zeta_0}{h} \int_{R}^{R+h} [rH_{0z} \sin\phi \exp(-jk_0 r \cos\phi) +$$

$$+ \frac{j}{k_0} \sum_{n=1}^{\infty} nd_n \sin(n\phi) H_n^{(2)}(k_0 r)]dr \qquad (2.2.39)$$

Thus, equation (2.2.39) involves the integrals of the form,

$$I_1 = A_1 \int_{r_1}^{r_2} \exp(-jar)dr$$

$$I_2 = A_2 \int_{r_1}^{r_2} \frac{H_n^{(2)}(k_0 r)}{r} \ dr$$

$$I_3 = A_3 \int_{r_1}^{r_2} r \exp(-jar)dr$$

and

$$I_4 = A_4 \int_{r_1}^{r_2} H_n^{(2)}(k_0 r)dr$$

Integrals I_1 and I_3 are simple and can be evaluated as,

$$I_1 = \frac{jA_1}{a} [\exp(-jar_2) - \exp(-jar_1)]$$

and

$$I_3 = jA_3 [\frac{r_2 \exp(-jar_2) - r_1 \exp(-jar_1)}{a} + - j \frac{\exp(-jar_2) - \exp(-jar_1)}{a^2}]$$

While I_2 and I_4 should be evaluated numerically. However, under the assumption that probe is small, the interval of integration is very small, and these can be approximated as,

$$I_2 \approx A_2 H_n^{(2)} \{k_0 \frac{(r_1+r_2)}{2}\} \ln(r_2/r_1)$$

and,

$$I_4 \approx A_4 (r_2-r_1) H_n^{(2)} \{k_0 \frac{(r_1+r_2)}{2}\}$$

Hence, an approximate expression for $V_{eq}^{TM,r}$ is found from equation (2.2.39) as,

$$V_{eq}^{TM,r} \approx \frac{4\zeta_0}{hk_0^2} H_{0z} \tan\phi \sec\phi \sin^2\left(\frac{k_0 h \cos\phi}{2}\right) \cdot$$

$$\cdot \exp(-jk_0 R \cos\phi) +$$

$$+ \frac{j\zeta_0}{hk_0} \sum_{n=1}^{\infty} nd_n \sin(n\phi)[(h-R)H_n^{(2)}\{k_0(R-\frac{h}{2})\}$$

$$\cdot \ln(\frac{R}{R-h}) +$$

$$+ (h+R)H_n^{(2)}\{k_0(R+\frac{h}{2})\}\ln(\frac{R+h}{R}) +$$

$$+ \frac{j\zeta_0}{k_0} \sum_{n=1}^{\infty} nd_n \sin(n\phi)[H_n^{(2)}\{k_0(R-\frac{h}{2})\}$$

$$- H_n^{(2)}\{k_0(R+\frac{h}{2})\}] \qquad (2.2.40)$$

Thus, the approximate expressions of V_{eq} (and hence load current, I_0) for individual probes are now known. In practice, the three probes are orthogonally connected with diode detectors across the load terminals. In that case the square of the current amplitudes of each is added up, assuming the detectors are behaving as square-law. In the following chapter, the theory presented here is verified experimentally and some of the theoretically computed results are also given.

CHAPTER 3

RESPONSE OF E-FIELD PROBE IN THE PROXIMITY OF HUMAN BODY-EXPERIMENTAL VERIFICATION

The simplified theory for the response of E-field probes is presented in the preceding chapter. Here in this chapter an attempt is made to verify that theory experimentally. For that purpose a cylindrical dielectric shell filled with saline water was used to simulate the human body. The experimental results thus obtained, are compared with computed ones, for both, including the effect of the wall thickness of the shell as well as by ignoring it. Also, the probe response near the empty shell is compared with theoretical results. Finally, some computed results of the probe-response near the body are given.

3.1 Set-up of the experimental system

The experimental set-up used for verification of the theory is shown in Figure 3.1.1. A GR type 1360-B signal generator was used as source. Since it had a built-in calibrated frequency dial and a variable attenuator, its output was used directly through a 10 dB pad, to excite the pyramidal horn antenna.

A plexiglass cylindrical dielectric shell (inner and outer radii 0.146 m and 0.1524 m, respectively, and 0.83 m high) was filled with saline water (salt/water = 1/75 by weight) to simulate the human body

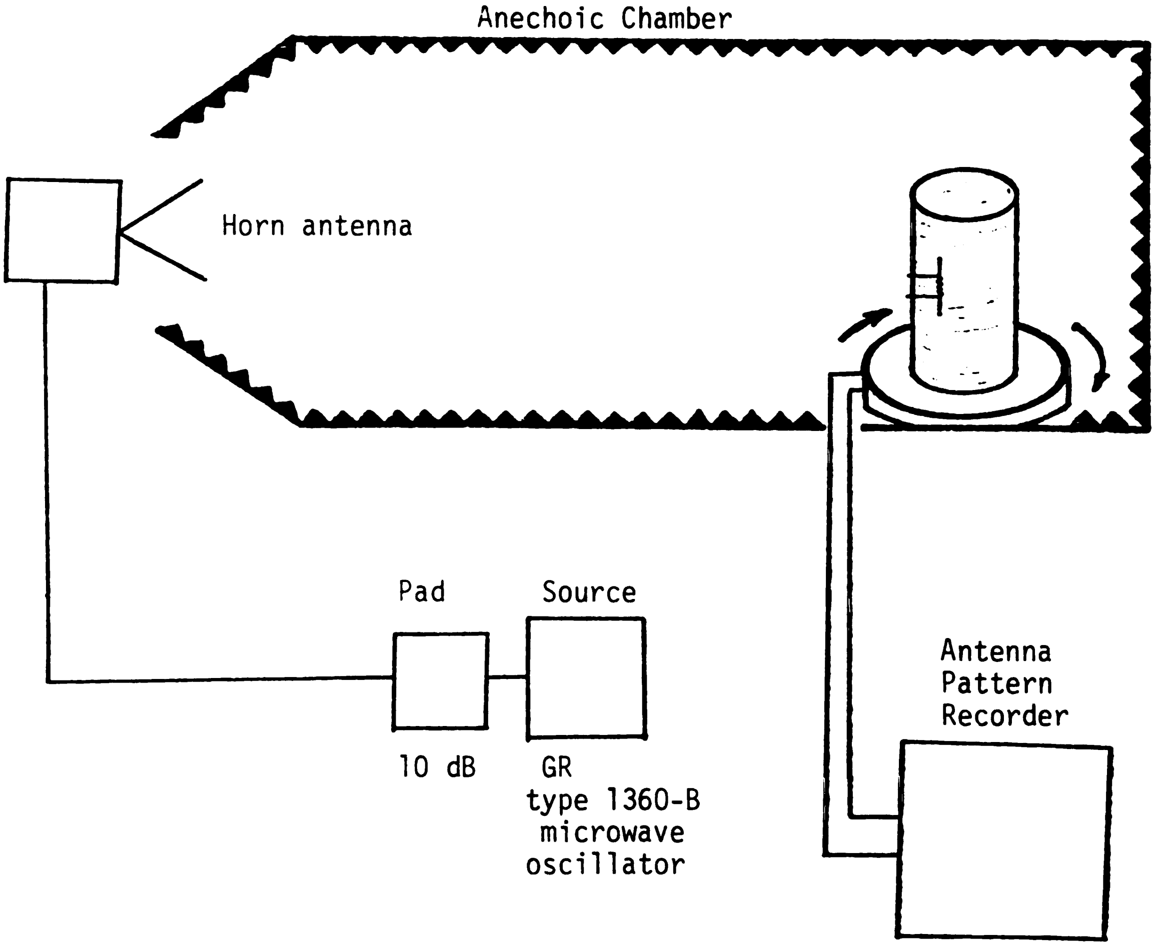

Fig. 3.1.1 Experimental set-up for recording the response of E-field probe near the cylindrical body.

[11,12]. A short probe with diode detector [22] was fixed at a suitable distance on the surface of the shell and the detector output was coupled to antenna pattern recorder (Scientific Atlanta) through the resistive leads of the probe [13]. The probe was oriented axially, azimuthally and radially with respect to the cylinder to measure the three components of the electric field on the surface of the cylinder. The polarization of the incident field was varied by changing the orientation of the transmitting horn antenna. The experiment was carried out at three different frequencies, viz, 2GHz, 2.45GHz and 3GHz for all the three, axial, azimuthal and radial field components near the body.

After the responses of the axial, the azimuthal and the radial probe are experimentally confirmed, the response of an orthogonal probe can be easily predicted by combining the responses of the former three single probes.

3.2 Results and inference

The experimental results obtained by the method described in the preceding section are illustrated in Figures 3.2.1 - 3.2.27 along with the corresponding computed results. Figure 3.2.1 shows the response of an axially aligned probe as function of azimuthal angle, ϕ, when a TE-polarized plane wave of 3GHz is incident on the saline water filled shell from $\phi = 180^o$ direction. In this case, the response shows a maximum on the front side (i.e., $\phi = 180^o$) and a very small output on the backside (i.e., $\phi = 0^o$). This type of probe response is understandable via shadow region formation behind a conducting body

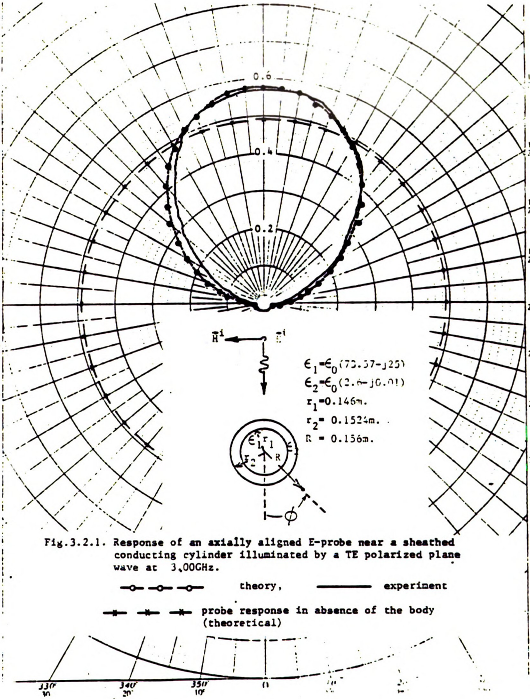

Fig.3.2.1. Response of an axially aligned E-probe near a sheathed conducting cylinder illuminated by a TE polarized plane wave at 3.00GHz.

—o— —o— —o— theory, ———— experiment

—*— —*— —*— probe response in absence of the body (theoretical)

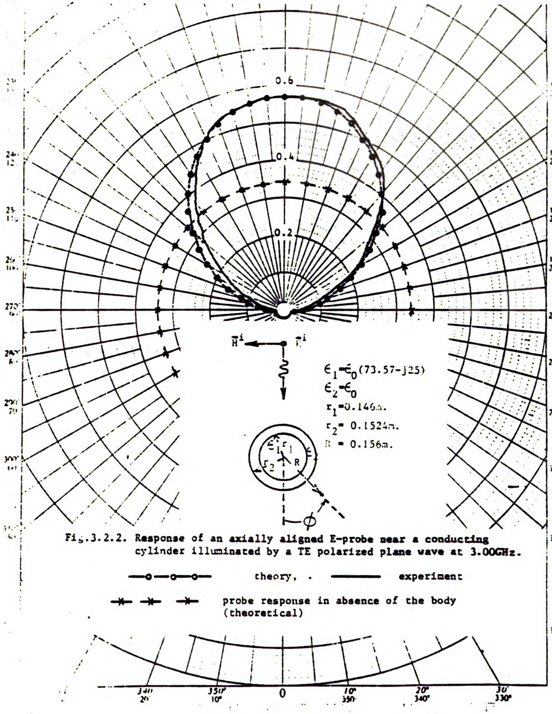

Fig.3.2.2. Response of an axially aligned E-probe near a conducting cylinder illuminated by a TE polarized plane wave at 3.00GHz.

—o—o—o— theory, . ———— experiment

—x— —x— —x— probe response in absence of the body (theoretical)

illuminated by EM wave. In this figure, the thickness of the shell was taken into account in theoretical results. These results are in good agreement with the experimentally recorded response of the probe. The theoretically computed response of the probe in the absence of the body is also shown in the same figure, which is in the form of a circle with a radius little smaller than the maximum of the response in the presence of the body. When the thickness of the shell is ignored (i.e., $\epsilon_2 = \epsilon_0$) in the computation, the results depicted in Figure 3.2.2 are still in good agreement. However, the response of the probe in the absence of the body is lower in this case in comparison with the previous case. In Figures 3.2.3 and 3.2.4, the experimentally recorded response of the probe at 2.45GHz is compared with the computed results, in the former the thickness of the shell is included while in the latter it is ignored. Again, in both figures the experimentally recorded results are in close agreement with theoretically predicted values, and the level of the probe response in the absence of the body is higher in the former case. A comparison of the experimentally observed response of the probe at 2GHz in Figures 3.2.5 and 3.2.6 also shows a good agreement with the theory, and the probe response in absence of the body is lower when the effect of the shell is ignored in Figure 3.2.6.

When a TM polarized plane wave of 3GHz is illuminating the sheathed conducting cylinder, the azimuthally as well as the axially aligned probe both respond. The response of an azimuthally aligned probe is illustrated in Figures 3.2.7 and 3.2.8, while that of a radially aligned probe is shown in Figures 3.2.13 and 3.2.14. The response of an azimuthally aligned probe shows a maximum on front side ($\phi = 180^0$)

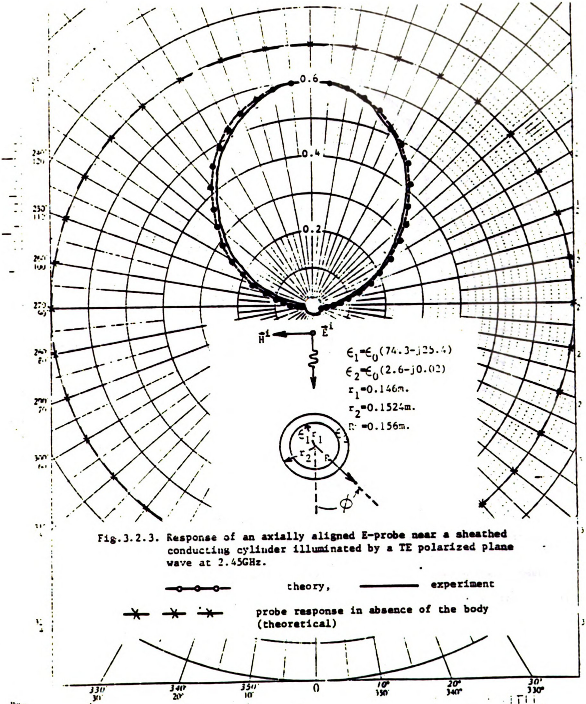

Fig.3.2.3. Response of an axially aligned E-probe near a sheathed conducting cylinder illuminated by a TE polarized plane wave at 2.45GHz.

theory, experiment

probe response in absence of the body (theoretical)

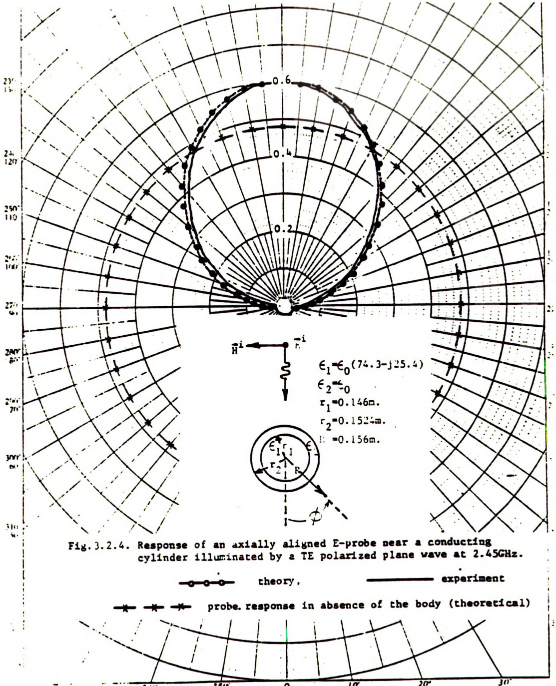

Fig. 3.2.4. Response of an axially aligned E-probe near a conducting cylinder illuminated by a TE polarized plane wave at 2.45GHz.

—o—o—o— theory, ———— experiment

—*— —*— —*— probe. response in absence of the body (theoretical)

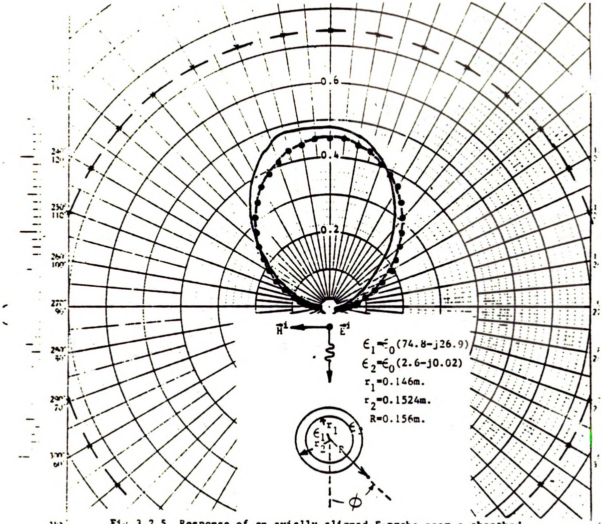

Fig.3.2.5. Response of an axially aligned E-probe near a sheathed conducting cylinder illuminated by a TE polarized plane wave at 2.00GHz.

—o—o—o— theory, ———— experiment

—✱— —✱— —✱— probe response in absence of the body (theoretical)

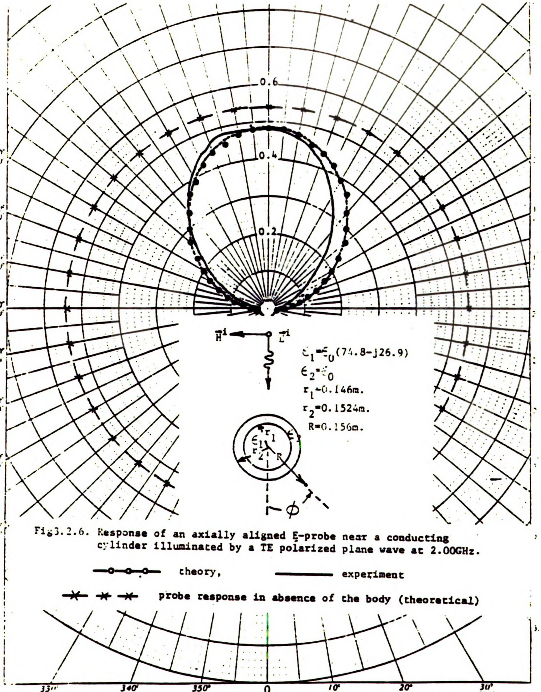

Fig3.2.6. Response of an axially aligned E_z-probe near a conducting cylinder illuminated by a TE polarized plane wave at 2.00GHz.

—o—o—o— theory, ——— experiment

—✕— ✕ —✕— probe response in absence of the body (theoretical)

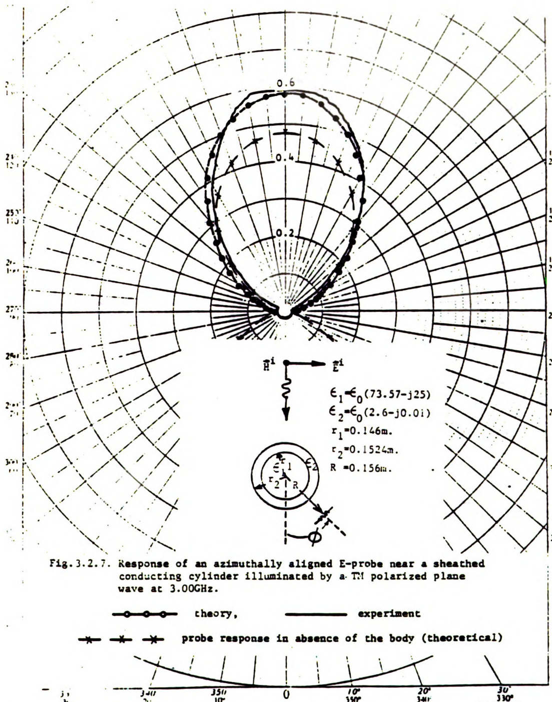

Fig. 3.2.7. Response of an azimuthally aligned E-probe near a sheathed conducting cylinder illuminated by a TM polarized plane wave at 3.00GHz.

—o—o—o— theory, ———— experiment

—x— —x— —x— probe response in absence of the body (theoretical)

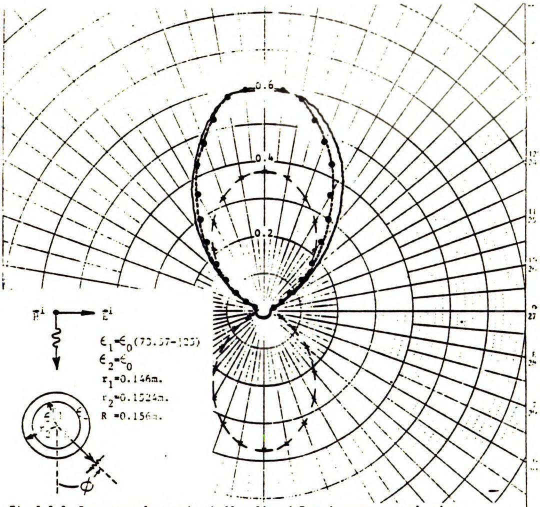

Fig.3.2.8. Response of an azimuthally aligned E-probe near a conducting cylinder illuminated by a TM polarized plane wave at 3.00GHz.

theory, experiment

probe response in absence of the body (theoretical)

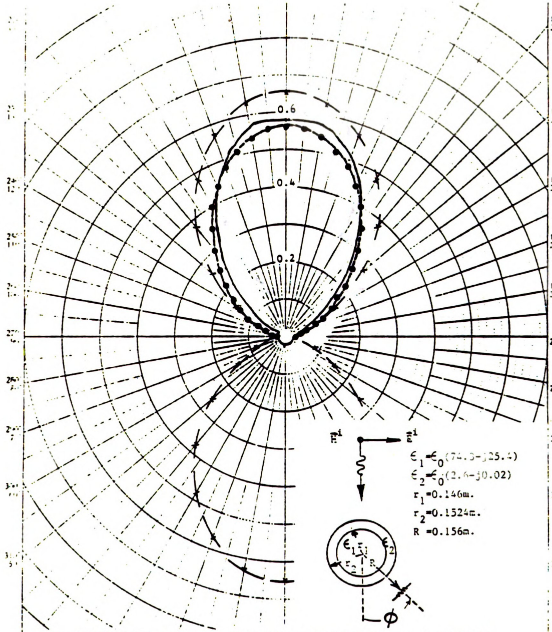

Fig. 3.2.9. Response of an azimuthally aligned E-probe near a sheathed conducting cylinder illuminated by a TM polarized plane wave at 2.45GHz.

—o—o—o— theory, ———————— experiment

—*— —*— —*— probe response in absence of the body (theoretical)

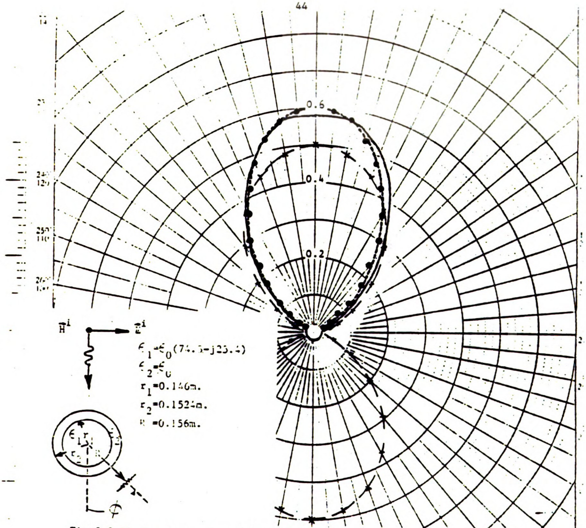

Fig.3.2.10. Response of an azimuthally aligned E-probe near a conducting cylinder illuminated by a TM polarized plane wave at 2.45GHz.

—o—o—o— theory, ———— experiment

— — — probe response in absence of the body (theoretical)

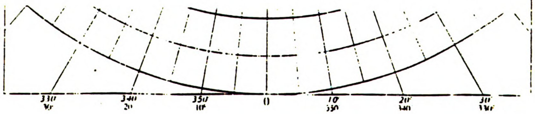

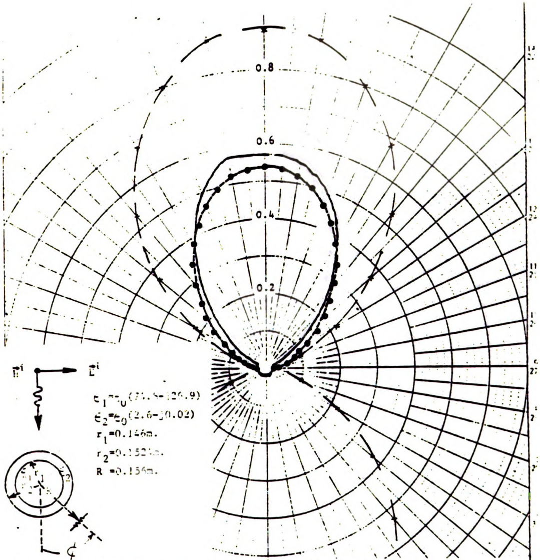

Fig.3.2.11. Response of an azimuthally aligned E-probe near a sheathed conducting cylinder illuminated by a TM polarized plane wave at 2.00GHz.

—o—o—●— theory, ———— experiment

—✱— —✱— —✱— probe response in absence of the body (theoretical)

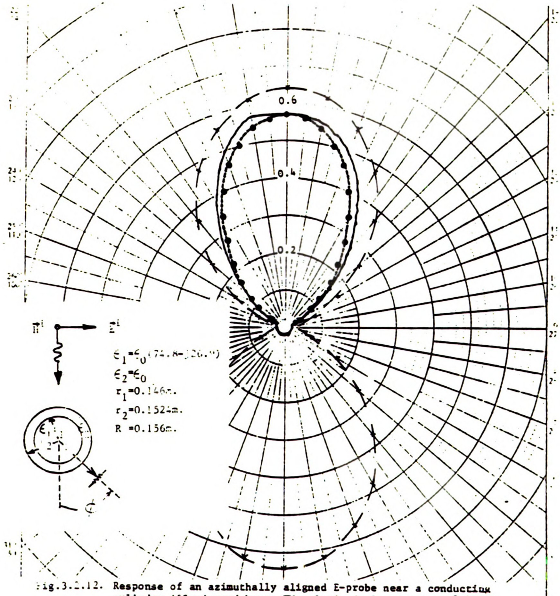

Fig.3.2.12. **Response of an azimuthally aligned E-probe near a conducting cylinder illuminated by a TM polarized plane wave at 2.00GHz.**

—o—o—o— theory, ———— **experiment**

—*— —*— —*— **probe response in absence of the body (theoretical)**

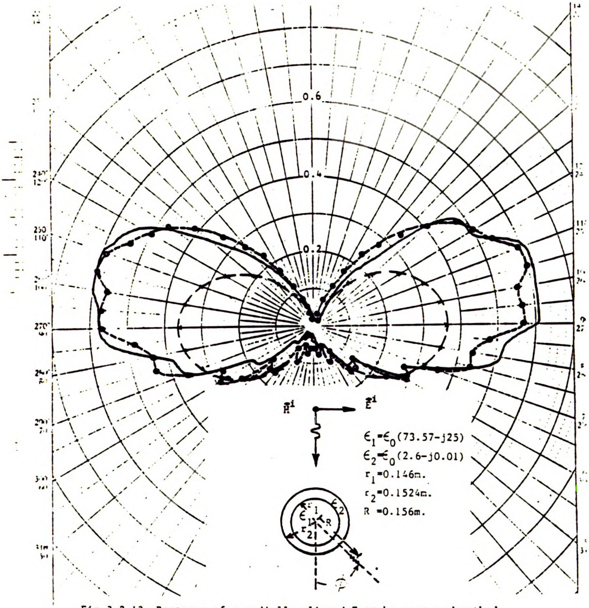

Fig.3.2.13. **Response of a radially aligned E-probe near a sheathed conducting cylinder illuminated by a TM polarized plane wave at 3.00GHz.**

theory, **experiment**

probe response in absence of the body (theoretical)

and a very small output on the backside ($\phi = 0^o$) in the presence of the body. Theoretically determined response of the azimuthally aligned probe in which the effect of the shell is included, is compared with the experimental results in Figure 3.2.7, while in Figure 3.2.8 only the saline water column is considered in theoretical computation. In both cases, the theoretical response is very close to experimental values. The probe response in the absence of the body is also depicted in Figures 3.2.7 and 3.2.8 for respective cases over $90^o \leq \phi \leq 270^o$ range. For $270^o \leq \phi \leq 360^o$ and $0^o \leq \phi \leq 90^o$, this is same as for $90^o \leq \phi \leq 270^o$, hence omitted for brevity. The shadow on the back side of the body and the higher response level in the absense of the body in Figure 3.2.7 in comparison with Figure 3.2.8 are noted.

The computed response of a radially aligned E-probe depicted in Figure 3.2.13 for 3GHz in which the effect of the shell is included, is in relatively better agreement with experimental result in comparison with that of Figure 3.2.14, where only the saline water column is considered for the theoretical calculations (i.e., $\epsilon_2 = \epsilon_0$). The calculated probe response in the absence of the body is a little smaller in the case of the sheathed conducting cylinder illustrated in Figure 3.2.13 with respect to the corresponding results in Figure 3.2.14 where sheath is ignored.

Figures 3.2.9 and 3.2.11 illustrate the response of an azimuthally aligned E-probe near a sheathed conducting cylinder illuminated by a TM polarized plane wave at 2.45GHz and 2GHz, respectively. The responses of a radially aligned probe for these cases are shown in Figures 3.2.15 and 3.2.17. The corresponding results when the effect

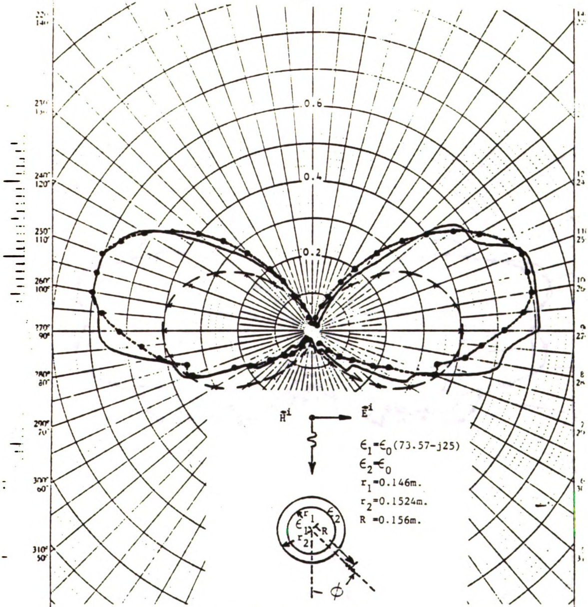

Fig. 3.2.14. Response of a radially aligned E-probe near a conducting cylinder illuminated by a TM polarized plane wave at 3.00GHz.

—o—o—o— theory, ———— experiment

—*— —*— —*— probe response in absence of the body (theoretical)

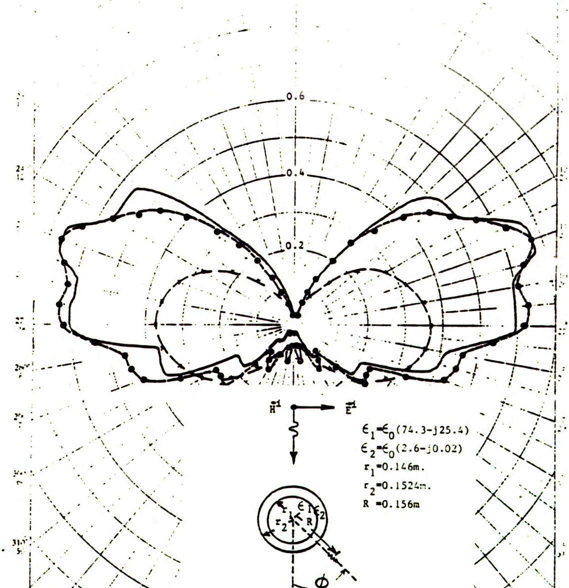

Fig.3.2.15. Response of a radially aligned E-probe near a sheathed conducting cylinder illuminated by a TM polarized plane wave at 2.45GHz.

—o—o—o— theory, ———— experiment

—+— —+— —+— probe response in absence of the body (theoretical)

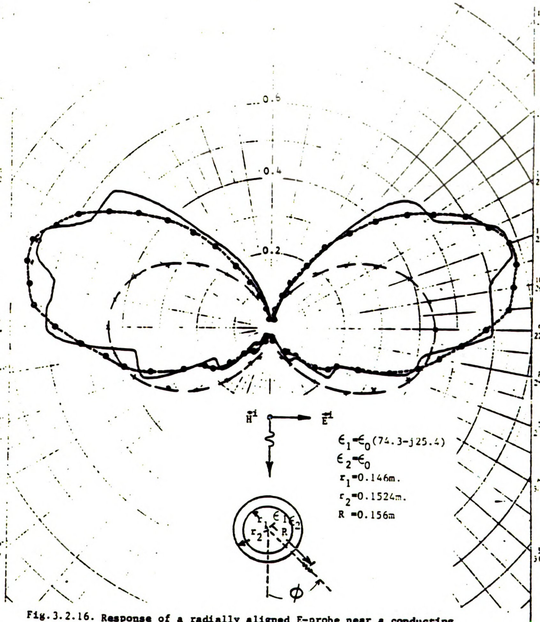

Fig.3.2.16. Response of a radially aligned E-probe near a conducting cylinder illuminated by a TM polarized plane wave at 2.45GHz.

—o—o—o— theory, ———— experiment

—+— —+— —+— probe response in absence of the body (theoretical)

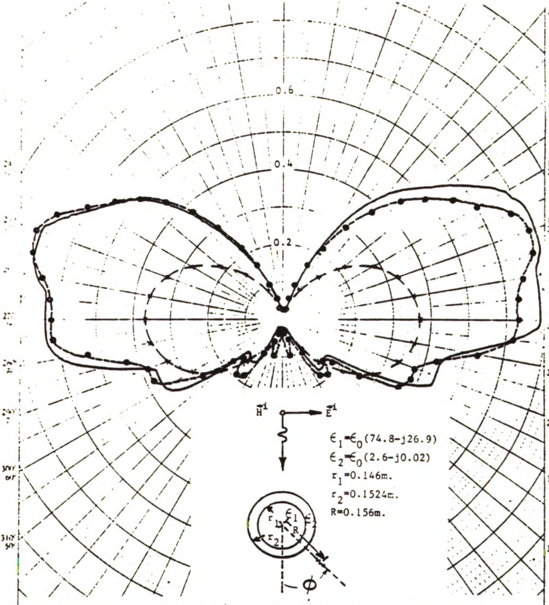

Fig. 3.2.17. Response of a radially aligned E-probe near a sheathed conducting cylinder illuminated by a TM polarized plane wave at 2.00GHz.

theory, experiment

probe response in absence of the body (theoretical)

of the sheath is ignored in the computation are compared with the respective experimental responses in Figures 3.2.10, 3.2.12, 3.2.16 and 3.2.18. The theoretically predicted results shown in these figures, are in fairly close agreement with the corresponding experimentally recorded responses at both frequencies, viz, 2.45GHz and 2GHz. General behaviour of these results is similar to that of corresponding 3GHz cases discussed earlier and therefore omitted here for brevity.

When a TE polarized plane wave of 3GHz frequency illuminates a cylindrical dielectric shell (i.e., $\epsilon_1 = \epsilon_0$) from $\phi = 180^o$ directtion, the response of the axially aligned E-probe in its proximity shows a large peak at $\phi = 0^o$ as depicted in Figure 3.2.19 alongwith a circular response computed when shell is not there. The experimentally observed response of the probe is still in close agreement with theoretically predicted results. Figures 3.2.20 and 3.2.21 illustrate these results for 2.45GHz and 2GHz, respectively. These responses are quite different from the one, shown in Figure 3.2.19 for 3GHz. However, these unusual probe responses can be accurately predicted theoretically.

The response of an azimuthally aligned E-probe near a cylindrical dielectric shell illuminated by a TM polarized plane wave at 3GHz is illustrated in Figure 3.2.22 alongwith the computed results of response in absence of the shell. Relatively higher response in $\phi = 0^o$ direction with respect to $\phi = 180^o$, and some depressions in the peaks when the shell is present are the main features to be noted. Figures 3.2.23 and 3.2.24 depict the response of the azimuthally aligned probe near the cylindrical dielectric shell for the illuminating TM polarized

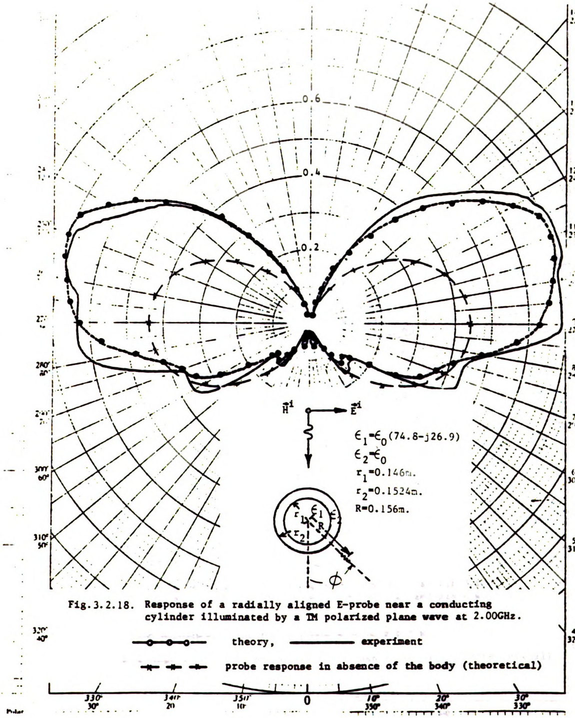

Fig. 3.2.18. Response of a radially aligned E-probe near a conducting cylinder illuminated by a TM polarized plane wave at 2.00GHz.

—o—o—o— theory, ———— experiment

—*— —*— —*— probe response in absence of the body (theoretical)

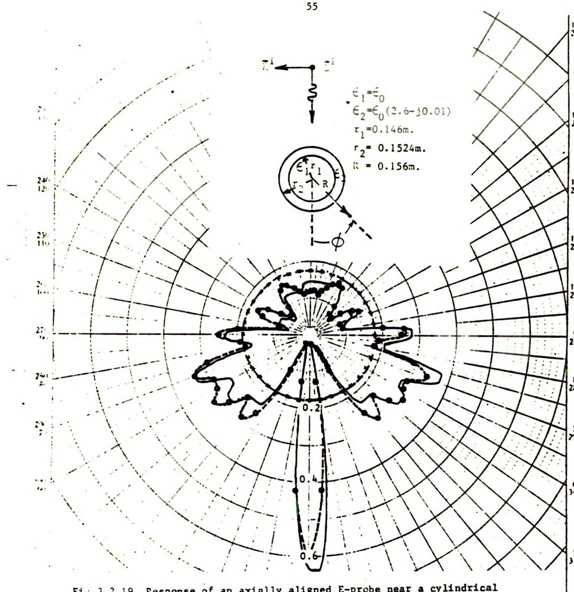

Fig.3.2.19. Response of an axially aligned E-probe near a cylindrical dielectric shell illuminated by a TE polarized plane wave at 3.00GHz.

—o—o—o— theory, ———— experiment

—▪— —▪— —▪— probe response in absence of the body (theoretical)

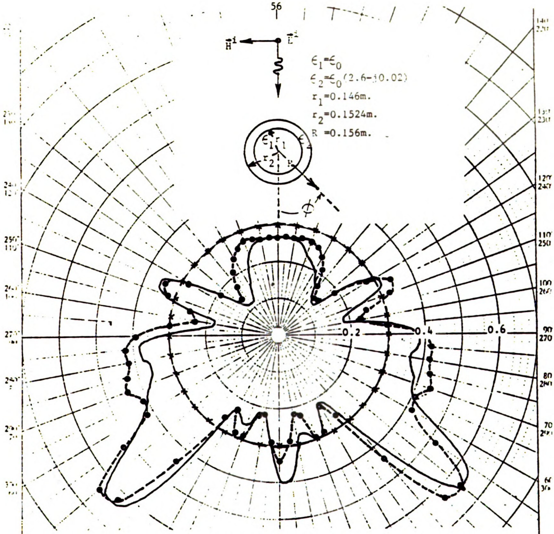

Fig.3.2.20. Response of an axially aligned E-probe near a cylindrical dielectric shell illuminated by a TE polarized plane wave at 2.45GHz.

—o—o—o— theory, ——— experiment

—x— —x— —x— probe response in absence of the body (theoretical)

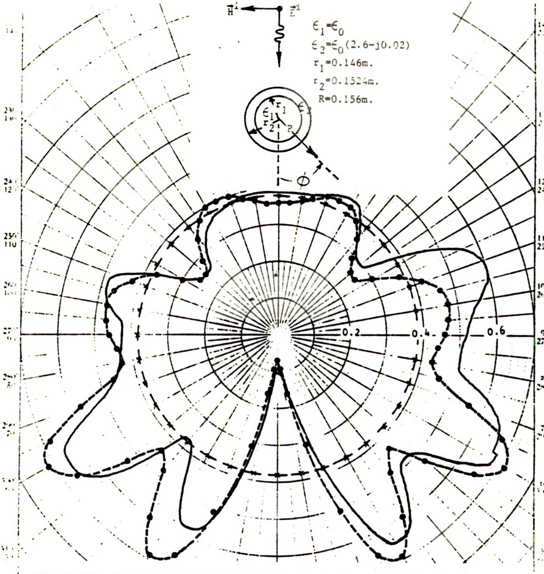

Fig.3.2.21. Response of an axially aligned E-probe near a cylindrical dielectric shell illuminated by a TE polarized plane wave at 2.00GHz.

—o—o—o— theory, ———— experiment

—✶— —✶— —✶— probe response in absence of the body (theoretical)

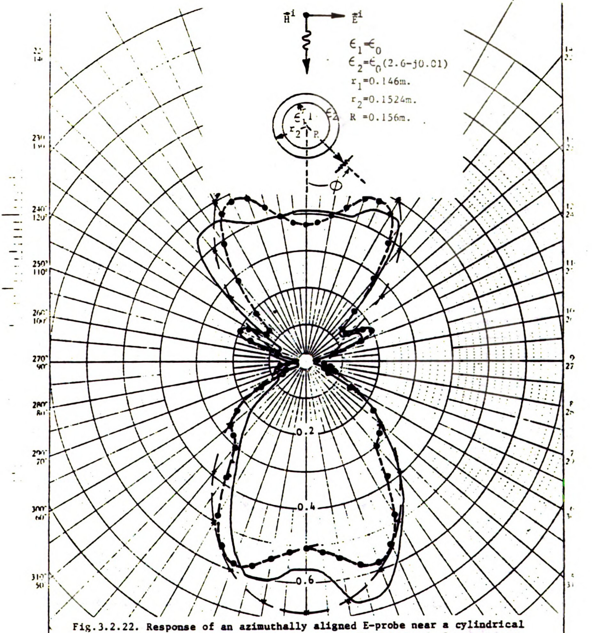

Fig.3.2.22. Response of an azimuthally aligned E-probe near a cylindrical dielectric shell illuminated by a TM polarized plane wave at 3.00GHz.

—o—o—o— theory, ———— experiment

—✱— —✱— —✱— probe response in absence of the body (theoretical)

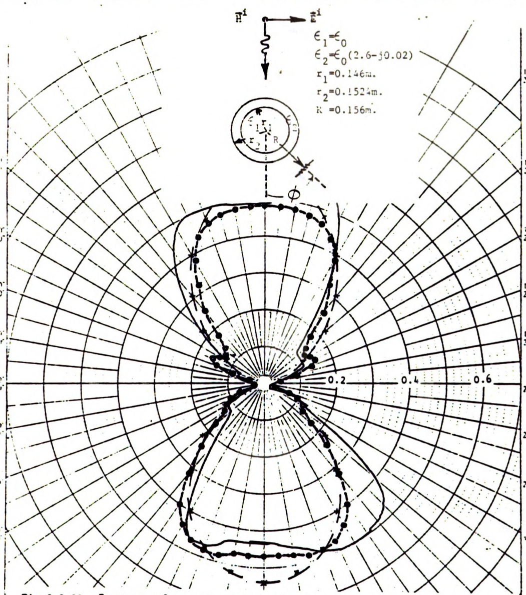

Fig.3.2.23. Response of an azimuthally aligned E-probe near a cylindrical dielectric shell illuminated by a TM polarized plane wave at 2.45GHz.

—o—o—o— theory, ———— experiment

—*— —*— —*— probe response in absence of the body (theoretical)

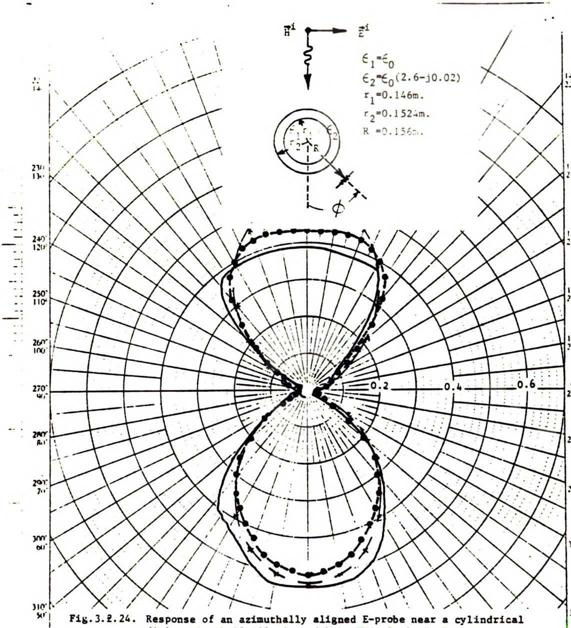

Fig.3.2.24. Response of an azimuthally aligned E-probe near a cylindrical dielectric shell illuminated by a TM polarized plane wave at 2.00GHz.

—o—o—o— theory, ———— experiment

—+— —+— —+— probe response in absence of the body (theoretical)

plane wave of 2.45GHz and 2GHz, respectively. A good agreement between experimentally recorded and computed results is found in all these figures.

Figures 3.2.25 - 3.2.27 illustrate the response of the radially aligned E-probe near a cylindrical dielectric shell illuminated by a TM polarized plane wave at 3GHz, 2.45GHz and 2GHz, respectively, alongwith the corresponding computed results with and without the dielectric shell. When a 3GHz TM wave is illuminating the shell, peaks in the probe response are observed at $\phi = 65^o$, 90^o, 270^o and 295^o while null for $\phi = 0^o$ and 180^o. The computed results are still very close to the experimentally observed response. Similar agreements are noted for 2.45GHz and 2GHz in Figues 3.2.26 and 3.2.27, respectively.

A 10 k Ohm resistor in parallel with a 6 pF capacitor is taken as load to the probe for the computations. The other related data are given in respective figures. The computer program developed for theoretically predicting the response of the probe is given in appendix A while the computer print-outs are included in appendix B.

3.3 Some theoretically computed results for the cylindrical biological body

Figures 3.3.1 to 3.3.3 illustrate the response of an orthogonal-probe-system as well as its individual components when the body is exposed to an incident plane wave field of 3GHz, 2.45GHz and 1.5GH , respectively. The permittivities of the body at these frequencies are also given there [11]. Polarization angle of the incident plane wave

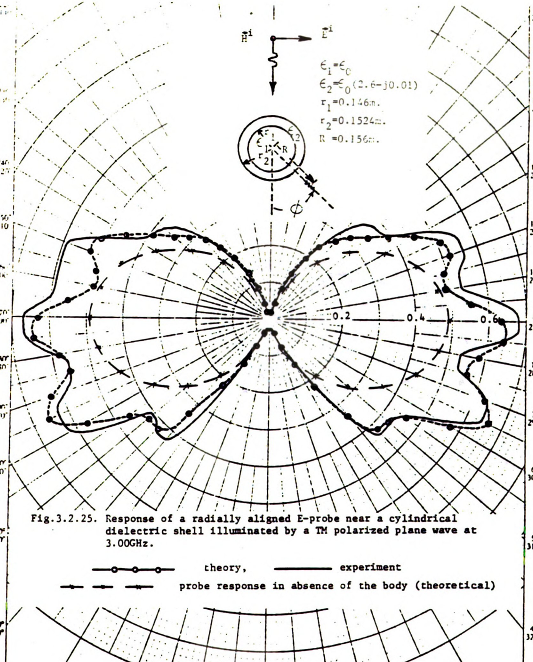

Fig.3.2.25. Response of a radially aligned E-probe near a cylindrical dielectric shell illuminated by a TM polarized plane wave at 3.00GHz.

—o—o—o— theory, ——— experiment

— x — x — probe response in absence of the body (theoretical)

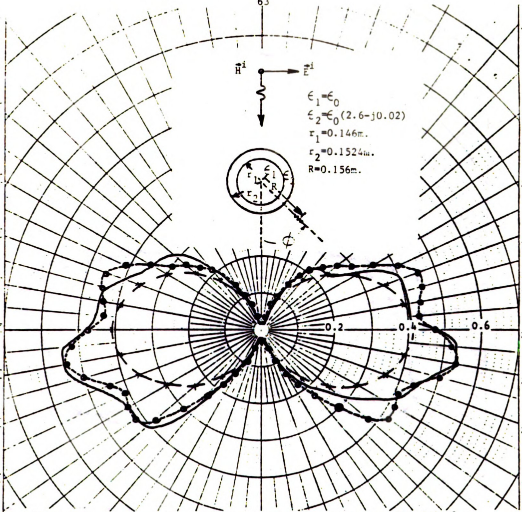

Fig.3.2.26. Response of a radially aligned E-probe near a cylindrical dielectric shell illuminated by a TM polarized plane wave at 2.45GHz.

—o—o—o— theory, ———— experiment

—*— —*— —*— probe response in absence of the body (theoretical)

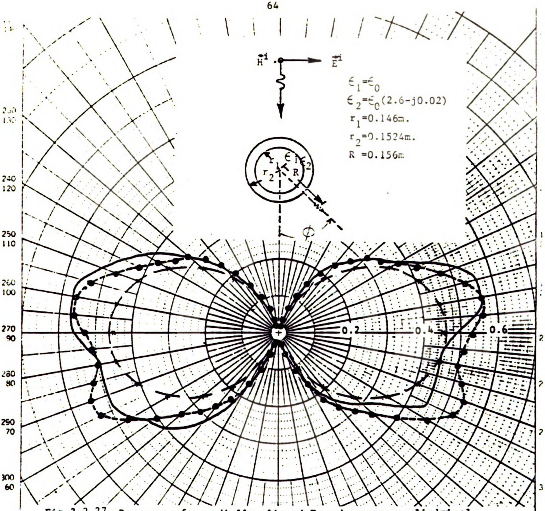

Fig.3.2.27. Response of a radially aligned E-probe near a cylindrical dielectric shell illuminated by a TM polarized plane wave at 2.00GHz.

—o—o—o— theory, ———— experiment

—x— —x— —x— probe response in absence of the body (theoretical)

is taken as 45^{o}. Hence TE as well as TM waves are equally incident. From these results, it seems that axial alongwith azimuthal component contributes dominantly at 3GHz and 2.45GHz. The response of orthogonally connected probe in the absence of the body is also shown in Figures 3.3.1 and 3.3.2, which indicates a little increase in the probe output for $\phi = 180^{o}$ and a shadow region formation for $\phi = 0^{o}$ in the presence of the body. At 1.5GHz as shown in Figure 3.3.3, the radial component dominates over the other two taken together.

Figures 3.3.4 to 3.3.6 depict the probe responses with polarization angle of 0^{o}, 30^{o}, 60^{o} and 90^{o} at aforementioned three frequencies. For 3GHz, the maximum occurs when polarization angle is $\theta = 0^{o}$ in Figure 3.3.4, while at the other two frequencies, viz, 2.45GHz and 2GHz, it is for $\theta = 90^{o}$.

Finally, Figure 3.3.7 shows the probe response as a function of spacing between the probe and the body at the azimuthal angles of 180^{o}, 135^{o} and 90^{o}, when the incident field is polarized at 45^{o}. As expected, this gives a standing wave pattern with decreasing amplitude as probe moves away from the body for each azimuthal angle. This is computed only at 2.45GHz.

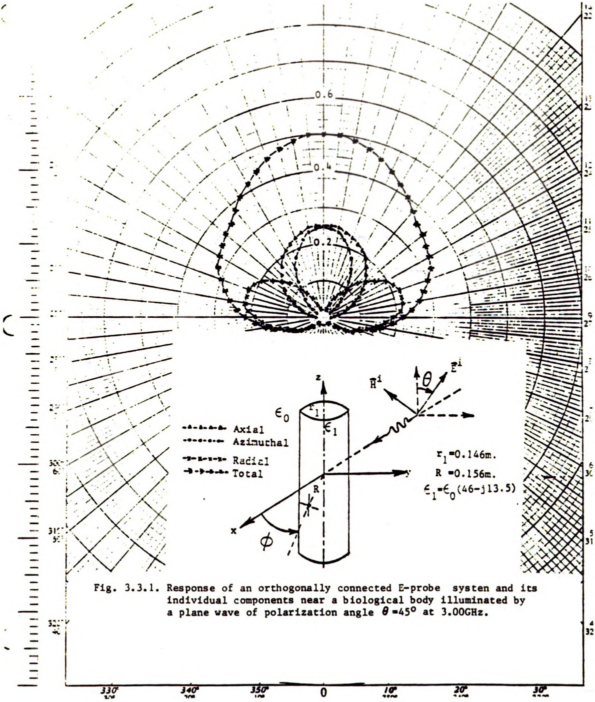

Fig. 3.3.1. Response of an orthogonally connected E-probe systen and its individual components near a biological body illuminated by a plane wave of polarization angle θ =45° at 3.00GHz.

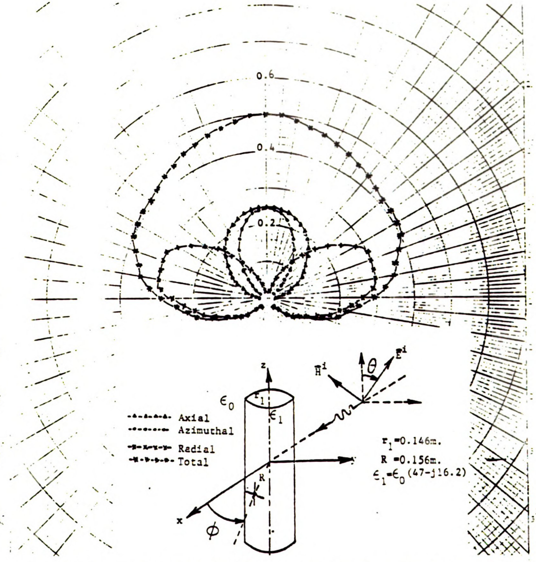

Fig.. 3.3.2. Response of an orthogonally connected E-probe system and its individual components near a biological body illuminated by a plane wave of polarization angle $\theta = 45^{\circ}$ at 2.45GHz.

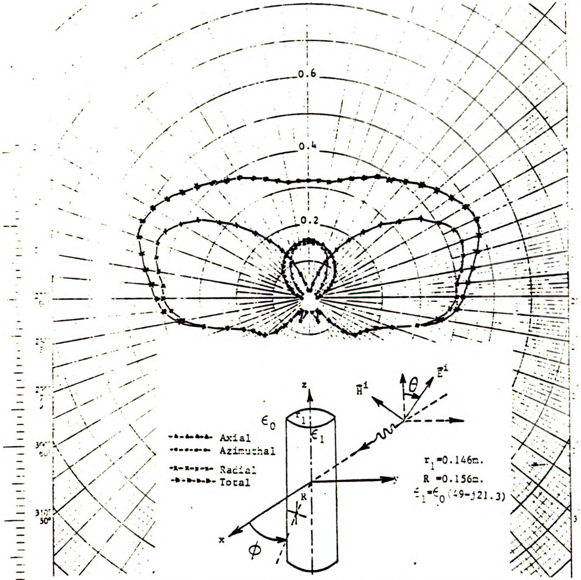

Fig. 3.3.3. Response of an orthogonally connected E-probe system and its individual components near a biological body illuminated by a plane wave of polarization angle $\theta=45^{\circ}$ at 1.5GHz.

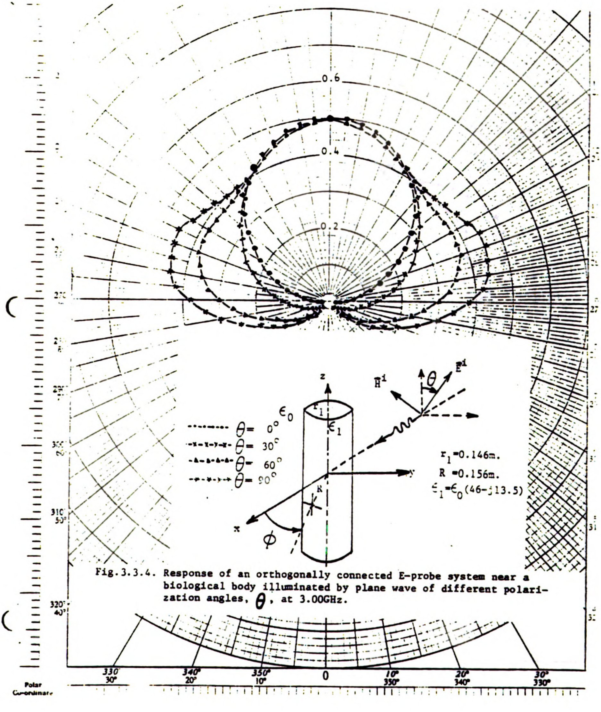

Fig.3.3.4. Response of an orthogonally connected E-probe system near a biological body illuminated by plane wave of different polarization angles, θ, at 3.00GHz.

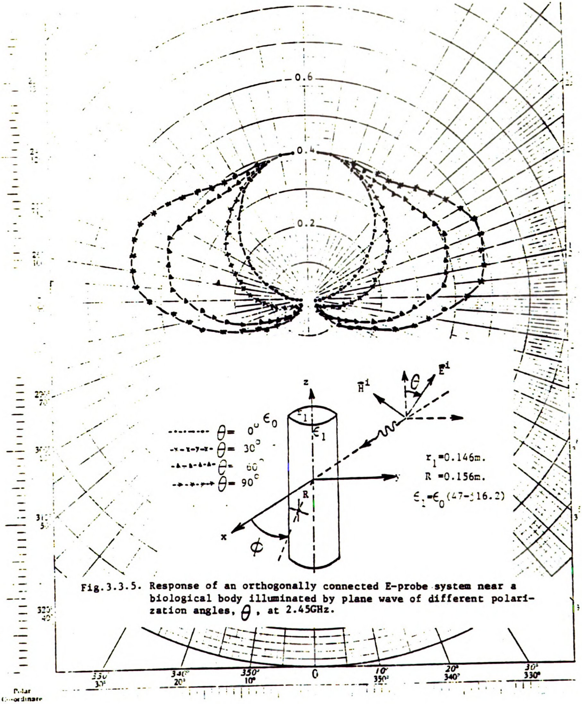

Fig.3.3.5. Response of an orthogonally connected E-probe system near a biological body illuminated by plane wave of different polarization angles, θ, at 2.45GHz.

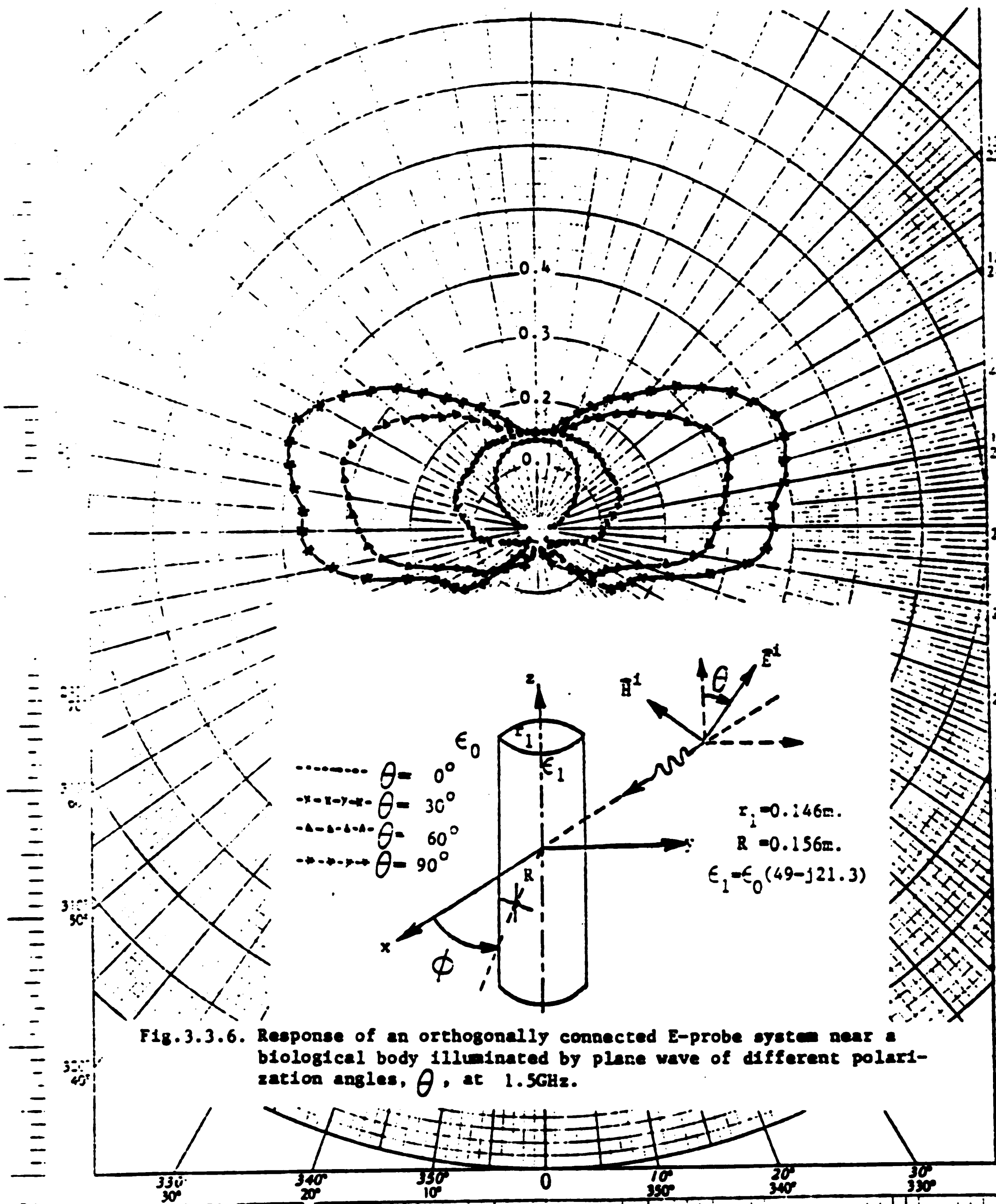

Fig.3.3.6. Response of an orthogonally connected E-probe system near a biological body illuminated by plane wave of different polarization angles, θ, at 1.5GHz.

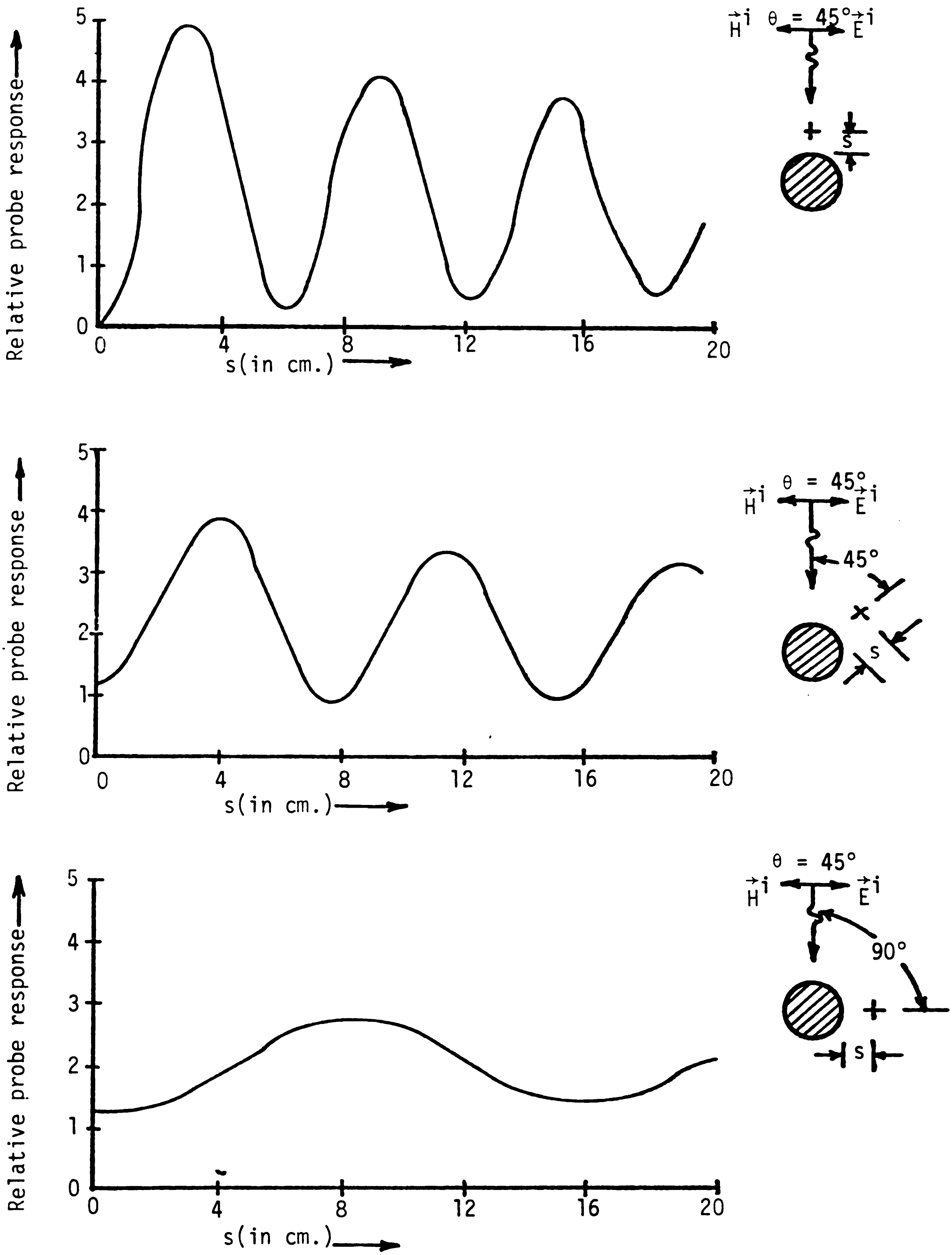

Fig. 3.3.7. Relative probe response as a function of spacing between the probe and the body at 2.45 GHz.

CHAPTER 4

SCATTERING OF EM WAVES BY SIMPLE MODELS OF HUMAN BODY

In this chapter, the scattering of EM waves by a human body will be studied. The purpose of this study is to provide a theoretical basis for the development of a distant life detection system. When a human subject is illuminated by an incident EM wave, the scattered wave from the human body is modulated by the body movements due to breathing and heart beat. If the backscattered wave is received and detected properly, the breathing and heart signals which modulate the backscattered wave can be measured. In our study, the microwave with a frequency in the X-band or the L-band will be employed and the human subject is located at a distance of 100 feet or farther from the antenna.

To analyse the nature of the backscattered field from the body, two simple models of human body, an infinite cylinder of complex permittivity with a time-varying radius and a sphere of complex permittivity with a time-varying radius, are considered. We aim to find the perturbance of the phase and the magnitude of the backscattered field due to the variation of the radius of the body model which simulates the breathing and heart beat.

4.1 Scattering of a TE-polarized EM wave by a circular cylinder of complex permittivity.

The EM wave scattered by an infinite cylinder of complex permittivity when it is illuminated by a TE-polarized wave can be determined following the procedure presented in Chapter 2. Here in this section, equations (2.1.18) and (2.1.25) to (2.1.27) are specialized for the case when $k_1 = k_2 = k$ and $r_2 = a$, as follows:

For $k_1 = k_2 = k$, equation (2.1.18) can be simplified using the wronskian formulas for Bessel function as

$$X_n\Big|_{k_2 = k_1 = k} = -1 \tag{4.1.1}$$

and from (2.1.26) and (4.1.1),

$$y_n\Big|_{\substack{k_2 = k_1 = k \\ r_2 = a}} = \frac{k}{k_0}\left[\frac{H_n^{(2)'}(ka) + H_n^{(1)'}(ka)}{H_n^{(2)}(ka) + H_n^{(1)}(ka)}\right]$$

Since,

$$H_n^{(2)'}(ka) + H_n^{(1)'}(ka) = 2\, J_n'(ka)$$

and

$$H_n^{(2)}(ka) + H_n^{(1)}(ka) = 2\, J_n(ka)$$

Therefore,

$$y_n\Big|_{\substack{k_2 = k_1 = k \\ r_2 = a}} = \left(\frac{k}{k_0}\right) \frac{J_n'(ka)}{J_n(ka)} \tag{4.1.2}$$

Hence, for the present case equation (2.1.25) may be written as

$$d_n = - E_{0z}\epsilon_n j^{-n} \frac{J_n(k_0a)}{H_n^{(2)}(k_0a)} \left\{ \frac{(\frac{k}{k_0}) \frac{J_n'(ka)}{J_n(ka)} - \frac{J_n'(k_0a)}{J_n(k_0a)}}{(\frac{k}{k_0}) \frac{J_n'(ka)}{J_n(ka)} - \frac{H_n^{(2)'}(k_0a)}{H_n^{(2)}(k_0a)}} \right\} \qquad (4.1.3)$$

Whereas the scattered electric field outside cylinder is given by

$$E_z^s(r,\phi) = \sum_{n=0}^{\infty} d_n \, H_n^{(2)}(k_0r) \cos(n\phi) \qquad (4.1.4)$$

Thus, the backscattered field, when k_0r is very large and the series is nicely converging such that the infinite series can be terminated at $n = N$ with $|k_0r| >> N$, is given by,

$$E_z^s(r,\phi = \pi) \simeq \sqrt{\frac{2}{\pi k_0 r}} \exp\{-j(k_0r - \frac{\pi}{4})\} \sum_{n=0}^{N} (-j)^n d_n \qquad (4.1.5)$$

Hence

$$|E_z^s(r,\phi = \pi)|^2 \simeq \frac{2}{\pi k_0 r}|T|^2$$

where

$$T \triangleq \sum_{n=0}^{N} (-j)^n d_n \triangleq (\frac{k_0a}{2}) \; (Q + jP) \qquad (4.1.6)$$

A computer program was prepared for computing $|E_z^s(r,\phi = \pi)|^2$, phase (in degrees) of $E_z^s(r,\phi = \pi)$, Q and P. The computed results for a highly conducting cylinder ($\sigma = 99.99 S/_m$ and $\epsilon_r = 1.0$) as well as for a cylinder with a conductivity of $0.668 S/_m$ and a zero relative permittivity (hypothetical case) are compared in Figure 4.1.1

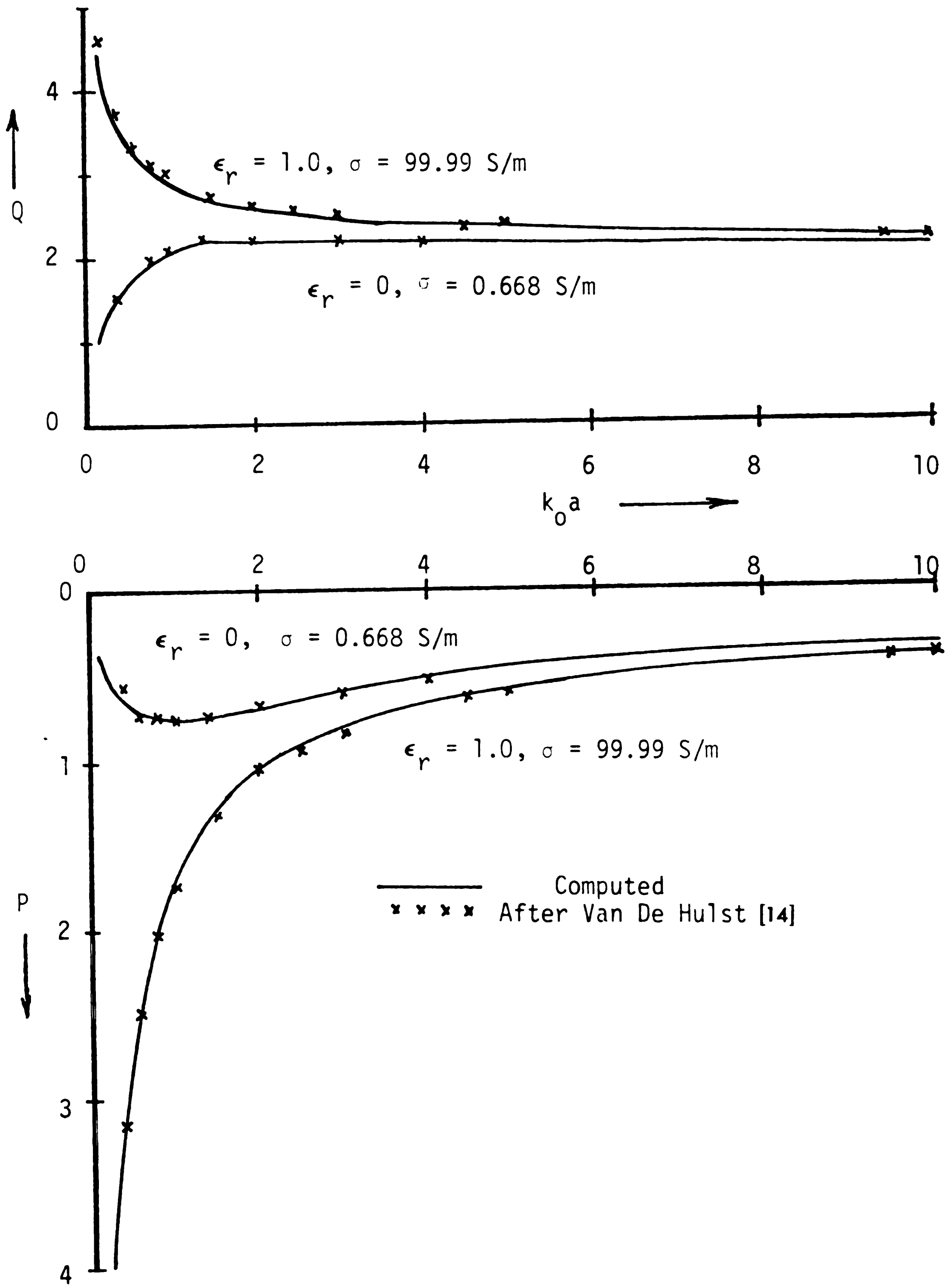

Fig. 4.1.1. Coefficients Q and P as a function of $k_o a$ (f = 3.0 GHz).

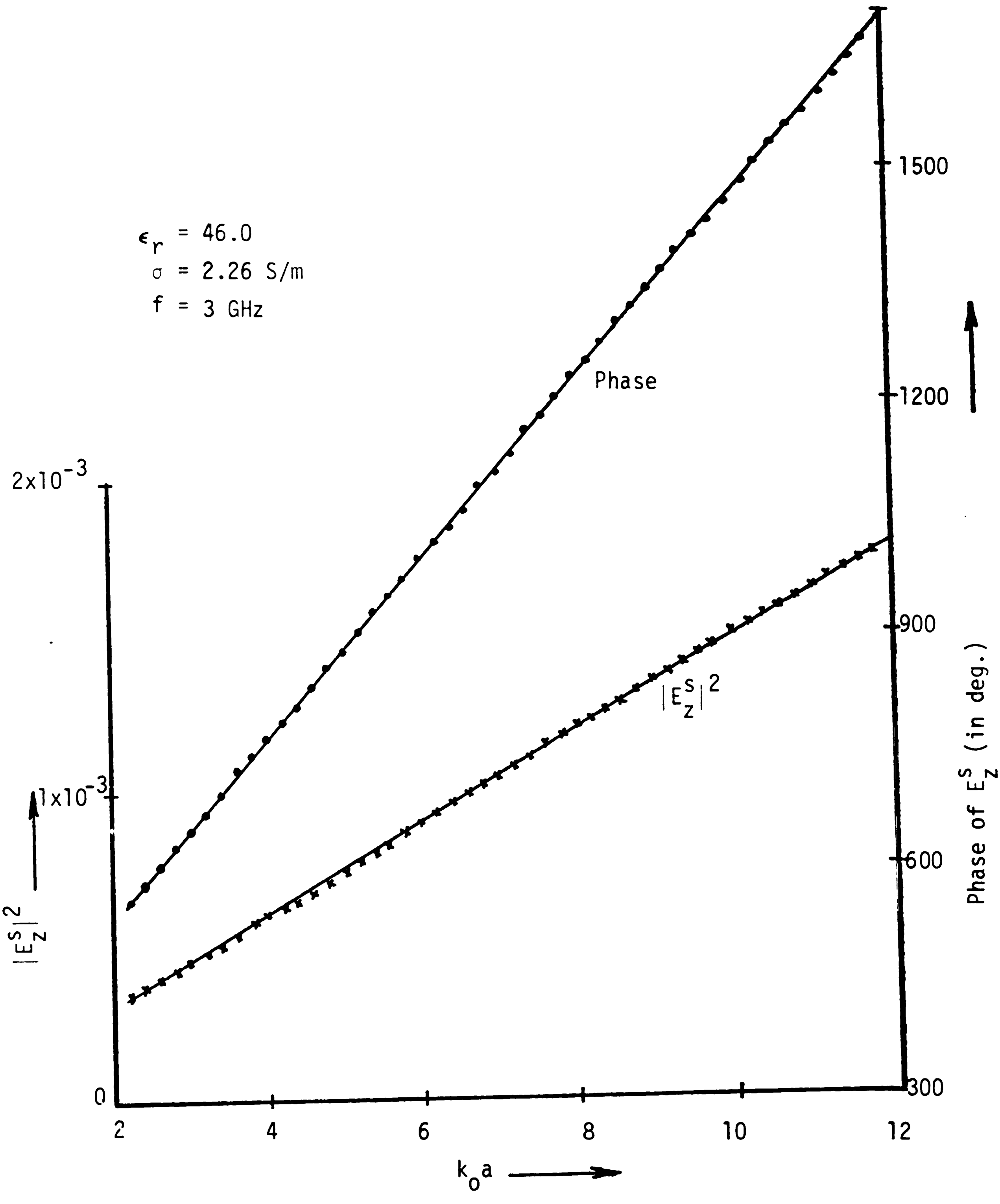

Fig. 4.1.2. Phase and square of the magnitude of the back scattered field E_z^s from a cylinder as a function of $k_o a$ at 3 GHz at a distance of 30.48m.

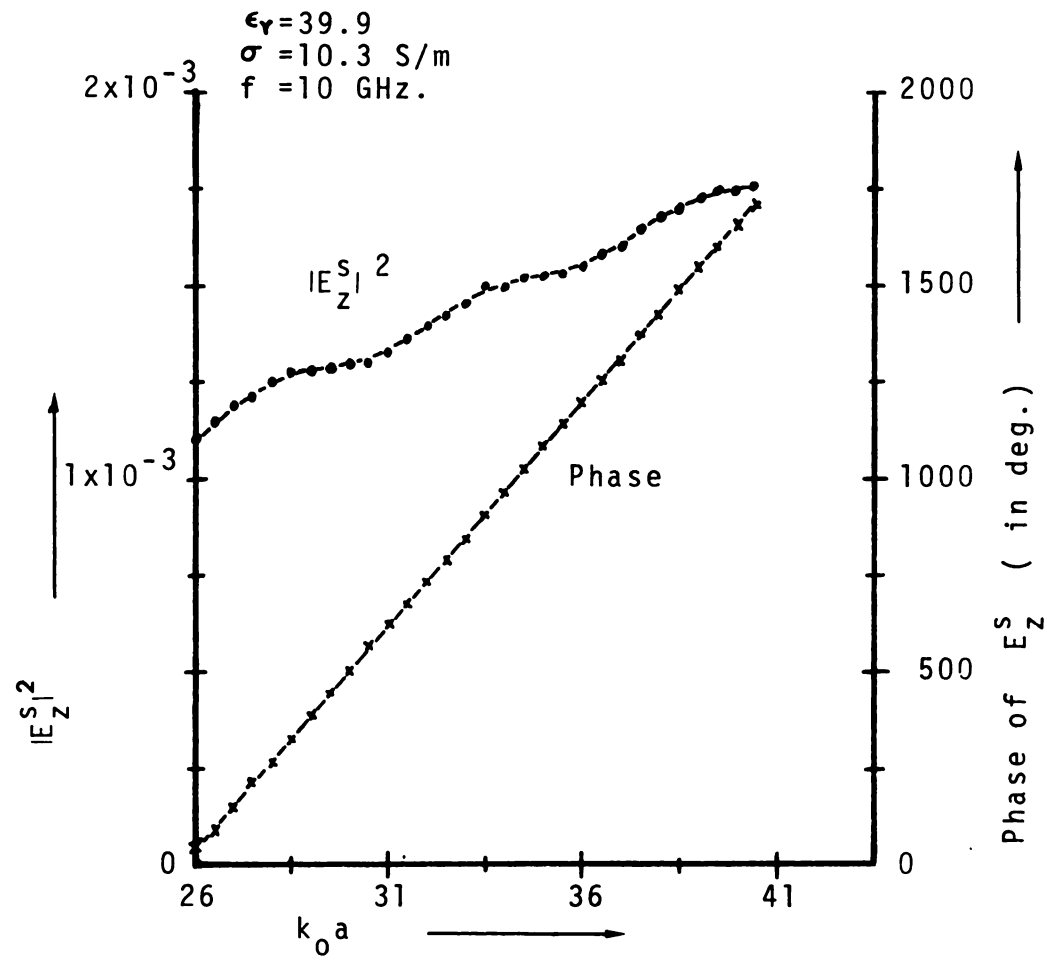

Fig.4.1.3. Phase and square of the magnitude of the back-scattered field E_z^s from a cylinder as a function of k_oa at 10 GHz at a distance of 30.48m.

with known results [14] which are in excellent agreement. Figures 4.1.2 and 4.1.3 depict $|E_z^s(r = 30.48m, \phi = \pi)|^2$ and phase of $E_z^s(r = 30.48m, \phi = \pi)$ as functions of k_0a for a cylinder of complex permittivity at 3GHz and 10GHz, respectively. At 3GHz, both the magnitude and phase of the backscattered field vary linearly with k_0a. However, at 10GHz, the magnitude of the backscattered field does not vary linearly with k_0a even though the phase still does. For this reason it is desirable to measure the phase of the backscattered field if the variation of 'a' is to be detected. The computer program and tabulated results print-outs are given in Appendix C.

4.2. Scattering of plane EM wave by a sphere of complex permittivity

In this section, the scattering of plane electromagnetic wave by a sphere of complex permittivity and radius a is considered. As shown in Figure 4.2.1, the x-polarized incident wave is propagating in positive z-direction. The time variation of $\exp(j\omega t)$ is assumed and suppressed throughout.

This scattering problem is treated as a boundary value problem. The partial differential equation being, of course, the vector Helmholtz equation,

$$\nabla^2 \vec{c} + k^2 \vec{c} = 0 \qquad (4.2.1)$$

Where $k = 2\pi/\lambda$, and $\vec{c}$ may be either the electric $\vec{E}$ or the magnetic field $\vec{H}$. Solutions of (4.2.1) are obtained in the form of infinite series containing unknown constants. To complete the

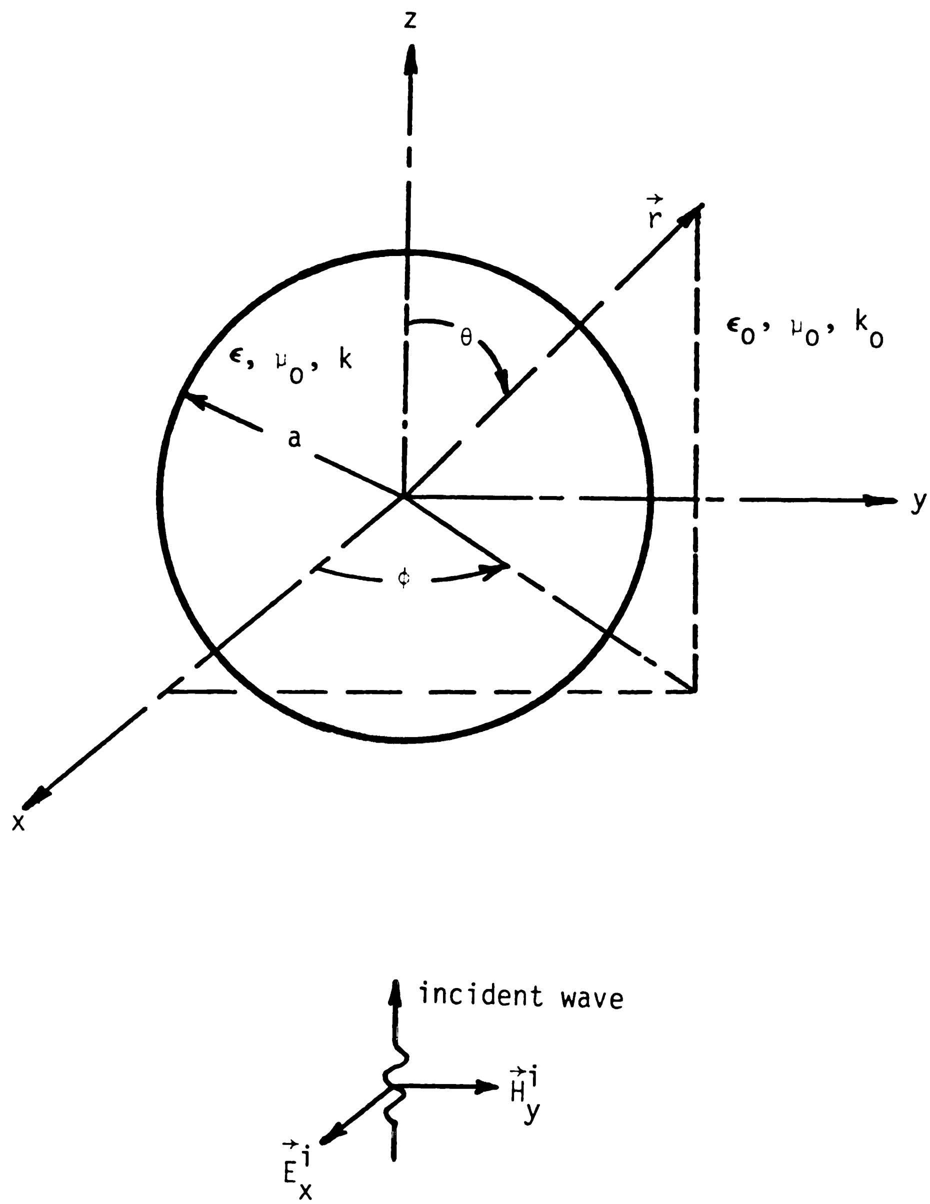

Fig. 4.2.1. Coordinate system for the sphere.

solution of the problem, these constants are determined by matching the boundary conditions for $\vec{E}$ and $\vec{H}$ on the surface of the sphere.

4.2.1 Solution to the vector Helmholtz equation in the spherical coordinate system

It can be proved that the solutions of the vector Helmholtz equation (4.2.1) in the spherical coordinate system are the spherical vector wave functions [15],

$$\vec{L}(r,\theta,\phi) = \nabla f(r,\theta,\phi) \tag{4.2.2}$$

$$\vec{M}(r,\theta,\phi) = \nabla \times [\vec{r} f(r,\theta,\phi)] \tag{4.2.3}$$

$$\vec{N}(r,\theta,\phi) = \frac{1}{k} \nabla \times \vec{M}(r,\theta,\phi) \tag{4.2.4}$$

Where $\vec{r}$ is the radial vector in spherical coordinates and $f(r,\theta,\phi)$ is the solution to the scalar Helmholtz equation,

$$\nabla^2 f(r,\theta,\phi) + k^2 f(r,\theta,\phi) = 0 \tag{4.2.5}$$

In the region surrounding the scatterer, $\nabla\cdot\vec{E} = \nabla\cdot\vec{H} = 0$. Since $\nabla\cdot\vec{L}(r,\theta,\phi) \neq 0$, only the $\vec{M}(r,\theta,\phi)$ and $\vec{N}(r,\theta,\phi)$ solutions can be used to represent $\vec{E}$ and $\vec{H}$.

It is well known that the solutions to equation (4.2.5) in spherical coordinate system are of the form,

$$f_{\substack{e \\ o}mn}(r,\theta,\phi) = z_n(kr) P_n^m(\cos\theta) \begin{Bmatrix} \cos(m\phi) \\ \sin(m\phi) \end{Bmatrix} \tag{4.2.6}$$

Where m and n can be any integer, e denotes "even" for the use of $\cos(m\phi)$ and 0 denotes "odd" for the use of $\sin(m\phi)$. $P_n^m(\cos\theta)$ is the associated Legendre polynomial, and $z_n(kr)$ represents the spherical Bessel functions of the first kind, $j_n(kr)$, of the second kind, $n_n(kr)$, spherical Hankel function of the first kind, $h_n^{(1)}(kr)$, or of the second kind, $h_n^{(2)}(kr)$, respectively.

The desired solutions to the vector Helmholtz equation are then the spherical vector wave functions obtained from equations (4.2.3), (4.2.4) and (4.2.6),

$$\vec{M}_{\substack{e\\o}mn} = \mp \frac{m}{\sin\theta} z_n(kr) P_n^m(\cos\theta) \begin{Bmatrix}\sin(m\phi)\\ \cos(m\phi)\end{Bmatrix} \hat{\theta} + \\ - z_n(kr)\left[\frac{\partial}{\partial\theta} P_n^m(\cos\theta)\right] \begin{Bmatrix}\cos(m\phi)\\ \sin(m\phi)\end{Bmatrix} \hat{\phi} \qquad (4.2.7)$$

and

$$\vec{N}_{\substack{e\\o}mn} = \frac{n(n+1)}{kr} z_n(kr) P_n^m(\cos\theta) \begin{Bmatrix}\cos(m\phi)\\ \sin(m\phi)\end{Bmatrix} \hat{r} + \\ + \frac{1}{kr}\frac{\partial}{\partial r}[r\, z_n(kr)]\left[\frac{\partial}{\partial\theta} P_n^m(\cos\theta)\right] \begin{Bmatrix}\cos(m\phi)\\ \sin(m\phi)\end{Bmatrix} \hat{\theta} + \\ \mp \frac{m}{kr\sin\theta} \frac{\partial}{\partial r}[r z_n(kr)] P_n^m(\cos\theta) \begin{Bmatrix}\sin(m\phi)\\ \cos(m\phi)\end{Bmatrix} \hat{\phi} \qquad (4.2.8)$$

4.2.2 Transformation of the plane wave into spherical coordinate system

The x-polarized plane EM wave propagating in +z direction can be represented as,

$$\vec{E}^i = \hat{x}E_0 \exp(-jk_0 z) = \hat{x}E_0 \exp(-jk_0 r \cos\theta) \qquad (4.2.9)$$

and

$$\vec{H}^i = \hat{y}\frac{E_0}{\zeta_0}\exp(-jk_0 z) = \hat{y}\frac{E_0}{\zeta_0}\exp(-jk_0 r \cos\theta) \qquad (4.2.10)$$

Where $\zeta_0 = \sqrt{\mu_0/\epsilon_0}$ intrinsic impedance of free space.

Since $\hat{x} = (\sin\theta\cos\phi)\hat{r} + (\cos\theta\cos\phi)\hat{\theta} - \sin\phi\,\hat{\phi}$, equation (4.2.9) can be written as,

$$\vec{E}^i = \left\{(\sin\theta\cos\phi)\hat{r} + (\cos\theta\cos\phi)\hat{\theta} - \sin\phi\,\hat{\phi}\right\}E_0 \exp(-jk_0 r \cos\theta) \qquad (4.2.11)$$

Now, after comparing equation (4.2.11) with (4.2.7) and (4.2.8), it can be concluded that

$$\vec{E}^i = E_0 \sum_{n=0}^{\infty} [a_n \vec{M}_{01n} + b_n \vec{N}_{e1n}] \qquad (4.2.12)$$

and, since the incident field is finite at $r = 0$, only first kind of Bessel functions are allowed for $\vec{M}_{01n}$ and $\vec{N}_{e1n}$. The coefficient b_n is determined by comparing r components of both the sides as follows:

$$\sin\theta\cos\phi\exp(-jk_0 r\cos\theta) = \sum_{n=0}^{\infty} b_n \frac{n(n+1)}{kr} j_n(k_0 r)P_n^1(\cos\theta)\cos\phi \qquad (4.2.13)$$

Now, noting that $\frac{d}{d\theta}\{\exp(-jk_0 r\cos\theta)\} = jk_0 r\sin\theta \quad \exp(-jk_0 r\cos\theta)$ and, $\exp(-jk_0 r\cos\theta) = \sum_{n=0}^{\infty}(-j)^n(2n+1)j_n(k_0 r).\ P_n(\cos\theta)$, b_n can be evaluated from eqaution (4.1.13) as,

$$b_n = (-j)^{n-1} \frac{(2n+1)}{n(n+1)} \tag{4.2.14}$$

To determine a_n, $\hat{r}$ component of $\vec{H}^i$ field is compared. Since $\hat{y} = (\sin\theta \sin\phi)\hat{r} + (\cos\theta \sin\phi)\hat{\theta} + \cos\phi\,\hat{\phi}$, equation (4.2.10) can be written as,

$$\vec{H}^i = \left\{ (\sin\theta \sin\phi)\hat{r} + (\cos\theta \sin\phi)\hat{\theta} + \cos\phi\,\hat{\phi} \right\} \frac{E_0}{\zeta_0} \exp(-jk_0 r \cos\theta) \tag{4.2.15}$$

Now from Maxwells's equations and equation (4.2.12), $\vec{H}^i$ is found to be,

$$\vec{H}^i = \frac{j}{\omega\mu_0} \sum_{n=0}^{\infty} [a_n \nabla X\vec{M}_{01n} + b_n \nabla X\vec{N}_{e1n}] \tag{4.1.16}$$

Since $\nabla X\vec{M}_{01n} = k_0\vec{N}_{01n}$ and $\nabla X\vec{N}_{e1n} = k_0\vec{M}_{e1n}$, equation (4.2.16) reduces to

$$\vec{H}^i = \frac{j}{\zeta_0} \sum_{n=0}^{\infty} [a_n\vec{N}_{01n} + b_n\vec{M}_{e1n}] \tag{4.2.17}$$

Now, comparing $\hat{r}$ components of equations (4.2.15) and (4.1.17), and after some mathematical manipulations, a_n is found as,

$$a_n = (-j)^n \frac{(2n+1)}{n(n+1)} \tag{4.2.18}$$

Thus $\vec{E}^i$ and $\vec{H}^i$ can be written as

$$\vec{E}^i = \sum_{n=1}^{\infty} (-j)^n \frac{(2n+1)}{n(n+1)} [\vec{M}^{(1)}_{01n} + j\vec{N}^{(1)}_{e1n}] \tag{4.2.19}$$

and

$$\vec{H}^{i} = \frac{-1}{\zeta_0} \sum_{n=1}^{\infty} (-j)^n \frac{(2n+1)}{n(n+1)} [\vec{M}^{(1)}_{e1n} - j\vec{N}^{(1)}_{01n}] \qquad (4.2.20)$$

Where superscript (1) on $\vec{M}$ and $\vec{N}$ denotes the first kind of the spherical Bessel function.

4.2.3 Construction of solution and computed results

When the incident EM wave represented by equations (4.2.19) and (4.2.20), illuminates the sphere, there should be a similar series of functions representing the fields scattered by as well as the fields transmitted into the spherical medium. Since the fields are finite at the origin and bounded at infinity, the appropriate expressions may be written as,

$$\vec{E}^{s} = E_0 \sum_{n=1}^{\infty} (-j)^n \frac{(2n+1)}{n(n+1)} [d_n \vec{M}^{(4)}_{01n} + je_n \vec{N}^{(4)}_{e1n}] \qquad (4.2.21)$$

$$\vec{H}^{s} = -\frac{E_0}{\zeta_0} \sum_{n=1}^{\infty} (-j)^n \frac{(2n+1)}{n(n+1)} [e_n \vec{M}^{(4)}_{e1n} - jd_n \vec{N}^{(4)}_{01n}] \qquad (4.2.22)$$

$$\vec{E}^{t} = E_0 \sum_{n=1}^{\infty} (-j)^n \frac{(2n+1)}{n(n+1)} [f_n \vec{M}^{(1)}_{01n} + jg_n \vec{N}^{(1)}_{e1n}] \qquad (4.2.23)$$

and

$$\vec{H}^{t} = -\frac{E_0}{\zeta} \sum_{n=1}^{\infty} (-j)^n \frac{(2n+1)}{n(n+1)} [g_n \vec{M}^{(1)}_{e1n} - jf_n \vec{N}^{(1)}_{01n}] \qquad (4.2.24)$$

Where superscript (4) on $\vec{M}$ and $\vec{N}$ in equation (4.2.21) and (4.2.22) represents the use of spherical Hankel function of second kind and ζ in equation (4.2.24) is intrinsic impedance of the medium. The superscripts s and t used in equations (4.2.21) - (4.2.24) represent scattered and transmitted fields, respectively.

Since the tangential fields must be continuous across the boundary at $r = a$, therefore,

$$(\vec{E}^i)_\theta + (\vec{E}^s)_\theta = (\vec{E}^t)_\theta \quad \text{at} \quad r = a \tag{4.2.25}$$

$$(\vec{E}^i)_\phi + (\vec{E}^s)_\phi = (\vec{E}^t)_\phi \quad \text{at} \quad r = a \tag{4.2.26}$$

$$(\vec{H}^i)_\theta + (\vec{H}^s)_\theta = (\vec{H}^t)_\theta \quad \text{at} \quad r = a \tag{4.2.27}$$

and,

$$(\vec{H}^i)_\phi + (\vec{H}^s)_\phi = (\vec{H}^t)_\phi \quad \text{at} \quad r = a \tag{4.2.28}$$

From equations (4.2.7), (4.2.8) and (4.2.19) - (4.2.28) one can get,

$$\sum_{n=1}^{\infty}(-j)^n \frac{(2n+1)}{n(n+1)} [j_n(k_0a) + d_nh_n^{(2)}(k_0a)-f_nj_n(ka)] \frac{P_n^1(\cos\theta)}{\sin\theta}$$

$$= \sum_{n=1}^{\infty}(-j)^{n-1} \frac{(2n+1)}{n(n+1)} [\frac{g_n}{ka} \frac{\partial}{\partial r} \{rj_n(kr)\} - \frac{e_n}{k_0a} \cdot$$

$$\cdot \frac{\partial}{\partial r} \{rh_n^{(2)}(k_0r)\} - \frac{1}{k_0a} \frac{\partial}{\partial r} \{rj_n(k_0r)\}]\Big|_{r=a} \frac{\partial}{\partial\theta}\{P_n^1(\cos\theta)\} \tag{4.2.29}$$

$$\sum_{n=1}^{\infty}(-j)^n \frac{(2n+1)}{n(n+1)} [j_n(k_0a) + d_nh_n^{(2)}(k_0a)-f_nj_n(ka)] \frac{\partial}{\partial\theta}\{P_n^1(\cos\theta)\}$$

$$= \sum_{n=1}^{\infty}(-j)^{n-1} \frac{(2n+1)}{n(n+1)} [\frac{g_n}{ka} \frac{\partial}{\partial r}\{rj_n(kr)\} - \frac{e_n}{k_0a} \frac{\partial}{\partial r}\{rh_n^{(2)}(k_0r)\}$$

$$- \frac{1}{k_0a} \frac{\partial}{\partial r} \{rj_n(k_0r)\}]\Big|_{r=a} \frac{P_n^1(\cos\theta)}{\sin\theta} \tag{4.2.30}$$

$$\sum_{n=1}^{\infty} (-j)^n \frac{(2n+1)}{n(n+1)} [j_n(k_0 a) + e_n h_n^{(2)}(k_0 a) - \frac{\zeta_0}{\zeta} g_n j_n(ka)] \frac{P_n^1(\cos\theta)}{\sin\theta}$$

$$= \sum_{n=1}^{\infty} (-j)^{n-1} \frac{(2n+1)}{n(n+1)} [\frac{\zeta_0}{\zeta} \frac{f_n}{ka} \frac{\partial}{\partial r} \{rj_n(kr)\} - \frac{1}{k_0 a} \cdot$$

$$\cdot \frac{\partial}{\partial r} \{rj_n(k_0 r)\} - \frac{d_n}{k_0 a} \frac{\partial}{\partial r} \{rh_n^{(2)}(k_0 r)\}]\Big|_{r=a} \frac{\partial}{\partial\theta} \{P_n^1(\cos\theta)\} \tag{4.2.31}$$

and,

$$\sum_{n=1}^{\infty} (-j)^n \frac{(2n+1)}{n(n+1)} [j_n(k_0 a) + e_n h_n^{(2)}(k_0 a) - \frac{\zeta_0}{\zeta} g_n j_n(ka)] \frac{\partial}{\partial\theta}\{P_n^1(\cos\theta)\}$$

$$= \sum_{n=1}^{\infty} (-j)^{n-1} \frac{(2n+1)}{n(n+1)} [\frac{\zeta_0}{\zeta} \frac{f_n}{ka} \frac{\partial}{\partial r}\{rj_n(kr)\} - \frac{1}{k_0 a} \cdot$$

$$\cdot \frac{\partial}{\partial r}\{rj_n(k_0 r)\} - \frac{d_n}{k_0 a} \frac{\partial}{\partial r}\{rh_n^{(2)}(k_0 r)\}]\Big|_{r=a} \frac{P_n^1(\cos\theta)}{\sin\theta} \tag{4.2.32}$$

Noting that $\frac{\partial}{\partial r}\{rz_n(k_0 r)\}\Big|_{r=a} = k_0 a z_n'(k_0 a) + z_n(k_0 a)$, and

$\left(\frac{P_n^1(\cos\theta)}{\sin\theta}\right)^2 \neq [\frac{\partial}{\partial\theta} \{P_n^1(\cos\theta)\}]^2$ for arbitrary n, equations (4.2.29) - (4.2.32) are always true if and only if,

$$j_n(k_0 a) + d_n h_n^{(2)}(k_0 a) - f_n j_n(ka) = 0 \tag{4.2.33}$$

$$g_n\{j_n'(ka) + \frac{j_n(ka)}{ka}\} - e_n\{h_n^{(2)'}(k_0 a) + \frac{h_n^{(2)}(k_0 a)}{k_0 a}\} - j_n'(k_0 a) - \frac{j_n(k_0 a)}{k_0 a} = 0 \tag{4.2.34}$$

$$j_n(k_0 a) + e_n h_n^{(2)}(k_0 a) - \frac{\zeta_0}{\zeta} g_n j_n(ka) = 0 \tag{4.2.35}$$

and,

$$\frac{\zeta_0}{\zeta} f_n\{j_n'(ka) + \frac{j_n(ka)}{ka}\} - d_n\{h_n^{(2)'}(k_0a) + \frac{h_n^{(2)}(k_0a)}{k_0a}\}$$

$$- j_n'(k_0a) - \frac{j_n(k_0a)}{k_0a} = 0 \qquad (4.2.36)$$

Thus, equations (4.2.33) - (4.2.36) can be solved for the unknown constants d_n, e_n, f_n and g_n. Since $\frac{\zeta_0}{\zeta} = \sqrt{\epsilon_r}$ and $k = k_0\sqrt{\epsilon_r}$, the constants d_n and e_n which are needed for the present problem, are found as,

$$d_n = \frac{\sqrt{\epsilon_r} j_n'(ka) j_n(k_0a) - j_n'(k_0a) j_n(ka)}{j_n(ka) h_n^{(2)'}(k_0a) - \sqrt{\epsilon_r}\, j_n'(ka) h_n^{(2)}(k_0a)} \qquad (4.2.37)$$

and,

$$e_n = \frac{\dfrac{j_n(k_0a) j_n'(ka)}{\sqrt{\epsilon_r}\, j_n(ka)} + \dfrac{j_n(k_0a)}{\sqrt{\epsilon_r} ka} - j_n(ka) - \dfrac{j_n(k_0a)}{k_0a}}{h_n^{(2)'}(k_0a) + \dfrac{h_n^{(2)}(k_0a)}{k_0a} - \dfrac{j_n'(ka) h_n^{(2)}(k_0a)}{\sqrt{\epsilon_r}\, j_n(ka)} - \dfrac{h_n^{(2)}(k_0a)}{\sqrt{\epsilon_r}\, ka}} \qquad (4.2.38)$$

Now, since d_n and e_n are evaluated in equations (4.2.37) and (4.2.38), the remaining two constants, f_n and g_n can be found from equations (4.2.36) and (4.2.35), respectively. The fields outside and inside the sphere are in turn, determined by equations (4.2.19) - (4.2.24).

For the present, the only backscattered field is of interest, which can be found after evaluating $\vec{M}$ and $\vec{N}$ for $\theta = 180^o$ and $\phi = 180^o$. Further, $\hat{r}$-component of the fields, which is due to $\hat{r}$ component of $\vec{N}$, is inversely proportional to r^2. Hence for large r, only transverse components, which are inversely proportional to r, survive. Hence,

$$\vec{E}^s(r \to \infty, \theta = \pi, \phi = \pi) \simeq \hat{\theta}\, E_\theta(r \to \infty, \theta = \pi, \phi = \pi) = E_{BS}$$

$$= -E_0 \sum_{n=1}^{\infty} (-j)^n \frac{(2n+1)}{n(n+1)} \left[d_n h_n^{(2)}(k_0 r) \left. \frac{P_n^1(\cos\theta)}{\sin\theta} \right|_{\theta=\pi} + j \frac{e_n}{k_0 r} \cdot \right.$$

$$\left. \cdot \frac{\partial}{\partial r} \{ r\, h_n^{(2)}(k_0 r) \} \frac{\partial}{\partial \theta} P_n^1(\cos\theta) \right|_{\theta=\pi} \qquad (4.2.39)$$

Since,

$$\frac{d}{d\theta} P_n^m(\cos\theta) = -\sqrt{1-\eta^2}\, \frac{dP_n^m}{d\eta} = \tfrac{1}{2}[(n-m+1)(n+m)\, P_n^{m-1} - P_n^{m+1}]$$

Therefore, $\frac{\partial}{\partial\theta} P_n^1(\cos\pi) = \tfrac{1}{2}[n(n+1)\, P_n^{(0)}(\cos\pi) - P_n^{(2)}(\cos\pi)]$

But, $P_n^{(2)}(\cos\pi) = P_n^{(2)}(-1) = 0$ and, $P_n^0(\cos\pi) = (-1)^n$.

Hence,

$$\frac{\partial}{\partial\theta} P_n^1(\cos\pi) = (-1)^n \frac{n(n+1)}{2} \qquad (4.2.40)$$

Also,

$$\left. \frac{P_n^1(\cos\theta)}{\sin\theta} \right|_{\theta=\pi} = -(-1)^n \frac{n(n+1)}{2} \qquad (4.2.41)$$

Therefore, equation (4.2.39) reduces to,

$$E_{BS} = -E_0 \sum_{n=1}^{\infty} j^n \frac{(2n+1)}{2} [-d_n h_n^{(2)}(k_0 r) + j e_n \{ h_n^{(2)'}(k_0 r) + \frac{h_n^{(2)}(k_0 r)}{k_0 r} \}] \qquad (4.2.42)$$

At this point if one defines another type of spherical Bessel functions [16] as follows,

$$\hat{Z}_n(\lambda x) = \sqrt{\frac{\pi\lambda x}{2}}\; Z_{n+\frac{1}{2}}(\lambda x) \tag{4.2.43}$$

Where $Z_{n+\frac{1}{2}}(\lambda x)$ are usual cylindrical Bessel functions. Then,

$$\hat{z}_n(\lambda x) = \frac{1}{\lambda x}\,\hat{Z}_n(\lambda x) \tag{4.2.44}$$

Also,

$$\hat{z}_n'(\lambda x) = \frac{\hat{Z}_n'(\lambda x)}{\lambda x} - \frac{1}{(\lambda x)^2}\,\hat{Z}_n(\lambda x) \tag{4.2.45}$$

and

$$\hat{z}_n'(\lambda x) + \frac{\hat{z}_n(\lambda x)}{\lambda x} = \frac{\hat{Z}_n'(\lambda x)}{\lambda x} \tag{4.2.46}$$

Therefore, equation (4.2.38) may be written as,

$$e_n = \frac{\hat{J}_n(k_0a)\hat{J}_n'(ka) - \sqrt{\epsilon_r}\;\hat{J}_n'(k_0a)\hat{J}_n(ka)}{\sqrt{\epsilon_r}\hat{H}_n^{(2)'}(k_0a)\hat{J}_n(ka) - \hat{H}_n^{(2)}(k_0a)\hat{J}_n'(ka)} \tag{4.2.47}$$

Further, using the relation,

$$z_n'(\lambda_1 x)z_n(\lambda_2 x) = \frac{\hat{Z}_n'(\lambda_1 x)\hat{Z}_n(\lambda_2 x)}{(\lambda_1 x)\cdot(\lambda_2 x)} - \frac{\hat{Z}_n(\lambda_1 x)\hat{Z}_n(\lambda_2 x)}{(\lambda_1 x)^2(\lambda_2 x)} \tag{4.2.48}$$

equation (4.2.37) may be written as,

$$d_n = \frac{\sqrt{\epsilon_r}\;\hat{J}_n'(ka)\hat{J}_n(k_0a) - \hat{J}_n'(k_0a)\hat{J}_n(ka)}{\hat{H}_n^{(2)'}(k_0a)\hat{J}_n(ka) - \sqrt{\epsilon_r}\;\hat{J}_n'(ka)\hat{H}_n^{(2)}(k_0a)} \tag{4.2.49}$$

The backscattered field, E_{BS}, may be written in terms of $\hat{Z}_n(k_0 r)$ as,

$$E_{BS} = \frac{-E_0}{2k_0 r} \sum_{n=1}^{\infty} j^n (2n+1)[-d_n \hat{H}_n^{(2)}(k_0 r) + j e_n \hat{H}_n^{(2)'}(k_0 r)] \qquad (4.2.50)$$

As a special case, when conductivity is very high, terms having $\sqrt{\epsilon_r}$ as a multiplying coefficient in equations (4.2.47) and (4.2.49) dominate and hence e_n and d_n reduce to

$$\lim_{\sigma \to \infty} e_n = -\hat{J}_n'(k_0 a)/\hat{H}_n^{(2)'}(k_0 a) \qquad (4.2.51)$$

and

$$\lim_{\sigma \to \infty} d_n = -\hat{J}_n(k_0 a)/\hat{H}_n^{(2)}(k_0 a) \qquad (4.2.52)$$

Here, it is to be noted that,

$$\lim_{k \to \infty} \hat{J}_n(ka) = \cos(ka - \frac{n\pi}{2} - \frac{\pi}{2}) = \sin(\frac{n\pi}{2} - ka) \qquad (4.2.53)$$

Therefore, this term is never zero even for the infinite conducitivity. Hence the expressions for e_n and d_n, as given by equations (4.2.47) and (4.2.49), approach relatively slowly to the perfectly conducting case in comparison to the fields scattered by an infinite cylinder.

It is a normal practice to determine the backscattering cross-section (also known as echo area) of the sphere, which is defined as,

$$A_e = \lim_{r \to \infty} (4\pi r^2 \frac{|E_{BS}|^2}{|E^i|^2}) = \lim_{r \to \infty} (4\pi r^2 \left|\frac{E_{BS}}{E_0}\right|^2) \qquad (4.2.54)$$

Normalized backscattering cross-section can be defined as

$$\overline{A}_e = A_e/\pi a^2 \tag{4.2.55}$$

where a is the radius of the sphere.

A computer program is prepared for calculating the E_{BS} as well as $\overline{A}_e$ from equations (4.2.50) and (4.2.55). The program is tested for its correctness with known data [14]. These data are plotted in Figure 4.2.2 for the case with a conductivity of 99.99 S/m and a relative permittivity of 1 as well as for the case with a conductivity of 2.21S/m and a relative permittivity of 7.8 at 3GHz; our computed results and the existing results are in excellent agreement. Figures 4.2.3 and 4.2.4 illustrate the change in $|E_{BS}|^2$ and phase angle of E_{BS} (in degrees) as a function of k_0a for the case with a conductivity of 2.28S/m and a relative permittivity of 46 at 3GHz, and for the case with a conductivity of 10.3S/m and a relative permittivity of 39.9 at 10GHz. These conductivity and relative permittivity represent the properties of the biological media at the specified frequencies [11]. The computer program and printout results are given in Appendix D.

From Figures 4.1.2, 4.1.3, 4.2.3 and 4.2.4, it may be observed that the phase of the backscattered field varies linearly with the change in k_0a while its magnitude does not have this linear relation. Therefore, for the detection of small change of a, which varies slowly with time, it is easier to detect the phase change in the backscattered field.

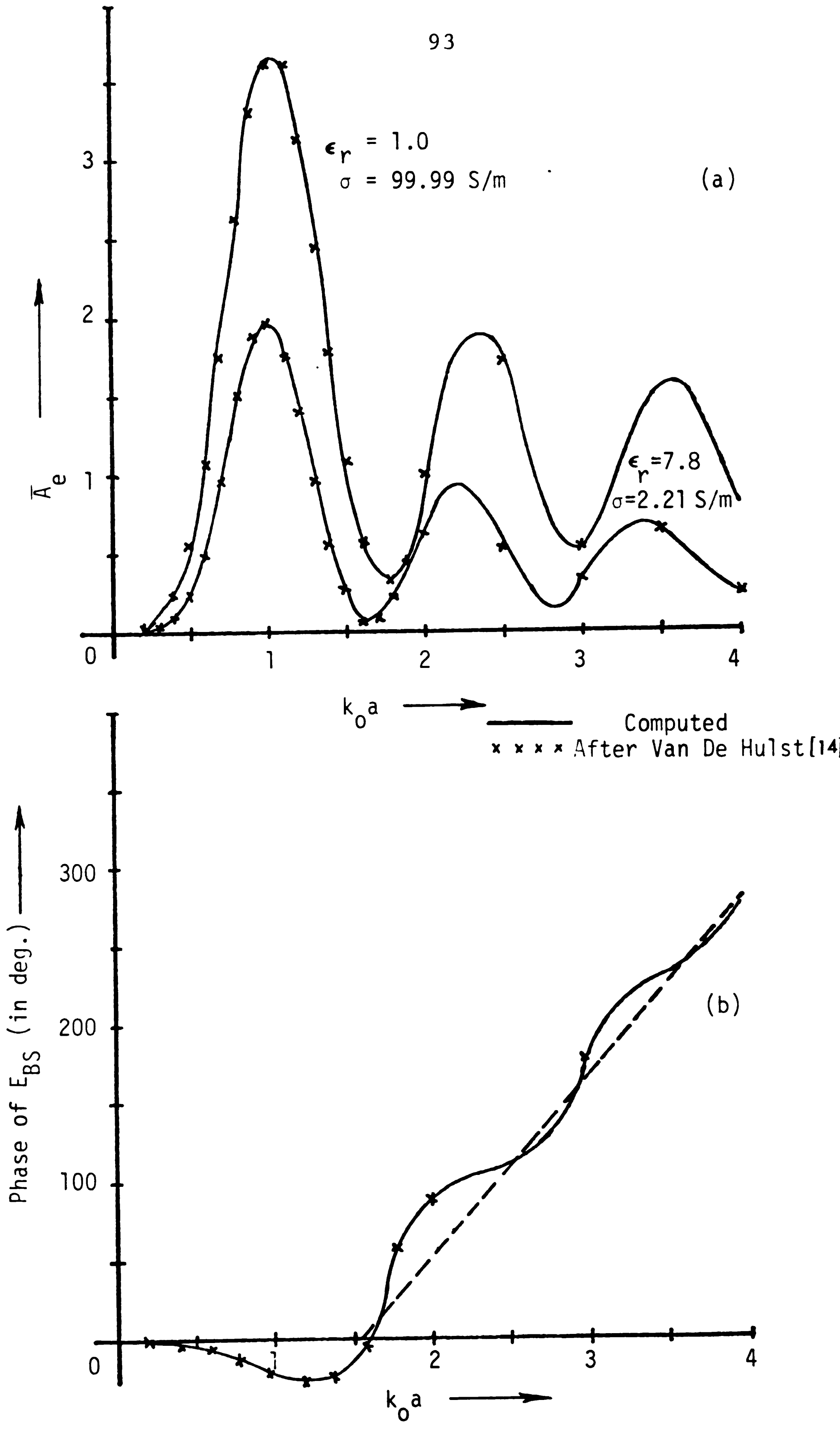

Fig. 4.2.2. Normalized backscattering cross section (a), and phase of backscattered field E_{BS}(b) from a sphere as a function of k_oa at 3 GHz.

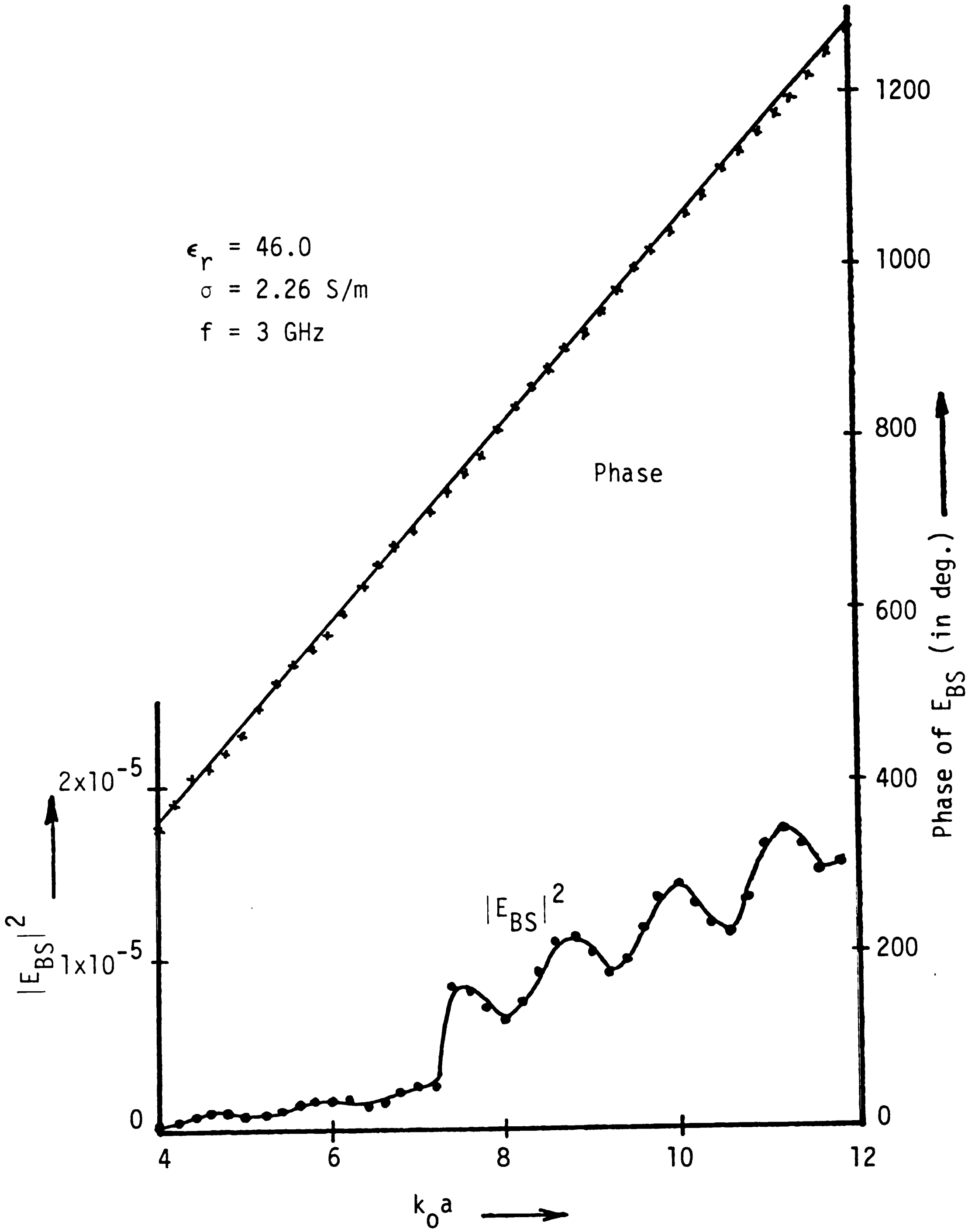

Fig. 4.2.3. Phase and square of the magnitude of the backscattered field E_{BS} from a sphere as a function of $k_o a$ at 3 GHz at a distance of 30.48m.

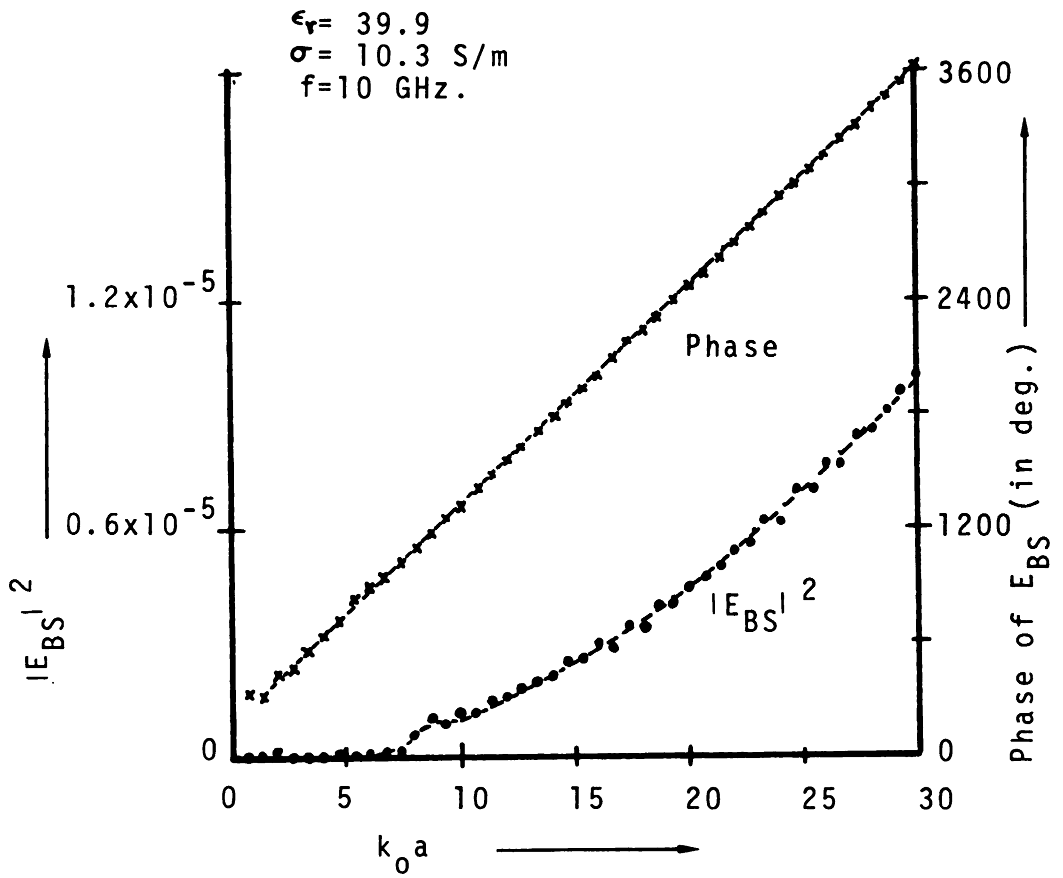

Fig.4.2.4. Phase and square of the magnitude of the back-scattered field E_{BS} from a sphere as a function of k_oa at 10GHz at a distance of 30.48m.

CHAPTER 5

THE DISTANT LIFE DETECTION SYSTEM DESIGN AND TESTING

In the preceding chapter, it has been observed that when the radius of a circular cylinder or a sphere changes, it affects the amplitude as well as phase of the return signal. However, in general, if the radius is changing in time as $r_0 u(t)$, the magnitude changes as $A_0 u_1(t)$, while the phase behaves as $\phi_0 u_2(t)$, i.e., they are not linearly related. Similarly, when a human being is exposed to an electromagnetic wave, the return signal is expected to vary in magnitude and phase with breathing as well as with heart beat. Although these variations may be related in a very complicated way, these give definite signals of life. In this chapter, two different systems, viz, the one based on a magic tee and the other, based on a circulator, are analyzed and tested for detecting the breathing as well as heart signals from long distances (~ 100 feet or over). The effects of body orientation, clothing and polarization of EM wave are also studied experimentally.

5.1 Analysis of the magic tee system

A simplified block diagram for detecting the breathing and heart signals using a magic tee is shown in Figure 5.1.1. The microwave signal is connected to the port 3 (H-arm) of the magic tee while a detector

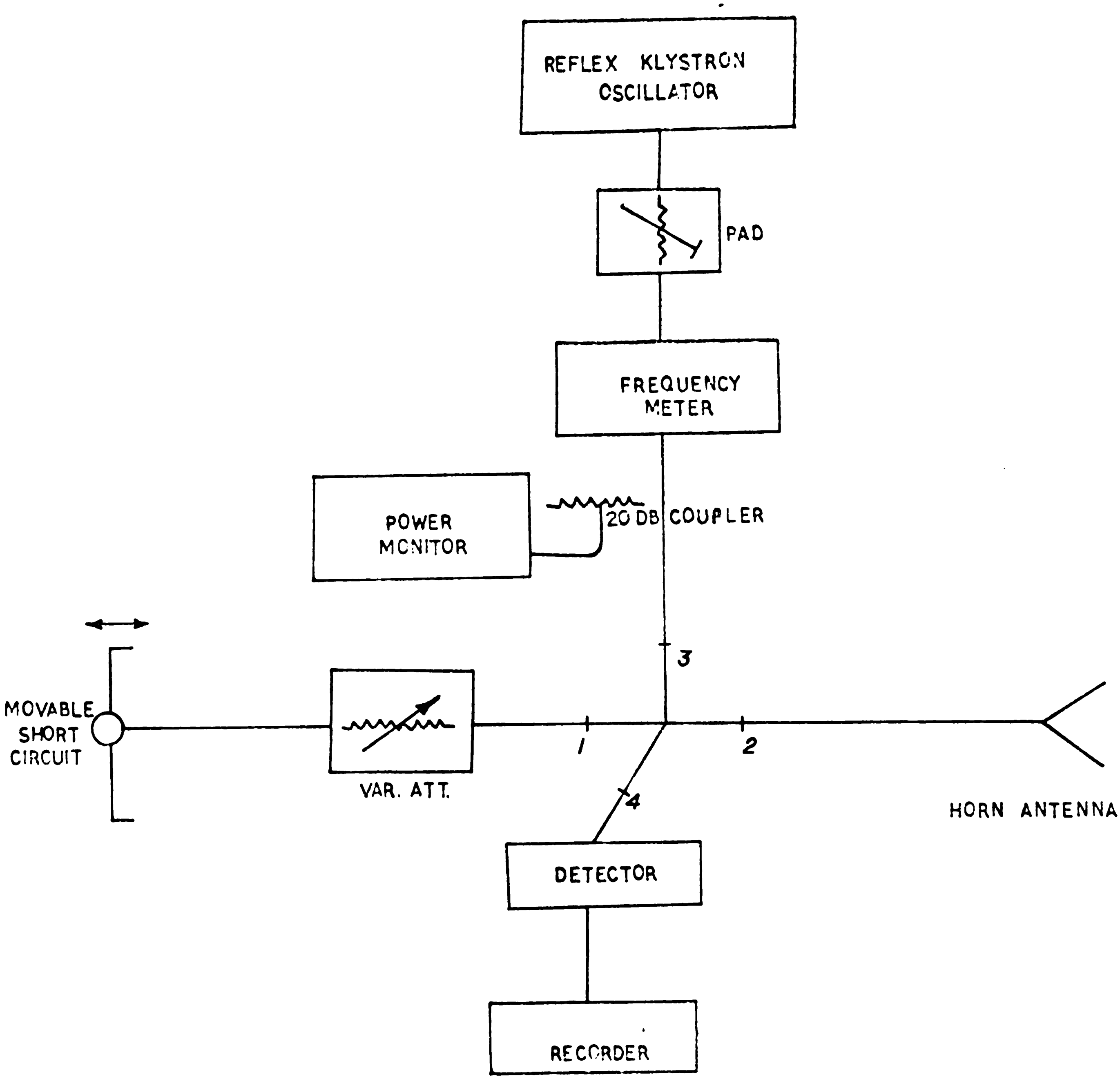

Fig. 5.1.1. Circuit diagram of an interferometer using a magic tee

(so far, it may be magnitude or phase detector) is connected to port 4 (E-arm). A variable attenuator and an adjustable short is connected at port 1, and an antenna at the port 2. When the EM wave is radiated by the antenna, it hits the different objects and the backscattered field is intercepted by the antenna and this signal works as an input to port 2. Hence, the effective impedance connected to port 2 may be considered as the antenna impedance and the impedance offered by different objects connected in parallel, through a transmission line of length ℓ. Now, if some parts of an object are vibrating, then the length ℓ and the impedance for that region is also changing, which, in turn, affects the reflection coefficient (both, magnitude and phase) at port 2. Hence, it can be assumed that an effective impedance $Z(t)$ is connected at port 2 [17, 18], which gives rise to a reflection coefficient $\Gamma_R(t)$ at this port. Also, it can be assumed for generality, that the detector gives rise to a reflection coefficient of Γ_D at port 4, attenuator and the short offers a reflection coefficient Γ_A at port 1. The source is also mismatched with a reflection coefficient of Γ_G at port 3. Hence, it can be described in terms of scattering parameters as follows [19],

$$\begin{bmatrix} b_1 \\ b_2 \\ b_3 \\ b_4 \end{bmatrix} = \begin{bmatrix} S_{11} & S_{12} & S_{13} & S_{14} \\ S_{21} & S_{22} & S_{23} & S_{24} \\ S_{31} & S_{32} & S_{33} & S_{34} \\ S_{41} & S_{42} & S_{43} & S_{44} \end{bmatrix} \begin{bmatrix} a_1 \\ a_2 \\ a_3 \\ a_4 \end{bmatrix} \tag{5.1.1}$$

Where a_i and b_i are the incoming signal to and the outgoing signal from the ith port of the magic tee junction, respectively. Furthermore, a_i and b_i are related as

$$a_1 = \Gamma_A b_1 \tag{5.1.2}$$

$$a_2 = \Gamma_R(t) b_2 \tag{5.1.3}$$

$$a_3 = b_G + \Gamma_G b_3 \tag{5.1.4}$$

$$a_4 = \Gamma_D b_4 \tag{5.1.5}$$

If the four port magic tee junction is perfect, the equation (5.1.1) may be written as

$$\begin{bmatrix} b_1 \\ b_2 \\ b_3 \\ b_4 \end{bmatrix} = \frac{1}{\sqrt{2}} \begin{bmatrix} 0 & 0 & 1 & 1 \\ 0 & 0 & -1 & 1 \\ 1 & -1 & 0 & 0 \\ 1 & 1 & 0 & 0 \end{bmatrix} \begin{bmatrix} \Gamma_A b_1 \\ \Gamma_R(t) b_2 \\ b_G + \Gamma_G b_3 \\ \Gamma_D b_4 \end{bmatrix} \tag{5.1.6}$$

Equation (5.1.6) represents 4 equations in 4 unknowns, viz, b_1, b_2, b_3 and b_4 which can be solved for known excitation b_G. However, the behaviour of b_4/b_G only need to be studied for the present problem. From equation (5.1.6),

$$\sqrt{2} b_1 \quad - \Gamma_G b_3 - \Gamma_D b_4 = b_G \tag{5.1.7}$$

$$\sqrt{2} b_2 + \Gamma_G b_3 - \Gamma_D b_4 = -b_G \tag{5.1.8}$$

$$-\Gamma_A b_1 + \Gamma_R(t) b_2 + \sqrt{2} b_3 = 0 \tag{5.1.9}$$

and,

$$-\Gamma_A b_1 - \Gamma_R(t) b_2 \qquad + \sqrt{2}\, b_3 = 0 \tag{5.1.10}$$

Thus, from equations (5.1.7) to (5.1.10),

$$\frac{b_4}{b_G} = \frac{\Gamma_A - \Gamma_R(t)}{2 - \Gamma_G \Gamma_R(t) - \Gamma_D \Gamma_R(t) - \Gamma_G \Gamma_A - \Gamma_D \Gamma_A + 2\Gamma_G \Gamma_D \Gamma_A \Gamma_R(t)} \tag{5.1.11}$$

Now, if source and detector are matched, $\Gamma_G = \Gamma_D = 0$, and equation (5.1.11) reduces to,

$$\frac{b_4}{b_G} = \frac{\Gamma_A - \Gamma_R(t)}{2} \tag{5.1.12}$$

Thus, equation (5.1.12) represents the ideal case. It is to be noted that if the source and/or detector is not matched, equation (5.1.11) should be used, while the imperfections of the magic tee can be incorporated by including appropriate coefficitents of [S] in equation (5.1.1) at the first place.

If $\Gamma_A = \rho_A \exp(-j\theta_A)$ and $\Gamma_R(t) = [\rho_R + \Delta\rho u_1(t) \exp\{-j\Delta\theta u_2(t)\}] \cdot \exp(-j\theta_R)$

Where $u_1(t)$ and $u_2(t)$ are arbitrary time function representing the effect due to the vibration of the body and $\rho_R \exp(-j\theta_R)$ represents the clutter, then,

$$\frac{b_4}{b_G} = \tfrac{1}{2}[\rho_A \exp(-j\theta_A)-\rho_R \exp(-j\theta_R)-\Delta\rho u_1(t) \exp\{-j[\theta_R + \Delta\theta u_2(t)]\}] \quad (5.1.13)$$

Therefore,

$$\begin{aligned}|b_4/b_G|^2 = \tfrac{1}{4}[\rho_A^2 + \rho_R^2 + \{\Delta\rho u_1(t)\}^2 - 2\rho_R\rho_A \cos(\theta_R-\theta_A) \\ - 2\rho_A\Delta\rho u_1(t) \cos\{\theta_R-\theta_A + \Delta\theta u_2(t)\} \\ + 2\rho_R\Delta\rho u_1(t) \cos\{\Delta\theta u_2(t)\}]\end{aligned} \quad (5.1.14)$$

If the attenuator and variable short is adjusted in such a way that $\rho_A = \rho_R$ and $\theta_A = \theta_R$, so that the clutter is cancelled, then equation (5.1.14) reduces to,

$$|b_4/b_G|^2 = \{\frac{\Delta\rho}{2} u_1(t)\}^2 \quad (5.1.15)$$

The phase angle θ_4 of b_4/b_G can be found from equation (5.1.13) as,

$$\theta_4 = \text{arc tan}\left[\frac{-\rho_A \sin\theta_A + \rho_R \sin\theta_R + \Delta\rho u_1(t)\sin\{\theta_R + \Delta\theta u_2(t)\}}{\rho_A \cos\theta_A - \rho_R \cos\theta_R - \Delta\rho u_1(t)\cos\{\theta_R + \Delta\theta u_2(t)\}}\right] \quad (5.1.16)$$

For $\rho_A = \rho_R$ and $\theta_A = \theta_R$, it reduces to,

$$\theta_4 = -\theta_R - \Delta\theta u_2(t) \quad (5.1.17)$$

Thus from equations (5.1.15) and (5.1.17), it may be noted that the magnitude detectors, which behave as square-law, will respond to the square of the half of the variations, while the phase detectors will respond linearly. Since these variations are assumed very small, the phase detectors may be preferred over the magnitude detectors for relatively large sensitivity.

5.2 Analysis of the circulator system

Figure 5.2.1 illustrates a simplified circuit using a three port circulator which can be used for detecting the breathing and heart signals. As discussed in the preceding section, the antenna is replaced by a load which offers a reflection coefficient $\Gamma_R(t)$. In general, any three port network can be described by,

$$\begin{bmatrix} b_1 \\ b_2 \\ b_3 \end{bmatrix} = \begin{bmatrix} S_{11} & S_{12} & S_{13} \\ S_{21} & S_{22} & S_{23} \\ S_{31} & S_{32} & S_{33} \end{bmatrix} \begin{bmatrix} a_1 \\ a_2 \\ a_3 \end{bmatrix} \tag{5.2.1}$$

Where a's and b's are as defined in the preceding section, and for the present system (tuner connected at port 2 in Figure 5.2.1 is ignored for time being),

$$a_1 = b_G + \Gamma_G\, b_1 \tag{5.2.2}$$

$$a_2 = \Gamma_R(t)\, b_2 \tag{5.2.3}$$

and

$$a_3 = \Gamma_D\, b_3 \tag{5.2.4}$$

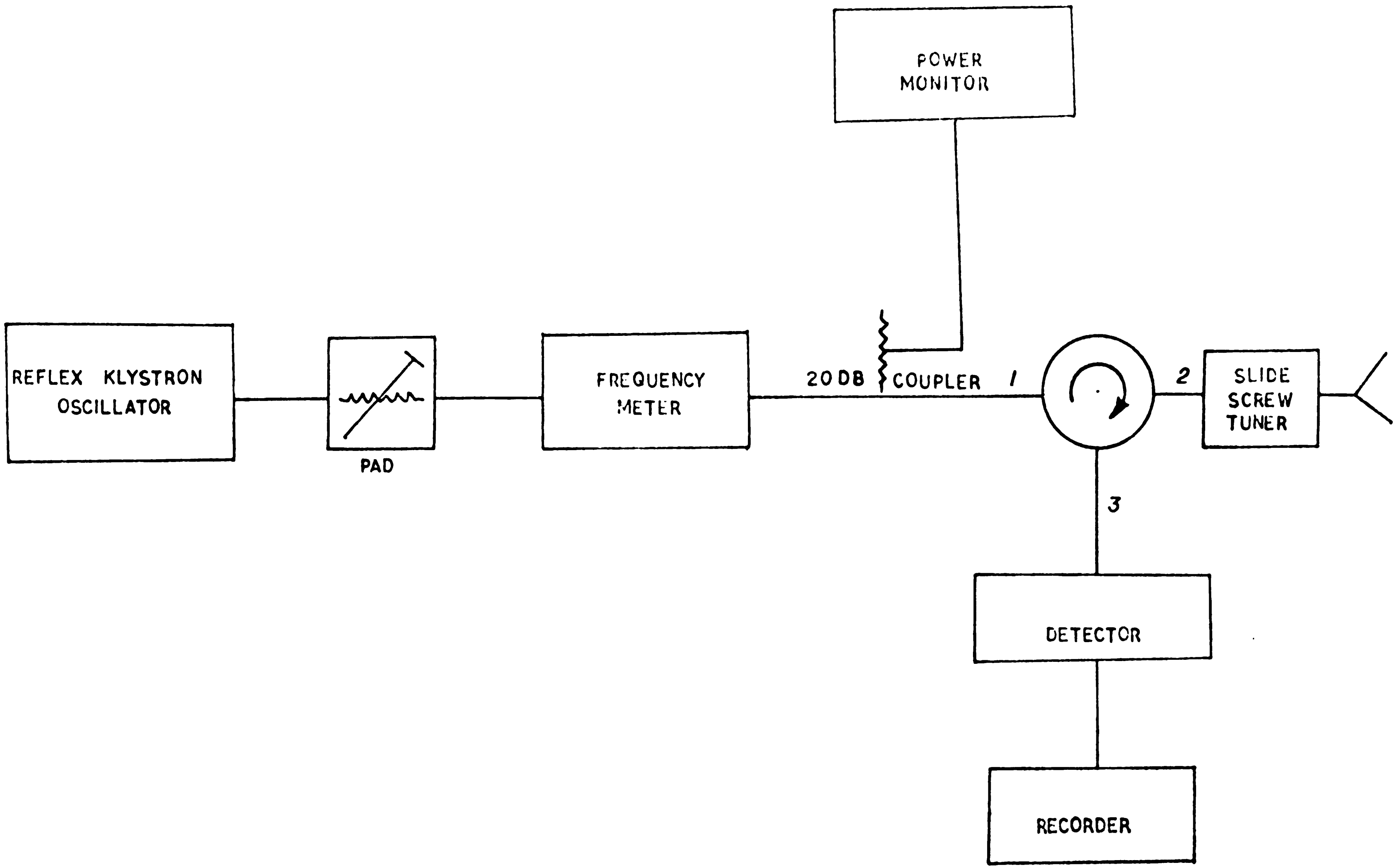

Fig.5.2.1. Circuit diagram of an interferometer using a circulator.

Thus, equations (5.2.1) - (5.2.4) give three algebraic equations in three unknowns, viz, b_1, b_2 and b_3, which can be solved easily. However, for the present problem, only b_3/b_G is of interest. Further, assuming that the three port circulator is an ideal circulator, its scattering matrix may be found as [20],

$$[S] = \begin{bmatrix} 0 & 0 & 1 \\ 1 & 0 & 0 \\ 0 & 1 & 0 \end{bmatrix} \tag{5.2.5}$$

Hence, from equations (5.2.1) - (5.2.5), b_3/b_G is found as,

$$\frac{b_3}{b_G} = \frac{\Gamma_R(t)}{1 - \Gamma_D\Gamma_G\Gamma_R(t)} \tag{5.2.6}$$

It can be simplified further assuming that the source and the detector are matched such that $\Gamma_G = \Gamma_D = 0$. Therefore,

$$b_3/b_G = \Gamma_R(t) \tag{5.2.7}$$

If

$$\Gamma_R(t) = [\rho_R + \Delta\rho u_1(t)\exp\{-j\Delta\theta u_2(t)\}]\exp(-j\theta_R)$$

Where $\rho_R \exp(-j\theta_R)$ is due to clutter and $\Delta\rho u_1(t)\exp\{-j\theta_R-j\Delta\theta u_2(t)\}$ is due to the vibration of the body, then the phase, θ_3, and the square of the magnitude of b_3/b_G is found as,

$$\theta_3 = \arctan\left[\frac{-\rho_R\sin\theta_R - \Delta\rho u_1(t)\sin\{\theta_R + \Delta\theta u_2(t)\}}{\rho_R\cos\theta_R + \Delta\rho u_1(t)\cos\{\theta_R + \Delta\theta u_2(t)\}}\right] \tag{5.2.8}$$

and

$$|b_3/b_G|^2 = \rho_R^2 + \{\Delta\rho u_1(t)\}^2 + 2\rho_R\Delta\rho u_1(t)\cos\{\Delta\theta u_2(t)\} \qquad (5.2.9)$$

Now, if the tuner connected at port 2 of the circulator is adjusted such that $\rho_R = 0$, or the clutter is cancelled, equations (5.2.8) and (5.2.9) reduce to,

$$\theta_3 = -\theta_R - \Delta\theta u_2(t) \qquad (5.2.10)$$

and

$$|b_3/b_G|^2 = [\Delta\rho u_1(t)]^2 \qquad (5.2.11)$$

Comparing equations (5.2.10) and (5.2.11) with (5.1.17) and (5.1.15), respectively, it may be noted that both systems have similar response. However, the circulator system has an advantage of having a 6 dB higher magnitude of the return signal in comparison to magic tee system.

5.3 The magic tee system for life detection

The schematic diagram of the X-band life detection system using a magic tee is shown in Figure 5.3.1. A klystron microwave generator generates a c.w. microwave at 9.35GHz with a power of about 10 mW. This wave is passed through an isolator, a frequency meter, a fixed attenuator, another isolator and a tuner before entering arm 1 of the hybrid T. This incoming wave is divided into arms 2 and 3 of the hybrid T. One wave $E_1 = A_1 \cos \omega t$ coming out of arm 2 of the hybrid T passes

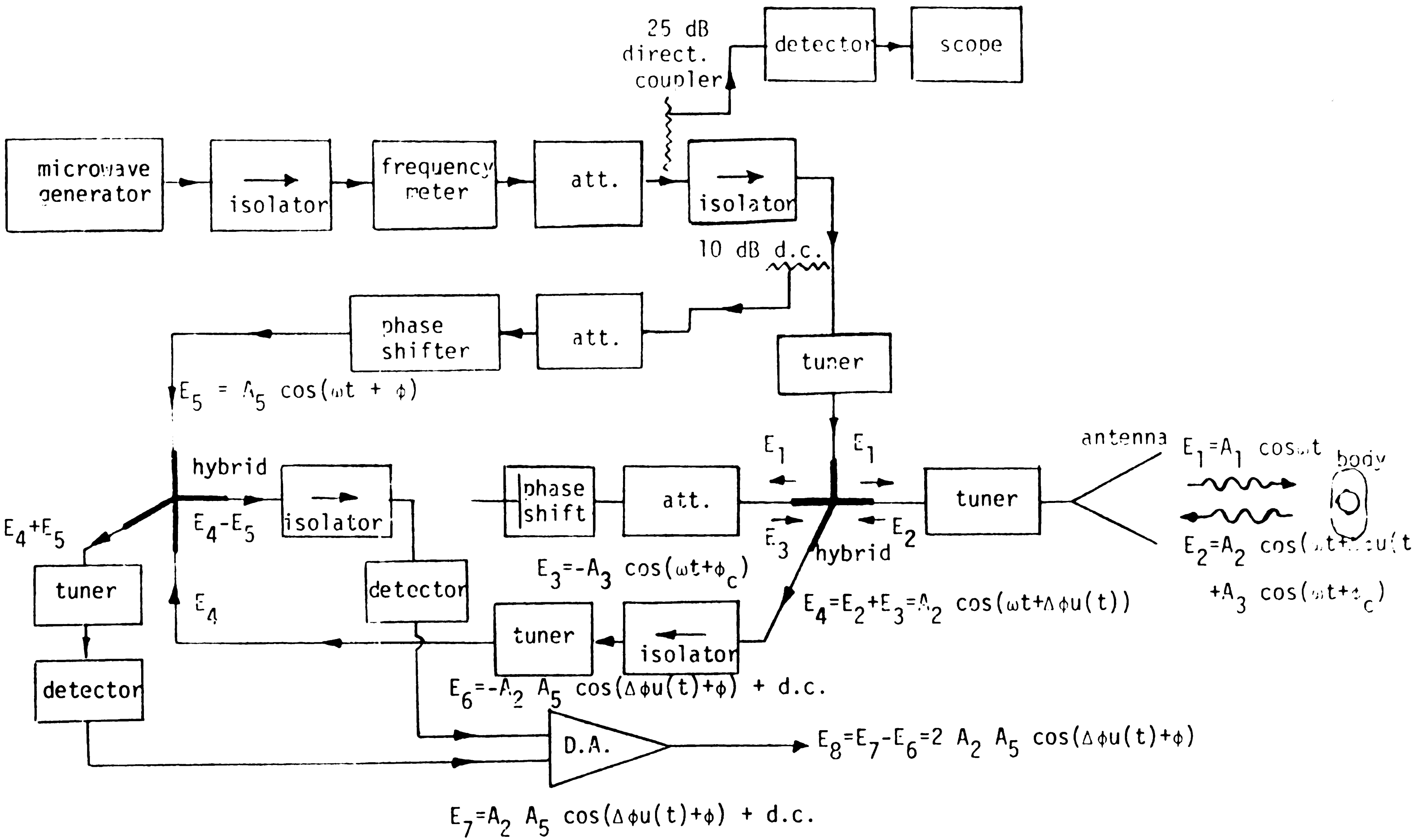

Fig.5.3.1 Schematic diagram of the x-band life detection system.

through another tuner and then radiates out through the antenna. In the beginning, the two tuners are adjusted in such a way that hybrid T behaves as a magic tee [21]. The wave radiated through the antenna illuminates the subject and the surrounding, and the reflected wave E_2 coming back to the antenna may consist of a scattered wave modulated by the subject's body motion caused by heart beat and breathing and a clutter wave reflected by the stationary surrounding. The modulated signal can be expressed as $A_2 \cos(\omega t + \Delta\phi u(t))$, where $\Delta\phi u(t)$ represents the phase perturbation caused by the heart beat and the breathing. The clutter wave can be expressed as $A_3 \cos(\omega t + \phi_c)$. Another wave E_1 coming through arm 3 of the hybrid T gives a reflected wave, $E_3 = -A_3 \cos(\omega t + \phi_c)$, which is the negative of the clutter wave, when the variable attenuator and the variable phase shifter (variable short) are properly adjusted. When E_2 and E_3 are combined in the hybrid T, the clutter wave is cancelled and the resultant wave E_4 coming out of arm 4 of the hybrid T contains only the modulated wave, $A_2 \cos(\omega t + \Delta\phi u(t))$. It is now aimed to measure the phase perturbation $\Delta\phi u(t)$ by mixing E_4 with a reference wave $E_5 = A_5 \cos(\omega t + \phi)$ in the second hybrid T (it is also tuned to behave like a magic tee). E_4 is fed into an arm of the second hybrid T after passing through an isolator and a tuner. The reference wave E_5 is obtained from the main wave-guide through a 10 dB directional coupler and its amplitude and phase are adjusted by a variable attenuator and a variable phase shifter before it is fed into another arm of the second hybrid T. The phase ϕ of E_5 is adjusted in such a way to maximize the sensitivity in the detection of $\Delta\phi u(t)$. As E_4 and E_5 are fed into two arms of the second hybrid T, two outputs from two other arms of the second hybrid T take the forms of E_4-E_5 and E_4+E_5. When these two waves are detected, the resultant outputs are E_6 and E_7. The wave E_6 consists of $-A_2A_5 \cos(\Delta\phi u(t) + \phi)$ and a d.c. component and, similarly, E_7 includes $A_2A_5 \cos(\Delta\phi u(t) + \phi)$ and a d.c. component. When E_6 and E_7 are fed into a differential amplifier, it gives an output of $2\ A_2A_5 \cos(\Delta\phi u(t) + \phi)$. This output signal is of extremely low frequency (heart beat or breathing frequency) and can be measured by a scope, a chart recorder or an acoustic indicator.

The typical measured heart and breathing signals by this X-band life detection system are shown in Figure 5.3.2. Figure 5.3.2(a) shows the recorded heart signals when the human subject was sitting at a distance of 17 feet facing the antenna which radiated a power of 4.5 mW at 9.35GHz. The heart signal was recorded when the subject was holding the breath. In this figure, the heart beat is clearly observed at an interval of about 0.87 second. The large signals at both ends of the recording are due to the breathing. As the distance between the human subject and the antenna was increased beyond 20 feet, the heart signal became obscure. However, the breathing signal was detected at a distance of upto about 90 feet. Figure 5.3.2(b) shows the recorded breathing signal of the human subject who sat at a distance of 80 feet facing the antenna. The subject was breathing at an interval of 2 to 3 seconds.

A significant improvement in the performance of the system was found when a phase-locked oscillator was used in place of klystron

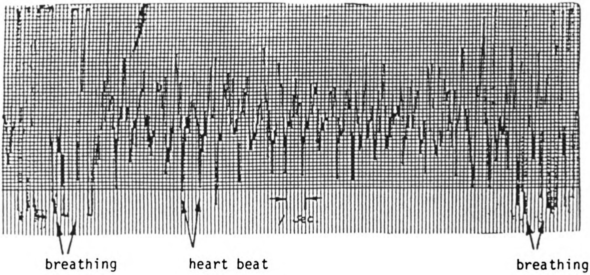

(a) Recorded heart signal; the human subject holding the breath at the distance of 17 feet. The heart beat is clearly seen at an interval of about 0.87 second. The large signals at both ends of the recording are due to breathing. The antenna radiated power is 4.5 mW.

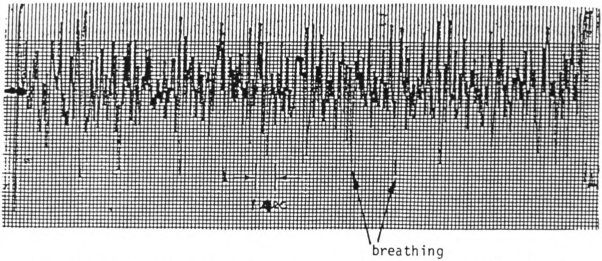

(b) Recorded breathing signal; the human subject at the ditance of 80 feet was breathing at an interval of 2 ~ 3 seconds. At this long distance only the breathing pattern can be clearly observed. The heart signal is immersed in the noise. The gain of the amplifier system was increased from case (a) for this recording.

Fig.5.3.2 Heart and breathing signals measured by the x-band life detection system.

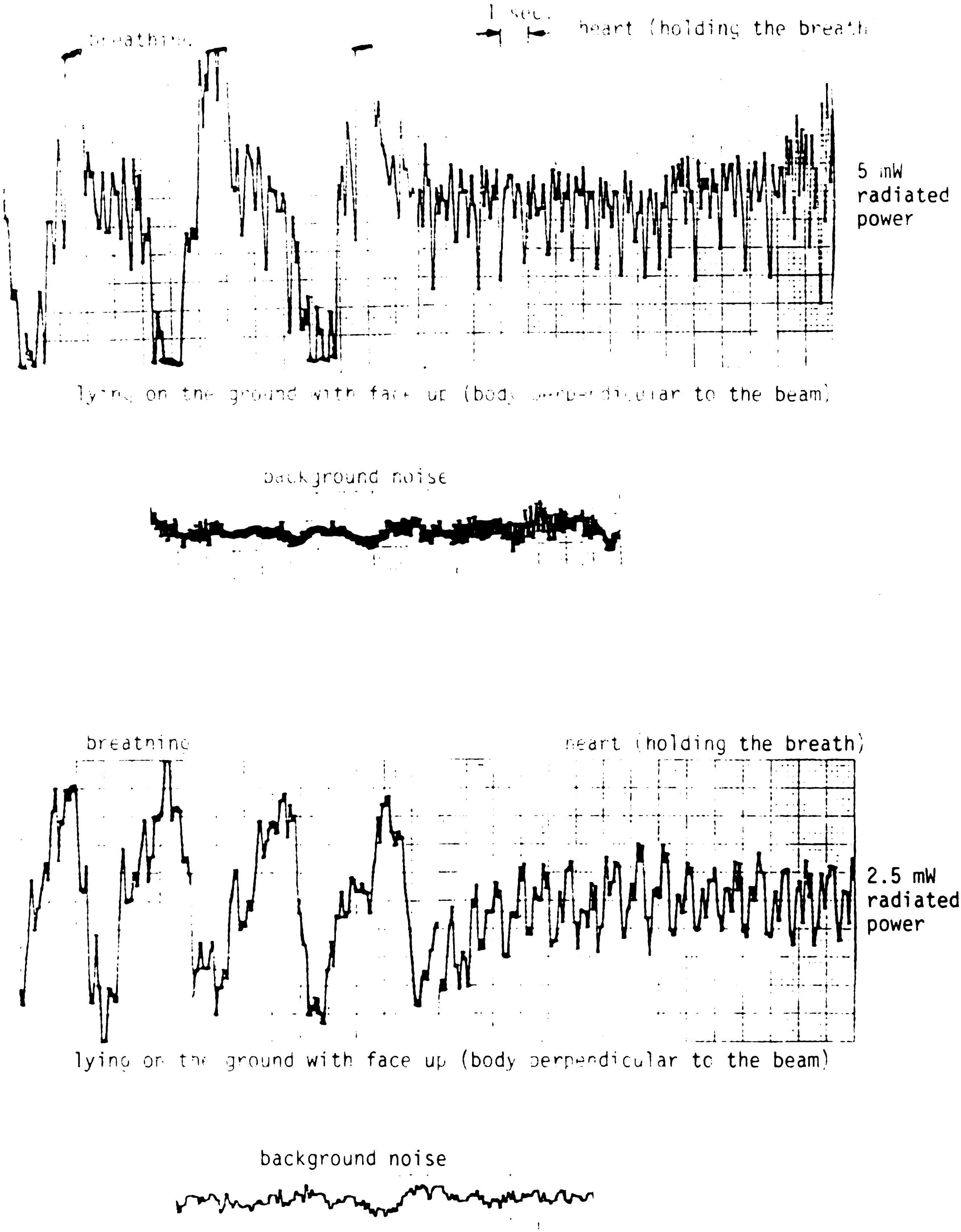

Fig5.3.3. Recorded heart and breathing signals of a human subject lying on the ground at a distance of 100 ft. The life detection system uses a magic T and the radiated power is 5 mW or 2.5 mW at 10 GHz.

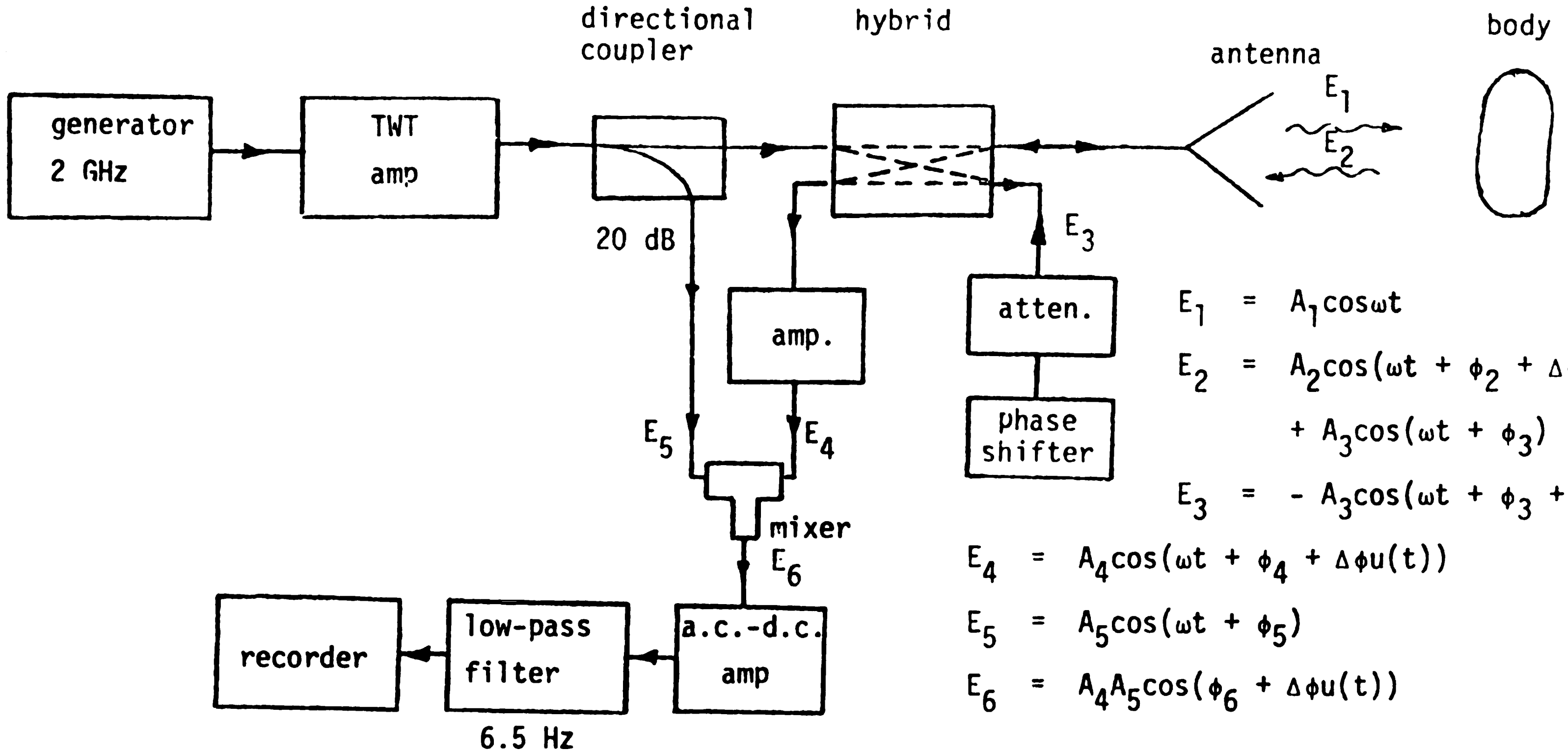

$$E_1 = A_1\cos\omega t$$

$$E_2 = A_2\cos(\omega t + \phi_2 + \Delta\phi u(t)) + A_3\cos(\omega t + \phi_3)$$

$$E_3 = -A_3\cos(\omega t + \phi_3 + 90^o)$$

$$E_4 = A_4\cos(\omega t + \phi_4 + \Delta\phi u(t))$$

$$E_5 = A_5\cos(\omega t + \phi_5)$$

$$E_6 = A_4A_5\cos(\phi_6 + \Delta\phi u(t))$$

Fig.5.3.4. **L-band life detection system**

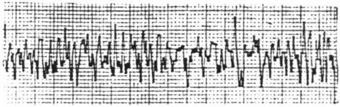

(a) background noise

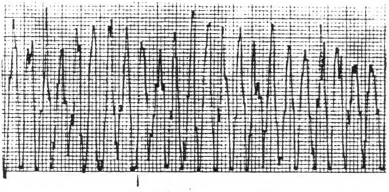

(b) recorded heart signal

Fig.5.3.5. Recorded heart signal of a human subject at a distance of 20 feet. The antenna radiated with a power of 0.5 W at 2 GHz.

source, and the second hybrid T detection scheme was replaced by a low-noise double-balanced mixer. After using a 30 dB microwave amplifier before double-balanced mixer, the system was able to pick the heart and breathing signals of a human subject lying on the ground at a distance of over 100 feet. Figure 5.3.3 depicts these results for a radiated power of 5 mW as well as 2.5 mW.

A similar detection system was realized in L-band at 2.0GHz using a 90^{o} hybrid, as shown in Figure 5.3.4. The recorded heart signal of a human subject at a distance of 20 feet are shown in Figure 5.3.5 alongwith the background noise. In this case noise level was high probably because of relatively less stable generator, and higher noise figure of TWT amplifiers and the mixer used in the system.

5.4 The circulator system for life detection

The schematic diagram of the X-band life detection system using a circulator is shown in Figure 5.4.1. A phase locked oscillator at 10GHz produces a stable output of about 20 mW. This output is amplified by a low-noise microwave amplifier to a power level of about 200 mW. The output of the amplifier is fed through a 6 dB directional coupler, a variable attenuator, a circulator and then to a horn antenna. The 6 dB directional coupler branches out 1/4 of the amplifier output to provide for a reference signal for clutter cancellation and another reference signal for the mixer. The variable attenuator controls the power level of the microwave to be radiated by the antenna. Usually, the radiated power was kept below 20 mW only. The microwave signal coming out of the variable attenuator is fed to the horn antenna through

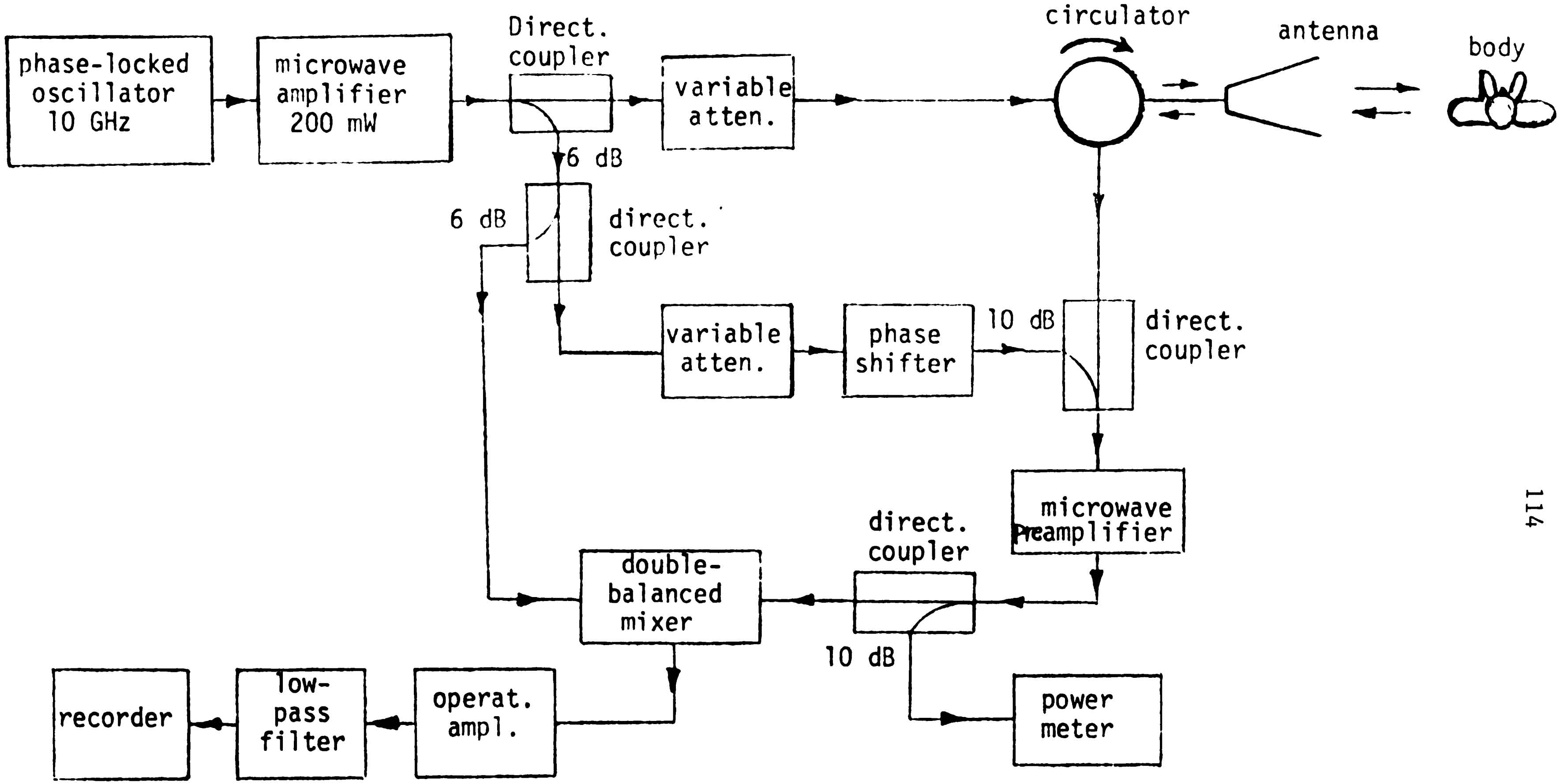

Fig. 5.4.1. Circuit diagram of the distant life detection system (without signal processing system).

a circulator. The horn antenna radiates a microwave beam of about 10^{o} beamwidth aiming at the human subject lying on the ground. The received signal by the antenna consists of a large clutter and a weak return signal scattered from the body. The large clutter signal is cancelled by a reference signal, the amplitude and phase of which are adjusted by a variable attenuator and a phaseshifter, in a 10 dB directional coupler. After this clutter cancellation, the output of the 10 dB directional coupler contains only the weak scattered signal from the body. This body-scattered signal is a 10GHz cw microwave modulated by the breathing and the heart beat. This signal is then amplified by a low-noise microwave preamplifier of 30 dB gain. The amplified, body-scattered signal is then mixed with another reference signal in a double-balanced mixer. In between the microwave preamplifier and the double-balanced mixer, a 10 dB directional coupler is inserted to take out a small portion of the amplified signal for monitoring its intensity. This monitoring is mainly for checking how well the clutter is cancelled. The mixing of the amplified, body-scattered signal and a reference signal (7 ~ 10 mW) in the double-balanced mixer produces a low frequency breathing and heart signals which modulate the scattered microwave from the body. This output from the mixer is amplified by an operational amplifier and then it passes through a low-pass filter (4 Hz cut-off) before reaching a recorder.

The typical measured breathing and heart signals are shown in Figures 5.4.2 - 5.4.4. For the results shown in Figure 5.4.2, the antenna radiated with a power of 45 mW at 10GHz and the microwave

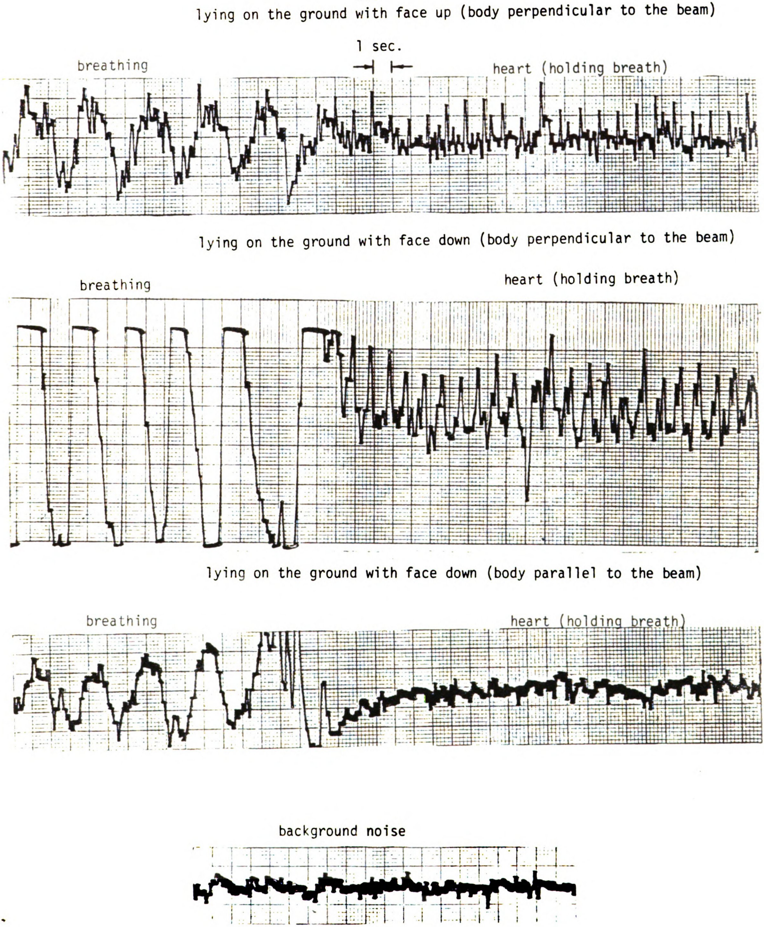

Fig.5.4.2 Heart and breathing signals of a human subject lying on the ground measured at a distance of 100 ft. with a power of 45 mW at 10 GHz.

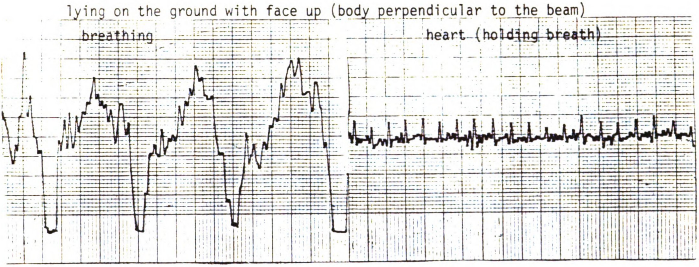

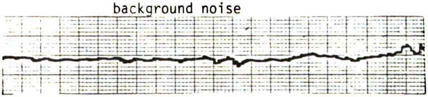

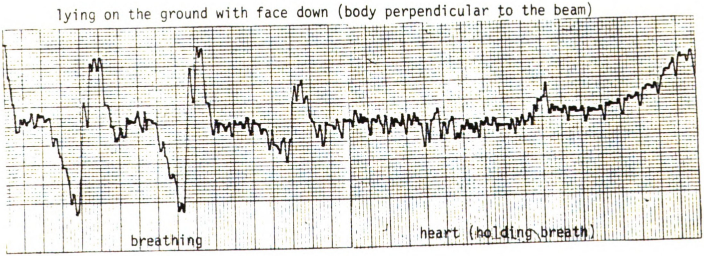

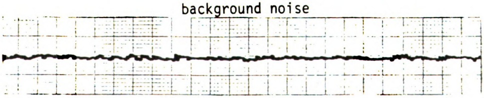

Fig.5.4.3. Heart and breathing signals of a human subject lying on the ground measured at a distance of 100 ft. with a power of 11.25 mW at 10 GHz. (Amplifier gain increased).

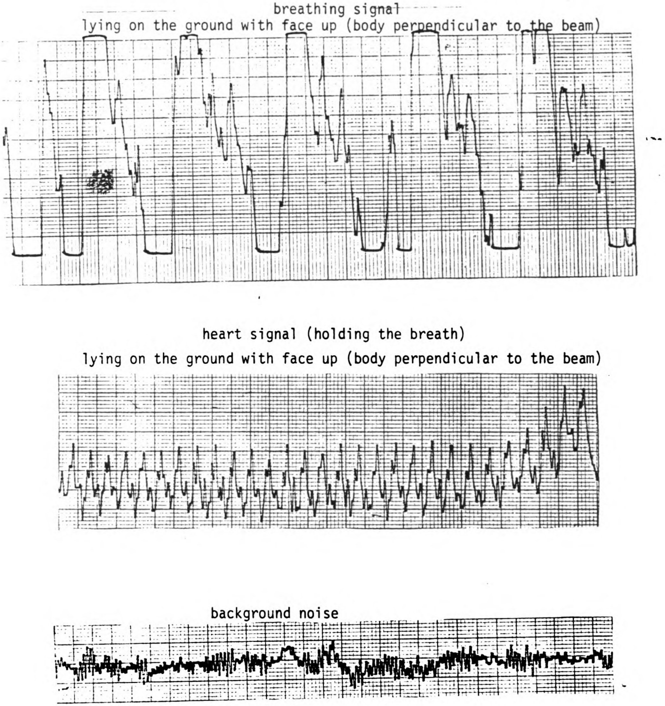

Fig.5.4.4.Heart and breathing signals of a human subject lying on the ground at a distance of 100 ft. measured with a microwave beam with a power of 4.5 mW at 10 GHz. (Amplifier gain further increased).

beam was aimed at a human subject lying on the ground at a distance of 100 feet. The top figure shows the results when the subject's body with face-up was perpendicular to the direction of the microwave beam. The left portion of this figure shows the breathing signals (superimposed with the heart signals) and the right portion of the figure indicates only the heart signal when the subject held the breathing. In this figure, both the breathing and heart signals are clearly recorded. The second figure from the top of Figure 5.4.2 shows the recorded breathing and heart signals when the same subject lay face-down on the ground at the same location. It is interesting to observe that with the face-down position, the breathing and heart signals unexpectedly became stronger than the face-up case. The third figure from the top of Figure 5.4.2 shows the recorded breathing and heart signals when the position of the human subject was rotated to the direction parallel to the microwave beam. For this case, the breathing signal was clearly measured but the heart signal became rather obscure. It was found that when the body position was slightly adjusted, the heart signal could be enhanced. The bottom figure of Figure 5.4.2 shows the recorded background noise. It is noted that the background noise varied from day to day depending on the movement of the machines, air conditioners and elevators in the building. On some occasions when the background noise was lower, it was easier to measure heart signals of human subjects lying in various positions at a distance of 100 feet or farther.

Figure 5.4.3 shows the measured breathing and heart signals of the same human subject when the antenna radiated power was reduced to 11 mW and the gain of the operational amplifier was increased. The

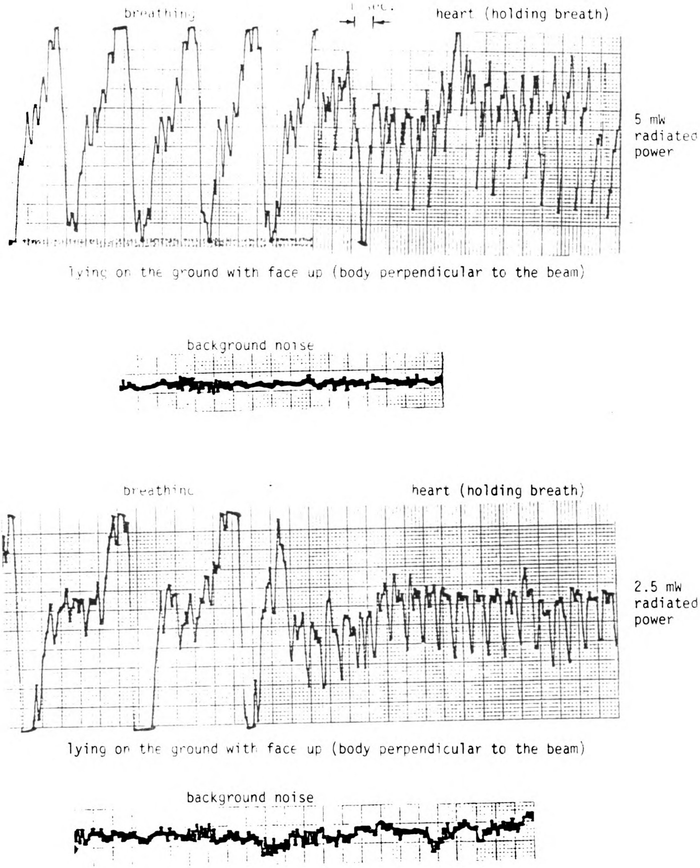

Fig 5.4.5. Recorded heart and breathing signals of a human subject lying on the ground at a distance of 100 ft. The life detection system uses a circulator and the radiated power is 5 mW or 2.5 mW at 10 GHz.

human subject lay at a distance of 100 feet with face-up or face-down position and with the body perpendicular to the direction of the microwave beam. It is observed in this figure that the breathing and heart signals were clearly recorded and the background noise was also reduced.

Figure 5.4.4 shows the measured breathing and heart signals of the same human subject lying at the same location when the antenna radiated power was further reduced to 4.5 mW and the gain of the operational amplifier was increased further. Surprisingly, with a lower radiated power the recorded heart signal seemed to be even clearer than the previous cases of higher radiated power. This phenomenon may be explained as follows. As the radiated power is increased, the clutter and the body scattered signals are both increased and when they exceed a certain level the microwave preamplifier may start to saturate. Therefore, the increase in the antenna radiated power may not enhance the amplitude and quality of the measured breathing and heart signals. Figure 5.4.5 illustrates the breathing and hearth signals of a human subject lying on the ground at a distance of 100 feet with radiated power of 5 mW or 2.5 mW only.

5.5 Effects of clutter cancellation, polarization, and the clothing of the human subject on the system performance

When the life detection system operates at different backgrounds, the nature of the clutter also varies. With the present system, it is easy to cancel or minimize different clutters with amplitude and phase adjustment in the cancellation circuit. When the clutter is not cancelled, the sum of the clutter and the body scattered signal can easily saturate the microwave preamplifier, and consequently, leading to the failure of heart signal detection. To study this effect a series of experiments were performed and the results are shown in Figures 5.5.1 - 5.5.2. In this series of experiments, the antenna radiated power was kept constant while the level of uncancelled clutter was varied by detuning the clutter cancellation circuit. The top figure of Figure 5.5.1 shows the recorded breathing and heart signals when the power level after the microwave preamplifier was 3 mW. This condition represents a good cancellation of the clutter and a significant portion of the input signal to the microwave preamplifier may consist of the body-scattered wave modulated by the heart beat. Because of this condition, the breathing and heart signals were clearly detected. The second figure from the top of Figure 5.5.1 indicates the recorded breathing and heart signals when the clutter was not very well cancelled, by purposely detuning the clutter cancellation circuit slightly, and the power level after the microwave preamplifier was increased to 5 mW. This increase in the output power of the microwave preamplifier was entirely due to an increased level of the uncancelled clutter because the antenna radiated power and the position of the human subject were unchanged from the previous case. Under this condition, the breathing and heart signals were still clearly recorded, implying that the microwave preamplifier was still working in the linear range. When the uncancelled clutter was further increased to a level that the microwave preamplifier output reached 60 mW, the recorded breathing and heart signals start to deteriorate as shown in the third figure from the top in Figure 5.5.1. This phenomenon clearly indicates the start of the saturation of the microwave preamplifier.

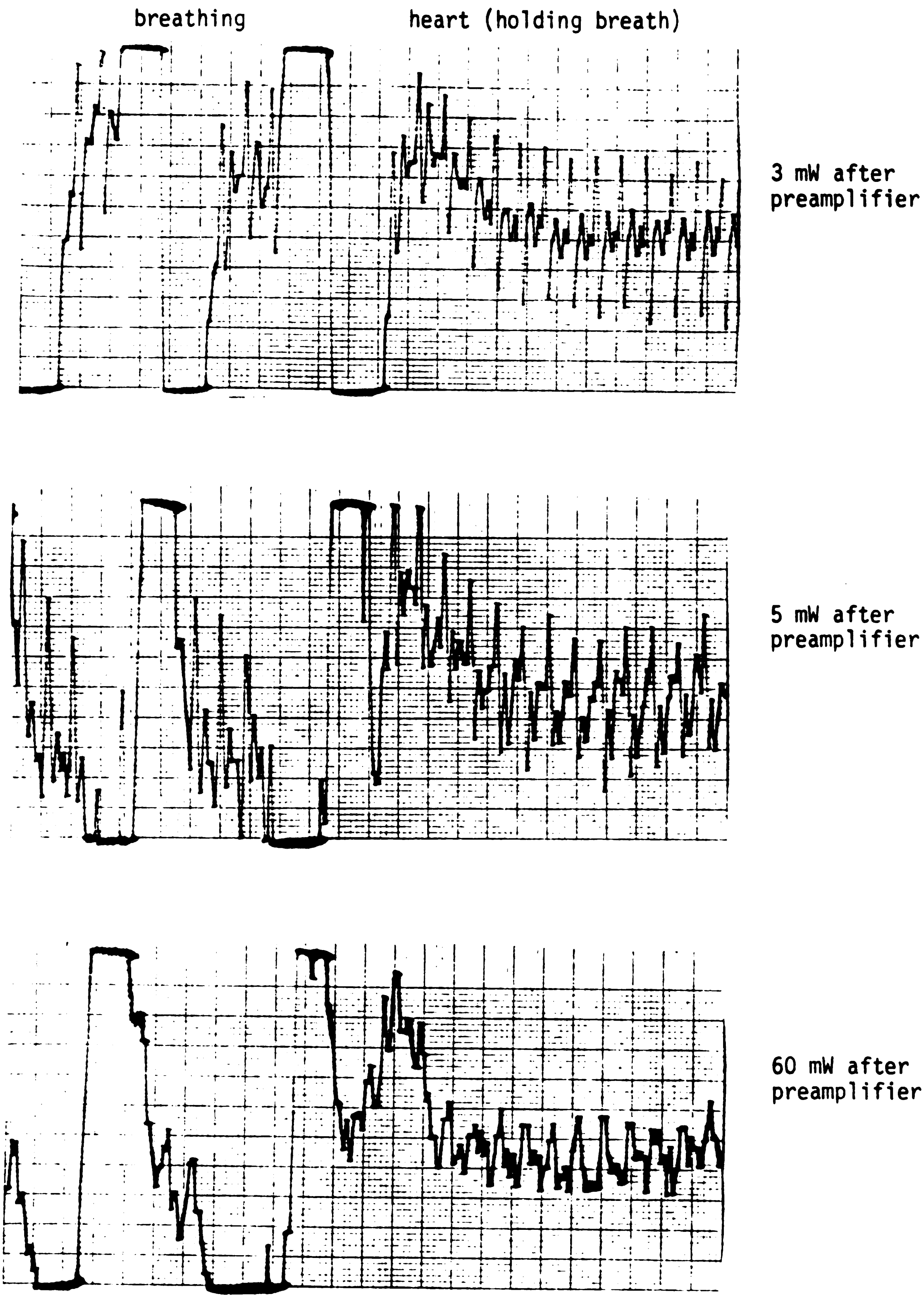

Fig.5.5.1.Performance of the system as a function of signal power level (heart signal plus clutter) input to the mixer.

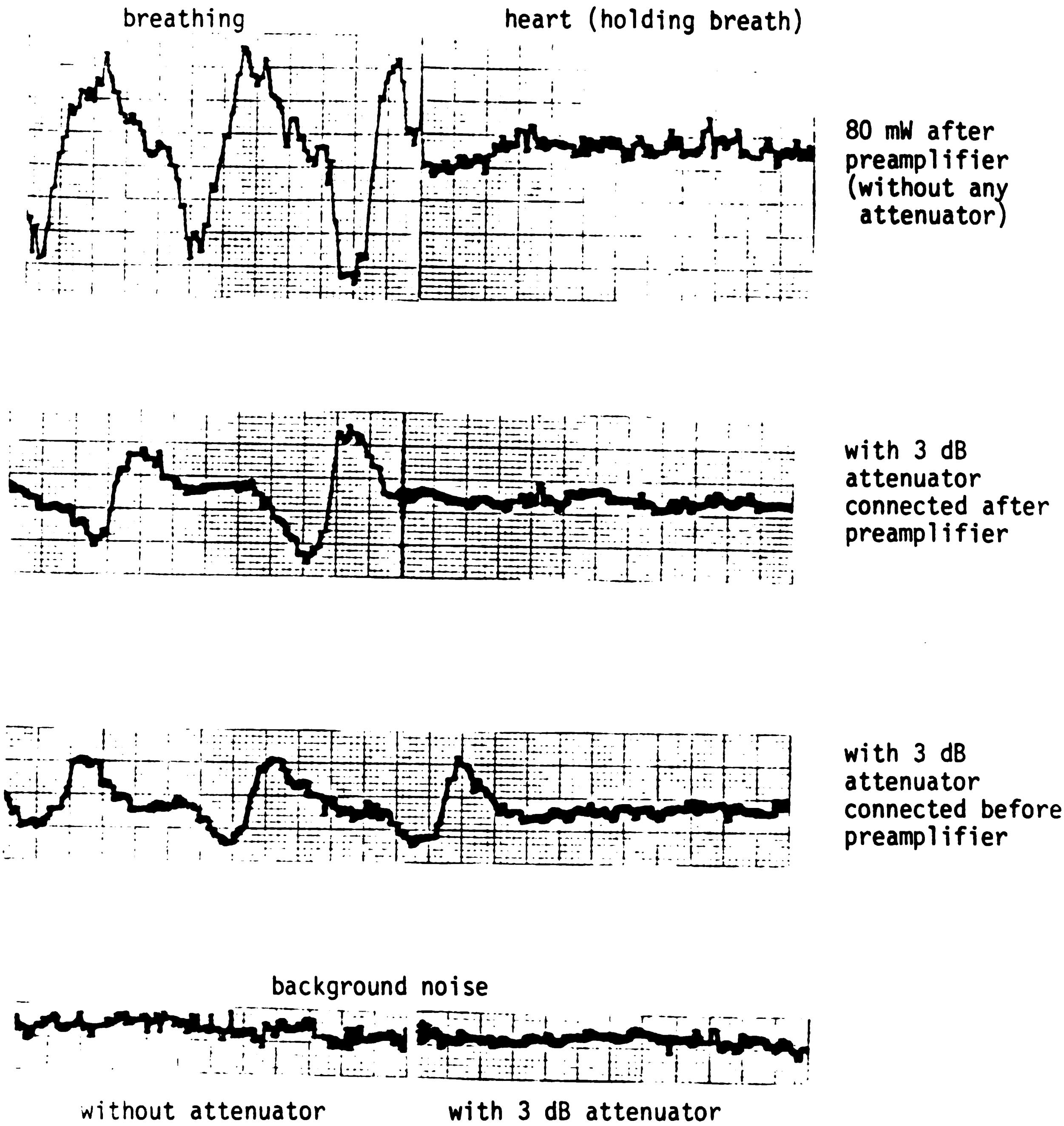

Fig.5.5.2 Effect of microwave preamplifier saturation on the system performance. The output of the preamplifier was 80 mW and the preamplifier was saturated due to a large uncancelled clutter. Under this condition, the heart signal was obscure even though the breathing signal was detectable. A 3 dB attenuator connected after the preamplifier can not recover the heart signal. The attenuator connected before the preamplifier can neither recover the heart signal because it reduced both the clutter and the body-scattered signal input to the preamplifier.

When the uncancelled clutter was increased to a level that the output of the microwave preamplifier became more than 80 mW, the saturation of the preamplifier caused the recorded heart signal to be quite obscure even though the breathing was still very clearly recorded. This phenomenon is shown in the first figure at the top of Figure 5.5.2. To further study this effect, a 3dB attenuator was inserted after and before the microwave preamplifier in an attempt to undo the saturation of the preamplifier. In either case, a clear heart signal could not be recovered due to the following probable reasons. When the 3dB attenuator was inserted after the microwave preamplifier (the second figure from the top in Figure 5.5.2), the saturated and distorted heart signals after the preamplifier were reduced in amplitude but its quality was not improved. Also from this experiment, it is observed that the deterioration of the heart signal was not due to the saturation of the double-balanced mixer, but rather was due to the saturation of the microwave preamplifier. When the 3dB attenuator was inserted before the preamplifier to undo the saturation of the preamplifier (the third figure from the top in Figure 5.5.2), a clear heart signal was not recorded either. The reason for this result was probably due to the fact that the 3dB attenuator while reduced the clutter it also reduced the body-scattered wave. Thus, the heart signal became too weak to be detected. The bottom figures in Figure 5.5.2 show the background noise levels in the experiment.

The results of Figures 5.5.1 - 5.5.2 indicate the importance of the clutter cancellation and the operating range of the microwave preamplifier. It is essential to operate the microwave preamplifier

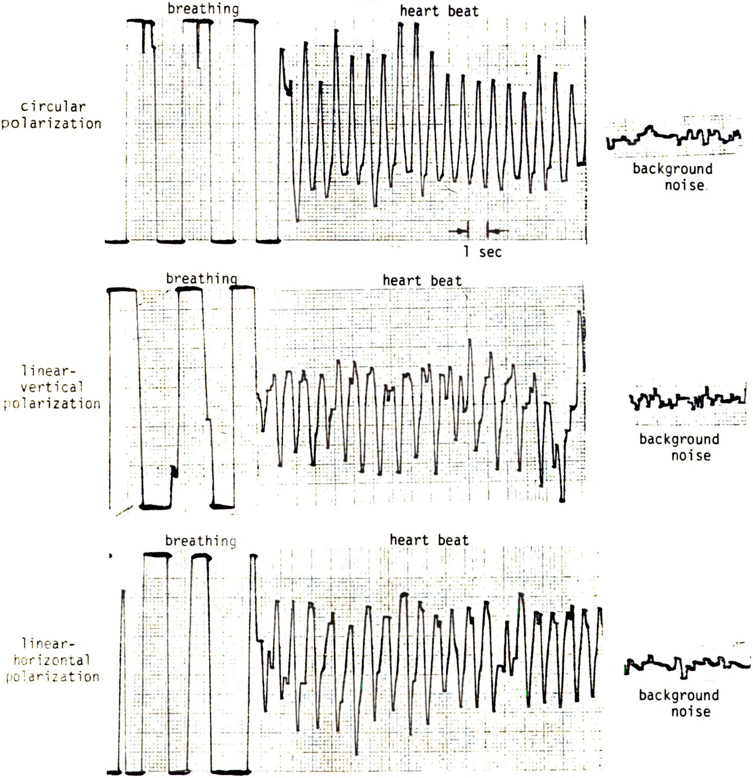

Fig.5.5.3. Measured breathing and heart signals from a human subject lying on the ground at a distance of 100 ft. with a microwave beam of 20 mW at 10 GHz with different polarizations; (1) circular polarization, (2) linear-vertical polarization and (3) linear-horizontal polarization.

in its linear range and to avoid the preamplifier saturation by a proper control of the clutter cancellation.

The second factor which may affect the system performance is the polarization of the microwave illuminating the human body. It was suspected that a certain type of polarization may lead to a best heart signal detection. To test this conjecture the circular polarization, the linear-vertical polarization, and the linear-horizontal polarization were employed. The circularly polarized wave was produced with a circularly polarized horn antenna commonly used in the car radar system. The linear-vertical and horizontal polarizations were produced by a home made pyramidal horn antenna. The results of the measured breathing and heart signals of a human subject lying on the ground at a distance of 100 feet with these three polarizations are shown in Figure 5.5.3. It is observed that the different polarizations did not cause a significant difference in the detection of breathing and heart signals when the human subject was lying on the ground at a distance of 100 feet. However, for shorter distances (20 ~ 40 feet) and the human subject lying on a metallic ground plane, the polarization effect on system performance is found to be more significant.

As one of the requirements, it is highly desirable to design a distant life detection system which performance is not significantly affected by the clothing of the human subject to be illuminated by the microwaves. Ideally, a microwave of particular frequency should be selected which can easily penetrate the clothing. It has been found that the X-band microwave at 10GHz can penetrate the clothing quite well as evidenced by the results shown in Figure 5.5.4. The top figure

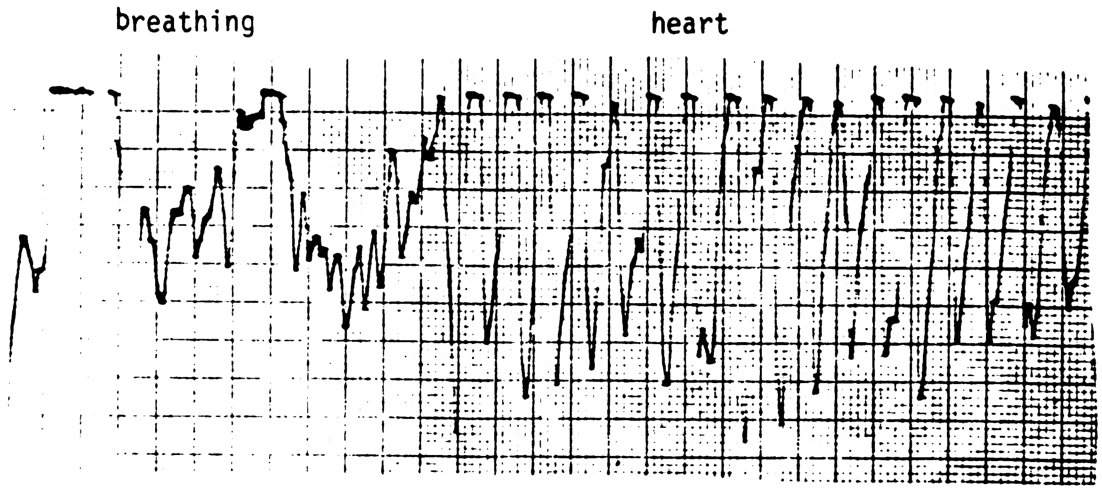

(a) recorded breathing and heart signal of a human subject with one layer of clothing lying on the ground at a distance of 100 ft

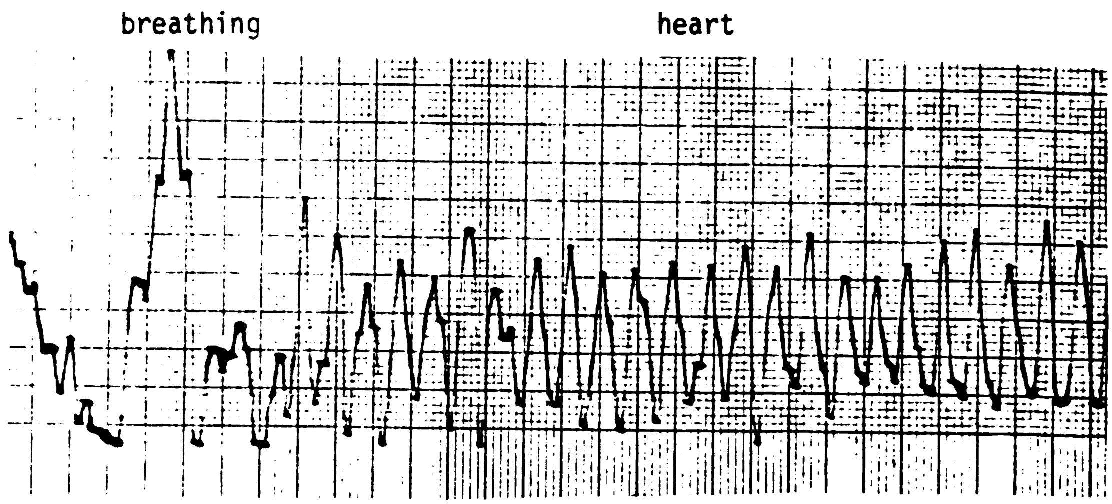

(b) recorded breathing and heart signals of the same human subject covered with four layers of clothing lying on the ground at a distance of 100 ft.

Fig.5.5.4. Effect of the clothing of the human subject on the performance of the distant life detection system.

of Figure 5.5.4 shows the measured breathing and heart signals of a human subject with one layer of clothing lying on the ground at a distance of 100 feet. The antenna radiated a linear-vertically polarized wave with a power of 10 mW. It is observed that both breathing and heart signals were clearly detected. The bottom figure in Figure 5.5.4 shows the recorded breathing and heart signals of the same human subject covered with four layers of clothing, three of them were heavy, lying at the same location. This result shows a slight reduction in the amplitude of the measured heart signal but the quality of the measured heart signal remains good. After many more experiments it is concluded that the effect of clothing on the heart signal detection is not significant at the X-band around 10 GHz.

5.6 Detection of breathing and heart signals through a concrete wall

For the completeness, the performance of the life detection system was also studied through a concrete wall. It may be interesting to test whether the system can detect the breathing and heart signals of human subjects located behind a concrete wall. Surprisingly enough, the system was able to detect the breathing and heart signals of a human subject sitting at a distance of 10 feet behind a concrete wall with an antenna radiated power of only 20 mW. With a higher radiated power, the detectable distance is expected to increase further. The results of this experiment are shown in Figure 5.6.1 where the measured breathing and heart signals of a human subject sitting behind a 6 inch concrete wall at a distance of 2, 7 or 10 feet are given. The antenna

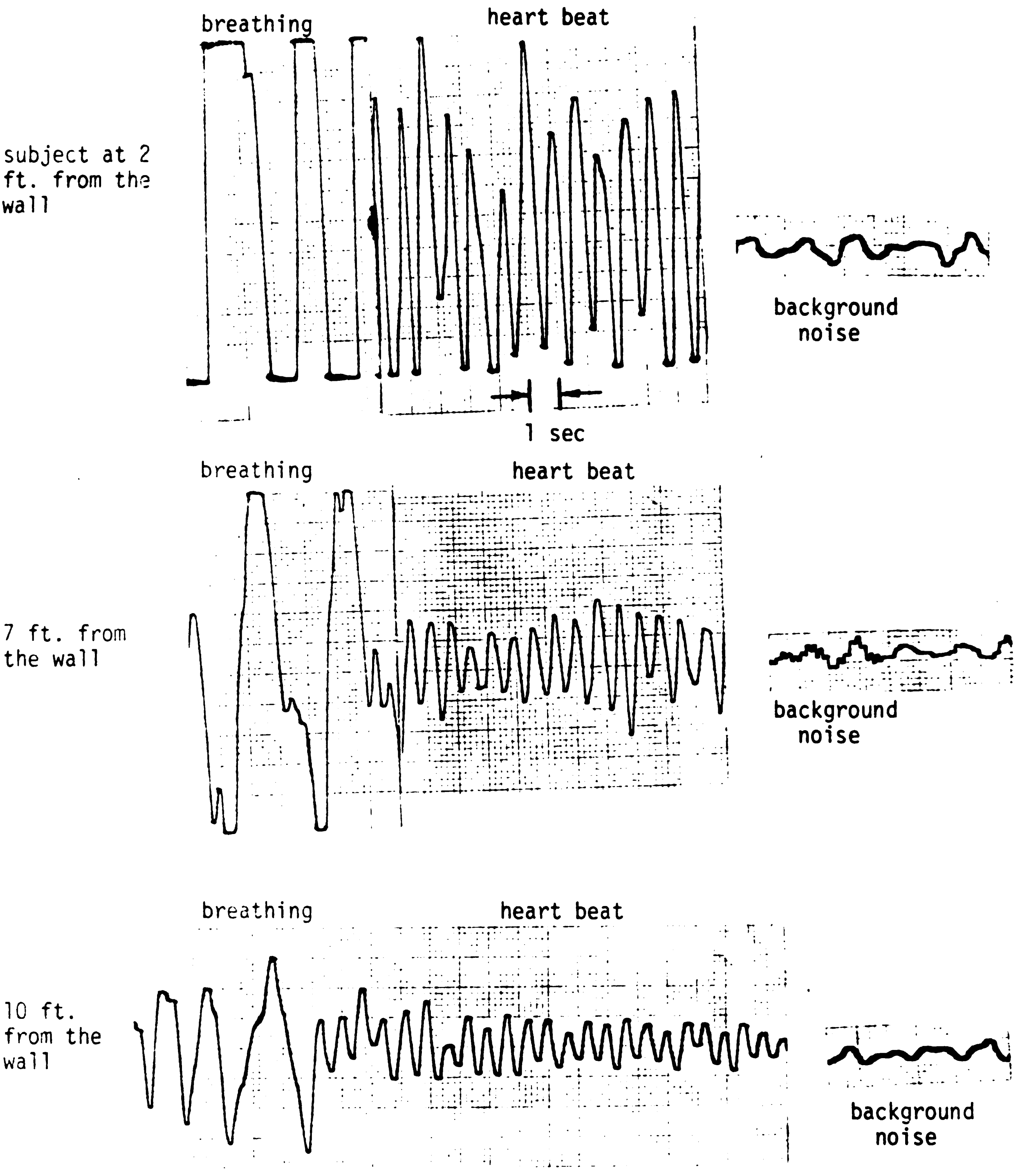

Fig.5.6.1. Measured breathing and heart signals from a human subject sitting behind a concrete wall (6" thick) at various distances. The antenna of the life detection system was located at the other side of the wall and radiated with a power of 20 mW at 10 GHz.

was located close to the wall and radiated with a power of 20 mW. In this experiment, it was necessary to use a matching (tuning) circuit between the antenna and the circulator to match the antenna through the wall, or to reduce a large reflection of microwave from the wall. In Figure 5.6.1, the breathing and heart signals are clearly recorded for all the three distances.

CHAPTER 6

SUMMARY

This thesis presents a study of the scattering of electromagnetic waves by the human body and also demonstrates some of its possible applications. The aim and scope of this study is presented in Chapter 1. In Chapter 2, the EM field near a cylindrical biological body illuminated by a plane wave is analysed and the responses of the single and orthogonal E-field probes located near the body-surface are determined. These results were experimentally verified in Chapter 3 using a cylindrical dielectric shell filled with saline solution at the frequencies of 2GHz, 2.45GHz and 3GHz. The theoretically computed results for the empty shell are also compared with the experimentally recorded probe responses. An excellent agreement is found between the theory and the experiments. Some additional theoretically computed results of the probe response near the biological body are also presented in this chapter. The shadowing effect due to the body and the difference in the probe response in the presence and in the absence of the body are noticed.

In Chapter 4, an expression for the backscattered electric field from a cylindrical body illuminated by a plane wave is obtained. The variations in the magnitude and phase of this backscattered field is then studied assuming the body-radius changes with time. In the latter part of this chapter, an expression for the backscattered electric field from a spherical body exposed to the plane EM waves is obtained and the effect of the change in the radius of the sphere with time on the magnitude and phase of the field is studied. It is noted that the change in the phase of the backscattered field is linear with the change in the radius of the cylindrical or spherical body. However, the magnitude of the return signal is not linearly affected by the change in the radius in both cases.

Two different techniques are presented in Chapter 5 for detecting the breathing and heart beats of humans from large distances. In one, a magic tee is used while in the other, a circulator is employed. The breathing and heart signals from the distance of upto 100 feet and also through a concrete wall are reported in this chapter. The application of these techniques for remotely detecting the physiological status of humans at distances or trapped living beings behind the barriers is noted.

REFERENCES

[1] K.M. Chen, "Interaction of electromagnetic fields with biological bodies", Research Topices in Electromagnetic Wave Theory, J.A. Kong, Ed., Ch. 13, Wiley-Interscience, NY, 1981.

[2] J.C. Lin, J. Kiernicki, M. Kiernicki and P.B. Wollschlaeger, "Microwave apexcardiography", IEEE Trans. Microwave Theory Tech., vol. MTT-27, No. 6, pp. 618-620, June 1979.

[3] D.W. Griffin, "MW interferometers for biological studies", Microwave J., vol. 21, No. 5, pp. 69-72, May 1978.

[4] E.C. Jordan and K.G. Balmain, "Electromagnetic Waves and Radiating Systems", Prentice-Hall, N.J., 1968; p. 535.

[5] W.L. Stutzman and G.A. Thiele, "Antenna Theory and Design", Wiley, N.Y., 1981; pp. 229-235.

[6] E.K. Miller, A.J. Poggio, G.J. Burke and E.S. Selden, "Analysis of wire antennas in the presence of a conducting half space. Part I. The vertical antenna in free space", Canadian J. Physics, vol. 50, pp. 879-888, 1972.

[7] ________, "Analysis of wire antennas in the presence of a conducting half space. Part II. The horizontal antenna in free space", Canadian J. Physics, vol. 50, pp. 2614-2627, 1972.

[8] R.W.P. King, "The Theory of Linear Antennas", Harvard University Press, Cambridge, Mass., 1956; pp. 191-192.

[9] R.S. Elliot, "Antenna Theory and Design", Prentice Hall, N.J., 1981; pp. 332-333.

[10] G. Arfken, "Mathematical Methods for Physicists", Academic Press, N.Y., 1970; p. 488.

[11] C.C. Johnson and A.W. Guy, "Nonionizing electromagnetic wave effects in biological materials and systems", Proc. IEEE, vol. 60, No. 6, pp. 692-718, June 1972.

[12] J.A. Saxton and J.A. Lane, "Electrical properties of sea water", Wireless Engineer, vol. 29, pp. 269-275, Oct. 1952.

[13] G.S. Smith, "Analysis of miniature electric field probes with resistive transmission lines", IEEE Trans. Microwave Theory Tech, vol. MTT-29, No. 11, pp. 1213-1224, Nov. 1981.

[14] H.C. Van De Hulst, "Light Scattering by Small Particles", Wiley, N.Y., 1957; pp. 285-286 and 313-320.

[15] J.A. Stratton, "Electromagnetic Theory", McGraw Hill, N.Y., 1941; pp. 563-573.

[16] S.A. Schelkunoff, "Electromagnetic Waves", D. Van Nostrand, N.J., 1943; pp. 51-52.

[17] A. Thansandote, S.S. Stuchly and J.S. Wright, "Microwave interferometer for measurements of small displacements", IEEE Trans. Instrum. Meas., vol IM-31, No. 4, pp. 227-232, Dec. 1982.

[18] P.C. Pedersen, C.C. Johnson, C.H. Durney and D.G. Bragg, "An investigation of the use of microwave radiation for pulmonary diagnostics", IEEE Trans. Biomed. Eng., vol. BME-23, No. 5, pp. 410-412, Sept. 1976.

[19] D.M. Kerns and R.W. Beatty, "Basic Theory of Waveguide Junctions and Introductory Microwave Network Analysis", Pergamon Press, N.Y., 1967; pp. 116-123.

[20] B. Lax and K.J. Button, "Microwave Ferrites and Ferrimagnetics", McGraw Hill, N.Y., 1962; pp. 518-522.

[21] T. Tamaru, "A note on bolometer mount efficiency measurement technique by impedance method in Japan", IEEE Trans. Microwave Theory Tech., vol. MTT-14, No. 9, p. 437, Sept. 1966.

[22] K.M. Chen, S. Rukspollmuang, and D.P. Nyquist, "Measurement of induced electric fields in a phantom model of man", Radio Science, vol. 17, No. 5S, pp. 49S-59S, Sept.-Oct. 1982.

[23] M. Goldstein, "Bessel Functions, for complex argument and order", AEC Computing and Applied Mathematics Center, Courant Institute of Mathematical Sciences, New York University. Nov. 1965.

APPENDIX A

Computer program for determining the response of an orthogonally connected E-probe system near the cylindrical body.

```
      PROGRAM SHELL (INPUT,OUTPUT,TAPE 10 = INPUT,TAPE 20 = OUTPUT)
      DIMENSION BJRE(75), BJIM(75),YRE(41), YIM(41)
      COMPLEX  BODY1,BODY2,WK1,WK2,WK1R1,WK2R1,WK2R2,ZLOAD,ZINPUT,FACTR2
     *,FACTR1,VEQPHI,CURENT,VEQRAD,DHARA,VEQTE,TELOAD
      COMMON WK1,WK2,WK1R1,WK2R1,WK2R2,CKO,CKOR,CKOR2
C     ******************************************************************
C     THIS PROGRAM COMPUTES THE LOAD CURRENT DETECTED BY E-FIELD PROBE
C     NEAR TWO CONCENTRIC CYLINDRICAL MEDIA OF  COMPLEX PERMITTIVITIES.
C     SIGMA1 AND SIGMA2 ARE CONDUCTIVITIES OF INNER AND OUTER MEDIA,
C     RESPECTIVELY,WHILE DIELC1 AND DIELC2 ARE RELATIVE PERMITTIVITIES.
C     IT READS THESE DATA AND FREQ FROM FORMATTED DATA CARDS.FIELD IS
C     MAGNITUDE OF INCIDENT E-FIELD,ANGLE IS ITS POLARIZATION ANGLE
C     MEASURED FROM THE  PLANE PASSING THRO, THE PROPAGATION AXIS AND
C     AXIS OF THE CYLINDER.R1 AND R2 ARE THE RADII OF INNER AND OUTER CYLINDERS.
C     HEIGHT IS HALF OF THE LENGTH OF PROBE LOCATED AT R FROM THE CYLINDER
C     AXIS. A 10 KOHM  RESISTOR IN PARALLEL WITH 6 PF CAPACITOR IS
C     ASSUMED LOAD FOR THE PROBE AND SQURE-LAW DETECTOR IS ASSUMED.
C     IN THE OUTPUT,IT PRINTS  THE CURRENTS FOR THREE INDIVIDUAL PROBES
C     AS WELL AS THE TOTAL CURRENT FOR THE THREE ORTHOGONALLY CONNECTED
C     PROBE SYSTEM AROUND CYLINDER AT 5 DEGREE INTERVAL.
C     ******************************************************************
      FIELD=2.0
      ANGLE=45.0
      HEIGHT=0.0065
      R1 = 0.146
      R2 = 0.1524
      R=0.156
      PI = 4.0 * ATAN (1.0)
      DO 99 M = 1,3
      READ(10,1)SIGMA1,SIGMA2,DIELC1,DIELC2,FREQ
1     FORMAT(2F6.4,2F5.2,E11.4)
      FREEMU = 4.0E-07*PI
      VACCUM = 8.854E-12
      PHIO=ATAN(HEIGHT/R)
      VELITE = 3.0E+08
      OMEGA = 2.0  * PI * FREQ
      CKO = OMEGA / VELITE
      DIER1 = DIELC1 * VACCUM
      DIER2 = DIELC2 * VACCUM
      BODY1 = CMPLX(DIER1,-(SIGMA1/OMEGA))
      BODY2 = CMPLX (DIER2,-(SIGMA2/OMEGA))
      SQROMG = OMEGA **2
      WK1 = CSQRT(SQROMG*FREEMU*BODY1)
      WK2 = CSQRT(SQROMG*FREEMU*BODY2)
      WK1R1 = WK1*R1
      WK2R1 = WK2*R1
      WK2R2 = WK2*R2
      CKOR2 = CKO*R2
      CKOR = CKO*R
      RLOAD=1.0E+04
      XLOAD=1.0E+12/(6.0*OMEGA)
```

```
      ZLOAD=RLOAD*CMPLX(0.0,-XLOAD)/CMPLX(RLOAD,-XLOAD)
      BETAH=CKO*HEIGHT
      RINPUT=18.3*(BETAH**2)*(1.0+0.086*(BETAH**2))
      XINPUT=-396.0*(1.0-0.383*(BETAH**2))/BETAH
      ZINPUT=CMPLX(RINPUT,XINPUT)
      FACTR1=ZINPUT+ZLOAD
      FACTR2=ZINPUT+ZLOAD
      ANGLRD=ANGLE*PI/180.
       WRITE(20,2) FREQ,FIELD,ANGLE
2     FORMAT(1H1,5X,11HFREQUENCY =,E11.4,5X,7HFIELD =,F5.2,5X,
     *7HANGLE =,F6.2,/)
      WRITE(20,75)
75    FORMAT(2X,6HPHI IN,3X,15HLOAD CURRENT SQ,3X,15HLOAD CURRENT SQ,
     *3X,15HLOAD CURRENT SQ,3X,15HLOAD CURRENT SQ)
      WRITE(20,750)
750   FORMAT(2X,3HDEG,6X,7HFOR PHI,11X,5HFOR R,13X,6HFOR TE,12X,
     *5HTOTAL,//)
      PHI = 0.0
      DO 4 I = 1,15
      DO 444 J = 1,5
      PHIR = PHI * PI / 180.0
      CALL TMPHI  (PHIR,VEQPHI,PHI0)
      CURENT=FIELD*VEQPHI*SIN(ANGLRD)/FACTR1
      CALL TMRAD  (PHI,VEQRAD,HEIGHT)
      DHARA=FIELD*VEQRAD*SIN(ANGLRD)/FACTR2
      CALL TEWAVE  (PHIR,VEQTE,HEIGHT)
      TELOAD=FIELD*VEQTE*COS(ANGLRD)/FACTR1
      AA=CABS(CURENT)
      BA=CABS(DHARA)
      CA=CABS(TELOAD)
      AASQ=AA**2
      BASQ=BA**2
      CASQ=CA**2
      DA=AASQ+BASQ+CASQ
      WRITE(20,200) PHI,AASQ,BASQ,CASQ,DA
200   FORMAT(2X,F6.2,3X,E11.4,7X,E11.4,7X,E11.4,7X,E11.4)
      PHI = PHI+5.0
      IF(PHI .GE.365.0) GO TO 99
444   CONTINUE
      WRITE (20,111)
111   FORMAT (1H0)
4     CONTINUE
99    CONTINUE
      STOP
       END
      SUBROUTINE TMPHI  ( PHIR,VEQTMF,PHI0)
      COMMON WK1,WK2,WK1R1,WK2R1,WK2R2,CKO,CKOR,CKOR2
      DIMENSION BJRE(75),BJIM(75),YRE(41),YIM(41)
      COMPLEX WK1,WK2,WK1R1,WK2R2,BSRS,DM,UP,HANKLR,UP1,HNKLR1,DERHKL,
     *COFCNT,BSERIS,X,Y,XANDY,VEQTMF ,WK2R1
      PI = 4.0 * ATAN (1.)
      R = CKOR/CKO
      BSRS = CMPLX (0.0,0.0)
      DO 44  N=1,20
      Q=FLOAT(N) - 1.0
      CALL DMPART (N,PI,DM,0.0)
      IF (ABS(CKOR) .LE. 50.0) GO TO 1
      FRONT= SQRT(2.0/(PI*CKOR) )
      UP=CMPLX(0.0,-CKOR+PI*(2.0*FLOAT(N)+1.0)/4.0)
      HANKLR= FRONT * CEXP (UP)
      UP1 = CMPLX(0.0,-CKOR+PI*(2.0*FLOAT(N+1)+1.0)/4.0)
```

```
      HNKLR1=FRONT*CEXP(UP1)
       GO TO 2
1     CALL COMBES(CKOR,0.0,0.0,0.0,N,BJRE,BJIM,YRE,YIM)
      HANKLR=CMPLX(BJRE(N),-YRE(N))
      HNKLR1=CMPLX(BJRE(N+1),-YRE(N+1))
2     DERHKL=(Q*HANKLR/CKOR)-HNKLR1
      IF(N-1)5,5,6
5     COFCNT=DM*PHIO*DERHKL
      GO TO 9
6     CX = -2.0/(Q*PHIO)
      QTETAR=Q*PHIR
       REMAIN=(1.0/Q)*(1.0-COS(Q*PHIO))*COS(QTETAR)
      COFCNT=-CX*DM*DERHKL*REMAIN
9     BSRS=BSRS+COFCNT
44    CONTINUE
      BSERIS=BSRS*CMPLX(0.0,1.0)
      X1=CKOR* COS(PHIR-(PHIO/2.0))
      Y1=CKOR*COS(PHIR+(PHIO/2.0))
      DOME1=COS(PHIR-(PHIO/4.0))
      DOME2=COS(PHIR+(PHIO/4.0))
      X=CMPLX(DOME1,0.0)*CMPLX(COS(X1),-SIN(X1))
      Y=DOME2*CMPLX(COS(Y1),-SIN(Y1))
      XANDY=(X+Y)*PHIO/2.0
      VEQTMF=R*(BSERIS+XANDY)
      RETURN
      END
      SUBROUTINE TMRAD (PHI,VEQTMR,HEIGHT)
      DIMENSION BJRE(75),BJIM(75),YRE(41),YIM(41)
      COMMON WK1,WK2,WK1R1,WK2R1,WK2R2,CKO,CKOR,CKOR2
      COMPLEX WK1,WK2,WK1R1,WK2R2,SERIES,DM,UP1,HN1,TERM1,UP2,HN2,
     *TERM2,TOTAL,C1,C2,C3,E1,E2,E3,BODYNO,VEQTMR ,WK2R1
      PI=4.0*ATAN(1.0)
      PHIR=PHI*PI/180.0
      R=CKOR/CKO
      SERIES=CMPLX(0.0,0.0)
      DO 44 N=1,20
      Q=FLOAT(N)-1.0
      CALL DMPART (N,PI,DM,0.0)
      RMINUS=R-HEIGHT/2.0
      RPLUS=R+HEIGHT/2.0
      ARGU1=CKO*RMINUS
      ARGU2=CKO*RPLUS
      IF(ABS(ARGU1) .LE.50.0) GO TO 1
      X1 = SQRT(2.0/(PI*ARGU1))
      UP1=CMPLX(0.0,-ARGU1+PI*(2.0*FLOAT(N)+1.0)/4.0)
      HN1=X1*CEXP(UP1)
      GO TO 2
1     CALL COMBES(ARGU1,0.0,0.0,0.0,N,BJRE,BJIM,YRE,YIM)
      HN1=CMPLX(BJRE(N),-YRE(N))
2     TERM1=(1.0+(1.0-R/HEIGHT)*ALOG(R/(R-HEIGHT)))*HN1
       IF (ABS(ARGU2) .LE. 50.0) GO TO 3
      X2=SQRT(2.0/(PI*ARGU2))
      UP2=CMPLX(0.0,-ARGU2+PI*(2.0*FLOAT(N)+1.0)/4.0)
      HN2=X2* CEXP(UP2)
      GO TO 4
3     CALL COMBES(ARGU2,0.0,0.0,0.0,N,BJRE,BJIM,YRE,YIM)
      HN2=CMPLX(BJRE(N),-YRE(N))
4     TERM2=((1.0+R/HEIGHT)*ALOG((R+HEIGHT)/R)-1.0)*HN2
      TOTAL=(Q/CKO)*DM*(TERM1+TERM2)*SIN(Q*PHIR)*CMPLX(0.0,1.0)
      SERIES=SERIES+TOTAL
44    CONTINUE
```

```
      IF(PHI.EQ.90.0) GO TO 6
      IF ( PHI .EQ. 270.0) GO TO 6
      C1=CMPLX(0.0,-CKO*R*COS(PHIR))
      C2=CMPLX(0.0,-CKO*(R-HEIGHT)*COS(PHIR))
      C3=CMPLX(0.0,-CKO*(R+HEIGHT)*COS(PHIR))
      E1=CEXP(C1)
      E2= CEXP(C2)
      E3=CEXP(C3)
      DINOM=HEIGHT*(CKO**2)
      TRIG=(SIN(PHIR))/((COS(PHIR))**2)
      BODYNO=(2.0*E1-E2-E3)*TRIG/DINOM
      GO TO 66
6     BODYNO = HEIGHT*SIN(PHIR)
66    VEQTMR=BODYNO+SERIES
      RETURN
      END
      SUBROUTINE TEWAVE (PHIR,EZRPHI,HEIGHT)
      COMMON WK1,WK2,WK1R1,WK2R1,WK2R2,CKO,CKOR,CKOR2
      DIMENSION BJRE(75),BJIM(75),YRE(41),YIM(41)
      COMPLEX WK1,WK2,WK1R1,WK2R2,WK2R1,VSERIS,DM,HANKEL,SUM,C6,C7,
     *EZRPHI
      PI=4.0*ATAN(1.0)
      VSERIS=CMPLX(0.0,0.0)
      DO 44 N=1,20
      Q=FLOAT(N)-1.0
      CALL DMPART (N,PI,DM,1.0)
      IF (ABS(CKOR) .LE. 50.0) GO TO 11
      C5=SQRT(2.0/PI*CKOR)
      TN2=CKOR-(2.0*Q+1.0)*PI/4.0
      BES=C5*COS(TN2)
      BES2=C5*SIN(TN2)
      HANKEL=CMPLX(BES,-BES2)
       GO TO 8
11    CALL COMBES (CKOR,0.0,0.0,0.0,N,BJRE,BJIM,YRE,YIM)
      HANKEL=CMPLX(BJRE(N),-YRE(N))
8     PHICOS=COS( Q*PHIR)
      SUM=DM*HANKEL*PHICOS
      VSERIS=VSERIS+SUM
44    CONTINUE
      C6=CMPLX(0.0,-CKOR*COS(PHIR))
      C7=CEXP(C6)
      EZRPHI=(C7+VSERIS)*HEIGHT
      RETURN
      END
      SUBROUTINE DMPART (N,PI,DM,TE)
      DIMENSION BJRE(75),BJIM(75),YRE(41),YIM(41)
      COMPLEX WK1R1,WK2R1,XN,WK2,WK1,WK2R2,B2,B3,HNKL,DHNKL,B4,C3,C4,
     *C34,COMPXJ,DECOM,DM
      COMMON WK1,WK2,WK1R1,WK2R1,WK2R2,CKO,CKOR,CKOR2
      CALL ABC (WK1R1,WK2R1,N,PI,XN,WK2,WK1,TE)
      CALL BCD (WK2R2,WK2,CKO,N,PI,XN,B2,TE)
      B3 = B2
      Q = N-1
      IF(ABS(CKOR2) .LE.50.0)  GO TO 1000
      ARGUO1 = CKOR2-(Q*PI/2.0)-(3.0*PI/4.0)
      ARGUO2 = ARGUO1+(PI/2.0)
      C1 = SQRT(2.0/(PI*CKOR2))
      B1=C1*COS(ARGUO1)
      B= COS(ARGUO2) * C1
      TN1 = CKOR2 - (2.0*Q+1.0)*PI/4.0
      BESEL2 = C1*SIN(TN1)
```

```
      HNKL = CMPLX(B,-BESEL2)
      GO TO 10
1000    CALL COMBES(CKOR2,0.0,0.0,0.0,N,BJRE,BJIM,YRE,YIM)
      B = BJRE(N)
      BI = BJRE(N+1)
      HNKL = CMPLX(BJRE(N),-YRE(N))
10    PART = Q*B/CKOR2
      DERBES=PART-BI
      B1 = DERBES/B
      C2 = 2.0/(PI*CKOR2*B)
      DHNKL = B1 * HNKL - C2 * CMPLX ( 0.0,1.0)
      B4 = DHNKL/HNKL
      C3 = (B1-B3)/(B3-B4)
      C4 = B/HNKL
      C34 = C3*C4
      IF(N-1) 20,20,16
20    EPCLON = 1.0
      GO TO 7
16    EPCLON = 2.0
7     COMPXJ = CMPLX (0.0,1.0)
      DECOM = COMPXJ**(N-1)
      DM = EPCLON * C34/DECOM
      RETURN
      END
      SUBROUTINE ABC (WK1R1,WK2R1,N,PI,XN,WK2,WK1,TE)
      DIMENSION  BJRE(75), BJIM(75), YRE(41), YIM(41)
      COMPLEX WK1,WK2,WK1R1,WK2R1,XN,DEBES1,B1,BI11,PART11,A1,DEBESH,
     *BH,COEFF1,BESEL2,PART21,BH21,DBES,HNL221,HNL121,WRON,DHL221,
     *DHL121, A2, A4, A3,CB1
      REWK11 = REAL (WK1R1)
      AMWK11 = AIMAG (WK1R1)
      REWK21 = REAL (WK2R1)
      AMWK21 = AIMAG (WK2R1)
      Q = N - 1
      IF (CABS(WK1R1) .LE. 50.0) GO TO 1
      ARGU11 = REWK11 - ( Q * PI / 2.0) - (3.0 * PI / 4.0)
      ARGU12 = ARGU11+ ( PI / 2.0 )
      CB1=CSQRT(2.0/(PI*WK1R1))
      BI11= CB1*CMPLX(COS(ARGU11),-SIN(ARGU11)*TANH(AMWK11))
      B1 = CMPLX (COS (ARGU12), - SIN (ARGU12) *TANH (AMWK11)) *CB1
      GO TO 10
1     CALL COMBES (REWK11,AMWK11,0.0,0.0,N,BJRE,BJIM,YRE,YIM)
      B1 = CMPLX (BJRE (N), BJIM (N) )
      BI11 = CMPLX (BJRE (N+1), BJIM (N+1) )
10    PART11 = Q * B1 / WK1R1
      DEBES1 = PART11 - BI11
      A1 = DEBES1 / B1
      IF (CABS (WK2R1) .LE. 50.0) GO TO 2
      ARGU21 = REWK21 - ( Q*PI/2.0) - (3.0 *PI / 4.0)
      ARGU22 = ARGU21 + (PI / 2.0)
      COEFF1 = CSQRT ( 2.0 / ( PI * WK2R1) )
      BH21=COEFF1*CMPLX(COS(ARGU21),-SIN(ARGU21)*TANH(AMWK21))
      BH = CMPLX (COS (ARGU22),-SIN(ARGU22)*TANH (AMWK21) )*COEFF1
      COSINE = ( EXP ( AMWK21) + EXP (-AMWK21) ) / 2.0
      TN = REWK21 - ( 2.0*Q+1.0)*PI/4.0
      BESEL2 = COEFF1*COSINE*(SIN(TN)+TANH(AMWK21)*COS(TN)*
     CCMPLX(0.0,1.0))
      GO TO 3
2     CALL COMBES (REWK21,AMWK21,0.0,0.0,N,BJRE,BJIM,YRE,YIM)
      BH = CMPLX ( BJRE (N), BJIM (N) )
      BH21 = CMPLX (BJRE(N+1), BJIM (N+1) )
```

```
      BESEL2 = CMPLX (YRE(N), YIM (N) )
3     PART21 = Q*BH / WK2R1
       DEBESH = PART21 - BH21
      DBES = DEBESH /BH
      HNL221 = BH + BESEL2 * CMPLX (0.0,-1.0)
      HNL121 = BH + BESEL2 * CMPLX (0.0, 1.0)
      WRON = 2.0 / (PI * WK2R1 * BH)
      DHL221 = DBES * HNL221 - WRON*CMPLX (0.0,1.0)
      DHL121 = DBES * HNL121 + WRON * CMPLX (0.0,1.0)
      IF(TE-1.0)5,6,6
5     A2=(WK1*DHL221)/(WK2*HNL221)
      A4=(WK1*DHL121)/(WK2*HNL121)
       GO TO 47
6     A2 = (WK2 * DHL221) / ( WK1 * HNL221)
      A4 = (WK2 * DHL121) / ( WK1 * HNL121)
47    A3 = HNL221 / HNL121
      XN = A3 * (A1-A2)/(A1-A4)
      RETURN
      END
      SUBROUTINE BCD (WK2R2,WK2,CKO,N,PI,XN,B2,TE)
      DIMENSION BJRE(75), BJIM(75),YRE(41), YIM(41)
      COMPLEX DEBES2,B,BESEL2,COEFF2,PART22,BI22,HNL222,HNL122,DBES2,
     *WRON2,DHL222,DHL122,UNUM,DINOM,B2,WK2R2,WK2,XN
      REWK22 = REAL (WK2R2)
      AMWK22 = AIMAG (WK2R2)
      Q = N - 1
      IF(CABS(WK2R2) .LE. 50.0) GO TO 1
      ARG21 = REWK22 - (Q*PI/2.0) - (3.0*PI/4.0)
      ARG22 = ARG21 + (PI /2.0)
      COEFF2 = CSQRT (2.0/(PI*WK2R2) )
      BI22=COEFF2*CMPLX(COS(ARG21),-SIN(ARG21)*TANH(AMWK22))
      B = CMPLX (COS (ARG22),-SIN(ARG22)*TANH(AMWK22) )*COEFF2
      COSINE = (EXP(AMWK22)+EXP(-AMWK22) )/2.0
      TN = REWK22 -(2.0*Q+1.0)*PI/4.0
      BESEL2=COEFF2*COSINE*(SIN(TN)+COS(TN)*TANH(AMWK22)*
     CCMPLX(0.0,1.0) )
      GO TO 10
1     CALL COMBES(REWK22,AMWK22,0.0,0.0,N,BJRE,BJIM,YRE,YIM)
      B = CMPLX (BJRE(N),BJIM(N) )
      BESEL2 = CMPLX (YRE(N),YIM(N) )
      BI22 = CMPLX (BJRE(N+1),BJIM(N+1) )
10    PART22 = Q*B/WK2R2
      HNL122 = B+BESEL2 * CMPLX (0.0,1.0)
      HNL222 = B+BESEL2*CMPLX(0.0,-1.0)
      DEBES2 = PART22 - BI22
      DBES2 = DEBES2 / B
      WRON2 = 2.0/(PI*WK2R2*B)
      DHL222 = DBES2 * HNL222 - WRON2 * CMPLX (0.0,1.0)
      DHL122 = DBES2 * HNL122+WRON2 * CMPLX (0.0,1.0)
      UNUM = DHL222-XN*DHL122
      DINOM = HNL222 - XN * HNL122
      IF (TE-1.0)5,6,6
5     B2=(CKO*UNUM)/(WK2*DINOM)
       GO TO 47
6     B2 = (WK2 *UNUM) / ( CKO * DINOM )
47    RETURN
      END
```

```
C       *****************************************************************
C       SUBROUTINE  " COMBES " [23]
C       *****************************************************************
        SUBROUTINE COMBES  (X,Y,ALPHA,BETA,N,BJRE,BJIM,YRE,YIM)
        DIMENSION BJRE(75),BJIM(75),YRE(41),YIM(41)
        CALL BEGIN(X,Y,N,K,R)
        CALL JRECUR(X,Y,ALPHA,BETA,K,R,BJRE,BJIM)
        CALL JSUM(ALPHA,BETA,K,BJRE,BJIM,SUMRA,SUMIA)
        CALL FACTOR(X,Y,ALPHA,BETA,Q,R)
        CALL JNORM(K,Q,R,SUMRA,SUMIA,BJRE,BJIM)
 7      CALL YSUM  (X,Y,ALPHA,BETA,K,BJRE,BJIM,ASUMR,ASUMI)
 8      CALL YGNU  (X,Y,ALPHA,BETA,Q,R,ASUMR,ASUMI,BJRE,BJIM,YRE,YIM)
 9      CALL WRONSK  (X,Y,BJRE,BJIM,YRE,YIM)
         BJSQ=BJRE(1)**2+BJIM(1)**2
         IF(BJSQ-.00000005)  14,14,15
  14    CALL YSUMP(X,Y,ALPHA,BETA,K,BJRE,BJIM,ASUMR,ASUMI)
        CALL YGNUP(X,Y,ALPHA,BETA,Q,R,ASUMR,ASUMI,BJRE,BJIM,YRE,YIM)
 15     IF  (N-1)10,12,11
 10     IF  (N)13,12,12
 13     CALL NEGN  (X,Y,ALPHA,BETA,N,BJRE,BJIM,YRE,YIM)
        GO TO 12
   11   CALL YRECUR(X,Y,N,BJRE,BJIM,YRE,YIM)
 12     RETURN
         END
CBES402  BEGIN SUBROUTINE                              PART 2 OF 16
        SUBROUTINE BEGIN(X,Y,N,K,R)
        SSQ=X**2+Y**2
        KTEN=SQRT(SSQ)+20.0
        NTEN=IABS(N)+10
        M=MAXO(KTEN,NTEN)  /2
        K=2*M+1
            R = K + 1
        RETURN
        END
CBES403  JRECUR SUBROUTINE                             PART 3 OF 16
        SUBROUTINE JRECUR(X,Y,ALPHA,BETA,K,R,BJRE,BJIM)
        DIMENSION BJRE(100),BJIM(100)
        RALPHA=R+ALPHA
        SSQ=X**2+Y**2
        BJRE(K+2)=0
        BJIM(K+2)=0
        BJRE(K+1)=1.0E-37
        BJIM(K+1)=0.0
        DO4I=1,K
        L1=K+1-I
        RALPHA=RALPHA-1.0
        A=((2.0*X*RALPHA)+(2.0*BETA*Y))/SSQ
        B=((-2.0*Y*RALPHA)+(2.0*BETA*X))/SSQ
        BJRE(L1)=(A*BJRE(L1+1))-(B*BJIM(L1+1))-BJRE(L1+2)
 4      BJIM(L1)=(B*BJRE(L1+1))+(A*BJIM(L1+1))-BJIM(L1+2)
        RETURN
        END
CBES404  JSUM SUBROUTINE                               PART 4 OF 16
        SUBROUTINE JSUM(ALPHA,BETA,K,BJRE,BJIM,SUMRA,SUMIA)
        DIMENSION BJRE(100),BJIM(100)
 801    SUMRA=(BJRE(3)*(ALPHA+2.0))-(BJIM(3)*BETA)
        SUMIA=(BETA*BJRE(3))+((ALPHA+2.0)*BJIM(3))
        GRE=1.0
        GIM=0
        S=1.0
        DO6I=5,K,2
        S=S+1.0
        GREN=((GRE*(ALPHA+S-1.0))-(BETA*GIM))/S
        GIM=((GIM*(ALPHA+S-1.0))+(BETA*GRE))/S
        GRE=GREN
        ALPTS=ALPHA+2.0*S
        GJR=GRE*BJRE(I)
        GJI=GIM*BJIM(I)
        GJRI=GRE*BJIM(I)
        GJIR=GIM*BJRE(I)
        SUMRB=ALPTS*(GJR-GJI)-BETA*(GJIR+GJRI)+SUMRA
        SUMIB=ALPTS*(GJIR+GJRI)-BETA*(GJI-GJR)+SUMIA
        IF(SUMRA) 15,21,15
   15   IF(ABS((SUMRB/SUMRA)-1.0)-.00000005)21,21,10
 21     IF(SUMIA)20,11,20
```

```
20     IF(ABS((SUMIB/SUMIA)-1.0)-.00000005)11,11,10
10     SUMRA=SUMRB
6      SUMIA=SUMIB
   11 RETURN
        END
CBES405  FACTOR SUBROUTINE                           PART 5 OF 16
       SUBROUTINE FACTOR(X,Y,ALPHA,BETA,Q,R)
       CALL LOGGAM(ALPHA+1.0,BETA,U,V)
       CALL COMLOG(X,Y,A1,B1)
       A2=ALPHA*A1-BETA*B1
       B2=BETA*A1+ALPHA*B1
       A2=-A2
       B2=-B2
       CALL COMEXP(A2,B2,A3,B3)
       A4=.6931471806*ALPHA
       B4=.6931471806*BETA
       CALL COMEXP(A4,B4,A5,B5)
       A6=A3*A5-B3*B5
       B6=B3*A5+A3*B5
       CALL COMEXP(U,V,A7,B7)
       Q=A6*A7-B6*B7
       R=B6*A7+A6*B7
       RETURN
        END
CBES406  COMLOG SUBROUTINE                           PART 6 OF 16
C      COMPLEX LOGARITHM - BRANCH CUT ON NEGATIVE REAL AXIS
       SUBROUTINE COMLOG(X,Y,A,B)
       PI=3.141592654
       A=.5*ALOG(X*X+Y*Y)
       IF(X)5,1,4
 1     B=.5*PI
       IF(Y)2,3,8
 2     B=-B
       GO TO 8
 3     B=0.
       GO TO 8
     4 B=ATAN(Y/X)
       GO TO 8
     5 B=ATAN(Y/X)
       IF(Y)6,7,7
 6     B=B-PI
       GO TO 8
 7     B=B+PI
 8     RETURN
        END
CBES407  COMEXP SUBROUTINE                           PART 7 OF 16
       SUBROUTINE COMEXP(X,Y,A,B)
       C=EXP(X)
       A=C*COS(Y)
       B=C*SIN(Y)
       RETURN
        END
CBES408  JNORM SUBROUTINE                            PART 8 OF 16
       SUBROUTINE JNORM(K,Q,R,SUMRA,SUMIA,BJRE,BJIM)
       DIMENSION BJRE(100),BJIM(100)
       S=((SUMRA+BJRE(1))*Q)-((SUMIA+BJIM(1))*R)
       T=((SUMIA+BJIM(1))*Q)+((SUMRA+BJRE(1))*R)
       IF(ABS(S)-ABS(T))100,101,101
 101   TS=T/S
       TSSQ=S*(1.0+(TS**2))
 12    DO13I=1,K
       BJREN=(BJRE(I)+BJIM(I)*TS)/TSSQ
       BJIM(I)=(BJIM(I)-BJRE(I)*TS)/TSSQ
 13    BJRE(I)=BJREN
       GO  TO  14
 100   ST=S/T
       STSQ=T*((ST**2)+1.0)
 102   DO103I=1,K
       BJREN=(BJRE(I)*ST+BJIM(I))/STSQ
       BJIM(I)=(BJIM(I)*ST-BJRE(I))/STSQ
 103   BJRE(I)=BJREN
    14 RETURN
        END
CBES409  YSUM SUBROUTINE                             PART 9 OF 16
       SUBROUTINE YSUM (X,Y,ALPHA,BETA,K,BJRE,BJIM,ASUMR,ASUMI)
       DIMENSION BJRE(100),BJIM(100)
       A1=ALPHA-1.0
       A2=A1-1.0
       A3=A1+ALPHA
       A4=BETA**2
       A5=2.0*A4
```

```
      ABSQ=(-A1)**2+A4
      GAMRE=((2.0+ALPHA)*(-A1)-A4)/ABSQ
      GAMIM=(BETA*3.0)/ABSQ
      ASUMR=GAMRE*BJRE(3)-GAMIM*BJIM(3)
      ASUMI=GAMIM*BJRE(3)+GAMRE*BJIM(3)
      T=1.0
      DO 500 I=5,K,2
      T=T+1.0
      B1=2.0*T
      F1=B1+ALPHA
      F2=A3+T
      F3=A1+T
      F5=T-ALPHA
      F6=A2+B1
      G1=F1*F2-A5
      G2=(F2+2.0*F1)*BETA
      H1=G1*F3-G2*BETA
      H2=G2*F3+G1*BETA
      P1=F5*F6+A4
      P2=(F5-F6)*BETA
      P3=P1**2+P2**2
      CRE=((H1*P1+H2*P2)/P3)/T
      CIM=((H2*P1-H1*P2)/P3)/T
      TEMP=-(CRE*GAMRE-CIM*GAMIM)
      GAMIM=-(CIM*GAMRE+CRE*GAMIM)
      GAMRE=TEMP
      BSUMR=GAMRE*BJRE(I)-GAMIM*BJIM(I)+ASUMR
      BSUMI=GAMIM*BJRE(I)+GAMRE*BJIM(I)+ASUMI
      IF(ABS((BSUMR/ASUMR)-1.0)-.00000005)521,521,510
  521 IF(ASUMI)520,511,520
  520 IF(ABS((BSUMI/ASUMI)-1.0)-.00000005)511,511,510
  510 ASUMR=BSUMR
  500 ASUMI=BSUMI
  511 RETURN
       END
CBES410  YGNU SUBROUTINE                             PART 10 OF 16
      SUBROUTINE YGNU(X,Y,ALPHA,BETA,Q,R,ASUMR,ASUMI,BJRE,BJIM,YRE,YIM)
      DIMENSION BJRE(100),BJIM(100),YRE(50),YIM(50)
      PI=3.141592654
      TPI=2.0/PI
      QRE=TPI*(Q**2-R**2)
      QIM=TPI*2.0*Q*R
      DRE=QRE*ASUMR-QIM*ASUMI
      DIM=QIM*ASUMR+QRE*ASUMI
      IF(ALPHA)1,2,1
  2   IF(BETA)1,3,1
  3   CALL YZERO(X,Y,ALPRE,ALPIM)
      GO TO 720
  1   PALPHA=PI*ALPHA
      COX=COS(PALPHA)
      SIX=SIN(PALPHA)
      EXY=EXP(PI*BETA)
      EXY1=1.0/EXY
      COSH=.5*(EXY+EXY1)
      SINH=.5*(EXY-EXY1)
      DEN=(SIX*COSH)**2+(COX*SINH)**2
      ERE=(SIX*COX)/DEN
      EIM=(-COSH*SINH)/DEN
      ABSQ3=2.0*(ALPHA**2+BETA**2)
      ALPRE=ERE-((QRE*ALPHA+BETA*QIM)/ABSQ3)
      ALPIM=EIM-((QIM*ALPHA-BETA*QRE)/ABSQ3)
  720 YRE(1)=ALPRE*BJRE(1)-ALPIM*BJIM(1)+DRE
      YIM(1)=ALPIM*BJRE(1)+ALPRE*BJIM(1)+DIM
      RETURN
       END
CBES411  YZERO SUBROUTINE                            PART 11 OF 16
      SUBROUTINE YZERO(X,Y,ALPRE,ALPIM)
      TPI=2.0/3.141592654
      CALL COMLOG(X,Y,A,B)
      ALPRE=TPI*(-.1159315157+A)
      ALPIM=TPI*B
      RETURN
       END
CBES412  WRONSK SUBROUTINE                           PART 12 OF 16
      SUBROUTINE WRONSK(X,Y,BJRE,BJIM,YRE,YIM)
      DIMENSION BJRE(100),BJIM(100),YRE(50),YIM(50)
      SSQ=X**2+Y**2
      TPI=2.0/3.141592654
      AZRE=TPI*X/SSQ
      AZIM=-TPI*Y/SSQ
      ZRE=BJRE(2)*YRE(1)-BJIM(2)*YIM(1)
```

```
      ZIM=BJIM(2)*YRE(1)+BJRE(2)*YIM(1)
      BZRE=ZRE-AZRE
      BZIM=ZIM-AZIM
      BJSQ=BJRE(1)**2+BJIM(1)**2
      CZRE=BJRE(1)/BJSQ
      CZIM=(-BJIM(1))/BJSQ
      YRE(2)=BZRE*CZRE-BZIM*CZIM
      YIM(2)=BZIM*CZRE+BZRE*CZIM
      RETURN
       END
CBES413  NEGN SUBROUTINE                                  PART 13 OF 16
      SUBROUTINE NEGN(X,Y,ALPHA,BETA,N,BJRE,BJIM,YRE,YIM)
      DIMENSION BJRE(100),BJIM(100),YRE(50),YIM(50)
      L=IABS(N)+1
      SSQ=X**2+Y**2
      TX=2.0*X
      TY=2.0*Y
      RALPHA=ALPHA
      A=(TX*RALPHA+TY*BETA)/SSQ
      B=(-TY*RALPHA+TX*BETA)/SSQ
      BJRE(2)=A*BJRE(1)-B*BJIM(1)-BJRE(2)
      BJIM(2)=B*BJRE(1)+A*BJIM(1)-BJIM(2)
      YRE(2)=A*YRE(1)-B*YIM(1)-YRE(2)
      YIM(2)=B*YRE(1)+A*YIM(1)-YIM(2)
      IF(L-3)3,2,2
    2 DO 1 I=3,L
      RALPHA=RALPHA-1.0
      A=(TX*RALPHA+TY*BETA)/SSQ
      B=(-TY*RALPHA+TX*BETA)/SSQ
      BJRE(I)=A*BJRE(I-1)-B*BJIM(I-1)-BJRE(I-2)
      BJIM(I)=B*BJRE(I-1)+A*BJIM(I-1)-BJIM(I-2)
      YRE(I)=A*YRE(I-1)-B*YIM(I-1)-YRE(I-2)
 1    YIM(I)=B*YRE(I-1)+A*YIM(I-1)-YIM(I-2)
    3 CONTINUE
      RETURN
       END
CBES414  YRECUR SUBROUTINE                                PART 14 OF 16
      SUBROUTINE YRECUR(X,Y,N,BJRE,BJIM,YRE,YIM)
      DIMENSION BJRE(100),BJIM(100),YRE(50),YIM(50)
      SSQ=X**2+Y**2
      TPI=2.0/3.141592654
      AZRE=TPI*X/SSQ
      AZIM=-TPI*Y/SSQ
      L=N+1
      IF(L-3)3,2,2
    2 DO 1 I=3,L
      ZRE=BJRE(I)*YRE(I-1)-BJIM(I)*YIM(I-1)
      ZIM=BJIM(I)*YRE(I-1)+BJRE(I)*YIM(I-1)
      BZRE=ZRE-AZRE
      BZIM=ZIM-AZIM
      BJSQ=BJRE(I-1)**2+BJIM(I-1)**2
      CZRE=BJRE(I-1)/BJSQ
      CZIM=(-BJIM(I-1))/BJSQ
      YRE(I)=BZRE*CZRE-BZIM*CZIM
    1 YIM(I)=BZIM*CZRE+BZRE*CZIM
    3 CONTINUE
      RETURN
       END
CBES415  YGNUP SUBROUTINE                                 PART 15 OF 16
      SUBROUTINE YGNUP(X,Y,ALPHA,BETA,Q,R,ASUMR,ASUMI,BJRE,BJIM,YRE,YIM)
      DIMENSION BJRE(100),BJIM(100),YRE(50),YIM(50)
      PI=3.141592654
      TPI=2.0/PI
      QRE=TPI*(Q**2-R**2)
      QIM=TPI*2.0*Q*R
      DRE=QRE*ASUMR-QIM*ASUMI
      DIM=QIM*ASUMR+QRE*ASUMI
      IF(ALPHA)1,2,1
 2    IF(BETA)1,3,1
 3    CALL YZERO(X,Y,ALPRE,ALPIM)
      GO TO 720
 1    PALPHA=PI*ALPHA
      COX=COS(PALPHA)
      SIX=SIN(PALPHA)
      EXY=EXP(PI*BETA)
      EXY1=1.0/EXY
      COSH=.5*(EXY+EXY1)
      SINH=.5*(EXY-EXY1)
      DEN=(SIX*COSH)**2+(COX*SINH)**2
      ERE=(SIX*COX)/DEN
      EIM=(-COSH*SINH)/DEN
```

```
      ABSQ3=2.0*(ALPHA**2+BETA**2)
      ALPRE=ERE-((QRE*ALPHA+BETA*QIM)/ABSQ3)
      ALPIM=EIM-((QIM*ALPHA-BETA*QRE)/ABSQ3)
 720  TRE=ALPRE*BJRE(2)-ALPIM*BJIM(2)+DRE
      TIM=ALPIM*BJRE(2)+ALPRE*BJIM(2)+DIM
      ALPRE=-(Q*X+R*Y)/(X**2+Y**2)
      ALPIM=-(X*R-Q*Y)/(X**2+Y**2)
      YRE(2)=ALPRE*BJRE(1)-ALPIM*BJIM(1)+TRE
      YIM(2)=ALPIM*BJRE(1)+ALPRE*BJIM(1)+TIM
      RETURN
       END
CBES416  YSUMP SUBROUTINE                                  PART 16 OF 16
      SUBROUTINE YSUMP(X,Y,ALPHA,BETA,K,BJRE,BJIM,ASUMR,ASUMI)
      DIMENSION BJRE(100),BJIM(100)
      A1=ALPHA-1.0
      A2=A1-1.0
      A3=A1+ALPHA
      A4=BETA**2
      A5=2.0*A4
      ABSQ=(-A1)**2+A4
      ROLDRE=((2.0+ALPHA)*(-A1)-A4)/ABSQ
      ROLDIM=(BETA*3.0)/ABSQ
      RES1=-ROLDRE/2.0
      VMS1=-ROLDIM/2.0
      STORE=3.*(ALPHA*X+BETA*Y)/(X**2+Y**2)
      STOIM=3.*(X*BETA-ALPHA*Y)/(X**2+Y**2)
      RES2=(ROLDRE*STORE-ROLDIM*STOIM)
      VMS2=(ROLDRE*STOIM+ROLDIM*STORE)
      ASUMR=RES1*BJRE(2)-VMS1*BJIM(2)
      ASUMR=ASUMR+RES2*BJRE(3)-VMS2*BJIM(3)
      ASUMI=VMS1*BJRE(2)+RES1*BJIM(2)
      ASUMI=ASUMI+VMS2*BJRE(3)+RES2*BJIM(3)
      T=1.0
      DO 500 I=3,K,2
      T=T+1.0
      B1=2.0*T
      F1=B1+ALPHA
      F2=A3+T
      F3=A1+T
      F5=T-ALPHA
      F6=A2+B1
      G1=F1*F2-A5
      G2=(F2+2.0*F1)*BETA
      H1=G1*F3-G2*BETA
      H2=G2*F3+G1*BETA
      P1=F5*F6+A4
      P2=(F5-F6)*BETA
      P3=P1**2+P2**2
      CRE=((H1*P1+H2*P2)/P3)/T
      CIM=((H2*P1-H1*P2)/P3)/T
      TEMP=-(CRE*ROLDRE-CIM*ROLDIM)
      RNEWIM=-(CIM*ROLDRE+CRE*ROLDIM)
      RNEWRE=TEMP
      RES1=(ROLDRE-RNEWRE)/2.0
      VMS1=(ROLDIM-RNEWIM)/2.0
      RES2=(RNEWRE*STORE-RNEWIM*STOIM)
      VMS2=(RNEWRE*STOIM+RNEWIM*STORE)
      BSUMR=RES1*BJRE(I+1)-VMS1*BJIM(I+1)+ASUMR
      BSUMI=VMS1*BJRE(I+1)+RES1*BJIM(I+1)+ASUMI
      BSUMR=RES2*BJRE(I+2)-VMS2*BJIM(I+2)+BSUMR
      BSUMI=VMS2*BJRE(I+2)+RES2*BJIM(I+2)+BSUMI
      IF(ABS((BSUMR/ASUMR)-1.0)-.00000005)521,521,510
 521  IF(ASUMI)520,511,520
 520  IF(ABS((BSUMI/ASUMI)-1.0)-.00000005)511,511,510
 510  ASUMR=BSUMR
      ASUMI=BSUMI
      ROLDIM=RNEWIM
 500  ROLDRE=RNEWRE
 511  RETURN
       END
      SUBROUTINE LOGGAM(X,Y,U,V)
CLOGGAM  LOG OF THE GAMMA FUNCTION OF COMPLEX ARGUMENTS  FORTRAN II
C THIS SUBROUTINE COMPUTES THE NATURAL LOG OF THE GAMMA FUNCTION FOR
C COMPLEX ARGUMENTS.  THE ROUTINE IS ENTERED BY THE STATEMENT
C     CALL LOGGAM(X,Y,U,V)
C WHERE   X IS THE REAL PART OF THE ARGUMENT
C         Y IS THE IMAGINARY PART OF THE ARGUMENT
C         U IS THE REAL PART OF THE RESULT
C         V IS THE IMAGINARY PART OF THE RESULT
      DIMENSION H(7)
      H(1)=2.269488974
```

```
      H(2)=1.517473649
      H(3)=1.011523068
      H(4)=5.256064690E-1
      H(5)=2.523809524E-1
      H(6) = 3.333333333E-2
      H(7) = 8.333333333E-2
      E2 = 1.57079632679
      E8 = 3.14159265359
       B1 = 0.0
      B2 = 0.0
      J = 2
      X 2  = X
 4    IF  (X) 1 ,2 ,3
 3    B6 = ATAN (Y/X)
      T = X **2
  5   B7 = Y ** 2  + T
C     REAL PART OF LOG
      T 1  = 0.5 * ALOG (B7)
      IF  ( X-2.0)7,7,6
 7    B1 = B1 + B6
      B2 = B2 + T1
      X = X + 1.0
      J = 1
      GO TO 4
 6    T3 = -Y* B6 + ( T1 * (X-0.5) - X + 9.189385332 E -1)
      T2 = B6 * (X-0.5) + Y*T1-Y
      T4 = X
      T 5  = -Y
      T1 = B7
      DO 8  I = 1 ,7
      T = H (I)/T1
      T4  = T*T4 + X
      T5 = - ( T* T5 + Y)
 8    T1 = T4**2 + T5 **2
      T3 = T4 - X + T3
      T2 = - T5 - Y + T2
      IF  (J-1) 9,9,10
 9     T3 = T3 - B2
      T2 = T2 - B1
   10 IF  ( X2) 11, 12, 12
 12   U = T3
      V = T 2
      X = X2
      RETURN
 11   U = T3 - E4
      V = T2 - E5
      X = X2
      RETURN
 2    T = 0.0
      IF  (Y) 13 , 14, 15
 13   B6 = -E2
      GO TO 5
 15   B6 = E2
      GO TO 5
 1     E4 = 0.0
      E5 = 0.0
      IE6 = 0
 16   E4 = E4 + 0.5 * ( ALOG ( X**2 + Y **2))
      E5 = E5 + ATAN (Y/X)
      IE6 = IE6 + 1
      X = X + 1.0
      IF  (X) 16, 17, 17
 17   IF ( MOD ( IE6,2)) 18, 4, 18
18     E5 = E5 + E8
      GO TO 4
 14   PRINT  19, X2 , Y
 19   FORMAT ( 29H ATTEMPTED TO TAKE LOGGAM OF 2HX=F6.0,1X2HY8F6.0)
      CALL  EXIT
      END
```

APPENDIX B

The probe response near the cylindrical body - computer print outs.

TABLE B-1 : Probe near a sheathed conducting cylinder.
Incident field = (2,45 deg.) V/m, f=3.0GHz.
(Figs. 3.2.1, 3.2.7, 3.2.13)

FREQUENCY = .3000E+10 FIELD = 2.00 ANGLE = 45.00

PHI IN DEG	LOAD CURRENT SQ FOR PHI	LOAD CURRENT SQ FOR R	LOAD CURRENT SQ FOR TE	LOAD CURRENT SQ TOTAL
0.00	.3827E-12	0.	.5644E-14	.3883E-12
5.00	.1332E-12	.1650E-10	.2209E-14	.1664E-10
10.00	.5525E-13	.2299E-10	.2770E-14	.2305E-10
15.00	.3807E-12	.4652E-11	.1097E-13	.5043E-11
20.00	.2973E-12	.1421E-10	.1487E-13	.1452E-10
25.00	.1186E-12	.3195E-10	.2202E-13	.3208E-10
30.00	.4483E-12	.1855E-10	.4384E-13	.1904E-10
35.00	.5884E-12	.1995E-10	.7381E-13	.2061E-10
40.00	.3852E-12	.4528E-10	.1216E-12	.4578E-10
45.00	.6387E-12	.4329E-10	.2133E-12	.4414E-10
50.00	.1014E-11	.3933E-10	.3611E-12	.4070E-10
55.00	.9425E-12	.6728E-10	.5898E-12	.6881E-10
60.00	.1123E-11	.7989E-10	.9554E-12	.8197E-10
65.00	.1757E-11	.7533E-10	.1519E-11	.7880E-10
70.00	.2095E-11	.9955E-10	.2364E-11	.1040E-09
75.00	.2441E-11	.1236E-09	.3609E-11	.1297E-09
80.00	.3513E-11	.1220E-09	.5384E-11	.1309E-09
85.00	.4759E-11	.1353E-09	.7806E-11	.1479E-09
90.00	.5956E-11	.1596E-09	.1100E-10	.1766E-09
95.00	.8075E-11	.1600E-09	.1508E-10	.1831E-09
100.00	.1111E-10	.1570E-09	.2013E-10	.1883E-09
105.00	.1433E-10	.1674E-09	.2619E-10	.2079E-09
110.00	.1840E-10	.1658E-09	.3322E-10	.2173E-09
115.00	.2399E-10	.1500E-09	.4111E-10	.2151E-09
120.00	.3040E-10	.1402E-09	.4983E-10	.2202E-09
125.00	.3740E-10	.1321E-09	.5851E-10	.2260E-09
130.00	.4577E-10	.1145E-09	.6746E-10	.2277E-09
135.00	.5545E-10	.9389E-10	.7622E-10	.2258E-09
140.00	.6547E-10	.7797E-10	.8456E-10	.2260E-09
145.00	.7549E-10	.6366E-10	.9229E-10	.2314E-09
150.00	.8568E-10	.4778E-10	.9928E-10	.2327E-09
155.00	.9566E-10	.3269E-10	.1054E-09	.2337E-09
160.00	.1046E-09	.2099E-10	.1105E-09	.2361E-09
165.00	.1116E-09	.1242E-10	.1146E-09	.2388E-09
170.00	.1171E-09	.5947E-11	.1176E-09	.2408E-09
175.00	.1204E-09	.1579E-11	.1194E-09	.2414E-09
180.00	.1216E-09	.2835E-36	.1200E-09	.2415E-09
185.00	.1204E-09	.1579E-11	.1194E-09	.2414E-09
190.00	.1171E-09	.5947E-11	.1176E-09	.2408E-09
195.00	.1116E-09	.1242E-10	.1146E-09	.2388E-09
200.00	.1046E-09	.2099E-10	.1105E-09	.2361E-09
205.00	.9566E-10	.3269E-10	.1054E-09	.2337E-09
210.00	.8568E-10	.4778E-10	.9928E-10	.2327E-09
215.00	.7549E-10	.6366E-10	.9229E-10	.2314E-09
220.00	.6547E-10	.7797E-10	.8456E-10	.2260E-09
225.00	.5545E-10	.9389E-10	.7622E-10	.2258E-09
230.00	.4577E-10	.1145E-09	.6746E-10	.2277E-09
235.00	.3740E-10	.1321E-09	.5851E-10	.2260E-09
240.00	.3040E-10	.1402E-09	.4983E-10	.2202E-09
245.00	.2399E-10	.1500E-09	.4111E-10	.2151E-09
250.00	.1840E-10	.1658E-09	.3322E-10	.2173E-09
255.00	.1433E-10	.1674E-09	.2619E-10	.2079E-09
260.00	.1111E-10	.1570E-09	.2013E-10	.1883E-09
265.00	.8075E-11	.1600E-09	.1508E-10	.1831E-09
270.00	.5956E-11	.1596E-09	.1100E-10	.1766E-09
275.00	.4759E-11	.1353E-09	.7806E-11	.1479E-09
280.00	.3513E-11	.1220E-09	.5384E-11	.1309E-09
285.00	.2441E-11	.1236E-09	.3609E-11	.1297E-09
290.00	.2095E-11	.9955E-10	.2364E-11	.1040E-09
295.00	.1757E-11	.7533E-10	.1519E-11	.7880E-10
300.00	.1123E-11	.7989E-10	.9554E-12	.8197E-10
305.00	.9425E-12	.6728E-10	.5898E-12	.6881E-10
310.00	.1014E-11	.3933E-10	.3611E-12	.4070E-10
315.00	.6387E-12	.4329E-10	.2133E-12	.4414E-10
320.00	.3852E-12	.4528E-10	.1216E-12	.4578E-10
325.00	.5884E-12	.1995E-10	.7381E-13	.2061E-10
330.00	.4483E-12	.1855E-10	.4384E-13	.1904E-10
335.00	.1186E-12	.3195E-10	.2202E-13	.3208E-10
340.00	.2973E-12	.1421E-10	.1487E-13	.1452E-10
345.00	.3807E-12	.4652E-11	.1097E-13	.5043E-11
350.00	.5525E-13	.2299E-10	.2770E-14	.2305E-10
355.00	.1332E-12	.1650E-10	.2209E-14	.1664E-10
360.00	.3827E-12	.2040E-34	.5644E-14	.3883E-12

TABLE B-2 : Probe near conducting cylinder.
Incident field = (2,45 deg.) V/m, f=3.0GHz.
(Figs. 3.2.2, 3.2.8, 3.2.14)

FREQUENCY = .3000E+10

PHI IN DEG	LOAD CURRENT SQ FOR PHI	LOAD CURRENT SQ FOR R	LOAD CURRENT SQ FOR TE	LOAD CURRENT SQ TOTAL
0.00	.2200E-12	0.	.6817E-14	.2268E-12
5.00	.9141E-13	.4002E-11	.2693E-14	.4096E-11
10.00	.3180E-13	.6626E-11	.3434E-14	.6661E-11
15.00	.2259E-12	.2526E-11	.1334E-13	.2765E-11
20.00	.2689E-12	.3461E-11	.1817E-13	.3736E-11
25.00	.1503E-12	.9834E-11	.2780E-13	.1001E-10
30.00	.2879E-12	.9998E-11	.5543E-13	.1034E-10
35.00	.5021E-12	.9021E-11	.9414E-13	.9617E-11
40.00	.4788E-12	.1678E-10	.1569E-12	.1741E-10
45.00	.5545E-12	.2419E-10	.2786E-12	.2502E-10
50.00	.8682E-12	.2600E-10	.4709E-12	.2734E-10
55.00	.1013E-11	.3421E-10	.7767E-12	.3600E-10
60.00	.1040E-11	.4899E-10	.1270E-11	.5130E-10
65.00	.1239E-11	.5892E-10	.2037E-11	.6219E-10
70.00	.1337E-11	.6917E-10	.3194E-11	.7370E-10
75.00	.1155E-11	.8771E-10	.4908E-11	.9378E-10
80.00	.9290E-12	.1051E-09	.7359E-11	.1134E-09
85.00	.6371E-12	.1167E-09	.1073E-10	.1281E-09
90.00	.2320E-12	.1306E-09	.1519E-10	.1460E-09
95.00	.1287E-13	.1447E-09	.2093E-10	.1656E-09
100.00	.2688E-12	.1507E-09	.2803E-10	.1790E-09
105.00	.1353E-11	.1512E-09	.3656E-10	.1891E-09
110.00	.3817E-11	.1502E-09	.4645E-10	.2004E-09
115.00	.8059E-11	.1442E-09	.5752E-10	.2097E-09
120.00	.1440E-10	.1317E-09	.6944E-10	.2156E-09
125.00	.2328E-10	.1167E-09	.8185E-10	.2218E-09
130.00	.3486E-10	.1012E-09	.9433E-10	.2303E-09
135.00	.4881E-10	.8455E-10	.1065E-09	.2399E-09
140.00	.6485E-10	.6740E-10	.1181E-09	.2501E-09
145.00	.8185E-10	.5151E-10	.1287E-09	.2621E-09
150.00	.9961E-10	.3780E-10	.1383E-09	.2757E-09
155.00	.1169E-09	.2621E-10	.1466E-09	.2898E-09
160.00	.1325E-09	.1662E-10	.1535E-09	.3026E-09
165.00	.1458E-09	.9187E-11	.1589E-09	.3139E-09
170.00	.1559E-09	.4004E-11	.1629E-09	.3227E-09
175.00	.1622E-09	.9862E-12	.1652E-09	.3284E-09
180.00	.1644E-09	.1100E-35	.1660E-09	.3304E-09
185.00	.1622E-09	.9862E-12	.1652E-09	.3284E-09
190.00	.1559E-09	.4004E-11	.1629E-09	.3227E-09
195.00	.1458E-09	.9187E-11	.1589E-09	.3139E-09
200.00	.1325E-09	.1662E-10	.1535E-09	.3026E-09
205.00	.1169E-09	.2621E-10	.1466E-09	.2898E-09
210.00	.9961E-10	.3780E-10	.1383E-09	.2757E-09
215.00	.8185E-10	.5151E-10	.1287E-09	.2621E-09
220.00	.6485E-10	.6740E-10	.1181E-09	.2501E-09
225.00	.4881E-10	.8455E-10	.1065E-09	.2399E-09
230.00	.3486E-10	.1012E-09	.9433E-10	.2303E-09
235.00	.2328E-10	.1167E-09	.8185E-10	.2218E-09
240.00	.1440E-10	.1317E-09	.6944E-10	.2156E-09
245.00	.8059E-11	.1442E-09	.5752E-10	.2097E-09
250.00	.3817E-11	.1502E-09	.4645E-10	.2004E-09
255.00	.1353E-11	.1512E-09	.3656E-10	.1891E-09
260.00	.2688E-12	.1507E-09	.2803E-10	.1790E-09
265.00	.1287E-13	.1447E-09	.2093E-10	.1656E-09
270.00	.2320E-12	.1306E-09	.1519E-10	.1460E-09
275.00	.6371E-12	.1167E-09	.1073E-10	.1281E-09
280.00	.9290E-12	.1051E-09	.7359E-11	.1134E-09
285.00	.1155E-11	.8771E-10	.4908E-11	.9378E-10
290.00	.1337E-11	.6917E-10	.3194E-11	.7370E-10
295.00	.1239E-11	.5892E-10	.2037E-11	.6219E-10
300.00	.1040E-11	.4899E-10	.1270E-11	.5130E-10
305.00	.1013E-11	.3421E-10	.7767E-12	.3600E-10
310.00	.8682E-12	.2600E-10	.4709E-12	.2734E-10
315.00	.5545E-12	.2419E-10	.2786E-12	.2502E-10
320.00	.4788E-12	.1678E-10	.1569E-12	.1741E-10
325.00	.5021E-12	.9021E-11	.9414E-13	.9617E-11
330.00	.2879E-12	.9998E-11	.5543E-13	.1034E-10
335.00	.1503E-12	.9834E-11	.2780E-13	.1001E-10
340.00	.2689E-12	.3461E-11	.1817E-13	.3736E-11
345.00	.2259E-12	.2526E-11	.1334E-13	.2765E-11
350.00	.3180E-13	.6626E-11	.3434E-14	.6661E-11
355.00	.9141E-13	.4002E-11	.2693E-14	.4096E-11
360.00	.2200E-12	.3540E-35	.6817E-14	.2268E-12

TABLE B-3 : Probe near a sheathed conducting cylinder.
Incident field = (2,45 deg.) V/m,f=2.45GHz,
(Figs. 3.2.3,3.2.9,3.2.15)

FREQUENCY = .2450E+10 FIELD = 2 00 ANGLE = 45.00

PHI IN DEG	LOAD CURRENT SQ FOR PHI	LOAD CURRENT SQ FOR R	LOAD CURRENT SQ FOR TE	LOAD CURRENT SQ TOTAL
0 00	.1554E-12	0.	.5590E-14	.1810E-12
5 00	.7945E-13	.8895E-11	.3083E-14	.8778E-11
10 00	.7204E-14	.1793E-10	.1608E-14	.1794E-10
15 00	.9526E-13	.1061E-10	.6907E-14	.1071E-10
20 00	.1893E-12	.3387E-11	.1338E-13	.3589E-11
25 00	.1314E-12	.1363E-10	.1777E-13	.1377E-10
30 00	.7275E-13	.2502E-10	.2891E-13	.2512E-10
35 00	.1751E-12	.2028E-10	.5335E-13	.2051E-10
40 00	.2987E-12	.1574E-10	.8818E-13	.1613E-10
45 00	.2819E-12	.2880E-10	.1375E-12	.2922E-10
50 00	.2535E-12	.4342E-10	.2196E-12	.4389E-10
55 00	.3857E-12	.4261E-10	.3527E-12	.4335E-10
60 00	.5790E-12	.4217E-10	.5528E-12	.4330E-10
65 00	.6681E-12	.5833E-10	.8495E-12	.5985E-10
70 00	.7530E-12	.7560E-10	.1286E-11	.7764E-10
75 00	.1050E-11	.7839E-10	.1904E-11	.8135E-10
80 00	.1535E-11	.8046E-10	.2747E-11	.8474E-10
85 00	.2032E-11	.9512E-10	.3867E-11	.1010E-09
90 00	.2617E-11	.1094E-09	.5324E-11	.1174E-09
95 00	.3572E-11	.1106E-09	.7171E-11	.1214E-09
100 00	.4945E-11	.1081E-09	.9439E-11	.1225E-09
105 00	.6539E-11	.1122E-09	.1214E-10	.1309E-09
110 00	.8375E-11	.1158E-09	.1526E-10	.1394E-09
115 00	.1075E-10	.1100E-09	.1876E-10	.1395E-09
120 00	.1378E-10	.9898E-10	.2250E-10	.1353E-09
125 00	.1726E-10	.8891E-10	.2642E-10	.1336E-09
130 00	.2104E-10	.8233E-10	.3041E-10	.1338E-09
135 00	.2519E-10	.7200E-10	.3435E-10	.1315E-09
140 00	.2978E-10	.5863E-10	.3815E-10	.1266E-09
145 00	.3460E-10	.4536E-10	.4172E-10	.1217E-09
150 00	.3931E-10	.3423E-10	.4498E-10	.1185E-09
155 00	.4366E-10	.2494E-10	.4786E-10	.1165E-09
160 00	.4754E-10	.1672E-10	.5030E-10	.1146E-09
165 00	.5084E-10	.9852E-11	.5226E-10	.1127E-09
170 00	.5340E-10	.4303E-11	.5388E-10	.1114E-09
175 00	.5504E-10	.1067E-11	.5455E-10	.1107E-09
180 00	.5560E-10	.1077E-36	.5484E-10	.1104E-09
185 00	.5504E-10	.1067E-11	.5455E-10	.1107E-09
190 00	.5340E-10	.4303E-11	.5388E-10	.1114E-09
195 00	.5084E-10	.9852E-11	.5226E-10	.1127E-09
200 00	.4754E-10	.1672E-10	.5030E-10	.1146E-09
205.00	.4366E-10	.2494E-10	.4786E-10	.1165E-09
210.00	.3931E-10	.3423E-10	.4498E-10	.1185E-09
215.00	.3460E-10	.4536E-10	.4172E-10	.1217E-09
220 00	.2978E-10	.5863E-10	.3815E-10	.1266E-09
225.00	.2519E-10	.7200E-10	.3435E-10	.1315E-09
230 00	.2104E-10	.8233E-10	.3041E-10	.1338E-09
235 00	.1726E-10	.8891E-10	.2642E-10	.1336E-09
240.00	.1378E-10	.9898E-10	.2250E-10	.1353E-09
245 00	.1075E-10	.1100E-09	.1875E-10	.1395E-09
250.00	.8375E-11	.1158E-09	.1526E-10	.1394E-09
255 00	.6539E-11	.1122E-09	.1214E-10	.1309E-09
260.00	.4945E-11	.1081E-09	.9439E-11	.1225E-09
265 00	.3572E-11	.1106E-09	.7171E-11	.1214E-09
270.00	.2617E-11	.1094E-09	.5324E-11	.1174E-09
275.00	.2032E-11	.9512E-10	.3867E-11	.1010E-09
280.00	.1535E-11	.8046E-10	.2747E-11	.8474E-10
285.00	.1050E-11	.7839E-10	.1904E-11	.8135E-10
290.00	.7530E-12	.7560E-10	.1286E-11	.7764E-10
295.00	.6681E-12	.5833E-10	.8495E-12	.5985E-10
300.00	.5790E-12	.4217E-10	.5528E-12	.4330E-10
305.00	.3857E-12	.4261E-10	.3527E-12	.4335E-10
310.00	.2535E-12	.4342E-10	.2196E-12	.4389E-10
315.00	.2819E-12	.2880E-10	.1375E-12	.2922E-10
320.00	.2987E-12	.1574E-10	.8818E-13	.1613E-10
325.00	.1751E-12	.2028E-10	.5335E-13	.2051E-10
330.00	.7275E-13	.2502E-10	.2891E-13	.2512E-10
335.00	.1314E-12	.1363E-10	.1777E-13	.1377E-10
340.00	.1893E-12	.3387E-11	.1338E-13	.3589E-11
345.00	.9526E-13	.1061E-10	.6907E-14	.1071E-10
350.00	.7204E-14	.1793E-10	.1608E-14	.1794E-10
355.00	.7945E-13	.8895E-11	.3083E-14	.8778E-11
360.00	.1554E-12	.5001E-35	.5590E-14	.1810E-12

TABLE B-4 : Probe near a conducting cylinder.
Incident field = (2,45 deg.) V/m, f=2.45GHz.
(Figs. 3.2.4, 3.2.10, 3.2.16)

FREQUENCY = .2450E+10

PHI IN DEG	LOAD CURRENT SQ FOR PHI	LOAD CURRENT SQ FOR R	LOAD CURRENT SQ FOR TE	LOAD CURRENT SQ TOTAL
0.00	.1755E-12	0	.7155E-14	.1827E-12
5.00	.9908E-13	.2782E-11	.3937E-14	.2885E-11
10.00	.1473E-13	.6272E-11	.2148E-14	.5289E-11
15.00	.9345E-13	.4740E-11	.9201E-14	.4843E-11
20.00	.2208E-12	.2064E-11	.1776E-13	.2302E-11
25.00	.2088E-12	.4788E-11	.2372E-13	.5000E-11
30.00	.1456E-12	.1023E-10	.3877E-13	.1042E-10
35.00	.2326E-12	.1160E-10	.7163E-13	.1191E-10
40.00	.4088E-12	.1054E-10	.1190E-12	.1107E-10
45.00	.4678E-12	.1440E-10	.1874E-12	.1505E-10
50.00	.4488E-12	.2288E-10	.3017E-12	.2363E-10
55.00	.5465E-12	.2886E-10	.4873E-12	.2990E-10
60.00	.7209E-12	.3178E-10	.7674E-12	.3327E-10
65.00	.7701E-12	.3858E-10	.1184E-11	.4053E-10
70.00	.6958E-12	.5064E-10	.1799E-11	.5313E-10
75.00	.6337E-12	.6135E-10	.2675E-11	.6466E-10
80.00	.5536E-12	.6811E-10	.3876E-11	.7254E-10
85.00	.3600E-12	.7580E-10	.5480E-11	.8164E-10
90.00	.1341E-12	.8638E-10	.7573E-11	.9409E-10
95.00	.3213E-13	.9494E-10	.1023E-10	.1052E-09
100.00	.1468E-12	.9812E-10	.1349E-10	.1118E-09
105.00	.6322E-12	.9837E-10	.1737E-10	.1164E-09
110.00	.1755E-11	.9810E-10	.2185E-10	.1217E-09
115.00	.3729E-11	.9578E-10	.2683E-10	.1263E-09
120.00	.6673E-11	.8945E-10	.3221E-10	.1283E-09
125.00	.1073E-10	.8006E-10	.3782E-10	.1286E-09
130.00	.1604E-10	.6979E-10	.4352E-10	.1293E-09
135.00	.2255E-10	.5955E-10	.4915E-10	.1312E-09
140.00	.3002E-10	.4913E-10	.5456E-10	.1337E-09
145.00	.3808E-10	.3862E-10	.5963E-10	.1363E-09
150.00	.4636E-10	.2868E-10	.6424E-10	.1393E-09
155.00	.5447E-10	.2000E-10	.6830E-10	.1428E-09
160.00	.6195E-10	.1289E-10	.7172E-10	.1466E-09
165.00	.6834E-10	.7328E-11	.7444E-10	.1501E-09
170.00	.7321E-10	.3297E-11	.7642E-10	.1529E-09
175.00	.7626E-10	.8319E-12	.7762E-10	.1547E-09
180.00	.7729E-10	.9985E-37	.7803E-10	.1553E-09
185.00	.7626E-10	.8319E-12	.7762E-10	.1547E-09
190.00	.7321E-10	.3297E-11	.7642E-10	.1529E-09
195.00	.6834E-10	.7328E-11	.7444E-10	.1501E-09
200.00	.6195E-10	.1289E-10	.7172E-10	.1466E-09
205.00	.5447E-10	.2000E-10	.6830E-10	.1428E-09
210.00	.4636E-10	.2868E-10	.6424E-10	.1393E-09
215.00	.3808E-10	.3862E-10	.5963E-10	.1363E-09
220.00	.3002E-10	.4913E-10	.5456E-10	.1337E-09
225.00	.2255E-10	.5955E-10	.4915E-10	.1312E-09
230.00	.1604E-10	.6979E-10	.4352E-10	.1293E-09
235.00	.1073E-10	.8006E-10	.3782E-10	.1286E-09
240.00	.6673E-11	.8945E-10	.3221E-10	.1283E-09
245.00	.3729E-11	.9578E-10	.2683E-10	.1263E-09
250.00	.1755E-11	.9810E-10	.2185E-10	.1217E-09
255.00	.6322E-12	.9837E-10	.1737E-10	.1164E-09
260.00	.1468E-12	.9812E-10	.1349E-10	.1118E-09
265.00	.3213E-13	.9494E-10	.1023E-10	.1052E-09
270.00	.1341E-12	.8638E-10	.7573E-11	.9409E-10
275.00	.3600E-12	.7580E-10	.5480E-11	.8164E-10
280.00	.5536E-12	.6811E-10	.3876E-11	.7254E-10
285.00	.6337E-12	.6135E-10	.2675E-11	.6466E-10
290.00	.6958E-12	.5064E-10	.1799E-11	.5313E-10
295.00	.7701E-12	.3858E-10	.1184E-11	.4053E-10
300.00	.7209E-12	.3178E-10	.7674E-12	.3327E-10
305.00	.5465E-12	.2886E-10	.4873E-12	.2990E-10
310.00	.4488E-12	.2288E-10	.3017E-12	.2363E-10
315.00	.4678E-12	.1440E-10	.1874E-12	.1505E-10
320.00	.4088E-12	.1054E-10	.1190E-12	.1107E-10
325.00	.2326E-12	.1160E-10	.7163E-13	.1191E-10
330.00	.1456E-12	.1023E-10	.3877E-13	.1042E-10
335.00	.2088E-12	.4788E-11	.2372E-13	.5000E-11
340.00	.2208E-12	.2064E-11	.1776E-13	.2302E-11
345.00	.9345E-13	.4740E-11	.9201E-14	.4843E-11
350.00	.1473E-13	.6272E-11	.2148E-14	.5289E-11
355.00	.9908E-13	.2782E-11	.3937E-14	.2885E-11
360.00	.1755E-12	.1353E-35	.7155E-14	.1827E-12

TABLE B-5 : Probe near a sheathed conducting cylinder. Incident field = (2,45 deg.) V/m, f=2.0GHz. (Figs. 3.2.5, 3.2.11, 3.2.17)

FREQUENCY = .2000E+10 FIELD = 2.00 ANGLE = 45 00

PHI IN DEG	LOAD CURRENT SQ FOR PHI	LOAD CURRENT SQ FOR R	LOAD CURRENT SQ FOR TE	LOAD CURRENT SQ TOTAL
0.00	.6830E-13	0.	.4807E-14	.7311E-13
5 00	.4430E-13	.4632E-11	.3199E-14	.4680E-11
10.00	.8126E-14	.1206E-10	.1587E-14	.1207E-10
15.00	.1536E-13	.1220E-10	.4576E-14	.1222E-10
20 00	.6127E-13	.5949E-11	.1114E-13	.6021E-11
25.00	.8862E-13	.3901E-11	.1696E-13	.4006E-11
30.00	.7010E-13	.1112E-10	.2253E-13	.1121E-10
35 00	.4588E-13	.1986E-10	.3440E-13	.1994E-10
40 00	.6570E-13	.2091E-10	.5794E-13	.2103E-10
45.00	.1214E-12	.1703E-10	.9393E-13	.1725E-10
50.00	.1623E-12	.1891E-10	.1446E-12	.1922E-10
55 00	.1867E-12	.2953E-10	.2199E-12	.2992E-10
60 00	.1729E-12	.4006E-10	.3340E-12	.4057E-10
65 00	.2338E-12	.4295E-10	.4992E-12	.4368E-10
70 00	.3577E-12	.4257E-10	.7272E-12	.4365E-10
75.00	.5063E-12	.4806E-10	.1036E-11	.4980E-10
80.00	.6567E-12	.5972E-10	.1450E-11	.6183E-10
85 00	.8536E-12	.6912E-10	.1997E-11	.7187E-10
90 00	.1178E-11	.7126E-10	.2699E-11	.7514E-10
95.00	.1665E-11	.7043E-10	.3573E-11	.7567E-10
100.00	.2277E-11	.7260E-10	.4632E-11	.7951E-10
105 00	.2990E-11	.7710E-10	.5877E-11	.8597E-10
110.00	.3859E-11	.7865E-10	.7299E-11	.8981E-10
115.00	.4978E-11	.7473E-10	.8870E-11	.8858E-10
120 00	.6383E-11	.6781E-10	.1056E-10	.8475E-10
125 00	.8023E-11	.6128E-10	.1232E-10	.8182E-10
130 00	.9825E-11	.5575E-10	.1412E-10	.7989E-10
135.00	.1176E-10	.4968E-10	.1591E-10	.7735E-10
140 00	.1383E-10	.4204E-10	.1764E-10	.7351E-10
145.00	.1600E-10	.3335E-10	.1928E-10	.6863E-10
150 00	.1818E-10	.2490E-10	.2079E-10	.6387E-10
155 00	.2024E-10	.1758E-10	.2212E-10	.5995E-10
160 00	.2206E-10	.1159E-10	.2326E-10	.5691E-10
165 00	.2355E-10	.6790E-11	.2418E-10	.5452E-10
170.00	.2465E-10	.3144E-11	.2485E-10	.5264E-10
175 00	.2533E-10	.8098E-12	.2526E-10	.5139E-10
180 00	.2556E-10	.1190E-36	.2539E-10	.5095E-10
185 00	.2533E-10	.8098E-12	.2526E-10	.5139E-10
190 00	.2465E-10	.3144E-11	.2485E-10	.5264E-10
195.00	.2355E 10	.6790E-11	.2418E-10	.5452E-10
200.00	.2206E-10	.1159E-10	.2326E-10	.5691E-10
205.00	.2024E-10	.1758E-10	.2212E-10	.5995E-10
210.00	.1818E-10	.2490E-10	.2079E-10	.6387E-10
215.00	.1600E-10	.3335E-10	.1928E-10	.6863E-10
220.00	.1383E-10	.4204E-10	.1764E-10	.7351E-10
225.00	.1176E-10	.4968E-10	.1591E-10	.7735E-10
230.00	.9825E-11	.5575E-10	.1412E-10	.7989E-10
235.00	.8023E-11	.6128E-10	.1232E-10	.8182E-10
240.00	.6383E-11	.6781E-10	.1056E-10	.8475E-10
245.00	.4978E-11	.7473E-10	.8870E-11	.8858E-10
250 00	.3859E-11	.7865E-10	.7299E-11	.8981E-10
255.00	.2990E-11	.7710E-10	.5877E-11	.8597E-10
260.00	.2277E-11	.7260E-10	.4632E-11	.7951E-10
265.00	.1665E-11	.7043E-10	.3573E-11	.7567E-10
270.00	.1178E-11	.7126E-10	.2699E-11	.7514E-10
275.00	.8536E-12	.6912E-10	.1997E-11	.7187E-10
280.00	.6567E-12	.5972E-10	.1450E-11	.6183E-10
285.00	.5063E-12	.4806E-10	.1036E-11	.4980E-10
290.00	.3577E-12	.4257E-10	.7272E-12	.4365E-10
295.00	.2338E-12	.4295E-10	.4992E-12	.4368E-10
300.00	.1729E-12	.4006E-10	.3340E-12	.4057E-10
305.00	.1867E-12	.2953E-10	.2199E-12	.2992E-10
310.00	.1623E-12	.1891E-10	.1446E-12	.1922E-10
315.00	.1214E-12	.1703E-10	.9393E-13	.1725E-10
320.00	.6570E-13	.2091E-10	.5794E-13	.2103E-10
325.00	.4588E-13	.1986E-10	.3440E-13	.1994E-10
330.00	.7010E-13	.1112E-10	.2253E-13	.1121E-10
335.00	.8862E-13	.3901E-11	.1696E-13	.4006E-11
340.00	.6127E-13	.5949E-11	.1114E-13	.6021E-11
345.00	.1536E-13	.1220E-10	.4576E-14	.1222E-10
350.00	.8126E-14	.1206E-10	.1587E-14	.1207E-10
355.00	.4430E-13	.4632E-11	.3199E-14	.4680E-11
360.00	.6830E-13	.1821E-36	.4807E-14	.7311E-13

TABLE B-6 : Probe near a conducting cylinder.
Incident field = (2,45 deg.) V/m, f=2.0GHz.
(Figs. 3.2.6,3.2.12,3.2,18)

FREQUENCY = .2000E+10

PHI IN DEG	LOAD CURRENT SQ FOR PHI	LOAD CURRENT SQ FOR R	LOAD CURRENT SQ FOR TE	LOAD CURRENT SQ TOTAL
0.00	.1340E-12	0.	.6553E-14	.1406E-12
5.00	.9142E-13	.1895E-11	.4365E-14	.1990E-11
10.00	.2368E-13	.5186E-11	.2160E-14	.5212E-11
15.00	.3066E-13	.5875E-11	.6193E-14	.5912E-11
20.00	.1178E-12	.3685E-11	.1511E-13	.3818E-11
25.00	.1888E-12	.2486E-11	.2315E-13	.2698E-11
30.00	.1765E-12	.5202E-11	.3110E-13	.5409E-11
35.00	.1372E-12	.9960E-11	.4794E-13	.1015E-10
40.00	.1719E-12	.1266E-10	.8106E-13	.1292E-10
45.00	.2847E-12	.1259E-10	.1316E-12	.1301E-10
50.00	.3770E-12	.1343E-10	.2032E-12	.1401E-10
55.00	.3858E-12	.1836E-10	.3097E-12	.1905E-10
60.00	.3639E-12	.2576E-10	.4717E-12	.2660E-10
65.00	.3848E-12	.3160E-10	.7072E-12	.3270E-10
70.00	.4245E-12	.3486E-10	.1034E-11	.3632E-10
75.00	.4004E-12	.3858E-10	.1479E-11	.4046E-10
80.00	.2952E-12	.4527E-10	.2079E-11	.4764E-10
85.00	.1733E-12	.5335E-10	.2871E-11	.5639E-10
90.00	.8734E-13	.5931E-10	.3888E-11	.6328E-10
95.00	.4739E-13	.6200E-10	.5154E-11	.6721E-10
100.00	.9239E-13	.6324E-10	.6686E-11	.7002E-10
105.00	.3303E-12	.6462E-10	.8489E-11	.7344E-10
110.00	.8806E-12	.6550E-10	.1055E-10	.7693E-10
115.00	.1819E-11	.6416E-10	.1282E-10	.7880E-10
120.00	.3200E-11	.6004E-10	.1527E-10	.7850E-10
125.00	.5097E-11	.5408E-10	.1782E-10	.7700E-10
130.00	.7574E-11	.4756E-10	.2043E-10	.7556E-10
135.00	.1062E-10	.4100E-10	.2302E-10	.7464E-10
140.00	.1414E-10	.3433E-10	.2553E-10	.7400E-10
145.00	.1794E-10	.2751E-10	2790E-10	.7335E-10
150.00	.2184E-10	.2080E-10	.3008E-10	.7271E-10
155.00	.2584E-10	.1464E-10	.3201E-10	.7229E-10
160.00	.2915E-10	.9408E-11	.3364E-10	.7220E-10
165.00	.3216E-10	.5295E-11	.3495E-10	.7241E-10
170.00	.3448E-10	.2353E-11	.3591E-10	.7274E-10
175.00	.3594E-10	.5886E-12	.3649E-10	.7302E-10
180.00	.3644E-10	.6590E-37	.3669E-10	.7313E-10
185.00	.3594E-10	.5886E-12	.3649E-10	.7302E-10
190.00	.3448E-10	.2353E-11	.3591E-10	.7274E-10
195.00	.3216E-10	.5295E-11	.3495E-10	.7241E-10
200.00	.2915E-10	.9408E-11	.3364E-10	.7220E-10
205.00	.2584E-10	.1464E-10	.3201E-10	.7229E-10
210.00	.2184E-10	.2080E-10	.3008E-10	.7271E-10
215.00	.1794E-10	.2751E-10	.2790E-10	.7335E-10
220.00	.1414E-10	.3433E-10	.2553E-10	.7400E-10
225.00	.1082E-10	.4100E-10	.2302E-10	.7464E-10
230.00	.7574E-11	.4756E-10	.2043E-10	.7556E-10
235.00	.5097E-11	.5408E-10	.1782E-10	.7700E-10
240.00	.3200E-11	.6004E-10	.1527E-10	.7850E-10
245.00	.1819E-11	.6416E-10	.1282E-10	.7880E-10
250.00	.8806E-12	.6550E-10	.1055E-10	.7693E-10
255.00	.3303E-12	.6462E-10	.8489E-11	.7344E-10
260.00	9239E-13	.6324E-10	.6686E-11	.7002E-10
265.00	.4739E-13	.6200E-10	.5154E-11	.6721E-10
270.00	.8734E-13	.5931E-10	.3888E-11	.6328E-10
275.00	.1733E-12	.5335E-10	.2871E-11	.5639E-10
280.00	.2952E-12	.4527E-10	.2079E-11	.4764E-10
285.00	.4004E-12	.3858E-10	.1479E-11	.4046E-10
290.00	.4245E-12	.3486E-10	.1034E-11	.3632E-10
295.00	.3848E-12	.3160E-10	.7072E-12	.3270E-10
300.00	.3639E-12	.2576E-10	.4717E-12	.2660E-10
305.00	.3858E-12	.1836E-10	.3097E-12	.1905E-10
310.00	.3770E-12	.1343E-10	.2032E-12	.1401E-10
315.00	.2847E-12	.1259E-10	.1316E-12	.1301E-10
320.00	.1719E-12	.1266E-10	.8106E-13	.1292E-10
325.00	.1372E-12	.9960E-11	.4794E-13	.1015E-10
330.00	.1765E-12	.5202E-11	.3110E-13	.5409E-11
335.00	.1888E-12	.2486E-11	.2315E-13	.2698E-11
340.00	.1178E-12	.3685E-11	.1511E-13	.3818E-11
345.00	.3066E-13	.5875E-11	.6193E-14	.5912E-11
350.00	.2368E-13	.5186E-11	.2160E-14	.5212E-11
355.00	.9142E-13	.1895E-11	.4365E-14	.1990E-11
360.00	.1340E-12	.9183E-36	.6553E-14	.1406E-12

TABLE B-7 : Probe near a cylindrical dielectric shell.
Incident field = (2,45 deg.) V/m, f=3.0GHz.
(Figs. 3.2.19,3.2.22,3.2.25)

FREQUENCY : .3000E+10 FIELD : 2.00 ANGLE : 45.00

PHI IN DEG	LOAD CURRENT SQ FOR PHI	LOAD CURRENT SQ FOR R	LOAD CURRENT SQ FOR TE	LOAD CURRENT SQ TOTAL
0.00	.7637E-10	0	.3514E-09	.4278E-09
5.00	.7786E-10	.5393E-13	.2473E-09	.3251E-09
10.00	.8092E-10	.3321E-12	.7459E-10	.1558E-09
15.00	.8452E-10	.2898E-11	.5064E-11	.9228E-10
20.00	8603E-10	.9078E-11	.1467E-11	.9857E-10
25.00	.8250E-10	.1758E-10	.6345E-11	.1084E-09
30.00	.7199E-10	.2809E-10	.6770E-10	.1678E-09
35.00	.5698E-10	.4854E-10	.1570E-09	.2605E-09
40.00	.4495E-10	.7142E-10	.1715E-09	.2878E-09
45.00	.4117E-10	.8704E-10	.1435E-09	.2717E-09
50.00	.4078E-10	.8814E-10	.1648E-09	.2938E-09
55.00	.3413E-10	.9449E-10	.1911E-09	.3197E-09
60.00	.2092E-10	.1179E-09	.1703E-09	.3092E-09
65.00	.1103E-10	.1367E-09	.1722E-09	.3200E-09
70.00	.9896E-11	.1305E-09	.2049E-09	.3451E-09
75.00	.1130E-10	.1164E-09	.1732E-09	.3009E-09
80.00	.1022E-10	.1198E-09	.1044E-09	.2342E-09
85.00	.7533E-11	.1322E-09	.1103E-09	.2500E-09
90.00	.5128E-11	.1304E-09	.1504E-09	.2860E-09
95.00	.3048E-11	.1134E-09	.1185E-09	.2350E-09
100.00	4083E-11	.1005E-09	.5392E-10	.1585E-09
105.00	.1194E-10	.1017E-09	.4735E-10	.1610E-09
110.00	2348E-10	.1074E-09	.8088E-10	.2118E-09
115.00	.2975E-10	.1050E-09	.9348E-10	.2283E-09
120.00	.2658E-10	.9342E-10	.7980E-10	.1998E-09
125.00	.1986E-10	.8004E-10	.5964E-10	.1595E-09
130.00	1903E-10	.7031E-10	.4346E-10	.1328E-09
135.00	.2812E-10	.6360E-10	.4209E-10	.1338E-09
140.00	.4363E-10	.5693E-10	.6125E-10	.1618E-09
145.00	5882E-10	.4872E-10	.8673E-10	.1943E-09
150.00	.6888E-10	.3915E-10	.9805E-10	.2059E-09
155.00	.7180E-10	.2909E-10	.9109E-10	.1920E-09
160.00	.6988E-10	.1951E-10	.7751E-10	.1667E-09
165.00	.6495E-10	.1128E-10	.6879E-10	.1450E-09
170.00	6005E-10	.5075E-11	.6749E-10	.1326E-09
175.00	.5658E-10	.1274E-11	.6981E-10	1277E-09
180.00	.5535E-10	.1210E-36	.7120E-10	1265E-09
185.00	5658E-10	.1274E-11	.6981E-10	.1277E-09
190.00	6005E-10	.5075E-11	.6749E-10	.1326E-09
195.00	.6495E-10	.1128E-10	.6879E-10	.1450E-09
200.00	.6988E-10	.1951E-10	.7751E-10	.1667E-09
205.00	.7180E-10	.2909E-10	.9109E-10	.1920E-09
210.00	.6888E-10	.3915E-10	.9805E-10	.2059E-09
215.00	5882E-10	.4872E-10	.8673E-10	.1943E-09
220.00	.4363E-10	.5693E-10	.6125E-10	.1618E-09
225.00	.2812E-10	.6360E-10	.4209E-10	1338E-09
230.00	.1903E-10	.7031E-10	.4346E-10	1328E-09
235.00	.1986E-10	.8004E-10	.5964E-10	.1595E-09
240.00	.2658E-10	.9342E-10	.7980E-10	.1998E-09
245.00	.2975E-10	.1050E-09	.9348E-10	.2283E-09
250.00	.2348E-10	.1074E-09	.8088E-10	.2118E-09
255.00	.1194E-10	.1017E-09	.4735E-10	.1610E-09
260.00	4083E-11	.1005E-09	.5392E-10	.1585E-09
265.00	.3048E-11	.1134E-09	.1185E-09	.2350E-09
270.00	.5128E-11	.1304E-09	.1504E-09	.2860E-09
275.00	.7533E-11	.1322E-09	.1103E-09	.2500E-09
280.00	.1022E-10	.1198E-09	.1044E-09	.2342E-09
285.00	.1130E-10	.1164E-09	.1732E-09	.3009E-09
290.00	.9896E-11	.1305E-09	.2049E-09	.3451E-09
295.00	.1103E-10	.1367E-09	.1722E-09	.3200E-09
300.00	.2092E-10	.1179E-09	.1703E-09	.3092E-09
305.00	.3413E-10	.9449E-10	.1911E-09	.3197E-09
310.00	.4078E-10	.8814E-10	.1648E-09	.2938E-09
315.00	.4117E-10	.8704E-10	.1435E-09	.2717E-09
320.00	.4495E-10	.7142E-10	.1715E-09	.2878E-09
325.00	.5698E-10	.4854E-10	.1570E-09	.2605E-09
330.00	.7199E-10	.2809E-10	.6770E-10	.1678E-09
335.00	.8250E-10	.1758E-10	.6345E-11	.1084E-09
340.00	.8603E-10	.9078E-11	.1467E-11	.9857E-10
345.00	.8452E-10	.2898E-11	.5064E-11	.9228E-10
350.00	.8092E-10	.3321E-12	.7459E-10	.1558E-09
355.00	.7786E-10	.5393E-13	.2473E-09	.3251E-09
360.00	.7637E-10	.3543E-36	.3514E-09	.4278E-09

TABLE B-8 : Probe near a cylindrical dielectric shell.
Incident field = (2,45 deg.) V/m, f=2.45GHz.
(Figs. 3.2.20, 3.2.23, 3.2.26)

FREQUENCY : .2450E+10 FIELD : 2.00 ANGLE : 45.00

PHI IN DEG	LOAD CURRENT SQ FOR PHI	LOAD CURRENT SQ FOR R	LOAD CURRENT SQ FOR TE	LOAD CURRENT SQ TOTAL
0.00	.5463E-10	0	.7313E-10	.1278E-09
5.00	.5481E-10	.1614E-12	.6246E-10	.1174E-09
10.00	.5525E-10	.9236E-12	.4693E-10	.1031E-09
15.00	.5568E-10	.3205E-11	.4942E-10	.1083E-09
20.00	.5571E-10	.7995E-11	.6255E-10	.1282E-09
25.00	.5477E-10	.1487E-10	.6204E-10	.1317E-09
30.00	.5198E-10	.2186E-10	.4993E-10	.1238E-09
35.00	.4631E-10	.2809E-10	.5684E-10	.1312E-09
40.00	.3758E-10	.3572E-10	.9507E-10	.1684E-09
45.00	.2754E-10	.4703E-10	.1337E-09	.2083E-09
50.00	.1931E-10	.5951E-10	.1388E-09	.2157E-09
55.00	.1497E-10	.6680E-10	.1103E-09	.1921E-09
60.00	.1345E-10	.6655E-10	.8907E-10	.1691E-09
65.00	.1164E-10	.6480E-10	.8862E-10	.1651E-09
70.00	.7948E-11	.6923E-10	.9402E-10	.1712E-09
75.00	.3733E-11	.7895E-10	.9249E-10	.1752E-09
80.00	.1080E-11	.8511E-10	.8987E-10	.1761E-09
85.00	.2351E-12	.8191E-10	.9000E-10	.1721E-09
90.00	.3235E-12	.7340E-10	.8283E-10	.1566E-09
95.00	.1606E-11	.6796E-10	.6443E-10	.1340E-09
100.00	.5284E-11	.6865E-10	.5005E-10	.1240E-09
105.00	.1103E-10	.7129E-10	.5395E-10	.1363E-09
110.00	.1613E-10	.7032E-10	.6805E-10	.1545E-09
115.00	.1792E-10	.6425E-10	.7225E-10	.1544E-09
120.00	.1651E-10	.5572E-10	.5938E-10	.1316E-09
125.00	.1477E-10	.4799E-10	.4045E-10	.1032E-09
130.00	.1586E-10	.4228E-10	.2925E-10	.8739E-10
135.00	.2091E-10	.3783E-10	.2961E-10	.8836E-10
140.00	.2878E-10	.3330E-10	.3674E-10	.9882E-10
145.00	.3728E-10	.2800E-10	.4484E-10	.1101E-09
150.00	.4459E-10	.2209E-10	.5113E-10	.1178E-09
155.00	.4986E-10	.1615E-10	.5517E-10	.1212E-09
160.00	.5313E-10	.1072E-10	.5718E-10	.1210E-09
165.00	.5487E-10	.6197E-11	.5752E-10	.1186E-09
170.00	.5566E-10	.2810E-11	.5680E-10	.1153E-09
175.00	.5596E-10	.7113E-12	.5588E-10	.1126E-09
180.00	.5602E-10	.5653E-37	.5548E-10	.1115E-09
185.00	.5596E-10	.7113E-12	.5588E-10	.1125E-09
190.00	.5566E-10	.2810E-11	.5680E-10	.1153E-09
195.00	.5487E-10	.6197E-11	.5752E-10	.1186E-09
200.00	.5313E-10	.1072E-10	.5718E-10	.1210E-09
205.00	.4986E-10	.1615E-10	.5517E-10	.1212E-09
210.00	.4459E-10	.2209E-10	.5113E-10	.1178E-09
215.00	.3728E-10	.2800E-10	.4484E-10	.1101E-09
220.00	.2878E-10	.3330E-10	.3674E-10	.9882E-10
225.00	.2091E-10	.3783E-10	.2961E-10	.8836E-10
230.00	.1586E-10	.4228E-10	.2925E-10	.8739E-10
235.00	.1477E-10	.4799E-10	.4045E-10	.1032E-09
240.00	.1651E-10	.5572E-10	.5938E-10	.1316E-09
245.00	.1792E-10	.6425E-10	.7225E-10	.1544E-09
250.00	.1613E-10	.7032E-10	.6805E-10	.1545E-09
255.00	.1103E-10	.7129E-10	.5395E-10	.1363E-09
260.00	.5284E-11	.6865E-10	.5005E-10	.1240E-09
265.00	.1606E-11	.6796E-10	.6443E-10	.1340E-09
270.00	.3235E-12	.7340E-10	.8283E-10	.1566E-09
275.00	.2351E-12	.8191E-10	.9000E-10	.1721E-09
280.00	.1080E-11	.8511E-10	.8987E-10	.1761E-09
285.00	.3733E-11	.7895E-10	.9249E-10	.1752E-09
290.00	.7948E-11	.6923E-10	.9402E-10	.1712E-09
295.00	.1164E-10	.6480E-10	.8862E-10	.1651E-09
300.00	.1345E-10	.6655E-10	.8907E-10	.1691E-09
305.00	.1497E-10	.6680E-10	.1103E-09	.1921E-09
310.00	.1931E-10	.5951E-10	.1388E-09	.2157E-09
315.00	.2754E-10	.4703E-10	.1337E-09	.2083E-09
320.00	.3758E-10	.3572E-10	.9507E-10	.1684E-09
325.00	.4631E-10	.2809E-10	.5684E-10	.1312E-09
330.00	.5198E-10	.2186E-10	.4993E-10	.1238E-09
335.00	.5477E-10	.1487E-10	.6204E-10	.1317E-09
340.00	.5571E-10	.7995E-11	.6255E-10	.1282E-09
345.00	.5568E-10	.3205E-11	.4942E-10	.1083E-09
350.00	.5525E-10	.9236E-12	.4693E-10	.1031E-09
355.00	.5481E-10	.1614E-12	.6246E-10	.1174E-09
360.00	.5463E-10	.8088E-37	.7313E-10	.1278E-09

TABLE B-9 : Probe near a cylindrical dielectric shell.
Incident field = (2,45 deg.) V/m, f=2.0GHz.
(Figs. 3.2.21, 3.2.24, 3.2.27)

FREQUENCY : .2000E+10 FIELD : 2.00 ANGLE : 45.00

PHI IN DEG	LOAD CURRENT SQ FOR PHI	LOAD CURRENT SQ FOR R	LOAD CURRENT SQ FOR TE	LOAD CURRENT SQ TOTAL
0.00	.4018E-10	0	.7143E-11	.4733E-10
5.00	.3977E-10	.2772E-12	.9196E-11	.4924E-10
10.00	.3858E-10	.1160E-11	.1712E-10	.5686E-10
15.00	.3678E-10	.2853E-11	.3304E-10	.7267E-10
20.00	.3460E-10	.5683E-11	.5379E-10	.9408E-10
25.00	.3226E-10	.9793E-11	.7015E-10	.1122E-09
30.00	.2990E-10	.1473E-10	.7334E-10	.1180E-09
35.00	.2741E-10	.1949E-10	.6340E-10	.1103E-09
40.00	.2446E-10	.2333E-10	.5044E-10	.9824E-10
45.00	.2066E-10	.2658E-10	.4663E-10	.9387E-10
50.00	.1597E-10	.3054E-10	.5558E-10	.1021E-09
55.00	.1097E-10	.3611E-10	.6946E-10	.1165E-09
60.00	.6709E-11	.4244E-10	.7652E-10	.1257E-09
65.00	.3971E-11	.4718E-10	.7156E-10	.1227E-09
70.00	.2720E-11	.4847E-10	.5943E-10	.1106E-09
75.00	.2210E-11	.4687E-10	.4900E-10	.9808E-10
80.00	.1759E-11	.4604E-10	.4605E-10	.9185E-10
85.00	.1376E-11	.4533E-10	.4605E-10	.9276E-10
90.00	.1576E-11	.4776E-10	.4811E-10	.9744E-10
95.00	.2612E-11	.5013E-10	.4921E-10	.1019E-09
100.00	.4015E-11	.5012E-10	.4932E-10	.1035E-09
105.00	.5021E-11	.4710E-10	.4822E-10	.1003E-09
110.00	.5375E-11	.4228E-10	.4484E-10	.9249E-10
115.00	.5700E-11	.3742E-10	.3890E-10	.8202E-10
120.00	.7055E-11	.3360E-10	.3220E-10	.7286E-10
125.00	.1014E-10	.3078E-10	.2771E-10	.6863E-10
130.00	.1481E-10	.2827E-10	.2733E-10	.7041E-10
135.00	.2024E-10	.2539E-10	.3064E-10	.7627E-10
140.00	.2538E-10	.2189E-10	.3555E-10	.8282E-10
145.00	.2948E-10	.1788E-10	.3981E-10	.8717E-10
150.00	.3227E-10	.1374E-10	.4217E-10	.8818E-10
155.00	.3388E-10	.9824E-11	.4259E-10	.8630E-10
160.00	.3464E-10	.6404E-11	.4173E-10	.8277E-10
165.00	.3490E-10	.3646E-11	.4039E-10	.7893E-10
170.00	.3493E-10	.1632E-11	.3914E-10	.7570E-10
175.00	.3489E-10	.4098E-12	.3832E-10	.7362E-10
180.00	.3487E-10	.4536E-37	.3804E-10	.7291E-10
185.00	.3489E-10	.4098E-12	.3832E-10	.7362E-10
190.00	.3493E-10	.1632E-11	.3914E-10	.7570E-10
195.00	.3490E-10	.3646E-11	.4039E-10	.7893E-10
200.00	.3464E-10	.6404E-11	.4173E-10	.8277E-10
205.00	.3388E-10	.9824E-11	.4259E-10	.8630E-10
210.00	.3227E-10	.1374E-10	.4217E-10	.8818E-10
215.00	.2948E-10	.1788E-10	.3981E-10	.8717E-10
220.00	.2538E-10	.2189E-10	.3555E-10	.8282E-10
225.00	.2024E-10	.2539E-10	.3064E-10	.7627E-10
230.00	.1481E-10	.2827E-10	.2733E-10	.7041E-10
235.00	.1014E-10	.3078E-10	.2771E-10	.6863E-10
240.00	.7055E-11	.3360E-10	.3220E-10	.7286E-10
245.00	.5700E-11	.3742E-10	.3890E-10	.8202E-10
250.00	.5375E-11	.4228E-10	.4484E-10	.9249E-10
255.00	.5021E-11	.4710E-10	.4822E-10	.1003E-09
260.00	.4015E-11	.5012E-10	.4932E-10	.1035E-09
265.00	.2612E-11	.5013E-10	.4921E-10	.1019E-09
270.00	.1576E-11	.4776E-10	.4811E-10	.9744E-10
275.00	.1376E-11	.4533E-10	.4605E-10	.9276E-10
280.00	.1759E-11	.4604E-10	.4605E-10	.9185E-10
285.00	.2210E-11	.4687E-10	.4900E-10	.9808E-10
290.00	.2720E-11	.4847E-10	.5943E-10	.1106E-09
295.00	.3971E-11	.4718E-10	.7156E-10	.1227E-09
300.00	.6709E-11	.4244E-10	.7652E-10	.1257E-09
305.00	.1097E-10	.3611E-10	.6946E-10	.1165E-09
310.00	.1597E-10	.3064E-10	.5558E-10	.1021E-09
315.00	.2066E-10	.2658E-10	.4663E-10	.9387E-10
320.00	.2446E-10	.2333E-10	.5044E-10	.9824E-10
325.00	.2741E-10	.1949E-10	.6340E-10	.1103E-09
330.00	.2990E-10	.1473E-10	.7334E-10	.1180E-09
335.00	.3226E-10	.9793E-11	.7015E-10	.1122E-09
340.00	.3460E-10	.5683E-11	.5379E-10	.9408E-10
345.00	.3678E-10	.2853E-11	.3304E-10	.7267E-10
350.00	.3858E-10	.1160E-11	.1712E-10	.5686E-10
355.00	.3977E-10	.2772E-12	.9196E-11	.4924E-10
360.00	.4018E-10	.1417E-36	.7143E-11	.4733E-10

TABLE B-10 : Probe near a cylindrical biological body.
Incident field = (2,45 deg.) V/m, f=3.0GHz.
(Fig. 3.3.1)

FREQUENCY : .3000E+10

PHI IN DEG	LOAD CURRENT SQ FOR PHI	LOAD CURRENT SQ FOR R	LOAD CURRENT SQ FOR TE	LOAD CURRENT SQ TOTAL
0.00	.1598E-12	0.	.7641E-14	.1674E-12
5.00	.6597E-13	.3267E-11	.2976E-14	.3336E-11
10.00	.2513E-13	.5371E-11	.3806E-14	.5400E-11
15.00	.1694E-12	.2057E-11	.1501E-13	.2242E-11
20.00	.1976E-12	.2984E-11	.2037E-13	.3202E-11
25.00	.1156E-12	.8211E-11	.3045E-13	.8357E-11
30.00	.2245E-12	.8305E-11	.6065E-13	.8591E-11
35.00	.3816E-12	.7868E-11	.1022E-12	.8352E-11
40.00	.3693D-12	.1462E-10	.1693E-12	.1516E-10
45.00	.4491E-12	.2077E-10	.2981E-12	.2152E-10
50.00	.6990E-12	.2277E-10	.5060E-12	.2397E-10
55.00	.8150E-12	.3056E-10	.8293E-12	.3221E-10
60.00	.8849E-12	.4342E-10	1347E-11	.4563E-10
65.00	1047E-11	.5237E-10	.2147E-11	.5557E-10
70.00	.1129E-11	.6253E-10	.3347E-11	.6701E-10
75.00	.1007E-11	.7956E-10	.5120E-11	.8569E-10
80.00	.8576E-12	.9518E-10	.7644E-11	.1037E-09
85.00	.6259E-12	.1066E-09	.1109E-10	.1184E-09
90.00	.3016E-12	.1203E-09	.1562E-10	.1363E-09
95.00	.1693E-12	.1334E-09	.2139E-10	.1550E-09
100.00	.4754E-12	.1394E-09	.2849E-10	.1684E-09
105.00	.1540E-11	.1409E-09	.3697E-10	.1794E-09
110.00	.3876E-11	.1405E-09	.4676E-10	.1912E-09
115.00	.7871E-11	.1350E-09	.5765E-10	.2006E-09
120.00	.1385E-10	.1239E-09	.6929E-10	.2070E-09
125.00	.2224E-10	.1103E-09	.8128E-10	.2138E-09
130.00	.3322E-10	.9589E-10	.9321E-10	.2223E-09
135.00	.4651E-10	.8019E-10	.1047E-09	.2314E-09
140.00	.6170E-10	.6407E-10	.1155E-09	.2413E-09
145.00	7823E-10	.4914E-10	.1254E-09	.2528E-09
150.00	.9529E-10	.3615E-10	.1343E-09	.2657E-09
155.00	1119E-09	.2506E-10	.1419E-09	.2788E-09
160.00	.1270E-09	.1589E-10	.1482E-09	.2911E-09
165.00	.1397E-09	.8798E-11	.1532E-09	.3018E-09
170.00	.1494E-09	.3846E-11	.1566E-09	.3101E-09
175.00	.1565E-09	.9503E-12	.1590E-09	.3165E-09
180.00	.1576E-09	.1071E-36	.1597E-09	.3173E-09
185.00	.1565E-09	.9503E-12	.1590E-09	.3165E-09
190.00	.1494E-09	.3846E-11	.1566E-09	.3101E-09
195.00	.1397E-09	.8798E-11	.1532E-09	.3018E-09
200.00	.1270E-09	.1589E-10	.1482E-09	.2911E-09
205.00	.1119E-09	.2506E-10	.1419E-09	.2788E-09
210.00	.9529E-10	.3615E-10	.1343E-09	.2657E-09
215.00	.7823E-10	.4914E-10	.1254E-09	.2528E-09
220.00	.6170E-10	.6407E-10	.1155E-09	.2413E-09
225.00	.4651E-10	.8019E-10	.1047E-09	.2314E-09
230.00	.3322E-10	.9589E-10	.9321E-10	.2223E-09
235.00	.2224E-10	.1103E-09	.8128E-10	.2138E-09
240.00	.1385E-10	.1239E-09	.6929E-10	.2070E-09
245.00	.7871E-11	.1350E-09	.5765E-10	.2006E-09
250.00	.3876E-11	.1405E-09	.4676E-10	.1912E-09
255.00	.1540E-11	.1409E-09	.3697E-10	.1794E-09
260.00	.4754E-12	.1394E-09	.2849E-10	.1684E-09
265.00	.1693E-12	.1334E-09	.2139E-10	.1550E-09
270.00	.3016E-12	.1203E-09	.1562E-10	.1363E-09
275.00	.6259E-12	.1066E-09	.1109E-10	.1184E-09
280.00	.8576E-12	.9518E-10	.7644E-11	.1037E-09
285.00	.1007E-11	.7956E-10	.5120E-11	.8569E-10
290.00	.1129E-11	.6253E-10	.3347E-11	.6701E-10
295.00	.1047E-11	.5237E-10	.2147E-11	.5557E-10
300.00	.8849E-12	.4342E-10	.1347E-11	.4563E-10
305.00	.8150E-12	.3056E-10	.8293E-12	.3221E-10
310.00	.6990E-12	.2277E-10	.5060E-12	.2397E-10
315.00	.4491E-12	.2077E-10	.2981E-12	.2152E-10
320.00	.3693E-12	.1462E-10	.1693E-12	.1516E-10
325.00	.3816E-12	.7868E-11	.1022E-12	.8352E-11
330.00	.2245E-12	.8305E-11	.6065E-13	.8591E-11
335.00	.1156E-12	.8211E-11	.3045E-13	.8357E-11
340.00	.1976E-12	.2984E-11	.2037E-13	.3202E-11
345.00	.1694E-12	.2057E-11	.1501E-13	.2242E-11
350.00	.2513E-13	.5371E-11	.3806E-14	.5400E-11
355.00	.6597E-13	.3267E-11	.2976E-14	.3336E-11
360.00	.1598E-12	.2922E-35	.7641E-14	.1674E-12

TABLE B-11 : Probe near a cylindrical biological body. Incident field = (2,45 deg.) V/m, f=2.45GHz. (Fig. 3.3.2)

FREQUENCY : .2450E+10

PHI IN DEG	LOAD CURRENT SQ FOR PHI	LOAD CURRENT SQ FOR R	LOAD CURRENT SQ FOR TE	LOAD CURRENT SQ TOTAL
0.00	.1305E-12	0	.8275E-14	.1387E-12
5.00	.7326E-13	.2391E-11	.4584E-14	.2469E-11
10.00	.1111E-13	.5360E-11	.2375E-14	.5373E-11
15.00	.7145E-13	.4015E-11	.1019E-13	.4098E-11
20.00	.1660E-12	.1807E-11	.1975E-13	.1993E-11
25.00	.1561E-12	.4281E-11	.2629E-13	.4463E-11
30.00	.1132E-12	.8973E-11	.4291E-13	.9129E-11
35.00	.1861E-12	.1008E-10	.7925E-13	.1035E-10
40.00	.3200E-12	.9369E-11	.1310E-12	.9820E-11
45.00	.3626E-12	.1310E-10	.2043E-12	.1367E-10
50.00	.3567E-12	.2062E-10	.3264E-12	.2130E-10
55.00	.4476E-12	.2581E-10	.5246E-12	.2678E-10
60.00	.5890E-12	.2874E-10	.8228E-12	.3015E-10
65.00	.6281E-12	.3542E-10	.1265E-11	.3731E-10
70.00	.5824E-12	.4648E-10	.1915E-11	.4896E-10
75.00	.5517E-12	.5605E-10	.2834E-11	.5943E-10
80.00	.4934E-12	.6254E-10	.4084E-11	.6711E-10
85.00	.3402E-12	.7027E-10	.5741E-11	.7635E-10
90.00	.1836E-12	.8031E-10	.7891E-11	.8839E-10
95.00	.1581E-12	.8813E-10	.1060E-10	.9869E-10
100.00	.3381E-12	.9128E-10	.1392E-10	.1055E-09
105.00	.8674E-12	.9209E-10	.1785E-10	.1108E-09
110.00	.1997E-11	.9223E-10	.2236E-10	.1166E-09
115.00	.3934E-11	.9008E-10	.2735E-10	.1214E-09
120.00	.6804E-11	.8414E-10	.3268E-10	.1236E-09
125.00	.1075E-10	.7554E-10	.3819E-10	.1245E-09
130.00	.1590E-10	.6612E-10	.4373E-10	.1258E-09
135.00	.2223E-10	.5653E-10	.4915E-10	.1279E-09
140.00	.2949E-10	.4662E-10	.5431E-10	.1304E-09
145.00	.3734E-10	.3661E-10	.5911E-10	.1331E-09
150.00	.4542E-10	.2722E-10	.6345E-10	.1361E-09
155.00	.5333E-10	.1903E-10	.6726E-10	.1396E-09
160.00	.6063E-10	.1229E-10	.7046E-10	.1434E-09
165.00	.6684E-10	.6995E-11	.7300E-10	.1468E-09
170.00	.7158E-10	.3146E-11	.7484E-10	.1496E-09
175.00	.7454E-10	.7930E-12	.7598E-10	.1513E-09
180.00	.7554E-10	.8639E-37	.7634E-10	.1519E-09
185.00	.7454E-10	.7930E-12	.7598E-10	.1513E-09
190.00	.7158E-10	.3146E-11	.7484E-10	.1496E-09
195.00	.6684E-10	.6995E-11	.7300E-10	.1468E-09
200.00	.6063E-10	.1229E-10	.7046E-10	.1434E-09
205.00	.5333E-10	.1903E-10	.6726E-10	.1396E-09
210.00	.4542E-10	.2722E-10	.6345E-10	.1361E-09
215.00	.3734E-10	.3661E-10	.5911E-10	.1331E-09
220.00	.2949E-10	.4662E-10	.5431E-10	.1304E-09
225.00	.2223E-10	.5653E-10	.4915E-10	.1279E-09
230.00	.1590E-10	.6612E-10	.4373E-10	.1258E-09
235.00	.1075E-10	.7554E-10	.3819E-10	.1245E-09
240.00	.6804E-11	.8414E-10	.3268E-10	.1236E-09
245.00	.3934E-11	.9008E-10	.2735E-10	.1214E-09
250.00	.1997E-11	.9223E-10	.2236E-10	.1166E-09
255.00	.8674E-12	.9209E-10	.1785E-10	.1108E-09
260.00	.3381E-12	.9128E-10	.1392E-10	.1055E-09
265.00	.1581E-12	.8813E-10	.1060E-10	.9869E-10
270.00	.1836E-12	.8031E-10	.7891E-11	.8839E-10
275.00	.3402E-12	.7027E-10	.5741E-11	.7635E-10
280.00	.4934E-12	.6254E-10	.4084E-11	.6711E-10
285.00	.5517E-12	.5605E-10	.2834E-11	.5943E-10
290.00	.5824E-12	.4648E-10	.1915E-11	.4896E-10
295.00	.6281E-12	.3542E-10	.1265E-11	.3731E-10
300.00	.5890E-12	.2874E-10	.8228E-12	.3015E-10
305.00	.4476E-12	.2581E-10	.5246E-12	.2678E-10
310.00	.3567E-12	.2062E-10	.3264E-12	.2130E-10
315.00	.3626E-12	.1310E-10	.2043E-12	.1367E-10
320.00	.3200E-12	.9369E-11	.1310E-12	.9820E-11
325.00	.1861E-12	.1008E-10	.7925E-13	.1035E-10
330.00	.1132E-12	.8973E-11	.4291E-13	.9129E-11
335.00	.1561E-12	.4281E-11	.2629E-13	.4463E-11
340.00	.1660E-12	.1807E-11	.1975E-13	.1993E-11
345.00	.7145E-13	.4015E-11	.1019E-13	.4098E-11
350.00	.1111E-13	.5360E-11	.2375E-14	.5373E-11
355.00	.7326E-13	.2391E-11	.4584E-14	.2469E-11
360.00	.1305E-12	.1141E-35	.8275E-14	.1387E-12

TABLE B-12 : Probe near a cylindrical biological body. Incident field = (2,45 deg.) V/m, f=1.5GHz. (Fig. 3.3.3)

FREQUENCY = .1500E+10

PHI IN DEG	LOAD CURRENT SQ FOR PHI	LOAD CURRENT SQ FOR R	LOAD CURRENT SQ FOR TE	LOAD CURRENT SQ TOTAL
0.00	.6471E-13	0	.6828E-14	.7154E-13
5.00	.5147E-13	.1104E-11	.5376E-14	.1161E-11
10.00	.2400E-13	.3544E-11	.2975E-14	.3571E-11
15.00	.8492E-14	.5440E-11	.3500E-14	.5452E-11
20.00	.2213E-13	.5489E-11	.8873E-14	.5520E-11
25.00	.5784E-13	.4078E-11	.1749E-13	.4154E-11
30.00	.9036E-13	.2982E-11	.2684E-13	.3099E-11
35.00	.9891E-13	.3871E-11	.3643E-13	.4006E-11
40.00	.8592E-13	.6910E-11	.5106E-13	.7047E-11
45.00	.7411E-13	.1064E-10	.7632E-13	.1079E-10
50.00	.8381E-13	.1324E-10	.1162E-12	.1344E-10
55.00	.1124E-12	.1416E-10	.1725E-12	.1445E-10
60.00	.1367E-12	.1451E-10	.2478E-12	.1489E-10
65.00	.1357E-12	.1608E-10	.3485E-12	.1655E-10
70.00	.1101E-12	.1964E-10	.4846E-12	.2024E-10
75.00	.7866E-13	.2442E-10	.6673E-12	.2517E-10
80.00	.5793E-13	.2869E-10	.9057E-12	.2966E-10
85.00	.4944E-13	.3128E-10	.1207E-11	.3253E-10
90.00	.4949E-13	.3235E-10	.1578E-11	.3397E-10
95.00	.6893E-13	.3295E-10	.2024E-11	.3504E-10
100.00	.1400E-12	.3392E-10	.2552E-11	.3661E-10
105.00	.3029E-12	.3516E-10	.3162E-11	.3861E-10
110.00	.5882E-12	.3585E-10	.3850E-11	.4029E-10
115.00	.1012E-11	.3525E-10	.4608E-11	.4087E-10
120.00	.1584E-11	.3317E-10	.5421E-11	.4017E-10
125.00	.2318E-11	.3000E-10	.6275E-11	.3859E-10
130.00	.3229E-11	.2633E-10	.7149E-11	.3671E-10
135.00	.4315E-11	.2260E-10	.8023E-11	.3494E-10
140.00	.5553E-11	.1897E-10	.8877E-11	.3340E-10
145.00	.6891E-11	.1544E-10	.9687E-11	.3202E-10
150.00	.8280E-11	.1200E-10	.1043E-10	.3069E-10
155.00	.9583E-11	.8728E-11	.1110E-10	.2941E-10
160.00	.1079E-10	.5785E-11	.1166E-10	.2823E-10
165.00	.1180E-10	.3332E-11	.1212E-10	.2725E-10
170.00	.1257E-10	.1503E-11	.1245E-10	.2652E-10
175.00	.1305E-10	.3785E-12	.1265E-10	.2608E-10
180.00	.1322E-10	.5486E-37	.1272E-10	.2593E-10
185.00	.1305E-10	.3785E-12	.1265E-10	.2608E-10
190.00	.1257E-10	.1503E-11	.1245E-10	.2652E-10
195.00	.1180E-10	.3332E-11	.1212E-10	.2725E-10
200.00	.1079E-10	.5785E-11	.1166E-10	.2823E-10
205.00	.9583E-11	.8728E-11	.1110E-10	.2941E-10
210.00	.8280E-11	.1200E-10	.1043E-10	.3069E-10
215.00	.6891E-11	.1544E-10	.9687E-11	.3202E-10
220.00	.5553E-11	.1897E-10	.8877E-11	.3340E-10
225.00	.4315E-11	.2260E-10	.8023E-11	.3494E-10
230.00	.3229E-11	.2633E-10	.7149E-11	.3671E-10
235.00	.2318E-11	.3000E-10	.6275E-11	.3859E-10
240.00	.1584E-11	.3317E-10	.5421E-11	.4017E-10
245.00	.1012E-11	.3525E-10	.4608E-11	.4087E-10
250.00	.5882E-12	.3585E-10	.3850E-11	.4029E-10
255.00	.3029E-12	.3516E-10	.3162E-11	.3861E-10
260.00	.1400E-12	.3392E-10	.2552E-11	.3661E-10
265.00	.6893E-13	.3295E-10	.2024E-11	.3504E-10
270.00	.4949E-13	.3235E-10	.1578E-11	.3397E-10
275.00	.4944E-13	.3128E-10	.1207E-11	.3253E-10
280.00	.5793E-13	.2869E-10	.9057E-12	.2966E-10
285.00	.7866E-13	.2442E-10	.6673E-12	.2517E-10
290.00	.1101E-12	.1964E-10	.4846E-12	.2024E-10
295.00	.1357E-12	.1608E-10	.3485E-12	.1655E-10
300.00	.1367E-12	.1451E-10	.2478E-12	.1489E-10
305.00	.1124E-12	.1416E-10	.1725E-12	.1445E-10
310.00	.8381E-13	.1324E-10	.1162E-12	.1344E-10
315.00	.7411E-13	.1064E-10	.7632E-13	.1079E-10
320.00	.8592E-13	.6910E-11	.5106E-13	.7047E-11
325.00	.9891E-13	.3871E-11	.3643E-13	.4006E-11
330.00	.9036E-13	.2982E-11	.2684E-13	.3099E-11
335.00	.5784E-13	.4078E-11	.1749E-13	.4154E-11
340.00	.2213E-13	.5489E-11	.8873E-14	.5520E-11
345.00	.8492E-14	.5440E-11	.3500E-14	.5452E-11
350.00	.2400E-13	.3544E-11	.2975E-14	.3571E-11
355.00	.5147E-13	.1104E-11	.5376E-14	.1161E-11
360.00	.6471E-13	.6883E-36	.6828E-14	.7154E-13

TABLE B-13 : Probe near a cylindrical biological body.
Incident field = (2,0 deg.) V/m, f=3.0GHz.
(Fig. 3.3.4)

FREQUENCY = .3000E+10 FIELD = 2.00 ANGLE = 0.00

PHI IN DEG	LOAD CURRENT SQ FOR PHI	LOAD CURRENT SQ FOR R	LOAD CURRENT SQ FOR TE	LOAD CURRENT SQ TOTAL
0.00	0	0	.1528E-13	.1528E-13
5.00	0	0	.5951E-14	.5951E-14
10.00	0	0	.7612E-14	.7612E-14
15.00	0	0	.3003E-13	.3003E-13
20.00	0	0	.4074E-13	.4074E-13
25.00	0	0	.6090E-13	.6090E-13
30.00	0	0	.1213E-12	.1213E-12
35.00	0	0	.2044E-12	.2044E-12
40.00	0	0	.3387E-12	.3387E-12
45.00	0	0	.5963E-12	.5963E-12
50.00	0	0	.1012E-11	.1012E-11
55.00	0	0	.1659E-11	.1659E-11
60.00	0	0	.2694E-11	.2694E-11
65.00	0	0	.4294E-11	.4294E-11
70.00	0	0	.6693E-11	.6693E-11
75.00	0	0	.1024E-10	.1024E-10
80.00	0	0	.1529E-10	.1529E-10
85.00	0	0	.2217E-10	.2217E-10
90.00	0	0	.3123E-10	.3123E-10
95.00	0	0	.4277E-10	.4277E-10
100.00	0	0	.5698E-10	.5698E-10
105.00	0	0	.7395E-10	.7395E-10
110.00	0	0	.9353E-10	.9353E-10
115.00	0	0	.1153E-09	.1153E-09
120.00	0	0	.1386E-09	.1386E-09
125.00	0	0	.1626E-09	.1626E-09
130.00	0	0	.1864E-09	.1864E-09
135.00	0	0	.2095E-09	.2095E-09
140.00	0	0	.2311E-09	.2311E-09
145.00	0	0	.2509E-09	.2509E-09
150.00	0	0	.2685E-09	.2685E-09
155.00	0	0	.2838E-09	.2838E-09
160.00	0	0	.2965E-09	.2965E-09
165.00	0	0	.3065E-09	.3065E-09
170.00	0	0	.3137E-09	.3137E-09
175.00	0	0	.3180E-09	.3180E-09
180.00	0	0	.3195E-09	.3195E-09
185.00	0	0	.3180E-09	.3180E-09
190.00	0	0	.3137E-09	.3137E-09
195.00	0	0	.3065E-09	.3065E-09
200.00	0	0	.2965E-09	.2965E-09
205.00	0	0	.2838E-09	.2838E-09
210.00	0	0	.2685E-09	.2685E-09
215.00	0	0	.2509E-09	.2509E-09
220.00	0	0	.2311E-09	.2311E-09
225.00	0	0	.2095E-09	.2095E-09
230.00	0	0	.1864E-09	.1864E-09
235.00	0	0	.1626E-09	.1626E-09
240.00	0	0	.1386E-09	.1386E-09
245.00	0	0	.1153E-09	.1153E-09
250.00	0	0	.9353E-10	.9353E-10
255.00	0	0	.7395E-10	.7395E-10
260.00	0	0	.5698E-10	.5698E-10
265.00	0	0	.4277E-10	.4277E-10
270.00	0	0	.3123E-10	.3123E-10
275.00	0	0	.2217E-10	.2217E-10
280.00	0	0	.1529E-10	.1529E-10
285.00	0	0	.1024E-10	.1024E-10
290.00	0	0	.6693E-11	.6693E-11
295.00	0	0	.4294E-11	.4294E-11
300.00	0	0	.2694E-11	.2694E-11
305.00	0	0	.1659E-11	.1659E-11
310.00	0	0	.1012E-11	.1012E-11
315.00	0	0	.5963E-12	.5963E-12
320.00	0	0	.3387E-12	.3387E-12
325.00	0	0	.2044E-12	.2044E-12
330.00	0	0	.1213E-12	.1213E-12
335.00	0	0	.6090E-13	.6090E-13
340.00	0	0	.4074E-13	.4074E-13
345.00	0	0	.3003E-13	.3003E-13
350.00	0	0	.7612E-14	.7612E-14
355.00	0	0	.5951E-14	.5951E-14
360.00	0	0	.1528E-13	.1528E-13

TABLE B-14 : Probe near a cylindrical biological body.
Incident field = (2,30 deg.) V/m, f=3.0GHz.
(Fig. 3.3.4)

FREQUENCY : .3000E+10 FIELD : 2.00 ANGLE : 30.00

PHI IN DEG	LOAD CURRENT SQ FOR PHI	LOAD CURRENT SQ FOR R	LOAD CURRENT SQ FOR TE	LOAD CURRENT SQ TOTAL
0.00	.7988E-13	0.	.1146E-13	.9135E-13
5.00	.3299E-13	.1634E-11	.4464E-14	.1671E-11
10.00	.1256E-13	.2685E-11	.5709E-14	.2704E-11
15.00	.8471E-13	.1029E-11	.2252E-13	.1136E-11
20.00	.9881E-13	.1492E-11	.3056E-13	.1621E-11
25.00	.5781E-13	.4108E-11	.4568E-13	.4209E-11
30.00	.1122E-12	.4153E-11	.9057E-13	.4356E-11
35.00	.1908E-12	.3934E-11	.1533E-12	.4278E-11
40.00	.1847E-12	.7310E-11	.2540E-12	.7748E-11
45.00	.2245E-12	.1039E-10	.4472E-12	.1106E-10
50.00	.3495E-12	.1138E-10	.7590E-12	.1249E-10
55.00	.4075E-12	.1528E-10	.1244E-11	.1693E-10
60.00	.4325E-12	.2171E-10	.2021E-11	.2416E-10
65.00	.5235E-12	.2619E-10	.3220E-11	.2993E-10
70.00	.5647E-12	.3127E-10	.5020E-11	.3685E-10
75.00	.5036E-12	.3978E-10	.7680E-11	.4796E-10
80.00	.4288E-12	.4759E-10	.1147E-10	.5949E-10
85.00	.3129E-12	.5332E-10	.1863E-10	.7027E-10
90.00	.1508E-12	.6017E-10	.2343E-10	.8374E-10
95.00	.8465E-13	.6671E-10	.3208E-10	.9887E-10
100.00	.2377E-12	.6971E-10	.4274E-10	.1127E-09
105.00	.7701E-12	.7046E-10	.5546E-10	.1267E-09
110.00	.1938E-11	.7026E-10	.7015E-10	.1423E-09
115.00	.3936E-11	.6752E-10	.8647E-10	.1579E-09
120.00	.6926E-11	.6193E-10	.1039E-09	.1728E-09
125.00	.1112E-10	.5516E-10	.1219E-09	.1882E-09
130.00	.1661E-10	.4794E-10	.1398E-09	.2044E-09
135.00	.2326E-10	.4009E-10	.1571E-09	.2204E-09
140.00	.3085E-10	.3203E-10	.1733E-09	.2362E-09
145.00	.3911E-10	.2457E-10	.1882E-09	.2518E-09
150.00	.4765E-10	.1808E-10	.2014E-09	.2671E-09
155.00	.5594E-10	.1253E-10	.2128E-09	.2813E-09
160.00	.6348E-10	.7946E-11	.2224E-09	.2938E-09
165.00	.6986E-10	.4399E-11	.2299E-09	.3041E-09
170.00	.7472E-10	.1923E-11	.2353E-09	.3119E-09
175.00	.7776E-10	.4752E-12	.2385E-09	.3168E-09
180.00	.7880E-10	.5355E-37	.2396E-09	.3184E-09
185.00	.7776E-10	.4752E-12	.2385E-09	.3168E-09
190.00	.7472E-10	.1923E-11	.2353E-09	.3119E-09
195.00	.6986E-10	.4399E-11	.2299E-09	.3041E-09
200.00	.6348E-10	.7946E-11	.2224E-09	.2938E-09
205.00	.5594E-10	.1253E-10	.2128E-09	.2813E-09
210.00	.4765E-10	.1808E-10	.2014E-09	.2671E-09
215.00	.3911E-10	.2457E-10	.1882E-09	.2518E-09
220.00	.3085E-10	.3203E-10	.1733E-09	.2362E-09
225.00	.2326E-10	.4009E-10	.1571E-09	.2204E-09
230.00	.1661E-10	.4794E-10	.1398E-09	.2044E-09
235.00	.1112E-10	.5516E-10	.1219E-09	.1882E-09
240.00	.6926E-11	.6193E-10	.1039E-09	.1728E-09
245.00	.3936E-11	.6752E-10	.8647E-10	.1579E-09
250.00	.1938E-11	.7026E-10	.7015E-10	.1423E-09
255.00	.7701E-12	.7046E-10	.5546E-10	.1267E-09
260.00	.2377E-12	.6971E-10	.4274E-10	.1127E-09
265.00	.8465E-13	.6671E-10	.3208E-10	.9887E-10
270.00	.1508E-12	.6017E-10	.2343E-10	.8374E-10
275.00	.3129E-12	.5332E-10	.1863E-10	.7027E-10
280.00	.4288E-12	.4759E-10	.1147E-10	.5949E-10
285.00	.5036E-12	.3978E-10	.7680E-11	.4796E-10
290.00	.5647E-12	.3127E-10	.5020E-11	.3685E-10
295.00	.5235E-12	.2619E-10	.3220E-11	.2993E-10
300.00	.4325E-12	.2171E-10	.2021E-11	.2416E-10
305.00	.4075E-12	.1528E-10	.1244E-11	.1693E-10
310.00	.3495E-12	.1138E-10	.7590E-12	.1249E-10
315.00	.2245E-12	.1039E-10	.4472E-12	.1106E-10
320.00	.1847E-12	.7310E-11	.2540E-12	.7748E-11
325.00	.1908E-12	.3934E-11	.1533E-12	.4278E-11
330.00	.1122E-12	.4153E-11	.9057E-13	.4356E-11
335.00	.5781E-13	.4108E-11	.4568E-13	.4209E-11
340.00	.9881E-13	.1492E-11	.3056E-13	.1621E-11
345.00	.8471E-13	.1029E-11	.2252E-13	.1136E-11
350.00	.1256E-13	.2685E-11	.5709E-14	.2704E-11
355.00	.3299E-13	.1634E-11	.4464E-14	.1671E-11
360.00	.7988E-13	.1461E-35	.1146E-13	.9135E-13

TABLE B-15 : Probe near a cylindrical biological body. Incident field = (2,60 deg.) V/m, f=3.0GHz. (Fig. 3.3.4)

FREQUENCY : .3000E+10 FIELD : 2.00 ANGLE : 60.00

PHI IN DEG	LOAD CURRENT SQ FOR PHI	LOAD CURRENT SQ FOR R	LOAD CURRENT SQ FOR TE	LOAD CURRENT SQ TOTAL
0.00	.2397E-12	0	.3821E-14	.2435E-12
5.00	.9896E-13	.4901E-11	.1488E-14	.5001E-11
10.00	.3769E-13	.8056E-11	.1903E-14	.8096E-11
15.00	.2541E-12	.3086E-11	.7507E-14	.3348E-11
20.00	.2964E-12	.4476E-11	.1019E-13	.4782E-11
25.00	.1734E-12	.1232E-10	.1523E-13	.1251E-10
30.00	.3367E-12	.1248E-10	.3032E-13	.1283E-10
35.00	.5723E-12	.1180E-10	.5110E-13	.1243E-10
40.00	.5540E-12	.2193E-10	.8466E-13	.2257E-10
45.00	.8736E-12	.3116E-10	.1491E-12	.3198E-10
50.00	.1048E-11	.3415E-10	.2530E-12	.3545E-10
55.00	.1223E-11	.4584E-10	.4146E-12	.4748E-10
60.00	.1297E-11	.6513E-10	.6735E-12	.6710E-10
65.00	.1570E-11	.7856E-10	.1073E-11	.8120E-10
70.00	.1694E-11	.9380E-10	.1673E-11	.9716E-10
75.00	.1511E-11	.1193E-09	.2560E-11	.1234E-09
80.00	.1286E-11	.1428E-09	.3822E-11	.1479E-09
85.00	.9388E-12	.1600E-09	.5543E-11	.1665E-09
90.00	.4523E-12	.1805E-09	.7809E-11	.1888E-09
95.00	.2540E-12	.2001E-09	.1069E-10	.2111E-09
100.00	.7131E-12	.2091E-09	.1425E-10	.2241E-09
105.00	.2310E-11	.2114E-09	.1849E-10	.2322E-09
110.00	.5814E-11	.2108E-09	.2338E-10	.2400E-09
115.00	.1181E-10	.2026E-09	.2882E-10	.2432E-09
120.00	.2078E-10	.1858E-09	.3484E-10	.2412E-09
125.00	.3336E-10	.1655E-09	.4064E-10	.2395E-09
130.00	.4982E-10	.1438E-09	.4660E-10	.2403E-09
135.00	.6977E-10	.1203E-09	.5236E-10	.2424E-09
140.00	.9255E-10	.9610E-10	.5777E-10	.2464E-09
145.00	.1173E-09	.7372E-10	.6272E-10	.2538E-09
150.00	.1429E-09	.5423E-10	.6713E-10	.2643E-09
155.00	.1678E-09	.3760E-10	.7095E-10	.2764E-09
160.00	.1905E-09	.2384E-10	.7412E-10	.2884E-09
165.00	.2096E-09	.1320E-10	.7662E-10	.2994E-09
170.00	.2242E-09	.5769E-11	.7842E-10	.3083E-09
175.00	.2333E-09	.1426E-11	.7951E-10	.3142E-09
180.00	.2364E-09	.1607E-36	.7987E-10	.3163E-09
185.00	.2333E-09	.1426E-11	.7951E-10	.3142E-09
190.00	.2242E-09	.5769E-11	.7842E-10	.3083E-09
195.00	.2096E-09	.1320E-10	.7662E-10	.2994E-09
200.00	.1905E-09	.2384E-10	.7412E-10	.2884E-09
205.00	.1678E-09	.3760E-10	.7095E-10	.2764E-09
210.00	.1429E-09	.5423E-10	.6713E-10	.2643E-09
215.00	.1173E-09	.7372E-10	.6272E-10	.2538E-09
220.00	.9255E-10	.9610E-10	.5777E-10	.2464E-09
225.00	.6977E-10	.1203E-09	.5236E-10	.2424E-09
230.00	.4982E-10	.1438E-09	.4660E-10	.2403E-09
235.00	.3336E-10	.1655E-09	.4064E-10	.2395E-09
240.00	.2078E-10	.1858E-09	.3484E-10	.2412E-09
245.00	.1181E-10	.2026E-09	.2882E-10	.2432E-09
250.00	.5814E-11	.2108E-09	.2338E-10	.2400E-09
255.00	.2310E-11	.2114E-09	.1849E-10	.2322E-09
260.00	.7131E-12	.2091E-09	.1425E-10	.2241E-09
265.00	.2540E-12	.2001E-09	.1069E-10	.2111E-09
270.00	.4523E-12	.1805E-09	.7809E-11	.1888E-09
275.00	.9388E-12	.1600E-09	.5543E-11	.1665E-09
280.00	.1286E-11	.1428E-09	.3822E-11	.1479E-09
285.00	.1511E-11	.1193E-09	.2560E-11	.1234E-09
290.00	.1694E-11	.9380E-10	.1673E-11	.9716E-10
295.00	.1570E-11	.7856E-10	.1073E-11	.8120E-10
300.00	.1297E-11	.6513E-10	.6735E-12	.6710E-10
305.00	.1223E-11	.4584E-10	.4146E-12	.4748E-10
310.00	.1048E-11	.3415E-10	.2530E-12	.3545E-10
315.00	.8736E-12	.3116E-10	.1491E-12	.3198E-10
320.00	.5540E-12	.2193E-10	.8466E-13	.2257E-10
325.00	.5723E-12	.1180E-10	.5110E-13	.1243E-10
330.00	.3367E-12	.1248E-10	.3032E-13	.1283E-10
335.00	.1734E-12	.1232E-10	.1523E-13	.1251E-10
340.00	.2964E-12	.4476E-11	.1019E-13	.4782E-11
345.00	.2541E-12	.3086E-11	.7507E-14	.3348E-11
350.00	.3769E-13	.8056E-11	.1903E-14	.8096E-11
355.00	.9896E-13	.4901E-11	.1488E-14	.5001E-11
360.00	.2397E-12	.4384E-36	.3821E-14	.2435E-12

TABLE B-16 : Probe near a cylindrical biological body. Incident field = (2,90 deg.) V/m, f=3.0GHz. (Fig. 3.3.4)

FREQUENCY = .3000E+10 FIELD = 2.00 ANGLE = 90.00

PHI IN DEG	LOAD CURRENT SQ FOR PHI	LOAD CURRENT SQ FOR R	LOAD CURRENT SQ FOR TE	LOAD CURRENT SQ TOTAL
0.00	.3195E-12	0	.2386E-41	.3195E-12
5.00	.1319E-12	.6534E-11	.9293E-42	.6666E-11
10.00	.5026E-13	.1074E-10	.1188E-41	.1079E-10
15.00	.3388E-12	.4115E-11	.4689E-41	.4454E-11
20.00	.3952E-12	.5968E-11	.6362E-41	.6363E-11
25.00	.2312E-12	.1642E-10	.9509E-41	.1665E-10
30.00	.4490E-12	.1661E-10	.1894E-40	.1706E-10
35.00	.7631E-12	.1574E-10	.3192E-40	.1650E-10
40.00	.7387E-12	.2924E-10	.5288E-40	.2998E-10
45.00	.8882E-12	.4154E-10	.9311E-40	.4244E-10
50.00	.1398E-11	.4553E-10	.1580E-39	.4693E-10
55.00	.1630E-11	.6113E-10	.2590E-39	.6276E-10
60.00	.1730E-11	.8884E-10	.4207E-39	.8857E-10
65.00	.2094E-11	.1047E-09	.6704E-39	.1068E-09
70.00	.2259E-11	.1251E-09	.1045E-38	.1273E-09
75.00	.2014E-11	.1591E-09	.1599E-38	.1611E-09
80.00	.1715E-11	.1904E-09	.2387E-38	.1921E-09
85.00	.1252E-11	.2133E-09	.3462E-38	.2146E-09
90.00	.6031E-12	.2407E-09	.4877E-38	.2413E-09
95.00	.3386E-12	.2668E-09	.6678E-38	.2672E-09
100.00	.9508E-12	.2788E-09	.8898E-38	.2798E-09
105.00	.3080E-11	.2818E-09	.1155E-37	.2849E-09
110.00	.7753E-11	.2810E-09	.1460E-37	.2888E-09
115.00	.1574E-10	.2701E-09	.1800E-37	.2858E-09
120.00	.2770E-10	.2477E-09	.2164E-37	.2754E-09
125.00	.4448E-10	.2206E-09	.2538E-37	.2651E-09
130.00	.6643E-10	.1918E-09	.2911E-37	.2582E-09
135.00	.9303E-10	.1604E-09	.3270E-37	.2534E-09
140.00	.1234E-09	.1281E-09	.3608E-37	.2515E-09
145.00	.1565E-09	.9829E-10	.3917E-37	.2547E-09
150.00	.1906E-09	.7231E-10	.4193E-37	.2629E-09
155.00	.2237E-09	.5013E-10	.4431E-37	.2739E-09
160.00	.2539E-09	.3178E-10	.4629E-37	.2857E-09
165.00	.2795E-09	.1780E-10	.4786E-37	.2970E-09
170.00	.2989E-09	.7692E-11	.4898E-37	.3066E-09
175.00	.3110E-09	.1901E-11	.4966E-37	.3129E-09
180.00	.3152E-09	.2142E-36	.4989E-37	.3152E-09
185.00	.3110E-09	.1901E-11	.4966E-37	.3129E-09
190.00	.2989E-09	.7692E-11	.4898E-37	.3066E-09
195.00	.2795E-09	.1780E-10	.4786E-37	.2970E-09
200.00	.2539E-09	.3178E-10	.4629E-37	.2857E-09
205.00	.2237E-09	.5013E-10	.4431E-37	.2739E-09
210.00	.1906E-09	.7231E-10	.4193E-37	.2629E-09
215.00	.1565E-09	.9829E-10	.3917E-37	.2547E-09
220.00	.1234E-09	.1281E-09	.3608E-37	.2515E-09
225.00	.9303E-10	.1604E-09	.3270E-37	.2534E-09
230.00	.6643E-10	.1918E-09	.2911E-37	.2582E-09
235.00	.4448E-10	.2206E-09	.2538E-37	.2651E-09
240.00	.2770E-10	.2477E-09	.2164E-37	.2754E-09
245.00	.1574E-10	.2701E-09	.1800E-37	.2858E-09
250.00	.7753E-11	.2810E-09	.1460E-37	.2888E-09
255.00	.3080E-11	.2818E-09	.1155E-37	.2849E-09
260.00	.9508E-12	.2788E-09	.8898E-38	.2798E-09
265.00	.3386E-12	.2668E-09	.6678E-38	.2672E-09
270.00	.6031E-12	.2407E-09	.4877E-38	.2413E-09
275.00	.1252E-11	.2133E-09	.3462E-38	.2146E-09
280.00	.1715E-11	.1904E-09	.2387E-38	.1921E-09
285.00	.2014E-11	.1591E-09	.1599E-38	.1611E-09
290.00	.2259E-11	.1251E-09	.1045E-38	.1273E-09
295.00	.2094E-11	.1047E-09	.6704E-39	.1068E-09
300.00	.1730E-11	.8884E-10	.4207E-39	.8857E-10
305.00	.1630E-11	.6113E-10	.2590E-39	.6276E-10
310.00	.1398E-11	.4553E-10	.1580E-39	.4693E-10
315.00	.8882E-12	.4154E-10	.9311E-40	.4244E-10
320.00	.7387E-12	.2924E-10	.5288E-40	.2988E-10
325.00	.7631E-12	.1574E-10	.3192E-40	.1650E-10
330.00	.4490E-12	.1661E-10	.1894E-40	.1706E-10
335.00	.2312E-12	.1642E-10	.9509E-41	.1665E-10
340.00	.3952E-12	.5968E-11	.6362E-41	.6363E-11
345.00	.3388E-12	.4115E-11	.4689E-41	.4454E-11
350.00	.5026E-13	.1074E-10	.1188E-41	.1079E-10
355.00	.1319E-12	.6534E-11	.9293E-42	.6666E-11
360.00	.3195E-12	.5845E-35	.2386E-41	.3195E-12

TABLE B-17 : Probe near a cylindrical biological body.
Incident field = (2,0 deg.) V/m, f=2.45GHz.
(Fig. 3.3.5)

FREQUENCY = .2450E+10   FIELD = 2.00   ANGLE = 0.00

PHI IN DEG	LOAD CURRENT SQ FOR PHI	LOAD CURRENT SQ FOR R	LOAD CURRENT SQ FOR TE	LOAD CURRENT SQ TOTAL
0.00	0.	0.	.1655E-13	.1655E-13
5.00	0.	0.	.9129E-14	.9129E-14
10.00	0.	0.	.4750E-14	.4750E-14
15.00	0.	0.	.2039E-13	.2039E-13
20.00	0.	0.	.3950E-13	.3950E-13
25.00	0.	0.	.5259E-13	.5259E-13
30.00	0.	0.	.6582E-13	.6582E-13
35.00	0.	0.	.1585E-12	.1585E-12
40.00	0.	0.	.2620E-12	.2620E-12
45.00	0.	0.	.4087E-12	.4087E-12
50.00	0.	0.	.6529E-12	.6529E-12
55.00	0.	0.	.1049E-11	.1049E-11
60.00	0.	0.	.1646E-11	.1646E-11
65.00	0.	0.	.2530E-11	.2530E-11
70.00	0.	0.	.3830E-11	.3830E-11
75.00	0.	0.	.5668E-11	.5668E-11
80.00	0.	0.	.8168E-11	.8168E-11
85.00	0.	0.	.1148E-10	.1148E-10
90.00	0.	0.	.1578E-10	.1578E-10
95.00	0.	0.	.2121E-10	.2121E-10
100.00	0.	0.	.2784E-10	.2784E-10
105.00	0.	0.	.3571E-10	.3571E-10
110.00	0.	0.	.4472E-10	.4472E-10
115.00	0.	0.	.5470E-10	.5470E-10
120.00	0.	0.	.6536E-10	.6536E-10
125.00	0.	0.	.7638E-10	.7638E-10
130.00	0.	0.	.8746E-10	.8746E-10
135.00	0.	0.	.9830E-10	.9830E-10
140.00	0.	0.	.1086E-09	.1086E-09
145.00	0.	0.	.1182E-09	.1182E-09
150.00	0.	0.	.1269E-09	.1269E-09
155.00	0.	0.	.1345E-09	.1345E-09
160.00	0.	0.	.1409E-09	.1409E-09
165.00	0.	0.	.1460E-09	.1460E-09
170.00	0.	0.	.1497E-09	.1497E-09
175.00	0.	0.	.1519E-09	.1519E-09
180.00	0.	0.	.1527E-09	.1527E-09
185.00	0.	0.	.1519E-09	.1519E-09
190.00	0.	0.	.1497E-09	.1497E-09
195.00	0.	0.	.1460E-09	.1460E-09
200.00	0.	0.	.1409E-09	.1409E-09
205.00	0.	0.	.1345E-09	.1345E-09
210.00	0.	0.	.1269E-09	.1269E-09
215.00	0.	0.	.1182E-09	.1182E-09
220.00	0.	0.	.1086E-09	.1086E-09
225.00	0.	0.	.9830E-10	.9830E-10
230.00	0.	0.	.8746E-10	.8746E-10
235.00	0.	0.	.7638E-10	.7638E-10
240.00	0.	0.	.6536E-10	.6536E-10
245.00	0.	0.	.5470E-10	.5470E-10
250.00	0.	0.	.4472E-10	.4472E-10
255.00	0.	0.	.3571E-10	.3571E-10
260.00	0.	0.	.2784E-10	.2784E-10
265.00	0.	0.	.2121E-10	.2121E-10
270.00	0.	0.	.1578E-10	.1578E-10
275.00	0.	0.	.1148E-10	.1148E-10
280.00	0.	0.	.8168E-11	.8168E-11
285.00	0.	0.	.5668E-11	.5668E-11
290.00	0.	0.	.3830E-11	.3830E-11
295.00	0.	0.	.2530E-11	.2530E-11
300.00	0.	0.	.1646E-11	.1646E-11
305.00	0.	0.	.1049E-11	.1049E-11
310.00	0.	0.	.6529E-12	.6529E-12
315.00	0.	0.	.4087E-12	.4087E-12
320.00	0.	0.	.2620E-12	.2620E-12
325.00	0.	0.	.1585E-12	.1585E-12
330.00	0.	0.	.6582E-13	.6582E-13
335.00	0.	0.	.5259E-13	.5259E-13
340.00	0.	0.	.3950E-13	.3950E-13
345.00	0.	0.	.2039E-13	.2039E-13
350.00	0.	0.	.4750E-14	.4750E-14
355.00	0.	0.	.9129E-14	.9129E-14
360.00	0.	0.	.1655E-13	.1655E-13

TABLE B-18 : Probe near a cylindrical biological body.
Incident field = (2,30 deg.) V/m, f=2.45GHz.
(Fig. 3.3.5)

FREQUENCY = .2450E+10 FIELD = 2.00 ANGLE = 30.00

PHI IN DEG	LOAD CURRENT SQ FOR PHI	LOAD CURRENT SQ FOR R	LOAD CURRENT SQ FOR TE	LOAD CURRENT SQ TOTAL
0.00	.6523E-13	0	.1241E-13	.7764E-13
5.00	.3663E-13	.1196E-11	.6847E-14	.1239E-11
10.00	.5554E-14	.2680E-11	.3562E-14	.2689E-11
15.00	.3572E-13	.2007E-11	.1529E-13	.2058E-11
20.00	.8300E-13	.9035E-12	.2963E-13	.1016E-11
25.00	.7804E-13	.2140E-11	.3944E-13	.2258E-11
30.00	.5659E-13	.4486E-11	.6436E-13	.4607E-11
35.00	.9306E-13	.5040E-11	.1189E-12	.5252E-11
40.00	.1600E-12	.4884E-11	.1965E-12	.5041E-11
45.00	.1813E-12	.6552E-11	.3065E-12	.7040E-11
50.00	.1783E-12	.1031E-10	.4897E-12	.1098E-10
55.00	.2238E-12	.1290E-10	.7869E-12	.1392E-10
60.00	.2945E-12	.1437E-10	.1234E-11	.1590E-10
65.00	.3140E-12	.1771E-10	.1897E-11	.1992E-10
70.00	.2912E-12	.2323E-10	.2872E-11	.2639E-10
75.00	.2758E-12	.2802E-10	.4251E-11	.3255E-10
80.00	.2467E-12	.3127E-10	.6126E-11	.3764E-10
85.00	.1701E-12	.3514E-10	.8612E-11	.4392E-10
90.00	.9182E-13	.4016E-10	.1184E-10	.5208E-10
95.00	.7906E-13	.4407E-10	.1590E-10	.6005E-10
100.00	.1691E-12	.4564E-10	.2088E-10	.6669E-10
105.00	.4337E-12	.4604E-10	.2678E-10	.7326E-10
110.00	.9985E-12	.4612E-10	.3354E-10	.8066E-10
115.00	.1967E-11	.4504E-10	.4102E-10	.8803E-10
120.00	.3402E-11	.4207E-10	.4902E-10	.9449E-10
125.00	.5375E-11	.3777E-10	.5729E-10	.1004E-09
130.00	.7952E-11	.3306E-10	.6560E-10	.1066E-09
135.00	.1112E-10	.2826E-10	.7372E-10	.1131E-09
140.00	.1475E-10	.2331E-10	.8147E-10	.1195E-09
145.00	.1867E-10	.1831E-10	.8867E-10	.1256E-09
150.00	.2271E-10	.1361E-10	.9518E-10	.1315E-09
155.00	.2667E-10	.9517E-11	.1009E-09	.1371E-09
160.00	.3031E-10	.6145E-11	.1057E-09	.1421E-09
165.00	.3342E-10	.3497E-11	.1095E-09	.1464E-09
170.00	.3579E-10	.1573E-11	.1123E-09	.1498E-09
175.00	.3727E-10	.3965E-12	.1139E-09	.1516E-09
180.00	.3777E-10	.4319E-37	.1145E-09	.1523E-09
185.00	.3727E-10	.3965E-12	.1139E-09	.1516E-09
190.00	.3579E-10	.1573E-11	.1123E-09	.1498E-09
195.00	.3342E-10	.3497E-11	.1095E-09	.1464E-09
200.00	.3031E-10	.6145E-11	.1057E-09	.1421E-09
205.00	.2667E-10	.9517E-11	.1009E-09	.1371E-09
210.00	.2271E-10	.1361E-10	.9518E-10	.1315E-09
215.00	.1867E-10	.1831E-10	.8867E-10	.1256E-09
220.00	.1475E-10	.2331E-10	.8147E-10	.1195E-09
225.00	.1112E-10	.2826E-10	.7372E-10	.1131E-09
230.00	.7952E-11	.3306E-10	.6560E-10	.1066E-09
235.00	.5375E-11	.3777E-10	.5729E-10	.1004E-09
240.00	.3402E-11	.4207E-10	.4902E-10	.9449E-10
245.00	.1967E-11	.4504E-10	.4102E-10	.8803E-10
250.00	.9985E-12	.4612E-10	.3354E-10	.8066E-10
255.00	.4337E-12	.4604E-10	.2678E-10	.7326E-10
260.00	.1691E-12	.4564E-10	.2088E-10	.6669E-10
265.00	.7906E-13	.4407E-10	.1590E-10	.6005E-10
270.00	.9182E-13	.4016E-10	.1184E-10	.5208E-10
275.00	.1701E-12	.3514E-10	.8612E-11	.4392E-10
280.00	.2467E-12	.3127E-10	.6126E-11	.3764E-10
285.00	.2758E-12	.2802E-10	.4251E-11	.3255E-10
290.00	.2912E-12	.2323E-10	.2872E-11	.2639E-10
295.00	.3140E-12	.1771E-10	.1897E-11	.1992E-10
300.00	.2945E-12	.1437E-10	.1234E-11	.1590E-10
305.00	.2238E-12	.1290E-10	.7869E-12	.1392E-10
310.00	.1783E-12	.1031E-10	.4897E-12	.1098E-10
315.00	.1813E-12	.6552E-11	.3065E-12	.7040E-11
320.00	.1600E-12	.4884E-11	.1965E-12	.5041E-11
325.00	.9306E-13	.5040E-11	.1189E-12	.5252E-11
330.00	.5659E-13	.4486E-11	.6436E-13	.4607E-11
335.00	.7804E-13	.2140E-11	.3944E-13	.2258E-11
340.00	.8300E-13	.9035E-12	.2963E-13	.1016E-11
345.00	.3572E-13	.2007E-11	.1529E-13	.2058E-11
350.00	.5554E-14	.2680E-11	.3562E-14	.2689E-11
355.00	.3663E-13	.1196E-11	.6847E-14	.1239E-11
360.00	.6523E-13	.5703E-36	.1241E-13	.7764E-13

TABLE B-19 : Probe near a cylindrical biological body.
Incident field = (2,60 deg.) V/m, f=2.45GHz.
(Fig. 3.3.5)

FREQUENCY : .2450E+10 FIELD : 2.00 ANGLE : 60 00

PHI IN DEG	LOAD CURRENT SQ FOR PHI	LOAD CURRENT SQ FOR R	LOAD CURRENT SQ FOR TE	LOAD CURRENT SQ TOTAL
0 00	.1957E-12	0	.4138E-14	.1998E-12
5 00	.1099E-12	.3587E-11	.2282E-14	.3699E-11
10 00	.1666E-13	.8040E-11	.1187E-14	.8058E-11
15 00	.1072E-12	.6022E-11	.5097E-14	.6134E-11
20 00	.2490E-12	.2710E-11	.9876E-14	.2969E-11
25 00	.2341E-12	.6421E-11	.1316E-13	.6668E-11
30 00	.1698E-12	.1346E-10	.2145E-13	.1365E-10
35 00	.2792E-12	.1512E-10	.3963E-13	.1544E-10
40 00	.4800E-12	.1405E-10	.6550E-13	.1460E-10
45 00	.5439E-12	.1966E-10	.1022E-12	.2030E-10
50 00	.5350E-12	.3093E-10	.1632E-12	.3162E-10
55 00	.6714E-12	.3871E-10	.2623E-12	.3965E-10
60 00	.8835E-12	.4311E-10	.4114E-12	.4440E-10
65 00	.9421E-12	.5313E-10	.6325E-12	.5471E-10
70 00	.8736E-12	.6969E-10	.9574E-12	.7152E-10
75 00	.8275E-12	.8407E-10	.1417E-11	.8631E-10
80 00	.7400E-12	.9381E-10	.2042E-11	.9659E-10
85 00	.5103E-12	.1054E-09	.2871E-11	.1088E-09
90 00	.2755E-12	.1205E-09	.3945E-11	.1247E-09
95 00	.2372E-12	.1322E-09	.5301E-11	.1377E-09
100 00	.5072E-12	.1369E-09	.6960E-11	.1444E-09
105 00	.1301E-11	.1381E-09	.8927E-11	.1484E-09
110 00	.2995E-11	.1384E-09	.1118E-10	.1525E-09
115 00	.5901E-11	.1351E-09	.1367E-10	.1547E-09
120 00	.1021E-10	.1262E-09	.1634E-10	.1528E-09
125 00	.1613E-10	.1133E-09	.1910E-10	.1485E-09
130 00	.2386E-10	.9917E-10	.2187E-10	.1449E-09
135 00	.3335E-10	.8479E-10	.2457E-10	.1427E-09
140 00	.4424E-10	.6992E-10	.2716E-10	.1413E-09
145 00	.5602E-10	.5492E-10	.2956E-10	.1405E-09
150 00	.6814E-10	.4083E-10	.3173E-10	.1407E-09
155 00	.8000E-10	.2855E-10	.3363E-10	.1422E-09
160 00	.9094E-10	.1843E-10	.3523E-10	.1446E-09
165 00	.1003E-09	.1049E-10	.3650E-10	.1473E-09
170 00	.1074E-09	.4718E-11	.3742E-10	.1495E-09
175 00	.1118E-09	.1190E-11	.3798E-10	.1510E-09
180 00	.1133E-09	.1296E-36	.3817E-10	.1515E-09
185 00	.1118E-09	.1190E-11	.3798E-10	.1510E-09
190 00	.1074E-09	.4718E-11	.3742E-10	.1495E-09
195 00	.1003E-09	.1049E-10	.3650E-10	.1473E-09
200 00	.9094E-10	.1843E-10	.3523E-10	.1446E-09
205 00	.8000E-10	.2855E-10	.3363E-10	.1422E-09
210 00	.6814E-10	.4083E-10	.3173E-10	.1407E-09
215 00	.5602E-10	.5492E-10	.2956E-10	.1405E-09
220 00	.4424E-10	.6992E-10	.2716E-10	.1413E-09
225 00	.3335E-10	.8479E-10	.2457E-10	.1427E-09
230 00	.2386E-10	.9917E-10	.2187E-10	.1449E-09
235 00	.1613E-10	.1133E-09	.1910E-10	.1485E-09
240 00	.1021E-10	.1262E-09	.1634E-10	.1528E-09
245 00	.5901E-11	.1351E-09	.1367E-10	.1547E-09
250 00	.2995E-11	.1384E-09	.1118E-10	.1525E-09
255 00	.1301E-11	.1381E-09	.8927E-11	.1484E-09
260 00	.5072E-12	.1369E-09	.6960E-11	.1444E-09
265 00	.2372E-12	.1322E-09	.5301E-11	.1377E-09
270 00	.2755E-12	.1205E-09	.3945E-11	.1247E-09
275 00	.5103E-12	.1054E-09	.2871E-11	.1088E-09
280 00	.7400E-12	.9381E-10	.2042E-11	.9659E-10
285 00	.8275E-12	.8407E-10	.1417E-11	.8631E-10
290 00	.8736E-12	.6969E-10	.9574E-12	.7152E-10
295 00	.9421E-12	.5313E-10	.6325E-12	.5471E-10
300 00	.8835E-12	.4311E-10	.4114E-12	.4440E-10
305 00	.6714E-12	.3871E-10	.2623E-12	.3965E-10
310 00	.5350E-12	.3093E-10	.1632E-12	.3162E-10
315 00	.5439E-12	.1966E-10	.1022E-12	.2030E-10
320.00	.4800E-12	.1405E-10	.6550E-13	.1460E-10
325.00	.2792E-12	.1512E-10	.3963E-13	.1544E-10
330.00	.1698E-12	.1346E-10	.2145E-13	.1365E-10
335.00	.2341E-12	.6421E-11	.1316E-13	.6668E-11
340.00	.2490E-12	.2710E-11	.9876E-14	.2969E-11
345.00	.1072E-12	.6022E-11	.5097E-14	.6134E-11
350 00	.1666E-13	.8040E-11	.1187E-14	.8058E-11
355.00	.1099E-12	.3587E-11	.2282E-14	.3699E-11
360.00	.1957E-12	.1711E-35	.4138E-14	.1998E-12

TABLE B-20 : Probe near a cylindrical biological body.
Incident field = (2,90 deg.) V/m, f=2.45GHz.
(Fig. 3.3.5)

FREQUENCY : .2450E+10 FIELD : 2.00 ANGLE : 90.00

PHI IN DEG	LOAD CURRENT SQ FOR PHI	LOAD CURRENT SQ FOR R	LOAD CURRENT SQ FOR TE	LOAD CURRENT SQ TOTAL
0.00	.2609E-12	0.	.2584E-41	.2609E-12
5.00	.1465E-12	.4783E-11	.1425E-41	.4929E-11
10.00	.2222E-13	.1072E-10	.7416E-42	.1074E-10
15.00	.1429E-12	.8029E-11	.3184E-41	.8172E-11
20.00	.3320E-12	.3614E-11	.6188E-41	.3946E-11
25.00	.3122E-12	.8561E-11	.8211E-41	.8873E-11
30.00	.2264E-12	.1795E-10	.1340E-40	.1817E-10
35.00	.3722E-12	.2016E-10	.2475E-40	.2053E-10
40.00	.6400E-12	.1874E-10	.4091E-40	.1938E-10
45.00	.7252E-12	.2621E-10	.6381E-40	.2693E-10
50.00	.7133E-12	.4123E-10	.1019E-39	.4195E-10
55.00	.8952E-12	.5162E-10	.1638E-39	.5251E-10
60.00	.1178E-11	.5748E-10	.2569E-39	.5865E-10
65.00	.1256E-11	.7084E-10	.3950E-39	.7210E-10
70.00	.1165E-11	.9292E-10	.5980E-39	.9406E-10
75.00	.1103E-11	.1121E-09	.8851E-39	.1132E-09
80.00	.9867E-12	.1251E-09	.1275E-38	.1261E-09
85.00	.6804E-12	.1405E-09	.1793E-38	.1412E-09
90.00	.3673E-12	.1606E-09	.2464E-38	.1610E-09
95.00	.3162E-12	.1763E-09	.3311E-38	.1766E-09
100.00	.6762E-12	.1826E-09	.4347E-38	.1832E-09
105.00	.1735E-11	.1842E-09	.5575E-38	.1859E-09
110.00	.3994E-11	.1845E-09	.6983E-38	.1885E-09
115.00	.7868E-11	.1802E-09	.8541E-38	.1880E-09
120.00	.1361E-10	.1683E-09	.1021E-37	.1819E-09
125.00	.2150E-10	.1511E-09	.1193E-37	.1726E-09
130.00	.3181E-10	.1322E-09	.1366E-37	.1640E-09
135.00	.4446E-10	.1131E-09	.1535E-37	.1575E-09
140.00	.5898E-10	.9323E-10	.1698E-37	.1522E-09
145.00	.7469E-10	.7323E-10	.1846E-37	.1479E-09
150.00	.9085E-10	.5444E-10	.1982E-37	.1453E-09
155.00	.1067E-09	.3807E-10	.2100E-37	.1447E-09
160.00	.1213E-09	.2458E-10	.2200E-37	.1458E-09
165.00	.1337E-09	.1399E-10	.2280E-37	.1477E-09
170.00	.1432E-09	.6291E-11	.2337E-37	.1495E-09
175.00	.1491E-09	.1586E-11	.2372E-37	.1507E-09
180.00	.1511E-09	.1728E-36	.2384E-37	.1511E-09
185.00	.1491E-09	.1586E-11	.2372E-37	.1507E-09
190.00	.1432E-09	.6291E-11	.2337E-37	.1495E-09
195.00	.1337E-09	.1399E-10	.2280E-37	.1477E-09
200.00	.1213E-09	.2458E-10	.2200E-37	.1458E-09
205.00	.1067E-09	.3807E-10	.2100E-37	.1447E-09
210.00	.9085E-10	.5444E-10	.1982E-37	.1453E-09
215.00	.7469E-10	.7323E-10	.1846E-37	.1479E-09
220.00	.5898E-10	.9323E-10	.1698E-37	.1522E-09
225.00	.4446E-10	.1131E-09	.1535E-37	.1575E-09
230.00	.3181E-10	.1322E-09	.1366E-37	.1640E-09
235.00	.2150E-10	.1511E-09	.1193E-37	.1726E-09
240.00	.1361E-10	.1683E-09	.1021E-37	.1819E-09
245.00	.7868E-11	.1802E-09	.8541E-38	.1880E-09
250.00	.3994E-11	.1845E-09	.6983E-38	.1885E-09
255.00	.1735E-11	.1842E-09	.5575E-38	.1859E-09
260.00	.6762E-12	.1826E-09	.4347E-38	.1832E-09
265.00	.3162E-12	.1763E-09	.3311E-38	.1766E-09
270.00	.3673E-12	.1606E-09	.2464E-38	.1610E-09
275.00	.6804E-12	.1405E-09	.1793E-38	.1412E-09
280.00	.9867E-12	.1251E-09	.1275E-38	.1261E-09
285.00	.1103E-11	.1121E-09	.8851E-39	.1132E-09
290.00	.1165E-11	.9292E-10	.5980E-39	.9406E-10
295.00	.1256E-11	.7084E-10	.3950E-39	.7210E-10
300.00	.1178E-11	.5748E-10	.2569E-39	.5865E-10
305.00	.8952E-12	.5162E-10	.1638E-39	.5251E-10
310.00	.7133E-12	.4123E-10	.1019E-39	.4195E-10
315.00	.7252E-12	.2621E-10	.6381E-40	.2693E-10
320.00	.6400E-12	.1874E-10	.4091E-40	.1938E-10
325.00	.3722E-12	.2016E-10	.2475E-40	.2053E-10
330.00	.2264E-12	.1795E-10	.1340E-40	.1817E-10
335.00	.3122E-12	.8561E-11	.8211E-41	.8873E-11
340.00	.3320E-12	.3614E-11	.6188E-41	.3946E-11
345.00	.1429E-12	.8029E-11	.3184E-41	.8172E-11
350.00	.2222E-13	.1072E-10	.7416E-42	.1074E-10
355.00	.1465E-12	.4783E-11	.1425E-41	.4929E-11
360.00	.2609E-12	.2281E-35	.2584E-41	.2609E-12

TABLE B-21 : Probe near a cylindrical biological body. Incident field = (2,0 deg.) V/m, f=1.5GHz. (Fig. 3.3.6)

FREQUENCY = .1500E+10   FIELD = 2.00   ANGLE = 0.00

PHI IN DEG	LOAD CURRENT SQ FOR PHI	LOAD CURRENT SQ FOR R	LOAD CURRENT SQ FOR TE	LOAD CURRENT SQ TOTAL
0.00	0.	0.	.1366E-13	.1366E-13
5.00	0.	0.	.1075E-13	.1075E-13
10.00	0.	0.	.5949E-14	.5949E-14
15.00	0.	0.	.7000E-14	.7000E-14
20.00	0.	0.	.1775E-13	.1775E-13
25.00	0.	0.	.3498E-13	.3498E-13
30.00	0.	0.	.5328E-13	.5328E-13
35.00	0.	0.	.7286E-13	.7286E-13
40.00	0.	0.	.1021E-12	.1021E-12
45.00	0.	0.	.1526E-12	.1526E-12
50.00	0.	0.	.2324E-12	.2324E-12
55.00	0.	0.	.3451E-12	.3451E-12
60.00	0.	0.	.4957E-12	.4957E-12
65.00	0.	0.	.6969E-12	.6969E-12
70.00	0.	0.	.9692E-12	.9692E-12
75.00	0.	0.	.1335E-11	.1335E-11
80.00	0.	0.	.1811E-11	.1811E-11
85.00	0.	0.	.2414E-11	.2414E-11
90.00	0.	0.	.3155E-11	.3155E-11
95.00	0.	0.	.4048E-11	.4048E-11
100.00	0.	0.	.5103E-11	.5103E-11
105.00	0.	0.	.6323E-11	.6323E-11
110.00	0.	0.	.7700E-11	.7700E-11
115.00	0.	0.	.9215E-11	.9215E-11
120.00	0.	0.	.1084E-10	.1084E-10
125.00	0.	0.	.1255E-10	.1255E-10
130.00	0.	0.	.1430E-10	.1430E-10
135.00	0.	0.	.1605E-10	.1605E-10
140.00	0.	0.	.1775E-10	.1775E-10
145.00	0.	0.	.1937E-10	.1937E-10
150.00	0.	0.	.2087E-10	.2087E-10
155.00	0.	0.	.2220E-10	.2220E-10
160.00	0.	0.	.2333E-10	.2333E-10
165.00	0.	0.	.2423E-10	.2423E-10
170.00	0.	0.	.2490E-10	.2490E-10
175.00	0.	0.	.2530E-10	.2530E-10
180.00	0.	0.	.2544E-10	.2544E-10
185.00	0.	0.	.2530E-10	.2530E-10
190.00	0.	0.	.2490E-10	.2490E-10
195.00	0.	0.	.2423E-10	.2423E-10
200.00	0.	0.	.2333E-10	.2333E-10
205.00	0.	0.	.2220E-10	.2220E-10
210.00	0.	0.	.2087E-10	.2087E-10
215.00	0.	0.	.1937E-10	.1937E-10
220.00	0.	0.	.1775E-10	.1775E-10
225.00	0.	0.	.1605E-10	.1605E-10
230.00	0.	0.	.1430E-10	.1430E-10
235.00	0.	0.	.1255E-10	.1255E-10
240.00	0.	0.	.1084E-10	.1084E-10
245.00	0.	0.	.9215E-11	.9215E-11
250.00	0.	0.	.7700E-11	.7700E-11
255.00	0.	0.	.6323E-11	.6323E-11
260.00	0.	0.	.5103E-11	.5103E-11
265.00	0.	0.	.4048E-11	.4048E-11
270.00	0.	0.	.3155E-11	.3155E-11
275.00	0.	0.	.2414E-11	.2414E-11
280.00	0.	0.	.1811E-11	.1811E-11
285.00	0.	0.	.1335E-11	.1335E-11
290.00	0.	0.	.9692E-12	.9692E-12
295.00	0.	0.	.6969E-12	.6969E-12
300.00	0.	0.	.4957E-12	.4957E-12
305.00	0.	0.	.3451E-12	.3451E-12
310.00	0.	0.	.2324E-12	.2324E-12
315.00	0.	0.	.1526E-12	.1526E-12
320.00	0.	0.	.1021E-12	.1021E-12
325.00	0.	0.	.7286E-13	.7286E-13
330.00	0.	0.	.5328E-13	.5328E-13
335.00	0.	0.	.3498E-13	.3498E-13
340.00	0.	0.	.1775E-13	.1775E-13
345.00	0.	0.	.7000E-14	.7000E-14
350.00	0.	0.	.5949E-14	.5949E-14
355.00	0.	0.	.1075E-13	.1075E-13
360.00	0.	0.	.1366E-13	.1366E-13

TABLE B-22 : Probe near a cylindrical biological body.
Incident field = (2,30 deg.) V/m, f=1.5GHz.
(Fig. 3.3.6)

FREQUENCY : .1500E+10 FIELD : 2.00 ANGLE : 30.00

PHI IN DEG	LOAD CURRENT SQ FOR PHI	LOAD CURRENT SQ FOR R	LOAD CURRENT SQ FOR TE	LOAD CURRENT SQ TOTAL
0.00	.3236E-13	0	.1024E-13	.4260E-13
5.00	.2573E-13	.5520E-12	.8063E-14	.5858E-12
10.00	.1200E-13	.1772E-11	.4462E-14	.1789E-11
15.00	.4246E-14	.2720E-11	.5250E-14	.2730E-11
20.00	.1106E-13	.2744E-11	.1331E-13	.2769E-11
25.00	.2892E-13	.2039E-11	.2623E-13	.2094E-11
30.00	.4518E-13	.1491E-11	.3996E-13	.1576E-11
35.00	.4945E-13	.1935E-11	.5464E-13	.2040E-11
40.00	.4296E-13	.3455E-11	.7659E-13	.3575E-11
45.00	.3706E-13	.5318E-11	.1145E-12	.5469E-11
50.00	.4191E-13	.6622E-11	.1743E-12	.6838E-11
55.00	.5621E-13	.7080E-11	.2588E-12	.7395E-11
60.00	.6837E-13	.7255E-11	.3718E-12	.7695E-11
65.00	.6786E-13	.8031E-11	.5227E-12	.8621E-11
70.00	.5505E-13	.9821E-11	.7269E-12	.1060E-10
75.00	.3933E-13	.1221E-10	.1001E-11	.1325E-10
80.00	.2897E-13	.1435E-10	.1359E-11	.1573E-10
85.00	.2472E-13	.1584E-10	.1810E-11	.1747E-10
90.00	.2474E-13	.1617E-10	.2366E-11	.1856E-10
95.00	.3446E-13	.1648E-10	.3036E-11	.1955E-10
100.00	.6999E-13	.1696E-10	.3827E-11	.2086E-10
105.00	.1515E-12	.1757E-10	.4742E-11	.2247E-10
110.00	.2941E-12	.1792E-10	.5775E-11	.2399E-10
115.00	.5059E-12	.1782E-10	.6912E-11	.2504E-10
120.00	.7919E-12	.1658E-10	.8132E-11	.2551E-10
125.00	.1159E-11	.1500E-10	.9412E-11	.2557E-10
130.00	.1614E-11	.1317E-10	.1072E-10	.2550E-10
135.00	.2158E-11	.1130E-10	.1204E-10	.2549E-10
140.00	.2776E-11	.9487E-11	.1332E-10	.2558E-10
145.00	.3446E-11	.7719E-11	.1453E-10	.2569E-10
150.00	.4130E-11	.5998E-11	.1565E-10	.2578E-10
155.00	.4791E-11	.4364E-11	.1665E-10	.2580E-10
160.00	.5393E-11	.2893E-11	.1750E-10	.2578E-10
165.00	.5900E-11	.1666E-11	.1818E-10	.2574E-10
170.00	.6286E-11	.7513E-12	.1867E-10	.2571E-10
175.00	.6526E-11	.1892E-12	.1898E-10	.2569E-10
180.00	.6608E-11	.2743E-37	.1908E-10	.2569E-10
185.00	.6526E-11	.1892E-12	.1898E-10	.2569E-10
190.00	.6286E-11	.7513E-12	.1867E-10	.2571E-10
195.00	.5900E-11	.1666E-11	.1818E-10	.2574E-10
200.00	.5393E-11	.2893E-11	.1750E-10	.2578E-10
205.00	.4791E-11	.4364E-11	.1665E-10	.2580E-10
210.00	.4130E-11	.5998E-11	.1565E-10	.2578E-10
215.00	.3446E-11	.7719E-11	.1453E-10	.2569E-10
220.00	.2776E-11	.9487E-11	.1332E-10	.2558E-10
225.00	.2158E-11	.1130E-10	.1204E-10	.2549E-10
230.00	.1614E-11	.1317E-10	.1072E-10	.2550E-10
235.00	.1159E-11	.1500E-10	.9412E-11	.2557E-10
240.00	.7919E-12	.1658E-10	.8132E-11	.2551E-10
245.00	.5059E-12	.1782E-10	.6912E-11	.2504E-10
250.00	.2941E-12	.1792E-10	.5775E-11	.2399E-10
255.00	.1515E-12	.1757E-10	.4742E-11	.2247E-10
260.00	.6999E-13	.1696E-10	.3827E-11	.2086E-10
265.00	.3446E-13	.1648E-10	.3036E-11	.1955E-10
270.00	.2474E-13	.1617E-10	.2366E-11	.1856E-10
275.00	.2472E-13	.1584E-10	.1810E-11	.1747E-10
280.00	.2897E-13	.1435E-10	.1359E-11	.1573E-10
285.00	.3933E-13	.1221E-10	.1001E-11	.1325E-10
290.00	.5505E-13	.9821E-11	.7269E-12	.1060E-10
295.00	.6786E-13	.8031E-11	.5227E-12	.8621E-11
300.00	.6837E-13	.7255E-11	.3718E-12	.7695E-11
305.00	.5621E-13	.7080E-11	.2588E-12	.7395E-11
310.00	.4191E-13	.6622E-11	.1743E-12	.6838E-11
315.00	.3706E-13	.5318E-11	.1145E-12	.5469E-11
320.00	.4296E-13	.3455E-11	.7659E-13	.3575E-11
325.00	.4945E-13	.1935E-11	.5464E-13	.2040E-11
330.00	.4518E-13	.1491E-11	.3998E-13	.1576E-11
335.00	.2892E-13	.2039E-11	.2623E-13	.2094E-11
340.00	.1106E-13	.2744E-11	.1331E-13	.2769E-11
345.00	.4246E-14	.2720E-11	.5250E-14	.2730E-11
350.00	.1200E-13	.1772E-11	.4482E-14	.1789E-11
355.00	.2573E-13	.5520E-12	.8063E-14	.5858E-12
360.00	.3236E-13	.3442E-36	.1024E-13	.4260E-13

TABLE B-23 : Probe near a cylindrical biological body. Incident field = (2,60 deg.) V/m, f=1.5GHz. (Fig. 3.3.6)

FREQUENCY = .1500E+10 FIELD = 2.00 ANGLE = 60.00

PHI IN DEG	LOAD CURRENT SQ FOR PHI	LOAD CURRENT SQ FOR R	LOAD CURRENT SQ FOR TE	LOAD CURRENT SQ TOTAL
0.00	.9707E-13	0	.3414E-14	.1005E-12
5.00	.7720E-13	.1656E-11	.2688E-14	.1736E-11
10.00	.3600E-13	.5317E-11	.1487E-14	.5354E-11
15.00	.1274E-13	.8160E-11	.1750E-14	.8175E-11
20.00	.3319E-13	.8233E-11	.4437E-14	.8271E-11
25.00	.8675E-13	.8118E-11	.8744E-14	.8213E-11
30.00	.1355E-12	.4472E-11	.1332E-13	.4621E-11
35.00	.1484E-12	.5806E-11	.1821E-13	.5973E-11
40.00	.1289E-12	.1037E-10	.2553E-13	.1052E-10
45.00	.1112E-12	.1595E-10	.3816E-13	.1610E-10
50.00	.1257E-12	.1987E-10	.5811E-13	.2005E-10
55.00	.1686E-12	.2124E-10	.8627E-13	.2150E-10
60.00	.2051E-12	.2176E-10	.1239E-12	.2209E-10
65.00	.2036E-12	.2409E-10	.1742E-12	.2447E-10
70.00	.1651E-12	.2946E-10	.2423E-12	.2987E-10
75.00	.1180E-12	.3664E-10	.3336E-12	.3709E-10
80.00	.8690E-13	.4304E-10	.4529E-12	.4358E-10
85.00	.7416E-13	.4692E-10	.6035E-12	.4759E-10
90.00	.7423E-13	.4852E-10	.7888E-12	.4938E-10
95.00	.1034E-12	.4943E-10	.1012E-11	.5054E-10
100.00	.2100E-12	.5087E-10	.1276E-11	.5236E-10
105.00	.4544E-12	.5272E-10	.1581E-11	.5476E-10
110.00	.8824E-12	.5377E-10	.1925E-11	.5658E-10
115.00	.1518E-11	.5287E-10	.2304E-11	.5670E-10
120.00	.2376E-11	.4975E-10	.2711E-11	.5484E-10
125.00	.3477E-11	.4499E-10	.3137E-11	.5161E-10
130.00	.4843E-11	.3950E-10	.3574E-11	.4791E-10
135.00	.6473E-11	.3391E-10	.4012E-11	.4439E-10
140.00	.8329E-11	.2846E-10	.4438E-11	.4123E-10
145.00	.1034E-10	.2316E-10	.4844E-11	.3834E-10
150.00	.1239E-10	.1799E-10	.5217E-11	.3560E-10
155.00	.1437E-10	.1309E-10	.5549E-11	.3302E-10
160.00	.1618E-10	.8678E-11	.5832E-11	.3069E-10
165.00	.1770E-10	.4999E-11	.6059E-11	.2876E-10
170.00	.1886E-10	.2254E-11	.6224E-11	.2734E-10
175.00	.1958E-10	.5677E-12	.6325E-11	.2647E-10
180.00	.1982E-10	.8229E-37	.6359E-11	.2618E-10
185.00	.1958E-10	.5677E-12	.6325E-11	.2647E-10
190.00	.1886E-10	.2254E-11	.6224E-11	.2734E-10
195.00	.1770E-10	.4999E-11	.6059E-11	.2876E-10
200.00	.1618E-10	.8678E-11	.5832E-11	.3069E-10
205.00	.1437E-10	.1309E-10	.5549E-11	.3302E-10
210.00	.1239E-10	.1799E-10	.5217E-11	.3560E-10
215.00	.1034E-10	.2316E-10	.4844E-11	.3834E-10
220.00	.8329E-11	.2846E-10	.4438E-11	.4123E-10
225.00	.6473E-11	.3391E-10	.4012E-11	.4439E-10
230.00	.4843E-11	.3950E-10	.3574E-11	.4791E-10
235.00	.3477E-11	.4499E-10	.3137E-11	.5161E-10
240.00	.2376E-11	.4975E-10	.2711E-11	.5484E-10
245.00	.1518E-11	.5287E-10	.2304E-11	.5670E-10
250.00	.8824E-12	.5377E-10	.1925E-11	.5658E-10
255.00	.4544E-12	.5272E-10	.1581E-11	.5476E-10
260.00	.2100E-12	.5087E-10	.1276E-11	.5236E-10
265.00	.1034E-12	.4943E-10	.1012E-11	.5054E-10
270.00	.7423E-13	.4852E-10	.7888E-12	.4938E-10
275.00	.7416E-13	.4692E-10	.6035E-12	.4759E-10
280.00	.8690E-13	.4304E-10	.4529E-12	.4358E-10
285.00	.1180E-12	.3664E-10	.3336E-12	.3709E-10
290.00	.1651E-12	.2946E-10	.2423E-12	.2987E-10
295.00	.2036E-12	.2409E-10	.1742E-12	.2447E-10
300.00	.2051E-12	.2176E-10	.1239E-12	.2209E-10
305.00	.1686E-12	.2124E-10	.8627E-13	.2150E-10
310.00	.1257E-12	.1987E-10	.5811E-13	.2005E-10
315.00	.1112E-12	.1595E-10	.3816E-13	.1610E-10
320.00	.1289E-12	.1037E-10	.2553E-13	.1052E-10
325.00	.1484E-12	.5806E-11	.1821E-13	.5973E-11
330.00	.1355E-12	.4472E-11	.1332E-13	.4621E-11
335.00	.8675E-13	.8118E-11	.8744E-14	.8213E-11
340.00	.3319E-13	.8233E-11	.4437E-14	.8271E-11
345.00	.1274E-13	.8160E-11	.1750E-14	.8175E-11
350.00	.3600E-13	.5317E-11	.1487E-14	.5354E-11
355.00	.7720E-13	.1656E-11	.2688E-14	.1736E-11
360.00	.9707E-13	.1032E-35	.3414E-14	.1005E-12

TABLE B-24 : Probe near a cylindrical biological body.
Incident field = (2,90 deg.) V/m, f=1.5GHz.
(Fig. 3.3.6)

FREQUENCY = .1500E+10 FIELD = 2.00 ANGLE = 90.00

PHI IN DEG	LOAD CURRENT SQ FOR PHI	LOAD CURRENT SQ FOR R	LOAD CURRENT SQ FOR TE	LOAD CURRENT SQ TOTAL
0.00	.1294E-12	0	.2132E-41	.1294E-12
5.00	.1029E-12	.2208E-11	.1679E-41	.2311E-11
10.00	.4800E-13	.7089E-11	.9290E-42	.7137E-11
15.00	.1698E-13	.1088E-10	.1093E-41	.1090E-10
20.00	.4426E-13	.1098E-10	.2771E-41	.1102E-10
25.00	.1157E-12	.8157E-11	.5461E-41	.8272E-11
30.00	.1807E-12	.5963E-11	.8319E-41	.6144E-11
35.00	.1978E-12	.7742E-11	.1138E-40	.7940E-11
40.00	.1718E-12	.1382E-10	.1595E-40	.1399E-10
45.00	.1482E-12	.2127E-10	.2383E-40	.2142E-10
50.00	.1676E-12	.2649E-10	.3629E-40	.2666E-10
55.00	.2249E-12	.2832E-10	.5388E-40	.2855E-10
60.00	.2735E-12	.2902E-10	.7740E-40	.2929E-10
65.00	.2716E-12	.3212E-10	.1088E-39	.3239E-10
70.00	.2202E-12	.3928E-10	.1513E-39	.3950E-10
75.00	.1573E-12	.4885E-10	.2084E-39	.4901E-10
80.00	.1159E-12	.5738E-10	.2828E-39	.5750E-10
85.00	.9888E-13	.6255E-10	.3769E-39	.6265E-10
90.00	.9897E-13	.6469E-10	.4926E-39	.6479E-10
95.00	.1379E-12	.6590E-10	.6321E-39	.6604E-10
100.00	.2800E-12	.6783E-10	.7968E-39	.6811E-10
105.00	.6059E-12	.7030E-10	.9873E-39	.7090E-10
110.00	.1176E-11	.7170E-10	.1202E-38	.7287E-10
115.00	.2023E-11	.7050E-10	.1439E-38	.7252E-10
120.00	.3168E-11	.6633E-10	.1693E-38	.6950E-10
125.00	.4637E-11	.5999E-10	.1959E-38	.6463E-10
130.00	.6457E-11	.5266E-10	.2232E-38	.5912E-10
135.00	.8630E-11	.4521E-10	.2506E-38	.5384E-10
140.00	.1111E-10	.3795E-10	.2772E-38	.4905E-10
145.00	.1378E-10	.3088E-10	.3025E-38	.4466E-10
150.00	.1652E-10	.2399E-10	.3258E-38	.4051E-10
155.00	.1917E-10	.1746E-10	.3466E-38	.3662E-10
160.00	.2157E-10	.1157E-10	.3642E-38	.3314E-10
165.00	.2360E-10	.6665E-11	.3784E-38	.3027E-10
170.00	.2514E-10	.3005E-11	.3888E-38	.2815E-10
175.00	.2610E-10	.7570E-12	.3951E-38	.2686E-10
180.00	.2643E-10	.1097E-36	.3972E-38	.2643E-10
185.00	.2610E-10	.7570E-12	.3951E-38	.2686E-10
190.00	.2514E-10	.3005E-11	.3888E-38	.2815E-10
195.00	.2360E-10	.6665E-11	.3784E-38	.3027E-10
200.00	.2157E-10	.1157E-10	.3642E-38	.3314E-10
205.00	.1917E-10	.1746E-10	.3466E-38	.3662E-10
210.00	.1652E-10	.2399E-10	.3258E-38	.4051E-10
215.00	.1378E-10	.3088E-10	.3025E-38	.4466E-10
220.00	.1111E-10	.3795E-10	.2772E-38	.4905E-10
225.00	.8630E-11	.4521E-10	.2506E-38	.5384E-10
230.00	.6457E-11	.5266E-10	.2232E-38	.5912E-10
235.00	.4637E-11	.5999E-10	.1959E-38	.6463E-10
240.00	.3168E-11	.6633E-10	.1693E-38	.6950E-10
245.00	.2023E-11	.7050E-10	.1439E-38	.7252E-10
250.00	.1176E-11	.7170E-10	.1202E-38	.7287E-10
255.00	.6059E-12	.7030E-10	.9873E-39	.7090E-10
260.00	.2800E-12	.6783E-10	.7968E-39	.6811E-10
265.00	.1379E-12	.6590E-10	.6321E-39	.6604E-10
270.00	.9897E-13	.6469E-10	.4926E-39	.6479E-10
275.00	.9888E-13	.6255E-10	.3769E-39	.6265E-10
280.00	.1159E-12	.5738E-10	.2828E-39	.5750E-10
285.00	.1573E-12	.4885E-10	.2084E-39	.4901E-10
290.00	.2202E-12	.3928E-10	.1513E-39	.3950E-10
295.00	.2716E-12	.3212E-10	.1088E-39	.3239E-10
300.00	.2735E-12	.2902E-10	.7740E-40	.2929E-10
305.00	.2249E-12	.2832E-10	.5388E-40	.2855E-10
310.00	.1676E-12	.2649E-10	.3629E-40	.2666E-10
315.00	.1482E-12	.2127E-10	.2383E-40	.2142E-10
320.00	.1718E-12	.1382E-10	.1595E-40	.1399E-10
325.00	.1978E-12	.7742E-11	.1138E-40	.7940E-11
330.00	.1807E-12	.5963E-11	.8319E-41	.6144E-11
335.00	.1157E-12	.8157E-11	.5461E-41	.8272E-11
340.00	.4426E-13	.1098E-10	.2771E-41	.1102E-10
345.00	.1698E-13	.1088E-10	.1093E-41	.1090E-10
350.00	.4800E-13	.7089E-11	.9290E-42	.7137E-11
355.00	.1029E-12	.2208E-11	.1679E-41	.2311E-11
360.00	.1294E-12	.1377E-35	.2132E-41	.1294E-12

TABLE B-25 : Probe response vs. separation between the probe and the body along phi = 180 deg. (Fig. 3.3.7)

FREQUENCY : 2450E+10 FIELD : 2 00 ANGLE : 45 00 PHI :180 00

S IN M	LOAD CURRENT SQ FOR PHI	LOAD CURRENT SQ FOR R	LOAD CURRENT SQ FOR TE	LOAD CURRENT SQ TOTAL
0 0000	2718E-11	1963E-36	2556E-11	5274E-11
0040	1325E-10	1732E-36	1270E-10	2595E-10
0080	3753E-10	1422E-36	3729E-10	7482E-10
0120	7076E-10	1071E-36	7132E-10	1421E-09
0160	1070E-09	7224E-37	1085E-09	2156E-09
0200	1402E-09	4151E-37	1425E-09	2827E-09
0240	1649E-09	1810E-37	1677E-09	3325E-09
0280	1773E-09	4076E-38	1800E-09	3573E-09
0320	1758E-09	1744E-39	1779E-09	3537E-09
0360	1610E-09	5813E-38	1620E-09	3230E-09
0400	1354E-09	1924E-37	1352E-09	2706E-09
0440	1035E-09	3786E-37	1022E-09	2057E-09
0480	7035E-10	5860E-37	6833E-10	1387E-09
0520	4125E-10	7834E-37	3905E-10	8030E-10
0560	2061E-10	9434E-37	1883E-10	3944E-10
0600	1138E-10	1046E-36	1058E-10	2195E-10
0640	1460E-10	1079E-36	1515E-10	2974E-10
0680	2929E-10	1042E-36	3131E-10	6060E-10
0720	5266E-10	9424E-37	5599E-10	1086E-09
0760	8059E-10	7973E-37	8481E-10	1654E-09
0800	1084E-09	6274E-37	1129E-09	2212E-09
0840	1314E-09	4560E-37	1355E-09	2668E-09
0880	1459E-09	3048E-37	1490E-09	2949E-09
0920	1498E-09	1916E-37	1514E-09	3012E-09
0960	1425E-09	1279E-37	1424E-09	2849E-09
1000	1255E-09	1177E-37	1238E-09	2493E-09
1040	1016E-09	1577E-37	9867E-10	2003E-09
1080	7487E-10	2379E-37	7130E-10	1462E-09
1120	4963E-10	3437E-37	4613E-10	9576E-10
1160	2992E-10	4577E-37	2719E-10	5711E-10
1200	1877E-10	5629E-37	1741E-10	3618E-10
1240	1780E-10	6447E-37	1813E-10	3593E-10
1280	2690E-10	6925E-37	2898E-10	5588E-10
1320	4434E-10	7014E-37	4792E-10	9226E-10
1360	6708E-10	6722E-37	7162E-10	1387E-09
1400	9124E-10	6112E-37	9606E-10	1873E-09
1440	1128E-09	5287E-37	1172E-09	2300E-09
1480	1283E-09	4374E-37	1315E-09	2597E-09
1520	1351E-09	3506E-37	1367E-09	2718E-09
1560	1324E-09	2801E-37	1321E-09	2646E-09
1600	1207E-09	2347E-37	1186E-09	2393E-09
1640	1019E-09	2191E-37	9857E-10	2005E-09
1680	7938E-10	2336E-37	7529E-10	1547E-09
1720	5671E-10	2738E-37	5265E-10	1094E-09
1760	3763E-10	3324E-37	3434E-10	7197E-10
1800	2516E-10	3994E-37	2326E-10	4842E-10
1840	2123E-10	4644E-37	2110E-10	4233E-10
1880	2631E-10	5179E-37	2804E-10	5435E-10
1920	3942E-10	5525E-37	4276E-10	8218E-10
1960	5825E-10	5641E-37	6270E-10	1209E-09

TABLE B-26 : Probe response vs. separation between the probe and the body along phi = 135 deg. (Fig.3.3.7)

FREQUENCY : 2450E+1C FIELD : 2 00 ANGLE : 45 00 PHI :135 00

S IN M	LOAD CURRENT SQ FOR PHI	LOAD CURRENT SQ FOR R	LOAD CURRENT SQ FOR TE	LOAD CURRENT SQ TOTAL
0 0000	2252E-11	8758E-10	1551E-11	9139E-10
0040	4770E-11	8106E-10	7788E-11	9362E-10
0080	1097E-10	7228E-10	2280E-10	1061E-09
0120	2054E-10	6198E-10	4465E-10	1272E-09
0160	3270E-10	5105E-10	7087E-10	1546E-09
0200	4637E-10	4035E-10	9867E-10	1854E-09
0240	6022E-10	3070E-10	1252E-09	2161E-09
0280	7283E-10	2281E-10	1477E-09	2433E-09
0320	8288E-10	1717E-10	1639E-09	2640E-09
0360	8928E-10	1405E-10	1724E-09	2757E-09
0400	9133E-10	1349E-10	1722E-09	2770E-09
0440	8877E-10	1527E-10	1635E-09	2675E-09
0480	8184E-10	1898E-10	1474E-09	2482E-09
0520	7126E-10	2407E-10	1255E-09	2209E-09
0560	5816E-10	2988E-10	1004E-09	1884E-09
0600	4393E-10	3568E-10	7455E-10	1542E-09
0640	3010E-10	4089E-10	5076E-10	1217E-09
0680	1815E-10	4498E-10	3144E-10	9457E-10
0720	9352E-11	4756E-10	1854E-10	7545E-10
0760	4628E-11	4845E-10	1323E-10	6631E-10
0800	4425E-11	4765E-10	1588E-10	6796E-10
0840	8706E-11	4535E-10	2596E-10	8001E-10
0880	1692E-10	4188E-10	4212E-10	1009E-09
0920	2807E-10	3767E-10	6238E-10	1281E-09
0960	4086E-10	3323E-10	8435E-10	1584E-09
1000	5381E-10	2905E-10	1055E-09	1883E-09
1040	6542E-10	2556E-10	1233E-09	2143E-09
1080	7437E-10	2310E-10	1359E-09	2334E-09
1120	7966E-10	2189E-10	1419E-09	2434E-09
1160	8072E-10	2197E-10	1406E-09	2433E-09
1200	7744E-10	2327E-10	1323E-09	2331E-09
1240	7025E-10	2556E-10	1181E-09	2140E-09
1280	5999E-10	2853E-10	9969E-10	1882E-09
1320	4786E-10	3180E-10	7914E-10	1588E-09
1360	3526E-10	3499E-10	5885E-10	1291E-09
1400	2363E-10	3773E-10	4116E-10	1025E-09
1440	1429E-10	3973E-10	2800E-10	8201E-10
1480	8255E-11	4080E-10	2080E-10	6985E-10
1520	6180E-11	4084E-10	2027E-10	6729E-10
1560	8233E-11	3991E-10	2634E-10	7448E-10
1600	1411E-10	3815E-10	3817E-10	9043E-10
1640	2306E-10	3579E-10	5428E-10	1131E-09
1680	3399E-10	3314E-10	7269E-10	1398E-09
1720	4558E-10	3050E-10	9120E-10	1673E-09
1760	5646E-10	2818E-10	1076E-09	1923E-09
1800	6535E-10	2643E-10	1200E-09	2118E-09
1840	7123E-10	2542E-10	1271E-09	2237E-09
1880	7342E-10	2524E-10	1279E-09	2266E-09
1920	7169E-10	2587E-10	1225E-09	2201E-09
1960	6630E-10	2721E-10	1116E-09	2051E-09

TABLE B-27 : Probe response vs. separation between the probe and the body along phi = 90 deg. (Fig. 3.3.7)

FREQUENCY : .2450E+10 FIELD : 2.00 ANGLE : 45.00 PHI : 90.00

S IN M	LOAD CURRENT SQ FOR PHI	LOAD CURRENT SQ FOR R	LOAD CURRENT SQ FOR TE	LOAD CURRENT SQ TOTAL
0.0000	.1077E-11	.9810E-10	.2147E-12	.9939E-10
.0040	.4418E-12	.9328E-10	.1126E-11	.9485E-10
.0080	.1727E-12	.8996E-10	.3348E-11	.9348E-10
.0120	.1243E-12	.8755E-10	.6819E-11	.9449E-10
.0160	.2075E-12	.8566E-10	.1149E-10	.9735E-10
.0200	.3671E-12	.8400E-10	.1731E-10	.1017E-09
.0240	.5689E-12	.8240E-10	.2421E-10	.1072E-09
.0280	.7910E-12	.8072E-10	.3211E-10	.1138E-09
.0320	.1020E-11	.7889E-10	.4089E-10	.1208E-09
.0360	.1247E-11	.7687E-10	.5041E-10	.1285E-09
.0400	.1467E-11	.7468E-10	.6050E-10	.1366E-09
.0440	.1676E-11	.7226E-10	.7096E-10	.1449E-09
.0480	.1873E-11	.6971E-10	.8157E-10	.1532E-09
.0520	.2057E-11	.6707E-10	.9210E-10	.1612E-09
.0560	.2228E-11	.6439E-10	.1023E-09	.1689E-09
.0600	.2385E-11	.6176E-10	.1119E-09	.1760E-09
.0640	.2529E-11	.5920E-10	.1207E-09	.1824E-09
.0680	.2661E-11	.5683E-10	.1284E-09	.1878E-09
.0720	.2781E-11	.5471E-10	.1348E-09	.1923E-09
.0760	.2889E-11	.5289E-10	.1397E-09	.1955E-09
.0800	.2987E-11	.5142E-10	.1430E-09	.1974E-09
.0840	.3076E-11	.5036E-10	.1446E-09	.1980E-09
.0880	.3155E-11	.4973E-10	.1444E-09	.1973E-09
.0920	.3227E-11	.4954E-10	.1424E-09	.1951E-09
.0960	.3291E-11	.4980E-10	.1386E-09	.1917E-09
.1000	.3348E-11	.5050E-10	.1332E-09	.1870E-09
.1040	.3400E-11	.5159E-10	.1263E-09	.1813E-09
.1080	.3446E-11	.5306E-10	.1180E-09	.1745E-09
.1120	.3488E-11	.5483E-10	.1087E-09	.1671E-09
.1160	.3525E-11	.5686E-10	.9866E-10	.1590E-09
.1200	.3559E-11	.5907E-10	.8811E-10	.1507E-09
.1240	.3590E-11	.6138E-10	.7740E-10	.1424E-09
.1280	.3617E-11	.6373E-10	.6688E-10	.1342E-09
.1320	.3643E-11	.6602E-10	.5685E-10	.1265E-09
.1360	.3666E-11	.6819E-10	.4765E-10	.1195E-09
.1400	.3687E-11	.7017E-10	.3954E-10	.1134E-09
.1440	.3706E-11	.7190E-10	.3280E-10	.1084E-09
.1480	.3723E-11	.7332E-10	.2761E-10	.1046E-09
.1520	.3738E-11	.7439E-10	.2413E-10	.1023E-09
.1560	.3752E-11	.7510E-10	.2247E-10	.1013E-09
.1600	.3764E-11	.7542E-10	.2264E-10	.1018E-09
.1640	.3774E-11	.7535E-10	.2463E-10	.1038E-09
.1680	.3782E-11	.7491E-10	.2835E-10	.1070E-09
.1720	.3789E-11	.7412E-10	.3363E-10	.1115E-09
.1760	.3794E-11	.7302E-10	.4029E-10	.1171E-09
.1800	.3796E-11	.7166E-10	.4805E-10	.1235E-09
.1840	.3797E-11	.7009E-10	.5664E-10	.1305E-09
.1880	.3796E-11	.6838E-10	.6573E-10	.1379E-09
.1920	.3792E-11	.6658E-10	.7499E-10	.1454E-09
.1960	.3787E-11	.6477E-10	.8408E-10	.1526E-09

APPENDIX C

Computer program and the print outs for the back scattered electric field from a cylindrical body of varying radius, illuminated by the plane EM waves.

```
C       *****************************************************************
C       THIS PROGRAM COMPUTES SQUARE OF THE MAGNITUDE AND PHASE OF BACK
C       SCATTERED FIELD FROM CYLINDER OF COMPLEX PERMITTIVITY. IT ALSO
C       PRINTS OUT THE PARAMETERS "Q" AND "P" , DEFINED IN THE TEXT. THE CY
C       LINDER IS ILLUMINATED BY PLANE WAVE, "A" IS RADIUS OF CYLINDER AND
C       "R" IS POINT OF OBSERVATION IN METERS. CONDUCTIVITY SIGMA,SOURCE
C       FREQUENCY AND RELATIVE PERMITTIVITY OF CYLINDER ARE REQUIRED AS
C       FORMATTED INPUT DATA. THIS PROGRAM NEEDS SUBROUTINE "COMBES" .
C       *****************************************************************
        PROGRAM HEART1 (INPUT,OUTPUT,TAPE 10 =INPUT,TAPE 20 = OUTPUT)
        DIMENSION BJRE(75),BJIM(75),YRE(41),YIM(41)
        COMPLEX BODY,WK,BN,HNKL,SERIES,TERMN ,AA ,PC
        PI=4.0*ATAN (1.0)
        R=30.48
        A=1./(PI*100.)
        READ (10,1) SIGMA,FREQ,DIELEC
1       FORMAT (F6.3,E11.4,F5.2)
        FREEMU=4.0E-07*PI
        VACUUM=8.854E-12
        VELITE=3.0E+08
        OMEGA=2.0*PI*FREQ
        WKO=OMEGA/VELITE
        DELCTR=DIELEC*VACUUM
        BODY=CMPLX(DELCTR,-(SIGMA/OMEGA))
        SQROMG=OMEGA**2
        WK=CSQRT(SQROMG*FREEMU*BODY)
        WRITE (20,57) SIGMA,FREQ,DIELEC
57      FORMAT (1H1,5X,14HCONDUCTIVITY =,F6.3,3X,11HFREQUENCY =,E11.4,
       *3X,14HPERMITTIVITY =,F5.2,//)
        WRITE(20,75)
75      FORMAT(     5X,3HKOA,10X,18HFIELD MAGNITUDE SQ,5X,12HPHASE IN DEG,
       *5X,14HREAL PART    Q,5X,14HIMAG PART    P,//)
        DO 9 I=1,12
        DO 99 J=1,5
        WKOR=WKO*R
        WKOA=WKO*A
        P1=SQRT(2.0/(PI*WKOR))
        P2=WKOR+(3.0*PI/4.0)
        PC=CMPLX(0.0,-  P2)
        SERIES=CMPLX(0.0,0.0)
        DO 999 N=1,30
        Q=FLOAT(N)-1.
        CALL COEFBN (N,WK,WKO,A,BN)
        IF ( ABS(WKOR)  .LE.50.0) GO TO 8
        C1=SQRT(2.0/(PI*WKOR))
        C2=WKOR-(2.0*Q+1.0)*PI/4.
        AA=CMPLX(0.0,-C2)
        HNKL=C1*CEXP(AA)
        GO TO 80
8       CALL COMBES (WKOR,0.0,0.0,0.0,N,BJRE,BJIM,YRE,YIM)
        HNKL=CMPLX(BJRE(N),-YRE(N))
80      Q1=Q*PI
        TERMN=(BN*HNKL*COS(Q1))/(P1*CEXP(PC))
        SERIES=SERIES+TERMN
999     CONTINUE
        X=REAL(SERIES)
        Y=AIMAG(SERIES)
        Z=Y/X
        PHASER=ATAN(Z)
        PHASEA=PHASER*180.0/PI
        AMPLI=(X**2+Y**2)*(P1**2)
        X1=(2.0/WKOA)*X
        Y1=(2.0/WKOA)*Y
        WRITE (20,11) WKOA,AMPLI,PHASEA,X1,Y1
11      FORMAT (F6.2,10X,E11.4,12X,E11.4,6X,E11.4,8X,E11.4)
        A=A+(1./(PI*100.))
99       CONTINUE
        WRITE(20,111)
111     FORMAT(1HO)
9       CONTINUE
        STOP
        END
        SUBROUTINE COEFBN (N,WK,WKO,A,BN)
        DIMENSION BJRE(75),BJIM(75),YRE(41),YIM(41)
        COMPLEX WK,WKA,C1,CB1,BI1,B,PART1,DERBES,X1,H,HI1,DERHAN,D,E,COMPX
```

```
     *J,BN,AAC
      PI=4.0*ATAN(1.0)
      WKOA=WKO*A
      WKA=WK*A
      REWKA=REAL(WKA)
      AMWKA=AIMAG(WKA)
      C1=WK/WKO
      Q=FLOAT(N-1)
      IF(CABS(WKA) .LE. 50.0) GO TO 1
      ARGU1=REWKA-(Q*PI/2.0)-(3.0*PI/4.0)
      ARGU2=ARGU1+(PI/2.0)
      CB1=CSQRT(2.0/(PI*WKA))
      BI1=CB1*CMPLX(COS(ARGU1),-SIN(ARGU1)*TANH(AMWKA))
      B=CB1*CMPLX(COS(ARGU2),-SIN(ARGU2)*TANH(AMWKA))
      GO TO 10
1     CALL COMBES (REWKA,AMWKA,0.0,0.0,N,BJRE,BJIM,YRE,YIM)
      B=CMPLX(BJRE(N),BJIM(N))
      BI1=CMPLX(BJRE(N+1),BJIM(N+1))
10     PART1=Q*B/WKA
      DERBES=PART1-BI1
      X1=C1*DERBES/B
      CALL COMBES (WKOA,0.0,0.0,0.0,N,BJRE,BJIM,YRE,YIM)
      C=(Q/WKOA)-(BJRE(N+1)/BJRE(N))
      H=CMPLX(BJRE(N),-YRE(N))
      HI1=CMPLX(BJRE(N+1),-YRE(N+1))
      DERHAN=(Q*H/WKOA)-HI1
      D=DERHAN/H
      E=(BJRE(N)/H)*(X1-C)/(X1-D)
      IF(N-1)20,20,16
20    EPCILN=1.0
      GO TO 7
16    EPCILN=2.0
7     AA=Q*PI/2.0
      AAC=CMPLX(0.0,AA)
      COMPXJ=CEXP(AAC)
      BN=-E*EPCILN/COMPXJ
      RETURN
      END
```

TABLE C-1 : Back scattered field from a conducting cylinder, coefficients Q and P vs. $k_o a$ (Fig. 4.1.1)

CONDUCTIVITY =99.990 FREQUENCY = .3000E+10 PERMITTIVITY = 1.00

KOA	FIELD MAGNITUDE SQ	PHASE IN DEG	REAL PART Q	IMAG PART P
.20	.1441E-03	-.4846E+02	.4367E+01	-.4929E+01
.40	.2982E-03	-.4095E+02	.3577E+01	-.3104E+01
.60	.4819E-03	-.3623E+02	.3237E+01	-.2372E+01
.80	.6952E-03	-.3282E+02	.3038E+01	-.1960E+01
1.00	.9386E-03	-.3019E+02	.2906E+01	-.1690E+01
1.20	.1212E-02	-.2806E+02	.2808E+01	-.1497E+01
1.40	.1515E-02	-.2631E+02	.2734E+01	-.1352E+01
1.60	.1848E-02	-.2482E+02	.2675E+01	-.1237E+01
1.80	.2211E-02	-.2354E+02	.2627E+01	-.1144E+01
2.00	.2602E-02	-.2242E+02	.2586E+01	-.1067E+01
2.20	.3024E-02	-.2149E+02	.2551E+01	-.1004E+01
2.40	.3474E-02	-.2060E+02	.2522E+01	-.9479E+00
2.60	.3953E-02	-.1980E+02	.2496E+01	-.8987E+00
2.80	.4461E-02	-.1908E+02	.2473E+01	-.8555E+00
3.00	.4998E-02	-.1843E+02	.2452E+01	-.8172E+00
3.20	.5564E-02	-.1783E+02	.2434E+01	-.7829E+00
3.40	.6158E-02	-.1728E+02	.2418E+01	-.7520E+00
3.60	.6781E-02	-.1677E+02	.2402E+01	-.7241E+00
3.80	.7433E-02	-.1630E+02	.2389E+01	-.6986E+00
4.00	.8113E-02	-.1586E+02	.2376E+01	-.6753E+00
4.20	.8822E-02	-.1546E+02	.2364E+01	-.6538E+00
4.40	.9560E-02	-.1507E+02	.2354E+01	-.6339E+00
4.60	.1033E-01	-.1472E+02	.2344E+01	-.6155E+00
4.80	.1112E-01	-.1438E+02	.2334E+01	-.5984E+00
5.00	.1194E-01	-.1406E+02	.2326E+01	-.5824E+00
5.20	.1279E-01	-.1376E+02	.2318E+01	-.5674E+00
5.40	.1367E-01	-.1347E+02	.2310E+01	-.5534E+00
5.60	.1458E-01	-.1320E+02	.2303E+01	-.5402E+00
5.80	.1552E-01	-.1294E+02	.2296E+01	-.5277E+00
6.00	.1648E-01	-.1270E+02	.2290E+01	-.5159E+00
6.20	.1747E-01	-.1247E+02	.2283E+01	-.5048E+00
6.40	.1849E-01	-.1224E+02	.2278E+01	-.4943E+00
6.60	.1954E-01	-.1203E+02	.2272E+01	-.4843E+00
6.80	.2061E-01	-.1183E+02	.2267E+01	-.4748E+00
7.00	.2172E-01	-.1164E+02	.2262E+01	-.4658E+00
7.20	.2285E-01	-.1145E+02	.2257E+01	-.4572E+00
7.40	.2401E-01	-.1127E+02	.2253E+01	-.4490E+00
7.60	.2520E-01	-.1110E+02	.2248E+01	-.4411E+00
7.80	.2641E-01	-.1093E+02	.2244E+01	-.4335E+00
8.00	.2766E-01	-.1078E+02	.2240E+01	-.4263E+00
8.20	.2893E-01	-.1062E+02	.2236E+01	-.4194E+00
8.40	.3023E-01	-.1047E+02	.2233E+01	-.4127E+00
8.60	.3156E-01	-.1033E+02	.2229E+01	-.4063E+00
8.80	.3291E-01	-.1019E+02	.2226E+01	-.4002E+00
9.00	.3429E-01	-.1006E+02	.2222E+01	-.3942E+00
9.20	.3570E-01	-.9930E+01	.2219E+01	-.3885E+00
9.40	.3714E-01	-.9805E+01	.2216E+01	-.3830E+00
9.60	.3861E-01	-.9684E+01	.2213E+01	-.3777E+00
9.80	.4010E-01	-.9567E+01	.2210E+01	-.3726E+00
10.00	.4162E-01	-.9454E+01	.2208E+01	-.3676E+00
10.20	.4317E-01	-.9344E+01	.2205E+01	-.3628E+00
10.40	.4475E-01	-.9237E+01	.2202E+01	-.3582E+00
10.60	.4636E-01	-.9133E+01	.2200E+01	-.3537E+00
10.80	.4799E-01	-.9032E+01	.2197E+01	-.3493E+00
11.00	.4965E-01	-.8934E+01	.2195E+01	-.3451E+00
11.20	.5134E-01	-.8839E+01	.2193E+01	-.3410E+00
11.40	.5305E-01	-.8746E+01	.2191E+01	-.3370E+00
11.60	.5480E-01	-.8655E+01	.2188E+01	-.3331E+00
11.80	.5657E-01	-.8567E+01	.2186E+01	-.3294E+00
12.00	.5837E-01	-.8481E+01	.2184E+01	-.3257E+00

TABLE C-2 : Back scattered field from a cylindrical body, coefficients Q and P vs. koa (Fig. 4.1.1)

CONDUCTIVITY : .668 FREQUENCY : .3000E+10 PERMITTIVITY : 0.00

KOA	FIELD MAGNITUDE SQ	PHASE IN DEG	REAL PART Q	IMAG PART P
.20	.4099E-05	-.2010E+02	.1043E+01	-.3816E+00
.40	.3623E-04	-.2338E+02	.1515E+01	-.6551E+00
.60	.1089E-03	-.2226E+02	.1766E+01	-.7226E+00
.80	.2305E-03	-.2074E+02	.1947E+01	-.7372E+00
1.00	.3997E-03	-.1983E+02	.2062E+01	-.7477E+00
1.20	.6076E-03	-.1934E+02	.2126E+01	-.7480E+00
1.40	.8505E-03	-.1873E+02	.2164E+01	-.7339E+00
1.60	.1127E-02	-.1816E+02	.2187E+01	-.7172E+00
1.80	.1433E-02	-.1761E+02	.2199E+01	-.6981E+00
2.00	.1769E-02	-.1708E+02	.2205E+01	-.6776E+00
2.20	.2134E-02	-.1656E+02	.2208E+01	-.6566E+00
2.40	.2529E-02	-.1607E+02	.2209E+01	-.6361E+00
2.60	.2952E-02	-.1560E+02	.2208E+01	-.6164E+00
2.80	.3404E-02	-.1515E+02	.2206E+01	-.5975E+00
3.00	.3886E-02	-.1474E+02	.2204E+01	-.5797E+00
3.20	.4396E-02	-.1434E+02	.2202E+01	-.5630E+00
3.40	.4935E-02	-.1397E+02	.2200E+01	-.5472E+00
3.60	.5503E-02	-.1362E+02	.2197E+01	-.5325E+00
3.80	.6100E-02	-.1330E+02	.2194E+01	-.5186E+00
4.00	.6726E-02	-.1299E+02	.2192E+01	-.5055E+00
4.20	.7381E-02	-.1270E+02	.2189E+01	-.4932E+00
4.40	.8064E-02	-.1242E+02	.2186E+01	-.4816E+00
4.60	.8775E-02	-.1216E+02	.2184E+01	-.4706E+00
4.80	.9516E-02	-.1192E+02	.2181E+01	-.4603E+00
5.00	.1028E-01	-.1168E+02	.2179E+01	-.4505E+00
5.20	.1108E-01	-.1146E+02	.2176E+01	-.4412E+00
5.40	.1191E-01	-.1125E+02	.2174E+01	-.4324E+00
5.60	.1276E-01	-.1105E+02	.2172E+01	-.4240E+00
5.80	.1364E-01	-.1085E+02	.2170E+01	-.4160E+00
6.00	.1455E-01	-.1067E+02	.2167E+01	-.4084E+00
6.20	.1549E-01	-.1049E+02	.2165E+01	-.4011E+00
6.40	.1646E-01	-.1033E+02	.2163E+01	-.3941E+00
6.60	.1745E-01	-.1016E+02	.2161E+01	-.3875E+00
6.80	.1848E-01	-.1001E+02	.2159E+01	-.3811E+00
7.00	.1953E-01	-.9860E+01	.2158E+01	-.3750E+00
7.20	.2061E-01	-.9717E+01	.2156E+01	-.3691E+00
7.40	.2172E-01	-.9579E+01	.2154E+01	-.3635E+00
7.60	.2285E-01	-.9446E+01	.2152E+01	-.3581E+00
7.80	.2401E-01	-.9317E+01	.2151E+01	-.3528E+00
8.00	.2521E-01	-.9194E+01	.2149E+01	-.3478E+00
8.20	.2642E-01	-.9074E+01	.2147E+01	-.3430E+00
8.40	.2767E-01	-.8958E+01	.2146E+01	-.3383E+00
8.60	.2895E-01	-.8847E+01	.2144E+01	-.3338E+00
8.80	.3025E-01	-.8739E+01	.2143E+01	-.3294E+00
9.00	.3158E-01	-.8634E+01	.2141E+01	-.3252E+00
9.20	.3294E-01	-.8532E+01	.2140E+01	-.3211E+00
9.40	.3433E-01	-.8434E+01	.2139E+01	-.3171E+00
9.60	.3574E-01	-.8338E+01	.2137E+01	-.3133E+00
9.80	.3718E-01	-.8246E+01	.2136E+01	-.3096E+00
10.00	.3865E-01	-.8155E+01	.2135E+01	-.3059E+00
10.20	.4015E-01	-.8068E+01	.2134E+01	-.3024E+00
10.40	.4168E-01	-.7983E+01	.2132E+01	-.2990E+00
10.60	.4323E-01	-.7900E+01	.2131E+01	-.2957E+00
10.80	.4481E-01	-.7819E+01	.2130E+01	-.2925E+00
11.00	.4642E-01	-.7741E+01	.2129E+01	-.2894E+00
11.20	.4806E-01	-.7664E+01	.2128E+01	-.2864E+00
11.40	.4972E-01	-.7590E+01	.2127E+01	-.2834E+00
11.60	.5141E-01	-.7517E+01	.2126E+01	-.2805E+00
11.80	.5313E-01	-.7446E+01	.2125E+01	-.2777E+00
12.00	.5488E-01	-.7377E+01	.2124E+01	-.2750E+00

TABLE C-3 : Back scattered field from a cylindrical biological body vs. koa at 3.0GHz. (Fig. 4.1.2)

CONDUCTIVITY : 2.260 FREQUENCY : .3000E+10 PERMITTIVITY :46.00

KOA	FIELD MAGNITUDE SQ	PHASE IN DEG	REAL PART O	IMAG PART P
.20	.1831E-03	-.2868E+02	.8511E+01	-.3562E+01
.40	.5861E-04	-.2018E+02	.1970E+01	-.7244E+00
.60	.1291E-03	.1601E+02	.1997E+01	.5731E+00
.80	.1112E-03	.3280E+02	.1215E+01	.7833E+00
1.00	.1875E-03	.6084E+02	.7319E+00	.1312E+01
1.20	.1954E-03	.8125E+02	.1944E+00	.1283E+01
1.40	.2389E-03	-.7410E+02	-.3317E+00	.1165E+01
1.60	.2485E-03	-.5114E+02	-.5781E+00	.8418E+00
1.80	.2853E-03	-.2675E+02	-.9191E+00	.4632E+00
2.00	.3099E-03	-.3519E+01	-.9637E+00	.5928E-01
2.20	.3458E-03	.1974E+02	-.8727E+00	-.3132E+00
2.40	.3704E-03	.4267E+02	-.6469E+00	-.5962E+00
2.60	.3989E-03	.6588E+02	-.3443E+00	-.7891E+00
2.80	.4244E-03	.8915E+02	-.1195E-01	-.8070E+00
3.00	.4550E-03	-.6757E+02	.2876E+00	-.7209E+00
3.20	.4847E-03	-.4445E+02	.5387E+00	-.5285E+00
3.40	.5147E-03	-.2142E+02	.6814E+00	-.2673E+00
3.60	.5423E-03	.1601E+01	.7093E+00	.1983E-01
3.80	.5701E-03	.2469E+02	.6262E+00	.2879E+00
4.00	.5984E-03	.4781E+02	.4506E+00	.4970E+00
4.20	.6282E-03	.7089E+02	.2143E+00	.6185E+00
4.40	.6579E-03	-.8809E+02	-.4365E-01	.6380E+00
4.60	.6871E-03	-.6309E+02	-.2829E+00	.5574E+00
4.80	.7153E-03	-.4009E+02	-.4676E+00	.3936E+00
5.00	.7437E-03	-.1706E+02	-.5720E+00	.1755E+00
5.20	.7726E-03	.5974E+01	-.5832E+00	-.6103E-01
5.40	.8023E-03	.2899E+02	-.5033E+00	-.2788E+00
5.60	.8318E-03	.5197E+02	-.3480E+00	-.4450E+00
5.80	.8608E-03	.7495E+02	-.1441E+00	-.5358E+00
6.00	.8894E-03	-.8207E+02	.7520E-01	-.5400E+00
6.20	.9181E-03	-.5908E+02	.2755E+00	-.4599E+00
6.40	.9473E-03	-.3608E+02	.4263E+00	-.3107E+00
6.60	.9769E-03	-.1311E+02	.5059E+00	-.1178E+00
6.80	.1006E-02	.9860E+01	.5042E+00	.8763E-01
7.00	.1035E-02	.3282E+02	.4237E+00	.2733E+00
7.20	.1064E-02	.5579E+02	.2794E+00	.4110E+00
7.40	.1111E-02	.7838E+02	.9954E-01	.4840E+00
7.60	.1141E-02	-.7864E+02	-.9599E-01	.4779E+00
7.80	.1170E-02	-.5567E+02	-.2713E+00	.3973E+00
8.00	.1200E-02	-.3271E+02	-.3986E+00	.2567E+00
8.20	.1229E-02	-.9758E-01	-.4622E+00	.7947E-01
8.40	.1258E-02	.1321E+02	-.4510E+00	-.1058E+00
8.60	.1288E-02	.3617E+02	-.3895E+00	-.2701E+00
8.80	.1317E-02	.5913E+02	-.2321E+00	-.3883E+00
9.00	.1347E-02	.8209E+02	-.6159E-01	-.4430E+00
9.20	.1376E-02	-.7498E+02	.1148E+00	-.4272E+00
9.40	.1406E-02	-.5201E+02	.2693E+00	-.3448E+00
9.60	.1435E-02	-.2906E+02	.3784E+00	-.2102E+00
9.80	.1464E-02	-.6106E+01	.4259E+00	-.4557E-01
10.00	.1494E-02	.1684E+02	.4058E+00	.1229E+00
10.20	.1524E-02	.3979E+02	.3225E+00	.2867E+00
10.40	.1553E-02	.6274E+02	.1804E+00	.3895E+00
10.60	.1582E-02	.8568E+02	.3099E-01	.4105E+00
10.80	.1612E-02	-.7137E+02	-.1302E+00	.3884E+00
11.00	.1641E-02	-.4843E+02	-.2681E+00	.3022E+00
11.20	.1671E-02	-.2548E+02	-.3814E+00	.1722E+00
11.40	.1700E-02	-.2540E+01	-.3964E+00	.1758E-01
11.60	.1730E-02	.2040E+02	-.3686E+00	-.1371E+00
11.80	.1759E-02	.4334E+02	-.2836E+00	-.2878E+00
12.00	.1789E-02	.6628E+02	-.1655E+00	-.3539E+00

TABLE C-4 : Back scattered field from a cylindrical biological body vs. koa at 10.0GHz. (Fig. 4.1.3)

CONDUCTIVITY =10.300 FREQUENCY = .1000E+11 PERMITTIVITY =39.90

KOA	FIELD MAGNITUDE SQ	PHASE IN DEG	REAL PART Q	IMAG PART P
25.99	.1112E-02	.4552E+02	.1898E+00	.1928E+00
26.49	.1147E-02	-.7339E+02	-.7318E-01	.2453E+00
27.00	.1188E-02	-.1584E+02	-.2460E+00	.6979E-01
27.50	.1219E-02	.4153E+02	-.1903E+00	-.1686E+00
28.00	.1248E-02	-.8109E+02	.3911E-01	-.2498E+00
28.50	.1269E-02	-.2391E+02	.2288E+00	-.1014E+00
29.01	.1273E-02	.3348E+02	.2055E+00	.1358E+00
29.51	.1280E-02	-.8879E+02	-.5125E-02	.2428E+00
30.01	.1298E-02	-.3103E+02	-.2058E+00	.1238E+00
30.52	.1310E-02	.2678E+02	-.2121E+00	-.1070E+00
31.02	.1332E-02	.8473E+02	-.2168E-01	-.2348E+00
31.52	.1365E-02	-.3749E+02	.1863E+00	-.1429E+00
32.02	.1394E-02	.2013E+02	.2193E+00	.8036E-01
32.53	.1425E-02	.7780E+02	.4913E-01	.2272E+00
33.03	.1462E-02	-.4473E+02	-.1847E+00	.1832E+00
33.53	.1488E-02	.1255E+02	-.2249E+00	-.5008E-01
34.03	.1503E-02	.6995E+02	-.7819E-01	-.2143E+00
34.54	.1517E-02	-.5259E+02	.1372E+00	-.1794E+00
35.04	.1522E-02	.4825E+01	.2222E+00	.1915E-01
35.54	.1527E-02	.6276E+02	.1008E+00	.1958E+00
36.04	.1547E-02	-.5929E+02	-.1116E+00	.1879E+00
36.55	.1575E-02	-.1486E+01	-.2174E+00	.5677E-02
37.05	.1605E-02	.5628E+02	-.1202E+00	-.1801E+00
37.55	.1643E-02	-.6606E+02	.8773E-01	-.1978E+00
38.06	.1678E-02	-.8641E+01	.2131E+00	-.3238E-01
38.56	.1700E-02	.4879E+02	.1411E+00	.1611E+00
39.06	.1723E-02	-.7372E+02	-.5985E-01	.2043E+00
39.56	.1742E-02	-.1632E+02	-.2027E+00	.5938E-01
40.07	.1749E-02	.4118E+02	-.1573E+00	-.1378E+00
40.57	.1756E-02	-.8113E+02	.3193E-01	-.2048E+00

APPENDIX D

Computer program and the print outs for the back scattered electric field from a spherical body of varying radius, illuminated by the plane EM waves.

```
C       ******************************************************************
C       THIS PROGRAM COMPUTES SQUARE OF THE MAGNITUDE AND PHASE OF THE SCAT
C       TERED FIELD FROM SPHERE OF COMPLEX PERMITTIVITY. IT ALSO PRINTS OUT
C       THE BACK SCATTERING CROSS SECTION NORMALIZED BY CROSS SECTION OF
C       THE SPHERE. THE SPHERE IS ILLUMINATED BY PLANE WAVE. "A" IS RADIUS
C       OF THE SPHERE AND "R" IS POINT OF OBSERVATION IN METERS. CONDUCTI
C       VITY OF THE SPHERE SIGMA,FREQUENCY OF PLANE WAVE AND RELATIVE
C       PERMITTIVITY OF THE SPHERE ARE REQUIRED AS FORMATTED INPUT DATA.
C       THIS PROGRAM NEEDS SUBROUTINE " COMBES ".
C       ******************************************************************
        PROGRAM HEART2 (INPUT,OUTPUT,TAPE 10 =INPUT,TAPE 20=OUTPUT)
        DIMENSION BJRE (75),BJIM(75),YRE(41),YIM(41)
        COMPLEX BODY,WK,SERIES,COMPXJ,AN,TERM1,DN,CN,HNKL1,HNKL2,DHNKL,
       *TERM3,BRAKET,SUM,ARGU1,ARGU2,HNKL11,TERM2,ARGU3,BODY1
        PI=4.0*ATAN (1.0)
        R=30.48
        A=0.01/PI
        READ (10,1) SIGMA,FREQ,DIELEC
1       FORMAT (F6.3,E11.4,F5.2)
        WRITE (20,57) SIGMA,FREQ,DIELEC
57      FORMAT (1H1,5X,14HCONDUCTIVITY =,F6.3,3X,11HFREQUENCY =,E11.4,
       *3X,14HPERMITTIVITY =,F5.2,//)
        FREEMU=4.0E-07*PI
        VACUUM=8.854E-12
        VELITE=3.0E+08
        OMEGA=2.0*PI*FREQ
        WKO=OMEGA/VELITE
        DELCTR=DIELEC*VACUUM
        BODY=CMPLX(DELCTR,-(SIGMA/OMEGA))
        BODY1=BODY/VACUUM
        SQROMG=OMEGA**2
        WK=CSQRT (SQROMG*FREEMU*BODY)
        WKOR=WKO*R
        WRITE(20,75)
75      FORMAT(     5X,3HKOA,10X,18HFIELD MAGNITUDE SQ,5X,12HPHASE IN DEG,
       *5X,14HREAL PART OF E,5X,14HIMAG PART OF E,5X,22HSCAT-CROSS-SEC BY
       *AREA,//)
        DO 9 I=1,12
        DO 99 J=1,5
        WKOA=WKO*A
        SERIES=CMPLX(0.0,0.0)
        DO 999 NW=1,30
        N=NW+1
        Q=FLOAT (N-1)
        C1=SQRT(PI*WKOR/2.0)
        C2=(Q+1.)*SQRT(PI/(2.0*WKOR))
        IF (ABS(WKOR) .GT. 50.) GO TO 10
        CALL COMBES (WKOR,0.0,0.5,0.0,N,BJRE,BJIM,YRE,YIM)
        B1=C1*BJRE(N)
        B2=C2*BJRE(N)
        B3=C1*BJRE(N+1)
        BD1=B2-B3
        HNKL1=C1*CMPLX(BJRE(N),-YRE(N))
        HNKL2=C1*CMPLX(BJRE(N+1),-YRE(N+1))
        DHNKL=(C2/C1)*HNKL1-HNKL2
        GO TO 100
10       CC2=Q+1.
        CC3=Q*PI/2.0
        CC7=SQRT(PI*WKOR/2.0)
        X1=CC3-WKOR
        B1=SIN(X1)
        BD1=(CC2/WKOR)*SIN(X1)+COS(X1)
        ARGU1=CMPLX(0.0,(X1+(PI/2.0)))
        ARGU2=CMPLX(0.0,X1)
        HNKL1=CEXP(ARGU1)
        HNKL11=CEXP(ARGU2)
        DHNKL=(CC2/WKOR)*HNKL1+HNKL11
100     COEFF=Q*PI/2.
        ARGU3=CMPLX(0.0,COEFF)
        AN1=((2.0*Q)+1.0)/(Q*(Q+1.0))
        COMPXJ=CEXP(ARGU3)
        AN=AN1/COMPXJ
        TERM1=AN*CMPLX(B1,BD1)
        CALL CNDN (WK,WKO,A,BODY1,N,CN,DN)
         TERM2=AN*DN*HNKL1*(-1.)
```

```
      TERM3=AN*CN*DHNKL
      BRAKET=TERM2+TERM3*CMPLX(0.0,1.0)
C     ***********************************************************************
C     TERM1 SHOUD BE ADDED TO "BRAKET" TO GET THE TOTAL FIELD AT "R".
C     HOWEVER, SCATTERING CROSS SECTION IN THAT CASE WILL BE DIFFERENT
C     FROM PRINT OUT RESULTS.
C     ***********************************************************************
      C3=(-1.)**NW
      C4=Q*(Q+1.)
      SUM=C3*C4*BRAKET
      SERIES=SERIES+SUM
999   CONTINUE
      X=REAL(SERIES)*(-1.)
      Y=AIMAG(SERIES)*(-1.)
      Z=Y/X
      AMPLI=(X**2+Y**2)/(4.0*(WKOR**2))
      PHASER=ATAN(Z)
      PHASEA=PHASER*180.0/PI
      AMP=(4.0*(R**2))/(A**2)
      AMP2=AMP*AMPLI
      WRITE (20,11)WKOA,AMPLI,PHASEA,X,Y,AMP2
11    FORMAT (3X,F6.2,10X,E11.4,12X,E11.4,8X,E11.4,8X,E11.4,8X,E11.4)
      A=A+(1./(PI*100.))
99    CONTINUE
      WRITE(20,111)
111   FORMAT(1HO)
9     CONTINUE
      STOP
      END

      SUBROUTINE CNDN (WK,WKO,A,BODY,N,CN,DN)
      DIMENSION BJRE(75),BJIM(75),YRE(41),YIM(41)
      COMPLEX WK,WKA,BODY,C1,SBFWKA,DSBFKA,D1,D2,HNKL,HNKL1,DHNKL,C9,
     *AURG1,AURG2,EPCILN,CN,DN,DN1,DN2,CN1,CN2
      PI=4.0*ATAN(1.0)
      WKA=WK*A
      WKOA=WKO*A
      EPCILN=CSQRT(BODY)
      REWKA=REAL(WKA)
      AEMWKA=AIMAG(WKA)
      Q=FLOAT (N-1)
      C1=CSQRT(PI*WKA/2.0)
      C2=Q+1.
      C3=Q*PI/2.
      C4=C3-REWKA
      C5=-AEMWKA
      C6=(EXP(C5)+EXP(-C5))/2.0
      C7=SQRT(PI*WKOA/2.0)
      C8=SQRT(PI/(2.0*WKOA))
      C9=CSQRT(PI/(2.0*WKA))
      IF (CABS(WKA) .GT. 50.0) GO TO 9
      CALL COMBES(REWKA,AEMWKA,0.5,0.0,N,BJRE,BJIM,YRE,YIM)
      SBFWKA=C1*CMPLX(BJRE(N),BJIM(N))
      DSBFKA=C2*C9*CMPLX(BJRE(N),BJIM(N))-C1*CMPLX(BJRE(N+1),BJIM(N+1))
      GO TO 1
9     F1=SIN(C4)
      F2=TANH(C5)*COS(C4)
      D1=C2*(C6/WKA)*CMPLX(F1,F2)
      F3=COS(C4)
      F4=TANH(C5)*SIN(C4)
      D2=C6*CMPLX(F3,-F4)
      DSBFKA=D1+D2
      SBFWKA=C6*CMPLX(F1,F2)
1     IF (ABS(WKOA) .GT. 50.) GO TO 99
      CALL COMBES (WKOA,0.0,0.5,0.0,N,BJRE,BJIM,YRE,YIM)
      SBFWKO=C7*BJRE(N)
      DSBFKO=C2*C8*BJRE(N)-C7*BJRE(N+1)
      HNKL=C7*CMPLX(BJRE(N),-YRE(N))
      HNKL1=C7*CMPLX(BJRE(N+1),-YRE(N+1))
      DHNKL=C2*C8*CMPLX(BJRE(N),-YRE(N))-HNKL1
      GO TO 11
99    X1=C3-WKOA
      SBFWKO=SIN(X1)
      DSBFKO=(C2/WKOA)*SIN(X1)+COS(X1)
      AURG1=CMPLX(0.0,(X1+(PI/2.0)))
      AURG2=CMPLX(0.0,X1)
      HNKL1=CEXP(AURG2)
      HNKL=CEXP(AURG1)
      DHNKL=(C2/WKOA)*HNKL+HNKL1
```

```
11    CN1=EPCILN*SBFWKA*DSBFKO-SBFWKO*DSBFKA
      CN2=HNKL*DSBFKA-EPCILN*DHNKL*SBFWKA
      CN=CN1/CN2
      DN1=EPCILN*SBFWKO*DSBFKA-DSBFKO*SBFWKA
      DN2=DHNKL*SBFWKA-EPCILN*HNKL*DSBFKA
      DN=DN1/DN2
C     ***********************************************************************

C     CN1,CN2,DN1 AND DN2 CARDS SHOULD BE CHANGED FOR CONDUCTING SPHERE
C     BECAUSE THESE WONT GIVE CORRECT VALUES AS LIMITING CASE OF INFINITE
C     CONDUCTIVITY AND UNITY RELATIVE PERMITTIVITY.

C     ***********************************************************************
      RETURN
      END
```

TABLE D-1 : Back scattered field and normalized scattering cross-section of a conducting sphere vs. koa. (Fig. 4.2.2)

CONDUCTIVITY =99.990 FREQUENCY = .3000E+10 PERMITTIVITY = 1.00

KOA	FIELD MAGNITUDE SQ	PHASE IN DEG	REAL PART OF E	IMAG PART OF E	SCAT-CROSS-SEC BY AREA
.20	.1448E-10	-.1359E+00	.2391E-01	-.5673E-04	.1429E-01
.40	.9035E-09	-.1424E+01	.1888E+00	-.4692E-02	.2229E+00
.60	.9531E-08	-.5509E+01	.6106E+0C	-.5889E-C1	.1045E+01
.8C	.4209E-07	-.1351E+02	.1253E+01	-.3010E+00	.2598E+01
1.00	.9216E-07	-.2269E+02	.1760E+01	-.7359E+00	.3638E+01
1.20	.1133E-06	-.2783E+02	.1870E+01	-.9872E+00	.3106E+01
1.40	.8633E-07	-.2595E+02	.1660E+01	-.8078E+00	.1739E+01
1.60	.3717E-07	-.8430E+01	.1198E+01	-.1778E+00	.5732E+00
1.8C	.2698E-07	.5483E+02	.5944E+00	.8436E+00	.3287E+00
2.00	.1021E-06	.8906E+02	.3297E-01	.2007E+01	.1007E+01
2.20	.2189E-06	-.8189E+02	-.4147E+00	.2911E+01	.1786E+01
2.40	.2814E-06	-.7605E+02	-.8033E+00	.3235E+01	.1929E+01
2.60	.2380E-06	-.6702E+02	-.1197E+01	.2822E+C1	.1390E+01
2.80	.1415E-06	-.4574E+02	-.1650E+01	.1693E+01	.7127E+00
3.00	.1186E-06	-.2400E+01	-.2162E+01	.9061E-01	.5203E+00
3.20	.2356E-06	.3167E+02	-.2596E+01	-.1601E+01	.9084E+00
3.40	.4180E-06	.4785E+02	-.2726E+01	-.3012E+01	.1428E+01
3.60	.5170E-06	.5875E+02	-.2344E+01	-.3862E+01	.1575E+01
3.80	.4544E-06	.7172E+02	-.1328E+01	-.4022E+01	.1242E+01
4.00	.3183E-06	-.8564E+02	.2696E+00	-.3535E+01	.7855E+00
4.20	.2868E-06	-.4962E+02	.2180E+01	-.2563E+01	.6418E+00
4.40	.4441E-06	-.1807E+02	.3981E+01	-.1298E+01	.9055E+00
4.60	.6881E-06	.9157E+00	.5211E+01	.8329E-01	.1284E+01
4.80	.8188E-06	.1479E+02	.5497E+01	.1452E+01	.1403E+01
5.00	.7404E-06	.3022E+02	.4672E+01	.2721E+01	.1169E+01
5.20	.5710E-06	.5324E+02	.2842E+01	.3804E+01	.8336E+00
5.40	.5320E-06	.8554E+02	.3564E+00	.4569E+01	.7202E+00
5.60	.7269E-06	-.6477E+02	-.2283E+01	.4846E+01	.9151E+00
5.80	.1027E-05	-.4441E+02	-.4548E+01	.4455E+01	.1205E+01
6.00	.1188E-05	-.2854E+02	-.6015E+01	.3272E+01	.1302E+01
6.20	.1098E-05	-.1153E+02	-.6452E+01	.1317E+01	.1128E+01
6.40	.9002E-06	.1157E+02	-.5640E+01	-.1195E+01	.8676E+00
6.60	.8548E-06	.4162E+02	-.4343E+01	-.3858E+01	.7747E+00
6.80	.1083E-05	.6998E+02	-.2238E+01	-.6144E+01	.9248E+00
7.00	.1433E-05	-.8882E+02	.1547E+00	-.7521E+01	.1155E+01
7.20	.1625E-05	-.7157E+02	.2533E+01	-.7598E+01	.1237E+01
7.40	.1529E-05	-.5347E+02	.4625E+01	-.6244E+01	.1103E+01
7.60	.1307E-05	-.3039E+02	.6196E+01	-.3634E+01	.8932E+00
7.80	.1255E-05	-.1857E+01	.7036E+01	-.2281E+00	.8146E+00
8.00	.1512E-05	.2556E+02	.6970E+01	.3334E+01	.9328E+00
8.20	.1908E-05	.4730E+02	.5888E+01	.6379E+01	.1120E+01
8.40	.2131E-05	.6558E+02	.3792E+01	.8351E+01	.1192E+01
8.60	.2033E-05	.8446E+02	.8645E+00	.8918E+01	.1085E+01
8.80	.1791E-05	-.7252E+02	-.2526E+01	.8021E+01	.9131E+00
9.00	.1733E-05	-.4508E+02	-.5841E+01	.5856E+01	.8448E+00
9.20	.2013E-05	-.1835E+02	-.8461E+01	.2807E+01	.9389E+00
9.40	.2451E-05	.3769E+01	-.9816E+01	-.6466E+00	.1095E+01
9.60	.2705E-05	.2283E+02	-.9525E+01	-.4010E+01	.1159E+01
9.80	.2611E-05	.4231E+02	-.7508E+01	-.6835E+01	.1073E+01
10.00	.2353E-05	.6525E+02	-.4035E+01	-.8763E+01	.9290E+00
10.20	.2287E-05	-.8812E+02	.3114E+00	-.9497E+01	.8679E+00
10.40	.2586E-05	-.6193E+02	.4754E+01	-.8916E+01	.9440E+00
10.60	.3063E-05	-.3953E+02	.8482E+01	-.6999E+01	.1076E+01
10.80	.3350E-05	-.1985E+02	.1082E+02	-.3905E+01	.1134E+01
11.00	.3263E-05	.8945E-01	.1135E+02	.1772E-01	.1065E+01
11.20	.2993E-05	.2295E+02	.1001E+02	.4238E+01	.9420E+00
11.40	.2918E-05	.4895E+02	.7050E+01	.8094E+01	.8865E+00
11.60	.3232E-05	.7472E+02	.2977E+01	.1090E+02	.9481E+00
11.80	.3743E-05	-.8267E+02	-.1551E+01	.1206E+02	.1061E+01
12.00	.4063E-05	-.6249E+02	-.5849E+01	.1123E+02	.1114E+01

TABLE D-2 : Back scattered field and normalized scattering cross-section of a sphere of complex permittivity vs. koa. (Fig. 4.2.2)

CONDUCTIVITY = 2.210 FREQUENCY = .3000E+10 PERMITTIVITY = 7.80

KOA	FIELD MAGNITUDE SQ	PHASE IN DEG	REAL PART OF E	IMAG PART OF E	SCAT-CROSS-SEC BY AREA
.20	.1436E-10	.6323E+02	.6537E-02	.1286E-01	.5267E-02
.40	.9562E-09	.6366E+02	.5255E-01	.1061E+00	.8768E-01
.60	.1209E-07	.6039E+02	.2081E+00	.3661E+00	.4925E+00
.80	.6450E-07	.4686E+02	.6652E+00	.7098E+00	.1479E+01
1.00	.1333E-06	.3017E+02	.1209E+01	.7028E+00	.1955E+01
1.20	.1376E-06	.2099E+02	.1326E+01	.5088E+00	.1402E+01
1.40	.7805E-07	.2028E+02	.1004E+01	.3708E+00	.5842E+00
1.60	.1629E-07	.5228E+02	.2991E+00	.3867E+00	.9336E-01
1.80	.4918E-07	-.4705E+02	-.5787E+00	.6217E+00	.2227E+00
2.00	.1831E-06	-.3566E+02	-.1332E+01	.9555E+00	.6715E+00
2.20	.3044E-06	-.3321E+02	-.1768E+01	.1158E+01	.9227E+00
2.40	.2979E-06	-.2954E+02	-.1819E+01	.1031E+01	.7588E+00
2.60	.1755E-06	-.1677E+02	-.1537E+01	.4630E+00	.3810E+00
2.80	.9574E-07	.2408E+02	-.1082E+01	-.4835E+00	.1791E+00
3.00	.1899E-06	.6889E+02	-.6012E+00	-.1557E+01	.3098E+00
3.20	.4062E-06	.8636E+02	-.1549E+00	-.2436E+01	.5819E+00
3.40	.5532E-06	-.8456E+02	.2703E+00	-.2836E+01	.7020E+00
3.60	.4981E-06	-.7411E+02	.7400E+00	-.2600E+01	.5638E+00
3.80	.3288E-06	-.5362E+02	.1303E+01	-.1768E+01	.3340E+00
4.00	.2701E-06	-.1600E+02	.1913E+01	-.5486E+00	.2476E+00
4.20	.4418E-06	.1761E+02	.2427E+01	.7704E+00	.3674E+00
4.40	.7213E-06	.3587E+02	.2636E+01	.1906E+01	.5466E+00
4.60	.8598E-06	.4861E+02	.2348E+01	.2664E+01	.5961E+00
4.80	.7527E-06	.6353E+02	.1481E+01	.2976E+01	.4793E+00
5.00	.6607E-06	.8758E+02	.1213E+00	.2866E+01	.3291E+00
5.20	.5467E-06	-.5853E+02	-.1478E+01	.2416E+01	.2968E+00
5.40	.7956E-06	-.2995E+02	-.2960E+01	.1706E+01	.4003E+00
5.60	.1113E-05	-.1129E+02	-.3962E+01	.7913E+00	.5206E+00
5.80	.1225E-05	.3909E+01	-.4230E+01	-.2891E+00	.5343E+00
6.00	.1073E-05	.2180E+02	-.3684E+01	-.1473E+01	.4373E+00
6.20	.8804E-06	.4732E+02	-.2436E+01	-.2642E+01	.3360E+00
6.40	.9250E-06	.7828E+02	-.7484E+00	-.3607E+01	.3313E+00
6.60	.1241E-05	-.7577E+02	.1049E+01	-.4136E+01	.4179E+00
6.80	.1576E-05	-.5669E+02	.2640E+01	-.4018E+01	.5000E+00
7.00	.1654E-05	-.3970E+02	.3790E+01	-.3147E+01	.4953E+00
7.20	.1469E-05	-.1983E+02	.4366E+01	-.1575E+01	.4168E+00
7.40	.1294E-05	.6124E+01	.4332E+01	.4647E+00	.3468E+00
7.60	.1401E-05	.3493E+02	.3717E+01	.2596E+01	.3559E+00
7.80	.1771E-05	.5939E+02	.2595E+01	.4387E+01	.4270E+00
8.00	.2109E-05	.7890E+02	.1071E+01	.5458E+01	.4833E+00
8.20	.2151E-05	-.8275E+02	-.7086E+00	.5573E+01	.4694E+00
8.40	.1945E-05	-.6157E+02	-.2543E+01	.4698E+01	.4045E+00
8.60	.1801E-05	-.3667E+02	-.4175E+01	.2997E+01	.3572E+00
8.80	.1969E-05	-.8406E+01	-.5317E+01	.7858E+00	.3731E+00
9.00	.2380E-05	.1519E+02	-.5702E+01	-.1549E+01	.4310E+00
9.20	.2710E-05	.3512E+02	-.5157E+01	-.3627E+01	.4697E+00
9.40	.2720E-05	.5451E+02	-.3667E+01	-.5144E+01	.4516E+00
9.60	.2506E-05	.7655E+02	-.1411E+01	-.5897E+01	.3989E+00
9.80	.2400E-05	-.7780E+02	.1264E+01	-.5800E+01	.3666E+00
10.00	.2626E-05	-.5155E+02	.3851E+01	-.4867E+01	.3852E+00
10.20	.3066E-05	-.2857E+02	.5890E+01	-.3207E+01	.4323E+00
10.40	.3382E-05	-.8250E+01	.6971E+01	-.1011E+01	.4587E+00
10.60	.3365E-05	.1195E+02	.6874E+01	.1455E+01	.4394E+00
10.80	.3154E-05	.3452E+02	.5605E+01	.3855E+01	.3967E+00
11.00	.3091E-05	.5986E+02	.3382E+01	.5823E+01	.3748E+00
11.20	.3368E-05	.8520E+02	.5887E+00	.7005E+01	.3939E+00
11.40	.3828E-05	-.7204E+02	-.2311E+01	.7129E+01	.4321E+00
11.60	.4127E-05	-.5138E+02	-.4859E+01	.6078E+01	.4489E+00
11.80	.4089E-05	-.3054E+02	-.6671E+01	.3936E+01	.4308E+00
12.00	.3889E-05	-.7623E+01	-.7487E+01	.1002E+01	.3862E+00

TABLE D-3 : Back scattered field and normalized scattering cross-section of a spherical biological body vs. koa at 3.0GHz. (Fig. 4.2.3)

CONDUCTIVITY = 2 280 FREQUENCY = 3000E+10 PERMITTIVITY =46 00

KOA	FIELD MAGNITUDE SQ	PHASE IN DEG	REAL PART OF E	IMAG PART OF E	SCAT-CROSS-SEC BY AREA
20	1381E-10	7232E+02	4322E-02	1356E-01	.5055E-02
40	8481E-09	- 7062E+02	-.3702E-01	1052E+00	.7777E-01
60	2873E-07	.8224E+02	. 3024E+00	5745E+00	1171E+01
80	6877E-07	.5563E+02	.5670E+00	8291E+00	1576E+01
1 00	1835E-06	4276E+02	.1204E+01	.1114E+01	.2691E+01
1 20	1543E-06	3513E+02	.1231E+01	8659E+00	.1572E+01
1 40	1141E-06	4105E+02	.9756E+00	8495E+00	.8538E+00
1 60	3079E-07	6347E+02	.3002E+00	6013E+00	1765E+00
1 80	6565E-07	- 4333E+02	- 7138E+00	6735E+00	.2973E+00
2 00	2010E-06	-.2376E+02	- 1572E+01	6920E+00	.7373E+00
2 20	3768E-06	- 1811E+02	-.2235E+01	7310E+00	1142E+01
2 40	3900E-06	- 1269E+02	- 2334E+01	5254E+00	.9934E+00
2 60	2820E-06	.2594E+00	- 2034E+01	- 9207E-02	.6119E+00
2 80	1629E-06	3185E+02	-.1313E+01	- 8159E+00	3049E+00
3 00	2325E-06	7575E+02	- 4547E+00	- 1790E+01	3790E+00
3 20	4651E-06	- 8090E+02	4132E+00	- 2579E+01	.8663E+00
3 40	6898E-06	- 6853E+02	1164E+01	- 2961E+01	8755E+00
3 60	7022E-06	- 5710E+02	1744E+01	- 2695E+01	7949E+00
3 80	5380E-06	- 3933E+02	.2173E+01	- 1781E+01	5466E+00
4 00	4136E-06	- 8547E+01	.2436E+01	- 3661E+00	.3792E+00
4 20	5333E-06	.2629E+02	.2508E+01	.1239E+01	4436E+00
4 40	8480E-06	4943E+02	.2294E+01	2679E+01	6426E+00
4 60	1107E-05	.6486E+02	.1712E+01	3648E+01	7674E+00
4 80	1101E-05	.7980E+02	.7117E+00	.3955E+01	7009E+00
5 00	9006E-06	-.7983E+02	-.6421E+00	3578E+01	5285E+00
5 20	7853E-06	-.5057E+02	- 2156E+01	.2622E+01	4261E+00
5 40	9626E-06	- 1998E+02	-.3532E+01	1284E+01	4843E+00
5 60	1343E-05	.2752E+01	-.4433E+01	- 2139E+00	6281E+00
5 80	1622E-05	.2003E+02	- 4583E+01	- 1671E+01	7074E+00
6 00	1595E-05	.3720E+02	-.3853E+01	- 2825E+01	6500E+00
6 20	1374E-05	.5896E+02	- 2315E+01	-.3847E+01	.5243E+00
6 40	1279E-05	.8694E+02	-.2313E+00	- 4326E+01	4582E+00
6 60	1514E-05	-.6488E+02	.2001E+01	- 4267E+01	5099E+00
6 80	1946E-05	-.4238E+02	.3947E+01	- 3801E+01	.6173E+00
7 00	2237E-05	-.2388E+02	5239E+01	-.2319E+01	6698E+00
7 20	2192E-05	-.5212E+01	.5648E+01	- 5152E+00	6204E+00
7 40	8122E-05	.2707E+02	.9720E+01	4967E+01	.2176E+01
7 60	8044E-05	.4473E+02	.7718E+01	.7846E+01	.2043E+01
7 80	7008E-05	.8603E+02	.4119E+01	.9265E+01	.1890E+01
8 00	6345E-05	-.8699E+02	- 5073E+00	.9634E+01	.1454E+01
8 20	.7092E-05	-.5848E+02	-.5332E+01	.8895E+01	.1547E+01
8 40	.8961E-05	-.3463E+02	-.9434E+01	6516E+01	.1863E+01
8 60	1056E-04	-.1532E+02	-.1201E+02	3289E+01	.2095E+01
8 80	.1073E-04	.2963E+01	-.1253E+02	-.6486E+00	.2033E+01
9 00	.9850E-05	.2389E+02	-.1088E+02	-.4818E+01	.1748E+01
9 20	.6749E-05	.4958E+02	-.7345E+01	-.8625E+01	.1518E+01
9 40	.9337E-05	.7738E+02	-.2558E+01	-.1142E+02	.1550E+01
9 60	.1133E-04	-.7810E+02	.2657E+01	-.1261E+02	.1803E+01
9 80	.1328E-04	-.5779E+02	.7441E+01	-.1181E+02	.2029E+01
10.00	.1375E-04	-.3894E+02	.1105E+02	-.8927E+01	.2018E+01
10 20	.1270E-04	-.1823E+02	.1297E+02	- 4270E+01	.1791E+01
10 40	.1158E-04	.6475E+01	.1295E+02	.1470E+01	.1570E+01
10 60	.1195E-04	.3358E+02	.1103E+02	.7323E+01	.1560E+01
10 80	.1399E-04	.5851E+02	.7484E+01	.1222E+02	1760E+01
11.00	.1627E-04	.7968E+02	.2773E+01	.1520E+02	.1873E+01
11.20	.1710E-04	-.8095E+02	- 2492E+01	.1564E+02	.2000E+01
11 40	.1615E-04	-.6035E+02	-.7818E+01	.1338E+02	.1824E+01
11 60	.1483E-04	-.3641E+02	-.1187E+02	.8757E+01	.1617E+01
11 80	.1495E-04	-.9966E+01	-.1458E+02	.2562E+01	.1575E+01
12 00	.1696E-04	.1520E+02	-.1522E+02	-.4137E+01	.1728E+01

TABLE D-4 : Back scattered field and normalized scattering cross-section of a spherical biological body vs. koa at 10.0GHz. (Fig. 4.2.4)

CONDUCTIVITY =10.300 FREQUENCY = .1000E+11 PERMITTIVITY =35.90

KOA	FIELD MAGNITUDE SQ	PHASE IN DEG	REAL PART OF E	IMAG PART OF E	SCAT-CROSS-SEC BY AREA
.67	.3569E-08	-.1341E+02	.7420E+00	-.1768E+00	.1309E+01
1.33	.1155E-07	-.3702E+02	.1095E+01	-.8262E+00	.1059E+01
2.00	.1884E-07	.8281E+02	.2193E+00	.1739E+01	.7679E+00
2.67	.1997E-07	-.5613E+02	-.7300E+00	.1650E+01	.4578E+00
3.33	.5671E-07	.3433E+02	-.2511E+01	-.1715E+01	.8320E+00
4.00	.3590E-07	-.8171E+02	.3489E+00	-.2394E+01	.3658E+00
4.67	.1015E-06	-.4142E+01	.4057E+01	-.2938E+00	.7599E+00
5.33	.7580E-07	.7759E+02	.7606E+00	.3455E+01	.4401E+00
6.00	.1410E-06	-.3659E+02	-.3849E+01	.2857E+01	.6383E+00
6.67	.1475E-06	.5015E+02	-.3142E+01	-.3764E+01	.5409E+00
7.33	.1786E-06	-.6440E+02	.2332E+01	-.4866E+01	.5414E+00
8.00	.5991E-06	.2240E+02	.9137E+01	.3765E+01	.1526E+01
8.67	.9881E-06	-.7879E+02	-.2226E+01	.1236E+02	.2101E+01
9.33	.8391E-06	-.2779E+01	-.1168E+02	.5671E+00	.1570E+01
10.00	.1241E-05	.7083E+02	-.4689E+01	-.1343E+02	.2022E+01
10.67	.1168E-05	-.2893E+02	.1202E+02	-.6648E+01	.1659E+01
11.33	.1512E-05	.4240E+02	.1159E+02	.1059E+02	.1919E+01
12.00	.1564E-05	-.5604E+02	-.8889E+01	.1320E+02	.1759E+01
12.67	.1792E-05	.1485E+02	-.1652E+02	-.4380E+01	.1820E+01
13.33	.2012E-05	-.8387E+02	.1934E+01	-.1800E+02	.1844E+01
14.00	.2100E-05	-.1199E+02	.1810E+02	-.3844E+01	.1748E+01
14.67	.2507E-05	.6790E+02	.7606E+01	.1873E+02	.1900E+01
15.33	.2461E-05	-.3842E+02	-.1569E+02	.1245E+02	.1706E+01
16.00	.3016E-05	.3956E+02	-.1709E+02	-.1412E+02	.1821E+01
16.67	.2900E-05	-.6477E+02	.9268E+01	-.1967E+02	.1702E+01
17.33	.3520E-05	.1135E+02	.2348E+02	.4714E+01	.1910E+01
18.00	.3427E-05	.8870E+02	.5380E+00	.2363E+02	.1724E+01
18.67	.4012E-05	-.1658E+02	-.2461E+02	.7298E+01	.1877E+01
19.33	.4041E-05	.6182E+02	-.1212E+02	-.2262E+02	.1782E+01
20.00	.4502E-05	-.4415E+02	.1944E+02	-.1887E+02	.1835E+01
20.67	.4727E-05	.3458E+02	.2286E+02	.1575E+02	.1804E+01
21.33	.5012E-05	-.7137E+02	-.9132E+01	.2709E+02	.1795E+01
22.00	.5458E-05	.7043E+01	-.2960E+02	-.3657E+01	.1838E+01
22.67	.5570E-05	.8188E+02	-.4357E+01	-.2981E+02	.1767E+01
23.33	.6207E-05	-.2066E+02	.2976E+02	-.1122E+02	.1858E+01
24.00	.6200E-05	.5487E+02	.1829E+02	.2600E+02	.1755E+01
24.67	.6952E-05	-.4840E+02	-.2235E+02	.2517E+02	.1862E+01
25.33	.6821E-05	.2806E+02	-.2964E+02	-.1580E+02	.1758E+01
26.00	.7882E-05	-.7606E+02	.8527E+01	-.3434E+02	.1852E+01
26.67	.7735E-05	.1121E+01	.3550E+02	.6947E+00	.1773E+01
27.33	.8403E-05	.7844E+02	.8679E+01	.3598E+02	.1833E+01
28.00	.8828E-05	-.2599E+02	-.3371E+02	.1643E+02	.1794E+01
28.67	.9133E-05	.4912E+02	-.2525E+02	-.2917E+02	.1812E+01
29.33	.9580E-05	-.5328E+02	.2363E+02	-.3168E+02	.1815E+01
30.00	.9898E-05	.2187E+02	.3725E+02	.1503E+02	.1783E+01